2014

# Modelling of clogging in a permeable reactive barrier in acid sulfate soil terrain

Punyama Udeshini Pathirage
*University of Wollongong*

UNIVERSITY OF WOLLONGONG

**School of Civil, Mining and Environmental Engineering**

# MODELLING OF CLOGGING IN A PERMEABLE REACTIVE BARRIER IN ACID SULFATE SOIL TERRAIN

**Punyama Udeshini Pathirage**

**This thesis is presented as part of the requirement for the**
**Award of the Degree of**
**Doctor of Philosophy**
**of the**
**University of Wollongong**

**February 2014**

## THESIS CERTIFICATION

I, Punyama Udeshini Pathirage, declare that this thesis, submitted in fulfilment of the requirements for the award of Doctor of Philosophy, in the School of Civil, Mining and Environmental Engineering, University of Wollongong, is wholly my own work unless otherwise referenced or acknowledged. The document has not been submitted for qualification at any other academic institution.

P.U. Pathirage

*Sincerely dedicated to*

*my*

*Father and Mother*

## ABSTRACT

This study contains laboratory, field and numerical methodology to determine the feasibility and performance of a permeable reactive barrier (PRB) utilising low cost recycled concrete aggregates for the remediation of acidic groundwater in acid sulfate soil (ASS) terrain. The PRB was installed in the Shoalhaven Floodplain about 100 km South of Sydney (Australia), in an area where acidic groundwater generation from pyritic soil poses a severe environmental and socio-economic problem. High concentrations of dissolved aluminium ($Al^{3+}$) and total iron ($Fe^{2+}$ and $Fe^{3+}$) in the groundwater along with low pH reflected the acidic conditions caused by pyrite oxidation at the study site. Past remediation strategies through groundwater manipulation using engineering solutions such as weirs and modified floodgates were not effective in low-lying ASS terrain, as they increased the risk of flooding.

Long-term laboratory column experiments were carried out using synthetic groundwater. The column experiments investigated the acid neutralisation behaviour occurring within the PRB and the precipitation of Al and Fe from the acidic groundwater. In addition, column experiments revealed the potential of recycled concrete to remediate acidic groundwater from ASS by maintaining a near neutral pH and complete removal of $Al^{3+}$ and total Fe from the influent for a considerable period of time. Chemical armouring and clogging, caused as a result of secondary mineral precipitation, was also studied which reduced the efficiency of the reactive material. Moreover, chemical clogging reduces the porosity and hydraulic conductivity of the reactive medium. It was found that chemical armouring/clogging by secondary Al- and Fe- precipitates decreased the acid neutralisation capacity (ANC) of the recycled concrete by ~50% as compared to its theoretical ANC.

For the first time in Australia, this study mainly focuses on coupling geochemistry with geo-hydraulics to allow time-dependant modelling and performance verification with respect to the remediation of acidic groundwater. Chemical clogging of PRB due to mineral precipitates has rarely been quantified and this thesis presents an original modelling and experimental verification of the clogging model for PRBs in an ASS terrain. This study developed an innovative model, capturing the geochemical reaction kinetics coupled with transient groundwater flows. The modelling was incorporated into commercial numerical codes, MODFLOW and RT3D. An algorithm was developed for RT3D to simulate geochemical reactions occurring in the PRB. The experimental and field observed results were in good agreement with the model predictions, confirming that the porosity and hydraulic conductivity reduction due to mineral precipitation occurred at the start of permeation and continued until halfway through the testing phase.

Overall, this study provides a better understanding of the acid neutralisation process occurring inside the PRB for the remediation of contaminated groundwater from ASS terrain using recycled concrete aggregates as the reactive media. This first pilot-scale PRB confirms that it is a suitable environmentally friendly and cost-effective alternative compared to other conventionally utilised techniques for the in-situ treatment of acidic groundwater. Most importantly, the developed numerical model is beneficial for practising engineers and scientists who have to deal with ASS especially in the coastal low-lying areas of Australia.

## ACKNOWLEDGEMENTS

I am extremely grateful to my supervisor, Prof. Buddhima Indraratna for his enthusiastic and unconditional help and encouragement in all aspects of this research. His numerous comments, constructive criticism and suggestions during this research and preparation of thesis are greatly appreciated. I am very glad to be one of his PhD students because of his knowledge on the subject matter, patience and availability for any help, whenever needed albeit the heavy workload.

I also extend my sincere gratitude to my co-supervisors Dr. Laura Banasiak and A/Prof. Long D. Nghiem. The valuable suggestions, numerous comments and friendly gesture of Dr. Laura Banasiak during this study, including the support in field trips and review of the thesis chapters are gratefully acknowledged. The support I got from A/Prof. Long D. Nghiem especially during the laboratory work is highly appreciated.

I am very much grateful to the Australian Government for providing the financial support through the Endeavour Postgraduate Award and all the case officers at Austraining International for their continuous support. This dissertation would not have been possible without financial support from the Endeavour Scholarship Scheme.

I would like to acknowledge the Elsevier Publications for allowing me to use the technical data presented in numerous Figures, Tables, and some technical discussions in the journal paper published in Computers and Geotechnics.

The PRB project would also not have been a success without the generous support from Manildra Group. Therefore, I would like to thank Glennys Lugg (Environmental Scientist) and Manildra Group for technical advice and in-field assistance.

My appreciation is also extended to Dr. Gyanendra Regmi, for his continuous support throughout the PhD. His valuable suggestions during the experiments and numerical modelling are deeply appreciated.

I must thank the enthusiastic technical staff at University of Wollongong, Faculty of Engineering, for their assistance, friendship and entertainment. A special thank goes to Bob Rowlan and Frank Crabtree for their tireless help and knowledge in laboratory equipment preparation. Their friendly nature and hard work really helped me to get through the long days in the field. And also the help and suggestions I got from Dr. Cholachat Rujikiatkamjorn, Dr. Faisal Hai, Dr. Linda Tie, Alan Grant, Ian Laird, Ian Bridge, Fernando Escribano, Cameron Neilson and Ritchie McLean was immense during lab work, and thanks to all. I also extend my gratitude to undergraduate students, Benjamin Lawrance and Rebecca Davies for their support during lab and field work.

I would also like to thank the staff led by Graham Lancaster at the Southern Cross University Environmental Analysis Laboratory for performing part of the water chemical testing. Thank you to Prof. Brian Jones and technical staff at Department of Earth Science, UOW for mineralogical analysis of the samples.

I sincerely dedicate my utmost appreciation to my beloved husband, Nalin Senevirathne. Your continuous encouragement, understanding, patience, love and care throughout this study have been immeasurable. If it were not for you, nothing would have been a success.

Heartfelt acknowledgements are expressed to my loving father, C.H. Pathirage, my beautiful mother, Devani Pathirage and my sweet brother, Gayan Pathirage for their unconditional love and support during my PhD. I am the person today, because of my mother and father. And also I would like to thank my mother-in-law, Anula Abeysinghe and my father-in-law, A.M. Senevirathne and loving sisters-in-law, Chathurika and Niranjala for their understanding and care during my PhD.

Last but not least, my gratitude is extended to all my friends and colleagues at University of Wollongong, especially Nadeesha, Aminda, Kumara, Subhani, Wuditha, Nilu, Pradeepa, Thiru and Darshan for their warm friendship and support given from the day I stepped into Australia.

## LIST OF PUBLICATIONS ARISING FROM THIS THESIS

### Journal Publications

Indraratna B., **Pathirage P.U.**, Kerry R. and Banasiak L (2014). "Coupled hydro-geochemical modelling of a permeable reactive barrier for treating acidic groundwater". Computers and Geotechnics. 55, 429-439.

Banasiak L.J., Indraratna B., Lugg G., **Pathirage U**., McIntosh G. and Rendell N (2014). "Permeable reactive barrier rejuvenation by alkaline wastewater". Environmental Geotechnics. Available: http://www.icevirtuallibrary.com/content/article/10.1680/envgeo.13.00122.

Indraratna B and **Pathirage U**. "Modelling of clogging and performance monitoring in a PRB", Environmental Geotechnics, Special issue: Alternative Barriers (Abstract accepted)

### Conference Papers

Indraratna B., **Pathirage P.U.**, Banasiak L. and Nghiem, L.D (2012). "Column experiments carried out for the treatment of acidic groundwater in acid sulfate terrain at the Shoalhaven Floodplain, NSW". Proceedings of 3rd National Acid Sulfate Soil Conference, Melbourne, Australia

**Pathirage P.U.**, Indraratna B., Nghiem L.D., Banasiak L. and Regmi G (2012). "Armouring by precipitates and the associated reduction in hydraulic conductivity of recycled concrete aggregates used in a novel PRB for the treatment of acidic groundwater". 11th Australia New Zealand Conference on Geomechanics, Melbourne, Australia

Banasiak L., **Pathirage P.U.** and Indraratna B (2012). "Modeling of chemical armouring in a permeable reactive barrier in acid sulfate soil terrain)".

International Conference on Ground Improvement and Ground Control, Wollongong, Australia

**Pathirage U** and Indraratna B. "Modelling of mineral fouling in an alkaline permeable reactive barrier (PRB) in Australia". 14th International Conference of the International Association for Computer Methods and Advances in Geomechanics (IACMAG), Kyoto, Japan 2014 (Full paper accepted)

**Pathirage U** and Indraratna B. "A novel hydro-geochemical model for treating acidic groundwater utilizing a permeable reactive barrier". 7th International Congress on Environmental Geotechnics, Melbourne, Australia 2014 (Abstract accepted)

## LIST OF SYMBOLS

| | |
|---|---|
| $\Phi_k$ | Volume fraction of mineral |
| $S_{Fe^0}$ | Current reactive surface area of zero-valent iron ($m^2$) |
| $\varphi_{Fe^0}$ | Current volume fraction of zero-valent iron |
| $S^0_{Fe^0}$ | Initial reactive surface area of zero-valent iron ($m^2$) |
| $\varphi^0_{Fe^0}$ | Initial volume fraction of zero-valent iron |
| $\Phi$ | Soil porosity |
| $\widetilde{r}_c$ | Rate of all reactions that occur in the soil phase (either $MM^{-1}T^{-1}$ or $ML^3T^{-1}$ can be used) |
| $\Delta n_t$ | Reduction in porosity at time *t* |
| $\mu$ | Absolute viscosity of water |
| $\mu$, *C*, *D* | Integral constants |
| *b* | Aquifer thickness |
| $C_e$ and $C_{in}$ | External effluent and influent concentrations respectively |
| $C_{im}$ | Solid phase concentration of the $im^{th}$ species [either $MM^{-1}$ (contaminant mass per unit mass of porous media) or $ML^{-3}$ (contaminant mass per unit aqueous phase volume) unit basis can be used] |
| $C_k$ | Aqueous phase concentration of the $k^{th}$ species [$ML^{-3}$] |
| $C_{lim}$ | Acceptable concentration |
| $C_s$ | Concentration of source/sink [$ML^{-3}$] |
| $D_a$ | Dispersion tensor for the water phase components |
| $D_{ij}$ | Hydrodynamic dispersion coefficient [$L^2T^{-1}$] |
| *g* | Gravitational constant |
| *h* | Hydraulic head (m) |
| *K* | Hydraulic conductivity initially at time *t* |
| $\boldsymbol{K}$ | Saturated hydraulic conductivity tensor (m/s) |
| *k* | Total number of species |
| $K_0$ | Initial hydraulic conductivity |
| $k_{eff}$ | Effective rate coefficient ($molm^{-3}{}_{bulk}s^{-1}$) |
| $K_{eq}$ | Solubility constant (unit depends on the reaction) |
| $k_{ra}$ | Relative permeability of the porous medium with respect to the water phase (dimensionless) |
| $K_{xx}$, $K_{yy}$, $K_{zz}$ | Hydraulic conductivity along the *x*, *y*, and *z* coordinate axes respectively (L/T) |
| *l* | Length of the column or PRB thickness |
| *m* | Total number of aqueous-phase (mobile) species |
| *M* | Specific surface of the recycled concrete particles (ratio of surface area and bulk volume) |
| $M_k$ | Mineral molar volume ($m^3mol^{-1}$) |
| $N_c$ | Number of components |
| $N_m$ | Number of minerals |
| $n_o$ | Porosity at the start |
| $n_t$ | Porosity at time *t* |
| *Ø* | Porosity of the media ($m^3/m^3$) |
| $q_a$ | Darcy fluid flux (m/s) |

| | |
|---|---|
| $Q_a$ | Source–sink term (1/s) |
| $Q_i$ | Flow rate into the cell ($L^3T^{-1}$) |
| $Q_j^{ext}$ and $Q_j^{int}$ | External and internal source–sinks respectively |
| $q_s$ | Volumetric flux of water per unit volume of aquifer representing sources and sinks [$T^{-1}$] |
| $r$ | Reaction rate ($molm^{-3}_{bulk}s^{-1}$) |
| $r_c$ | Rate of all reactions that occur in the aqueous phase [$ML^3T^{-1}$] |
| $R_k$ | Overall reaction rate for the mineral ($molm^{-3}_{bulk}s^{-1}$) |
| $S_a$ | Volumetric water saturation of the aqueous phase ($m^3/m^3$) |
| $S_s$ | Specific storage coefficient (1/m) |
| $S_S$ | Specific storage of the porous material ($L^{-1}$) |
| $t$ | Time (s) |
| $T$ | Transmissivity |
| $T_j^a$ | Total water phase concentration of component $j$ ($kg/m^3$ $H_2O$) |
| $T_j^s$ | Total adsorbed component concentration |
| $v$ | Pore velocity [$LT^{-1}$] |
| $v_b$ | Groundwater flow velocity through the barrier |
| $V_P$ | Volume occupied by each mineral |
| $V_T$ | Total volume of the column |
| $W$ | PRB width |
| $W$ | Volumetric flux per unit volume representing sources and/or sinks of water ($T^{-1}$) |
| $\Delta h$ | Change in head over a time interval of $\Delta t$ |
| $\Delta V$ | Volume of the cell ($L^3$) |
| $\rho_w$ | Density of water |

## ABBREVIATIONS

| | |
|---|---|
| AAS | Atomic absorbance spectroscopy |
| AASS | Actual acid sulfate soil |
| ACBFS | Air-cooled blast-furnace slag |
| AHD | Australia height datum |
| ALD | Anoxic limestone drains |
| AMD | Acid mine drainage |
| ANC | Acid neutralisation capacity |
| ANC/FF | Acid neutralising factor |
| ASS | Acid sulfate soil |
| BTEX | Benzene-toluene-xylene mixture |
| C-A-H | Aluminate hydrated compounds |
| CRB | Continuous reactive barrier |
| DCE | Dichloroethylene |
| DEM | Digital elevation model |
| DLL | Dynamic link library |
| DO | Dissolved oxygen |
| EC | Electrical conductivity |
| EUS | Epizootic ulcerative syndrome |
| F&G | Funnel-and-gate barrier |
| IAP | Ion activity product |
| ICP-MS | Inductively coupled plasma-mass spectrometry |
| MODFLOW | Modular three dimensional finite difference groundwater flow model |
| NA | Net acidity |
| OLC | Open limestone channels |
| OLD | Oxic limestone drains |
| ORP | Oxygen reduction potential |
| OS | Operator-split numerical strategy |
| OW | Observation well |
| PASS | Potential acid sulfate soil |
| PCE | Tetrachloroethene |
| PRB | Permeable reactive barrier |
| PSA | Potential sulfidic acidity |
| PTC | Pressure transducer column |
| PV | Pore volume |
| QXRD | Quantitative X-ray diffraction |
| RA | Retained acidity |
| SC | Sampling column |
| SF | Safety factor |
| SI | Saturation index |
| SP | Sampling point |
| SRB | Sulfate reducing bacteria |
| TAA | Total actual acidity |
| TCE | Tetrachloroethylene |
| TST | Transition State Theory |
| VC | Vinyl chloride |
| VOC | Volatile organic compounds |
| ZVI | Zero valent iron |

## TABLE OF CONTENTS

## LIST OF FIGURES

## LIST OF TABLES

# Chapter 1 Introduction

## 1.1 Background of the study

Acidic groundwater generated from acid sulfate soil, which occupies over 200,000 $km^2$ of Australian land, is a major environmental and socio-economic problem. Changes in land use pattern (e.g. construction of deep flood mitigation drains) and hydrological systems (e.g. rainy and drought seasons) can promote the oxidation of ASS (pyrite) in shallow zones, with the associated generation of sulfuric acid in the soil, which results in mobilising toxic metals (aluminium (Al) and iron (Fe)) from the soil (Dent, 1992, Indraratna et al., 1995a, Regmi et al., 2009b). Therefore, the transportation of acidic water along with high concentrations of dissolved Al and Fe towards water bodies has significantly degraded the coastal environment of Australia.

A permeable reactive barrier (PRB) offers an in-situ technology for passive treatment of contaminated groundwater (Blowes et al., 2000, Li et al., 2006, Kalinovich et al., 2012, Kalinovich et al., 2008). It is a passive treatment method because groundwater flows through natural gradient and no pump and treat method involved. Recycled concrete has been recommended as a suitable reactive media for the PRB based on batch test analysis among 24 different types of alkaline materials (Golab et al., 2006) for its ability to remove Al and Fe effectively out of solution, and most importantly to maintain near neutral pH for a considerable time. A pilot-scale PRB (17.7 m × 1.2 m × 3.0 m) was installed in ASS terrain located in the Lower Shoalhaven Floodplain near the town of Bomaderry (about 100 km south of Sydney) in October 2006. The

PRB was filled with crushed recycled concrete ($d_{50}$ = 40 mm) and the trench was lined with geotextile fabric to protect the reactive media (media that the contaminants react with and get treated) from physical clogging by soil and other fine particles entering the barrier. A total of 36 observation wells and 15 piezometers were installed inside, up-gradient and down-gradient of the PRB to monitor phreatic surface variations, hydraulic gradients, permeability and groundwater chemistry. Groundwater elevation and water quality parameters such as pH, oxidation reduction potential (ORP) and temperature were directly measured in the field every month from October 2006 using water level meter and multi-parameter field electrode probes. In addition, pH, DO (dissolved oxygen), water pressure, and temperature were measured hourly by two multi-parameter automated data loggers installed within the barrier. Groundwater samples were collected frequently for analysis of Fe, Al, major cations and anions. To the knowledge of the authors, this is only the second pilot-scale PRB under reducing conditions that has been installed for treating acidic water from ASS after a natural limestone PRB reported by Waite et al. (2002).

Generally the performance of PRBs has been satisfactory worldwide for numerous geo-environmental applications (Blowes et al., 2000, McMahon et al., 1999, Puls et al., 1999a, Vidic, 2001, Naftz et al., 2002, Wilkin et al., 2003). On the other hand, questions remain about the long-term efficiency of PRBs that are expected to function for decades or longer (Li et al., 2006, Sarr, 2001, Indraratna et al., 2010). The performance of PRBs has been hindered by mineral fouling wherein the pore space is reduced by mineral precipitation in the reactive media. Fouling of the pore spaces reduces the porosity and hydraulic conductivity of the reactive medium (Indraratna et al., 2010, Regmi et al., 2009a, Mackenzie et al., 1999, Rowe et al.,

2000, Jeen et al., 2012), which then directly affects the reorientation of flow paths and changes reactive times.

## 1.2 Scope of this study

Although the proposed PRB approach to negate the groundwater acidity is a promising solution for specific sites, clogging and armouring (strong adhesion and complete pacification of the reactive surface by encrustation) of the barrier is a major hindrance that requires detailed study. Once the mechanisms of chemical clogging and armouring are understood, the design of PRBs and the selection of materials can be carried out to optimise long-term performance.

The intent of this study was to develop a model to understand mineral fouling (both clogging and armouring) in PRBs in ASS terrain, incorporating a calibrated flow and a reactive transport model to simulate mineral deposition and its effects on hydraulic parameters. To achieve this, a comprehensive geochemical algorithm describing the most dominant reactions was developed and coupled with a transient groundwater flow model. This model will be beneficial for practising engineers and scientists who have to deal with ASS especially in coastal areas of Australia. Clearly, the use of PRBs before the acidic leachate reaches nearby waterways and strategic infrastructure will benefit all downstream users of coastal waterways.

## 1.3 Research Aims and Outcomes

The ultimate goal of this project is not only to model the effectiveness of the PRB, but also to monitor and quantify its performance with respect to time-dependent chemical clogging and armouring with the help of analytical models and numerical software.

The specific aims of this doctoral thesis are to:

1. Establish a rational approach for quantifying chemical clogging/armouring of alkaline PRBs treating acid sulfate landscapes through geo-hydrological and geochemical modelling;

2. Develop a time-dependent porous medium flow model combining particle retention with chemical precipitation to determine the corresponding reduction in void space and effectiveness of the PRB, thereby analysing the inter-related effects of acidic flow induced clogging and PRB effectiveness, i.e. the longevity of such PRBs; and

3. Evaluate and quantify the in-situ effectiveness of the PRB through real-time monitoring of groundwater chemistry up-gradient and down-gradient of the barrier, and to examine the nature of precipitation causing clogging through chemical analysis of barrier specimens.

The following outcomes are expected to significantly contribute to advancing the current state-of-the-art in PRB technology, with particular reference to coastal acid sulfate landscapes:

- A novel approach for evaluating the performance and longevity of alkaline PRBs in the localised treatment of acidic groundwater by evaluating the chemical processes that cause clogging;

- A comprehensive numerical model incorporating chemical clogging/armouring that can be universally applied in the design and performance verification of PRBs in ASS landscapes.

## 1.4 Structure of the Thesis

This dissertation is divided into seven chapters. This first chapter introduces the background and aims of the thesis. It also outlines the structure and organisation of this thesis.

Chapter 2 of this thesis presents a relevant literature review. It provides a general background on ASS, their distribution and the processes involved in pyrite formation. The pyrite oxidation process and, the impacts of ASS on the surrounding landscape with particular reference to environmental, social and economic aspects are briefly outlined. The performance of different types of reactive material used for remediating contaminated groundwater is described, along with the risk of armouring and clogging on the performance of reactive materials. The performance of PRBs and the numerical approaches used to clarify their long-term performance is critically analysed in this chapter.

Chapter 3 examines the potential of recycled concrete aggregates to remediate acidic groundwater through detailed laboratory column experiments. The observed stepwise acid neutralisation behaviour is discussed in depth with special reference to chemical armouring and clogging due to secondary mineral precipitation and accumulation on void spaces.

Chapter 4 outlines the study site information of the pilot-scale PRB installed in the Shoalhaven Floodplain in Nowra, Australia. The monitoring network used to analyse performance of the PRB is detailed. A brief outlook for the chemical attributes of the soil and groundwater parameters at the field site are given. Finally, this chapter

examines the performance of the PRB by comparing water quality data up-gradient, inside and down-gradient of the PRB over a 6.5 year monitoring period.

Chapter 5 describes the development of the geochemical algorithm. This is the first step involved in modelling the groundwater flow and contaminant transport through PRB in ASS terrain. This chapter will focus on the chemical reactions involved in the acid neutralisation and metal removal, and most importantly how they are captured in the geochemical model.

Chapter 6 elaborates the multi-component reactive transport model developed for acidic groundwater remediation with the use of recycled concrete. This chapter shows how the geochemical algorithm developed (in Chapter 5) for the reactions taking place between recycled concrete and acidic groundwater can be used to model the fate and transport of contaminants. Moreover, the model application to laboratory column experiments and field PRB is illustrated in this chapter.

Chapter 7 concludes the major contributions of this research concerning the effectiveness of a PRB in remediating contaminated groundwater in ASS terrain and offers some recommendations for future work.

# Chapter 2 Literature Review

## 2.1 Introduction

Presence of ASS around coastal Australia has evoked many environmental and socio-economic problems. This chapter presents a general background on ASS, their spreading and gives a synopsis of the pyrite formation process. The impacts of ASS on the surrounding landscape with special reference to environmental, social and economic aspects are briefly outlined. A concise assessment of the currently practised geo-environmental techniques for active management of ASS is presented including the ASS preventative and active remediation techniques currently practiced within Australia along with their limitations.

The next part of the literature review provides a critical overview of the application of PRB technology in contaminated groundwater remediation. The results and outcomes of different types of reactive material used for remediating contaminated groundwater are presented. Moreover, the laboratory and field monitoring data is briefly illustrated, to show how the performance of PRBs is hindered by the risk of armouring and clogging on the reactive materials. The performance of PRBs and the numerical approaches used to clarify their long-term performance is critically analysed.

## 2.2 Acid Sulfate Soils

ASS contain iron sulfides (inorganic sulfur compounds) either in an oxidisable or partially oxidised state (Dent, 1986, Sammut et al., 1996a, White et al., 1997). They

are naturally generating soils and sediments, which can be the worst soils in the world because of their ability to generate sulfuric acid ($H_2SO_4$) and reduce the soil pH to as low as 2 (Dent and Pons, 1995). Pyrite ($FeS_2$) is the dominant iron sulfide in coastal Australia although there can be smaller concentrations in the forms of iron monosulfide (FeS), greigite ($Fe_2S_4$) and organic sulfides (Bush and Sullivan, 1997).

ASS contains sulfidic soil horizons or layers according to their oxidisable state, mainly named as Actual Acid Sulfate Soil (AASS) and Potential Acid Sulfate Soil (PASS). AASS is the soil layer or sediment layer that produces $H_2SO_4$ by the oxidation of iron sulfides. AASS develops more when the quantity of $H_2SO_4$, exceeds the acid neutralisation capacity (ANC) of the soil, when the pH drops below 4.0 (Pons et al., 1982). There is another layer of soil or sediment containing iron sulfides and/or other sulfidic material which are not yet been exposed to air and oxidised, thus is completely harmless to the environment. This layer is commonly known as PASS. The PASS layer prevents further oxidation and acidification of ASS by maintaining an anoxic environment in the soil. Usually ASS remains chemically inert under reducing conditions. When they oxidise, complex chemical changes take place, which has the ability to generate and store large amounts of $H_2SO_4$ in the soil. This will result in acidifying the soil pore water and frequently leaching unusually high concentrations of Al and Fe from the soil (Dent, 1986). AASS and PASS can be found in the same soil profile, where AASS usually in top of PASS (Fitzpatrick et al., 1993). The term acid sulfate soil which can be found in literature, usually refer to both AASS and PASS.

### 2.2.1 Formation of Acid Sulfate Soil

ASS and pyritic sediment usually occur in different geographical locations; however, coastal floodplains are the most common places for formation of ASS. The most favourable conditions for the formation of pyritic sediment in coastal floodplains are reducing environments with a supply of decomposed organic matter, sulfate ($SO_4^{2-}$), Fe and reducing bacteria (Figure 2.1). Iron oxides such as hematite and iron oxide ($Fe_2O_3$), oxyhydroxides (goethite (FeOOH)) and hydroxides are the common sources of Fe (Blunden, 2000). Dissolved $SO_4^{2-}$ is rich in seawater (~2700 mg/L). A sufficient amount of dissolved $SO_4^{2-}$ comes from the inundation of low-lying land by brackish water. In addition, wet conditions due to excess rainfall, long water retention times and regular tidal inundation can create an environment for the existence of $SO_4^{2-}$-reducing bacteria (SRB, *Desulfovibrio desulfuricans*). In such wetlands, *D. desulfuricans* reduces $SO_4^{2-}$ from the tidewater and $Fe_2O_3$ from the soil in the presence of simply decomposable organic matter to form pyrite (Dent, 1986, Dent and Pons, 1995). During this microbial oxidation, generated electrons, reduce ferric iron ($Fe^{3+}$) to ferrous iron ($Fe^{2+}$) (Fanning, 1993). Addition to that pyrite formation kinetics are enhanced due to the warmer temperatures and slightly acidic conditions, but their influence is very slow compared to the microbial oxidation (e.g. ~100 years to form 1% pyrite by mass) (Dent and Pons, 1995, Lin et al., 1995).

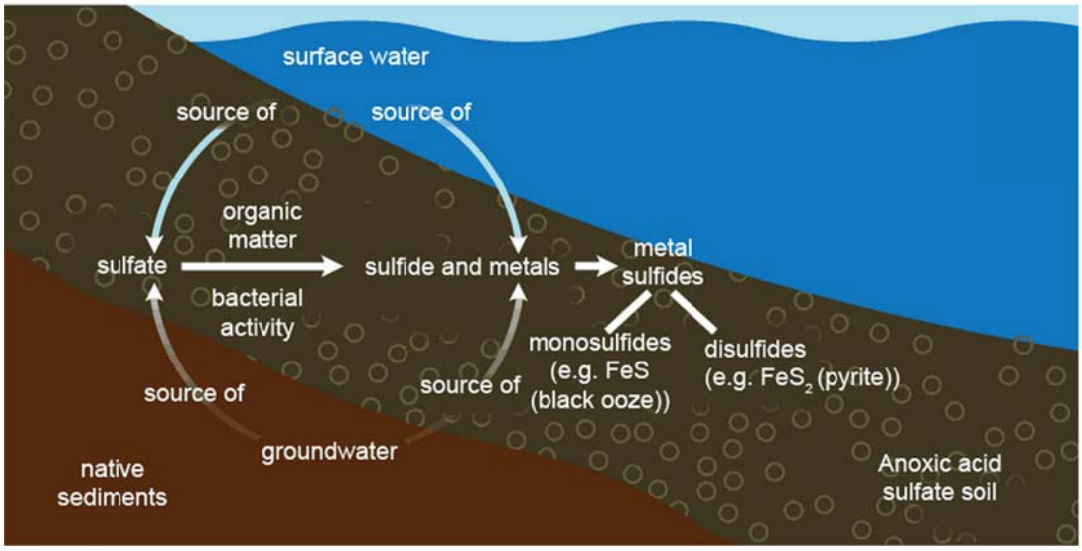


Figure 2.1 Formation and accumulation of ASS in an inundated scenario (Baldwin, 2011)

Dent (1986) has expressed the complex microbial-catalysed reaction involved in pyrite formation process as (Dent, 1986):

$$\underbrace{Fe_2O_{3(s)}}_{\text{iron}} + \underbrace{4SO_{4\ (aq)}^{2-}}_{\text{sulfate}} + \underbrace{8CH_2O}_{\text{organic matter}} + \tfrac{1}{2}O_2 \xrightarrow{\text{bacterial driven with reducing conditions}} \underbrace{FeS_{2(s)}}_{\text{pyrite}} + \underbrace{8HCO_3^-}_{\text{bicarbonate}} + 4H_2O \quad (2.1)$$

In these wet environments, bicarbonate ions ($HCO_3^-$) coming from Eqn. (2.1), remain soluble and mix with the groundwater by leaching and tidal flushing. The above reaction can occur in two stages; the first step invloved the bacterial reduction of $SO_4^{2-}$, in which the hydrogen sulfide ($H_2S$) forms first, as shown in Eqn. (2.2) (Bohn et al., 1989). Then $H_2S$ reacts with iron oxyhydroxides to produce pyrite, as shown in Eqn. (2.3).

$$SO_{4(aq)}^{2-} + 2CH_2O_{(s)} \xrightarrow{\text{bacteria}} H_2S_{(g)} + 2HCO_{3(aq)}^- \quad (2.2)$$

$$3H_2S_{(g)} + 2FeOOH_{(s)} \longrightarrow FeS_{(s)} + FeS_{2(s)} + 4H_2O_{(l)} \quad (2.3)$$

### 2.2.2 Pyrite Oxidation Process

Pyritic soil is moderately chemically inert if left undisturbed and inundated under the watertable (Dent and Pons, 1995, Indraratna et al., 1995b). However, once these inundated soil is disturbed, it can cause oxidation of pyrite resulting in the generation of $H_2SO_4$ (Stumm and Morgan, 1996, Lin et al., 1995). The pyrite oxidation process is a complex and not well recognised process because it involves chemical, physical and biological reactions (Dent, 1986). This complex series of reactions of pyrite with atmospheric $O_2$ and water can be simplified to:

$$\underbrace{FeS_2}_{\text{pyrite}} + \underbrace{\tfrac{7}{2}O_2}_{\text{atmospheric oxygen}} + H_2O \longrightarrow \underbrace{Fe^{2+}}_{\text{dissolved iron}} + 2SO_4^{2-} + \underbrace{2H^+}_{\text{acid}} \tag{2.4}$$

The reaction (Eqn. (2.4)) involves the conversion of pyrite ($FeS_2$) to $Fe^{2+}$ and $SO_4^{2-}$ when $O_2$ and water are present in the environment. The outcomes of Eqn. (2.4), which are dissolved $Fe^{2+}$, $SO_4^{2-}$ and $H^+$ can be easily transported in within porewater, groundwater and drainage water. With the presence of oxygen, $Fe^{2+}$ can be further oxidised to $Fe^{3+}$ as shown in Eqn. (2.5), which is soluble in acidic water at low pH (< 3.5). The $Fe^{3+}$ can form insoluble ferric hydroxide with the presence of water, at a pH greater than 3.5. This will result in generating more acidity as expressed in Eqn. (2.6).

$$\underbrace{Fe^{2+}}_{\text{dissolved iron}} + \underbrace{\tfrac{1}{4}O_2}_{\text{atmospheric oxygen}} + \underbrace{H^+}_{\text{acid}} \longrightarrow Fe^{3+} + \tfrac{1}{2}H_2O \tag{2.5}$$

$$Fe^{3+} + 3H_2O \Leftrightarrow \underbrace{Fe(OH)_3}_{\text{Floc}} + \underbrace{3H^+}_{\text{acid}} \tag{2.6}$$

Dent (1986) has combined Eqns. (2.4-2.6) to express the overall reaction for the complete oxidation of pyrite by:

$$FeS_2 + {}^{15}\!/_4\, O_2 + {}^{7}\!/_2\, H_2O \longrightarrow \underbrace{Fe(OH)_3}_{\text{Floc}} + 2SO_4^{2-} + 4H^+ \qquad (2.7)$$

*Acidithiobacillus ferrooxidans* is an iron-oxidising bacteria, which are acidophilic chemolithotrophic organisms that are global in pyritic environments (Nordstrom, 1982). *A. ferrooxidans* bacteria can catalyse and rapidly oxidise $Fe^{2+}$ to $Fe^{3+}$ by a factor > $10^6$ at pH 2.5–3.5 (Singer and Stumm, 1970, Jaynes et al., 1984). $Fe^{3+}$ can oxidise pyrite more hastily than by $O_2$ at pH less than 4.5, as shown in Eqn. (2.8) (Singer and Stumm, 1970), further generating more acid in the soil.

$$FeS_2 + 14Fe^{3+} + 8H_2O \xrightarrow{bacteria} 15Fe^{2+} + 2SO_4^{2-} + 16H^+ \qquad (2.8)$$

### 2.2.3 Distribution of Acid Sulfate Soils

ASS is spread out in the coastal wetlands of many locations worldwide. Although they occur mainly in low-lying coastal areas, they have been found in inland environments as well, where pedogenesis has been influenced by iron sulfide-rich rock (Kraus, 1998, Davison et al., 1985). Based on a survey done by van Breeman (1980) for Holocene coastal plains and tidal swamp sediments, it was estimated that there are 12-14 million hectares (ha) of ASS around the world. From this, two-thirds are found to be in Indonesia, Vietnam, Thailand, Malaysia and northern Australia (Ritsema et al., 2000). Table 2.1 shows an estimate of the worldwide distribution of ASS (Brinkman, 1982).

Table 2.1 Worldwide distribution of acid sulfate soil according to calculations of Brinkman (1982)

| Region | Area of ASS ($\times 10^6$ ha) |
|---|---|
| Africa | 3.7 |
| Asia | 6.7 |
| Latin America | 2.1 |
| Australia | 1.0 |

As shown in Figure 2.2, ASS in Australia is widely distributed in estuarine lowlands and coastal floodplains along the eastern (Walker, 1972) and northern Australia (White et al., 1996, Best, 2005). Moreover, some distribution can be seen in parts of Western Australia (White et al., 1997), South Australia and Victoria (Sammut et al., 1996a, Berner, 1984). In most of these regions, the sulfidic horizon is close to the mean sea level which arise a risk of oxidation.

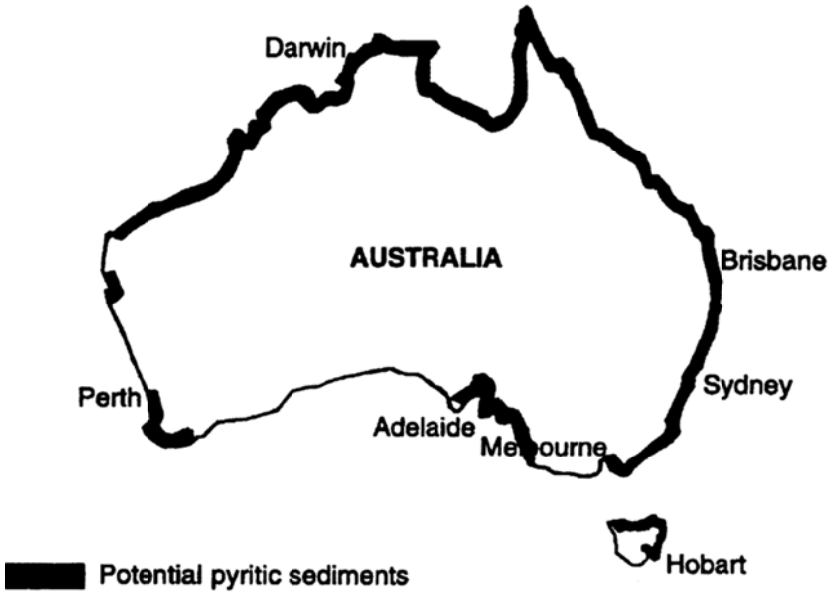


Figure 2.2 Acid sulfate soil distribution in Australia (Department of the Environment and Heritage 2006, National coastal acid sulfate soils)

White et al., (1997) mentioned that the ASS inhabits over 3 million ha of the Australian land. The entire estimated area of ASS in Australia contains 700 million tonnes of environmentally harmful sulfidic material. The total amount of sulfidic material present in 3 million ha of Australian land is equivalent to about 2.2 billion tonnes of $H_2SO_4$ if fully oxidised (Fitzpatrick et al., 2006). Figure 2.3 shows the total area of ASS in coastal NSW.

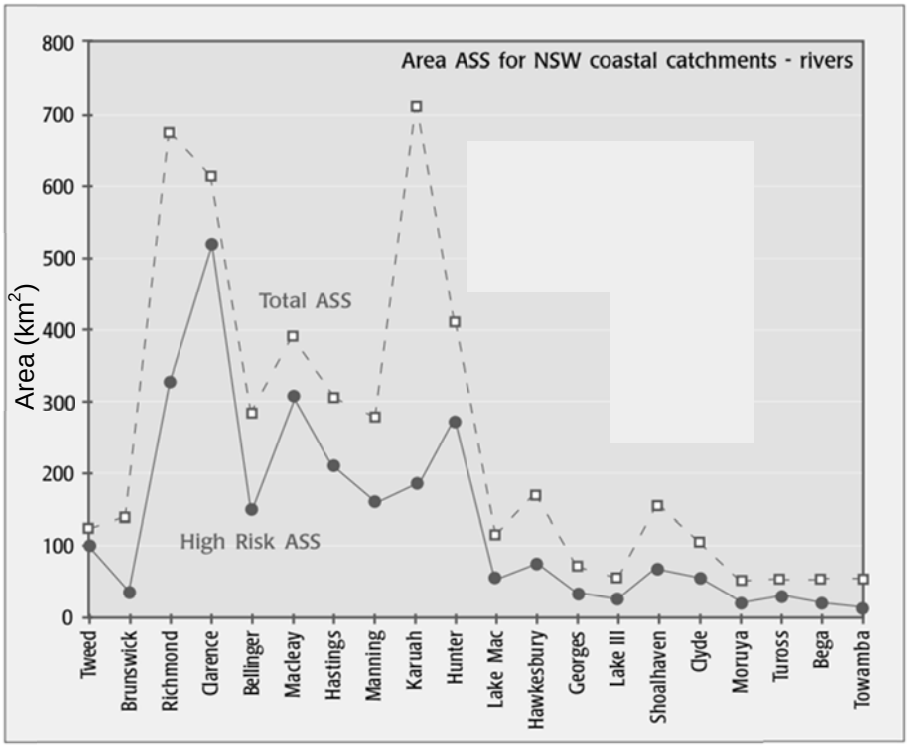


Figure 2.3 Area of high risk and total area of ASS in coastal NSW (White et al., 1999)

### 2.2.4 Environmental and socio-economic problems associated with ASS

Discharge of acidic and metal-rich water into aquifers and nearby surface water bodies from ASS is an intractable socio-environmental issue in many coastal regions around the world (Sammut et al., 1996b, Indraratna et al., 2005, Driscoll et al., 1980).

Following are some of the major environmental, social and economic impacts of ASS in coastal Australia (Figure 2.4).

One of the main impacts is the unfavourable conditions generated for soil productivity and plant growth. Major nutrients and trace elements cannot exist in soils below pH 4, and the presence of soluble toxic metals under acidic conditions is injurious to plant growth (Rorison, 1973). Lin et al. (2001) found that the ASS scalds have less organic matter and soluble phosphorus high salinity, acidity and soluble Al, Manganese and Zinc concentrations. ASS scalds are the bare lands where pyritic layers are close to the soil surface due to lack of alluvium coverage or where overlying peat has been washed or burned away.

(A) Acid scalds

(B) Fish kills

(C) Fe flocs


(D) Concrete corrosion


Figure 2.4 Impacts of acid sulfate soil in coastal Australia
(A and D: Baldwin (2011))

High concentrations of soil acidity also create unfavourable conditions for grass growth and other vegetation. This adversely and directly affects the dairy farming industry. Very few plants can bare the high acidity and high concentrations of toxic metals (e.g. Al and Fe) except sugar cane and tea tree. As a result of that many coastal Australian land have remained un-vegetated for many years. In south east NSW, UOW researchers (Blunden, 2000, Indraratna et al., 2002) have found that the Al concentration was three times higher than the accepted limits given in ANZECC guidelines (2000). These high concentrations of Al and Fe restrict the plant growth and promote grass which can tolerate the acidity such as smartweed (Sammut et al., 1996b). These environmental and ecological problems directly impact the potential revenue capacity.

Impact on the aquatic environment by the transportation of acidic water with high concentrations of dissolved Al and Fe towards water bodies (either by infiltration into aquifers or by discharging into nearby drains after rainfall events) is immense in Australia. Excessive use of groundwater in ASS terrains can lower the water table. This will result in further oxidation of ASS and the groundwater quality will be degraded due to highly acidic pH and high concentrations of soluble metals (Powell and Martens, 2005).

Aquatic marine organisms (e.g. fish, worms, shellfish and oysters) in Australia undergo death and epizootic ulcerative syndrome (EUS, commonly known as 'red-spot disease') as a direct effect of acidic groundwater. Moreover, the loss of aquatic biodiversity occur due to the high acidity, low dissolved $O_2$ and high Al, and overwhelming by Fe flocs (Lin and Melville, 1992, Sammut et al., 1996a, Sammut

and Melville, 1994, Dove, 2003, Driscoll et al., 1980). One of the biggest problems aroused in aquatic environment is the harmfulness of acidic drainage on breeding and nursery areas for reef fish as they result in chronic long-term effects.

In addition, ASS has numerous social and economic problems that are of national importance. In Australia, the damage to local fish and oyster farming industries due to acidic groundwater is estimated at several millions of dollars per year in NSW and QLD only (Indraratna et al., 1995b). There have been considerable financial losses in fish and oyster farming industries because of the loss of consumer confidence in product quality after fish kill events reported in these areas. As an example, the loss of discarded sea mullet due to EUS by NSW commercial fishers were estimated to be over one million dollars (Callinan et al., 1995).

ASS also has adverse effects on infrastructures due to acidic groundwater generated at ASS terrains. White and orange-red precipitates forming from Al and Fe respectively clog pipes and drains. Moreover, the weathering of ASS can form ettringite and gypsum minerals that are related to breakdown concrete structures (van Holst and Westerveld, 1973). High concentrations of $Fe^{2+}$ in groundwater precipitate as iron oxy/hydroxides and as an adverse effect, release $H^+$ ions, as shown in Eqn. (2.9).

$$Fe^{2+} + \tfrac{1}{2}O_2 + \tfrac{3}{2}H_2O \longrightarrow \underbrace{FeOOH\downarrow}_{\text{red-brown floc}} + \underbrace{2H^+}_{\text{acid}} \qquad (2.9)$$

One of the biggest problems of ASS occurs when neutral pH water meets acid and Fe-rich water, which will result in blocking or damaging surface water drain systems due to the precipitation of iron oxy/hydroxide.

Acid attack on concrete and steel infrastructures (e.g. foundations, bridge piers, culverts and pipelines) weakens the concrete, and rusts the steel reinforcing. This is a common problem observed in coastal Australia. In order to get rid of the acid corrosion, $SO_4^{2-}$-resistant concrete and galvanised steel have been suggested in the construction of public infrastructure in many parts of NSW. ASS in nature has a low load-bearing capacity due to their high volumetric moisture content. As a result, foundations built on ASS may settle or sink unequally because of the dewatering of the unconsolidated material.

### 2.2.5 Previous Management methods of Acid Sulfate Soils

As long as ASS can be left undisturbed, that would be the best way of minimising the impacts from ASS. That option is cost effective and environmentally friendly. In the meantime, ASS areas that have already been disturbed need to be treated. In Australia, various remediation methods have been practised and currently being used by government and private sectors to minimise the acidification and decrease the oxidation of ASS. The following is a critical review of some of the main preventive remediation techniques.

***Water Table Manipulation using v-notch weirs and self-tilting weirs***

As discussed previously, maintaining the groundwater table above the ASS horizon can prevent the exposure of ASS to atmospheric $O_2$, thus preventing oxidation. Groundwater manipulation techniques have been practised before in acid rock drainage. This method was successful for decreasing the oxidation of tailings by complete inundation of acid producing materials (Pedersen, 1983). Several researchers at the UOW (Indraratna et al., 1995b, Blunden et al., 1997) have found

that the handling of flood mitigation drain water levels can also affect the surrounding groundwater in ASS. The simple v-notch weirs installed by UOW research team (Indraratna et al., 1995b) could decrease acid production by maintaining the water table above the pyritic soil horizon in ASS terrains of coastal Australia.

A finite element model developed by Blunden et al. (1997), using a series of hydrologic and hydraulic procedures, revealed that the installation of weirs would allow the groundwater table to rise to a certain level without flooding. Therefore, the preliminary modelling work was carried forward by Blunden and Indraratna (2000), in which they undertook a detailed field and numerical study to uphold an elevated groundwater table above the pyritic soil horizon by installing three v-notch weirs near Berry, south east NSW (Figure 2.5). The pyrite oxidation analytical model developed by Blunden and Indraratna (2001) could precisely assess the management strategies at the sub-catchment scale and could demonstrate that the weirs had the ability to considerably decrease pyrite oxidation. As a successful outcome of the research carried out at UOW, water manipulation through weirs was adopted in coastal Australia during the last decade. This is a cost effective management strategy which can avoid further pyrite oxidation. The weirs were constructed from durable yet inexpensive materials (Golab and Indraratna, 2009). With the same basic mechanism of v-notch weirs with slight upgrading of the design, self-regulating tilting weirs were installed adjacent to the flood mitigation drains in ASS terrain (Figures 2.5 and 2.6).

Figure 2.5 V-notch weir installed near Berry, south east NSW, Australia (Blunden, 2000)

Figure 2.6 A self-regulating tilting weir (built in 2001 by the UOW ASS research team)

The installed weirs prevented the production of acid, but could not manage the discharge of stored acid. However, these techniques are not practical in low-lying ASS terrains because;

- they elevate the risk of flooding during heavy rainfall;
- the technique is limited to a smaller area near the region, hence not able to prevent pyrite oxidation far from the drain;
- they prevent the entry of tidal water, thus the water quality cannot be improved; and
- scheduled maintenance is required to clean up the drain due to the accumulation of sediments and growth of weeds.

***Tidal Buffering***

Various researchers (Pollard and Hannan, 1994, Williams and Watford, 1997, Dick and Osunkoya, 2000, Blunden, 2000) suggested improvements in drain water quality by tidal buffering within acid affected flood mitigation drains. The tidal flushing can facilitate acid neutralisation through diminishing the Al flocculation, raising the dissolved $O_2$ levels in groundwater, decreasing the 'acid reservoir effect' and enhancing the runoff during the wet periods (Glamore, 2003, Glamore and Indraratna, 2001, Indraratna et al., 2002, Portnoy and Giblin, 1997b, Portnoy and Giblin, 1997a).

Two types of modified two-way floodgates were installed by UOW researchers (Glamore and Indraratna, 2004, Glamore and Indraratna, 2002, Indraratna et al., 2002, Johnston et al., 2002) as an alternative solution to weirs and one-way floodgates near Berry, south east NSW. One of these was a winch-operated floodgate that lifts vertically (Figure 2.7 (a)). This can control the amount of water entering the drain. The other one is a more sophisticated automated *Smart Gate* system (Figure 2.7 (b)). This *Smart Gate* measures the real-time water quality parameters such as

pH, electrical conductivity (EC), DO and temperature and only if they are up to the standard limit, allows water to enter the drain (Figure 2.7, (Glamore, 2003, Indraratna et al., 2002)). The *Smart Gate* system is a computerised arrangement of real-time sensors that continually monitors the water chemistry and operates the mechanical winch of the floodgate according to the transmitted intelligent electronic signals.

(a)


(b)

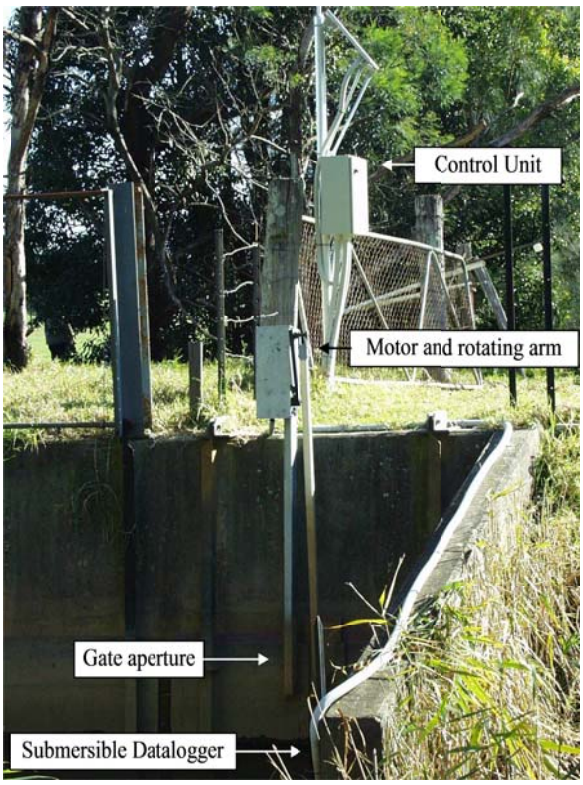


Figure 2.7 Modified Floodgates near Berry, south east NSW: (a) **T**wo-way floodgate, (b) Smart gate (Indraratna et al., 2002)

The results obtained from two-way floodgate show that the drain water quality has improved substantially upon re-establishment of tidal flushing (Figure 2.8). Moreover, surface water quality measured for continuous three years also showed an increase in drain water pH above 6, confirming its suitability for ASS remediation. Furthermore, Al and Fe were removed by precipitation during tidal buffering as their oxy/hydroxides (Glamore, 2003). Figure 2.9 clearly shows the rise of bicarbonate alkalinity up to 90 mg/L $CaCO_3$ in drain water after the setting up the two-way floodgates. Numerous local government agencies and councils use *Smart Gates* because of their ability to improve drain water.

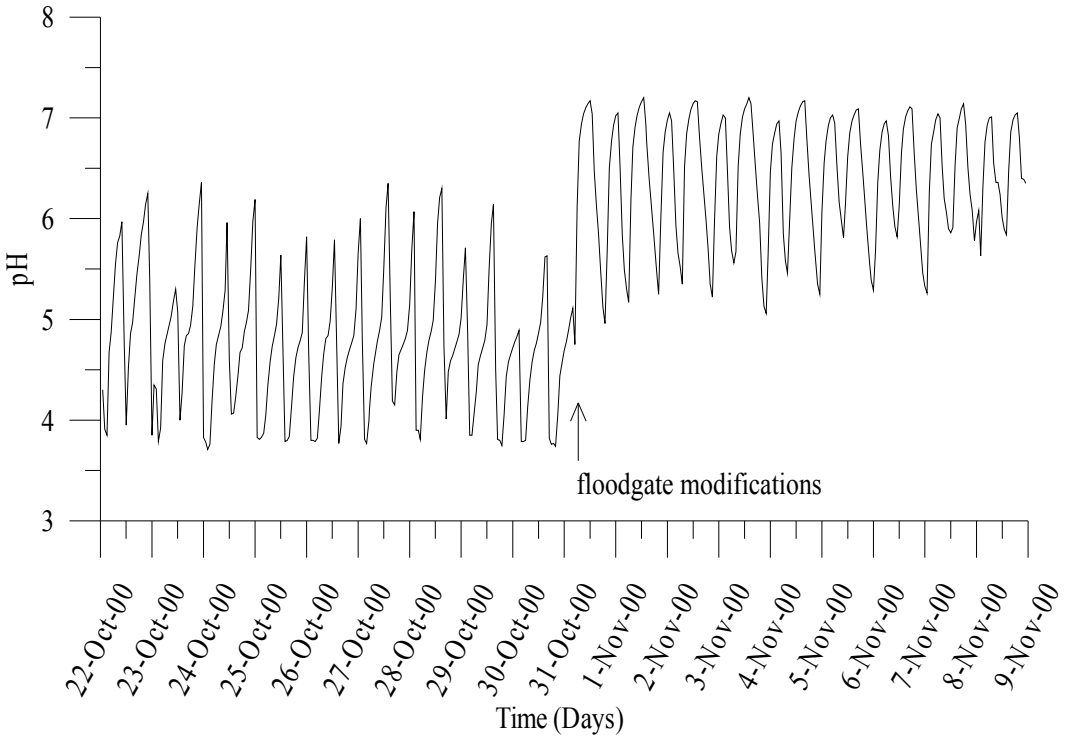


Figure 2.8 Modified Floodgates near Berry, south east NSW (Days 296-314) (Adapted from (Glamore, 2003))

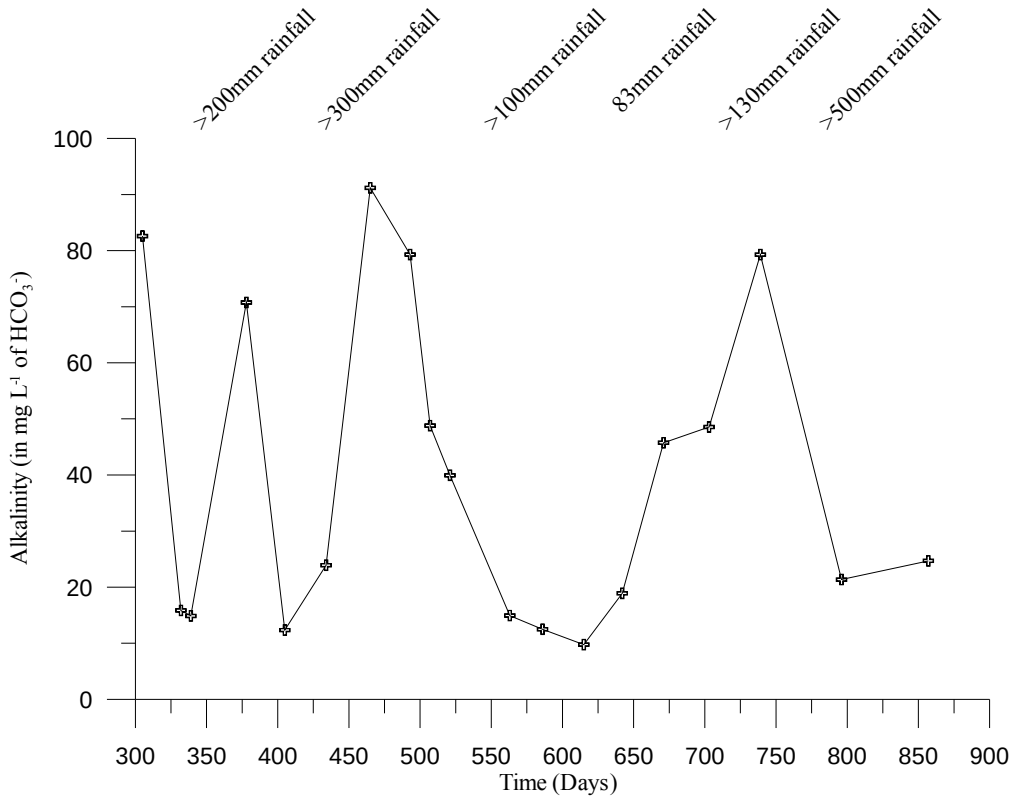


Figure 2.9 Bicarbonate concentrations within the drain after floodgate modifications with rainfall (Glamore, 2003)

Glamore (2003) reported that the performance of these floodgates was not sufficient especially in heavy rainfall events as the amount of alkalinity generated was not enough (10-90 mg/L $CaCO_3$ (Figure 2.9)). That is because the effectiveness of tidal buffering depends on several factors such as the concentration of buffering agents, the acid concentration within the drain and the hydrodynamics of the creek such as flow velocity (Indraratna et al., 2005). Two-way floodgates also have a risk of elevating the water table in low-lying areas with poor drainage. Maintenance is of paramount importance to clean the sensors and make sure the debris have not clogged the system, because the capital cost is high for electronic and mechanical devices controlling the *Smart Gates*.

### *Acid neutralisation through Liming*

Neutralisation of soil and groundwater acidity through liming has been widely applied in throughout the world for the management of ASS as an effective and easy remediation method. However, soil liming produces a metal-rich sludge in the soil (Benner et al., 1999a). This may result in subsequently leaching of metal ions when mixed with the acidic groundwater, hence becoming ineffective in the long-term (Pearson and McDonnell, 1975b, Webb and Sasowsky, 1994). Furthermore, soil liming around coastal Australia would be an expensive methodology to treat the whole estimated 3 million ha, although Dent (1992) suggested that raising the pH of the soil above 5 should be adequate to remediate ASS. Although this method can neutralise the acidity present in the top most soil layer with tidal flush, it releases very mobile acid into the creeks.

### *Lime-Fly ash Barrier*

A lime-fly ash barrier, suggested by researchers at the UOW (Banasiak, 2004, Indraratna et al., 2006), is a modification of the soil liming concept. It is a passive treatment system, which is relatively inexpensive for the benefit of the local farmers. Accordingly, an alkaline slurry was injected at shallow depth above the pyritic layer by radial grouting to form a semi-impermeable reactive horizontal barrier in ASS terrain near Berry, south east NSW. The alkaline slurry consisted of water, fine grained lime and fly ash (2:2:1) and was injected into the soil in a grid of 22 holes to form a 100 mm thick barrier. There were 31 observation wells to monitor the groundwater quality in an adjacent drain (Figure 2.10).

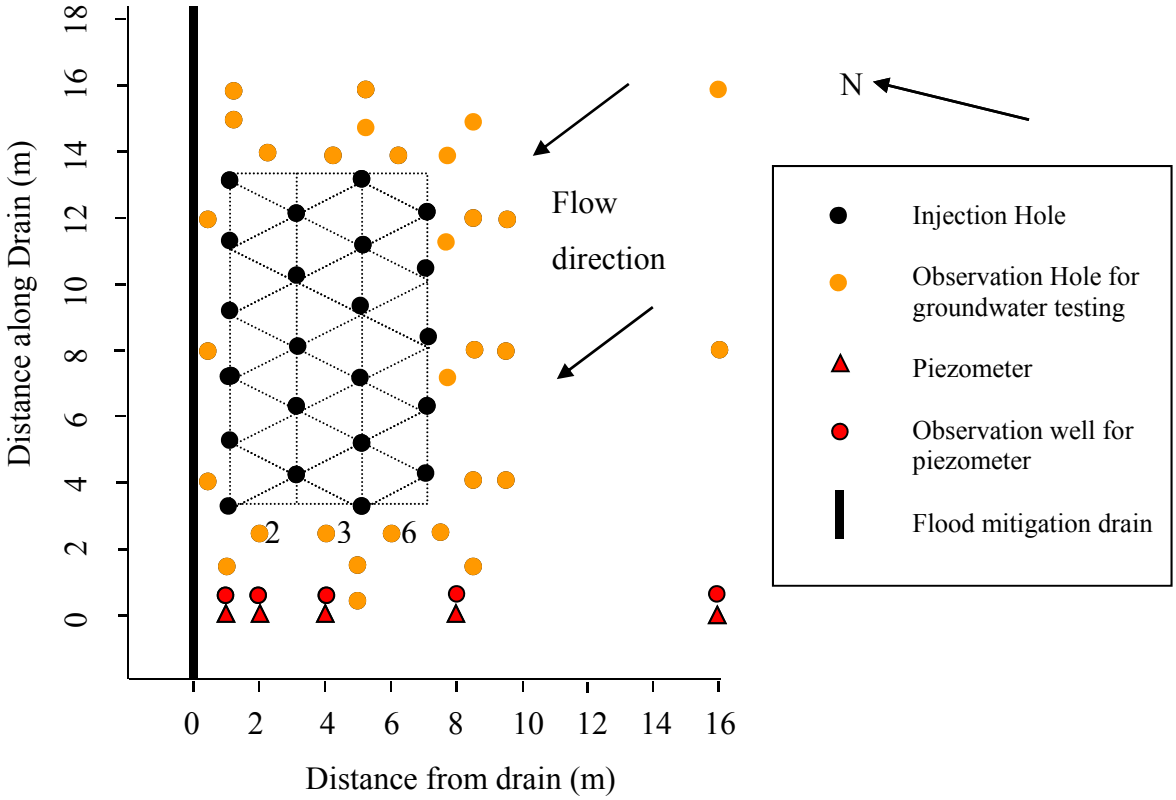


Figure 2.10 Layout of the horizontal semi-impermeable barrier installed in ASS, south east NSW (Banasiak, 2004)

Considerable improvements in groundwater were witnessed from the data taken from the observation wells for pH, Al and Fe concentrations. The average pH improved from 3.5 to 4.6, and Al and Fe concentrations were decreased from 65.5 to 20.3 mg/L and 161 to 42 mg/L, respectively (Figure 2.11) (Banasiak, 2004, Indraratna et al., 2006). The lime-fly ash barrier could reduce the infiltration of oxygen to the pyritic soil layer. As a result, the rate of pyrite oxidation decreased, in addition to neutralising any acidity stored in the soil.

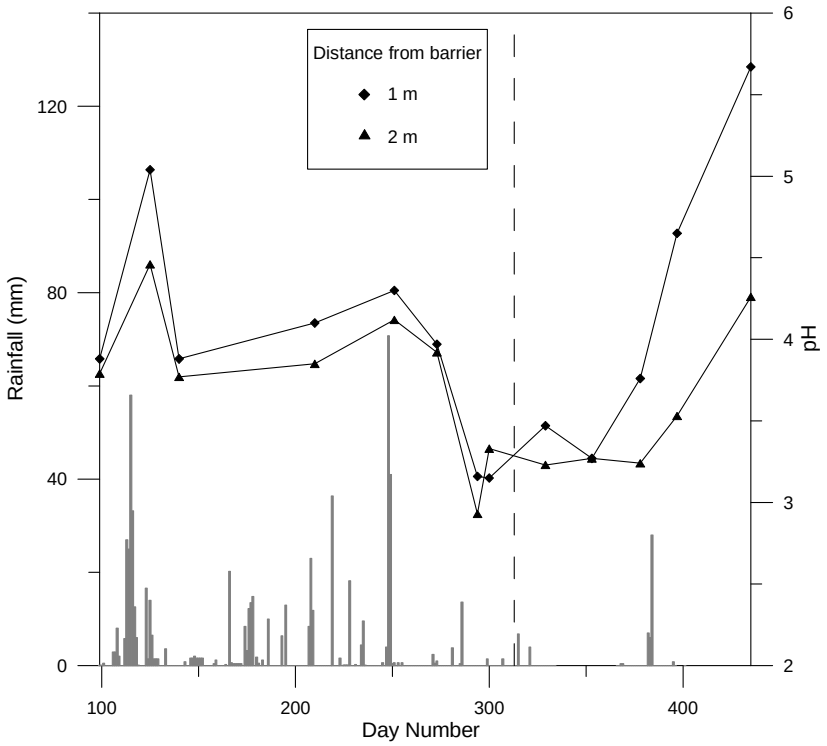


Figure 2.11 Average groundwater pH measured at 1 m and 2 m from the barrier and rainfall (Indraratna et al., 2006)

## 2.3 Permeable reactive barriers (PRBs)

A PRB is defined as an emplacement of reactive materials in the subsurface designed to intercept a contaminant plume, providing a flow path through the reactive media (Figure 2.12). The objective is to transform the contaminant(s) into environmentally acceptable forms to attain the remediation goals down-gradient of the barrier (Regmi et al., 2011a). The remediation is through physical, chemical and/or biological processes, including precipitation, sorption, and oxidation/reduction (Rumer and Ryan, 1995, Golab et al., 2006).

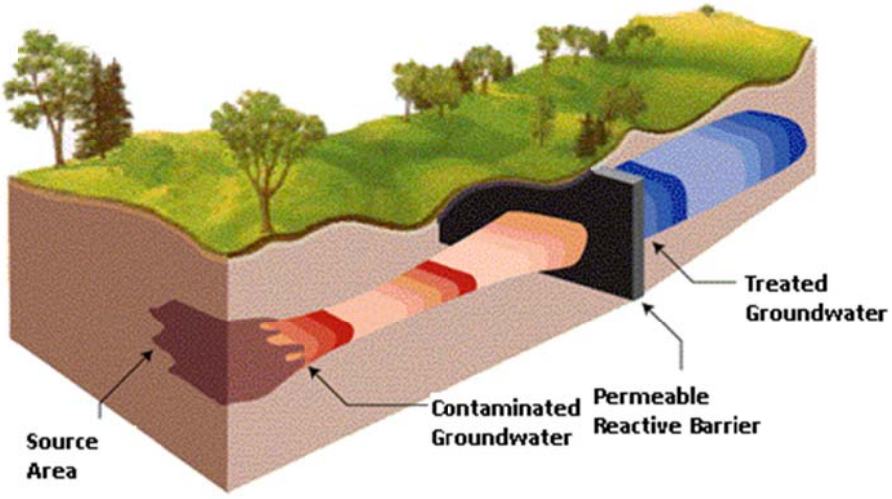


Figure 2.12 Diagram of a permeable reactive barrier (PRB) intercepting a plume of contaminated groundwater (Stewart, 2008)

In this remediation procedure, the reactivity of the reactive material is exhausted slowly providing the environment to remediate the contamination. As a result of PRB's long-term performance, they have the potential to treat contaminants over several years or decades (Gavaskar et al., 1998). Despite higher installation costs compared to conventional remediation techniques such as weirs and modified two-way floodgates, pump-and-treat methods, soil liming and direct addition of lime to streams; PRBs have low operation and maintenance costs. PRBs are proven to be promising, as they do not show any unexpected malfunction before the costs are recovered (Birke et al., 2003). Perhaps the only possible maintenance is the replacement of the reactive material once its reactive potential has been depleted or if it is clogged by precipitates and/or microorganisms (Vidic, 2001). Most importantly, land use patterns can remain unchanged as the remediation is happening underground and only monitoring wells are visible aboveground.

In practice, usually two types of PRB installations are used as shown in Figure 2.13: (a) continuous reactive barrier (CRB) and (b) funnel-and-gate (F&G) barrier. A CRB

is a trench filled with reactive material across the entire contaminated groundwater plume. In F&G barriers, sheet piles and slurry walls are constructed to direct the contaminated groundwater flow towards the gate containing the reactive material(s) which is located between the ends of the walls (Figure 2.13 (b)).

The first full-scale commercial zero valent iron (ZVI) PRB is a F&G type barrier installed at Sunnyvale, California (CA), USA in 1995 for treating chlorinated solvents TCE, dichloroethylene (DCE), vinyl chloride (VC), and chlorinated fluorocarbons (CFCs) (Birke et al., 2003). The concept was based on the first pilot-scale PRB (CRB type), which was installed at Borden, Ontario, Canada, in June 1991 after the concept development by the University of Waterloo in 1990. The application of PRBs for real world applications progressively increased after 1995 and till then, over 100 PRBs have been installed worldwide for remediation of different kind of contaminants (USEPA, 2002).

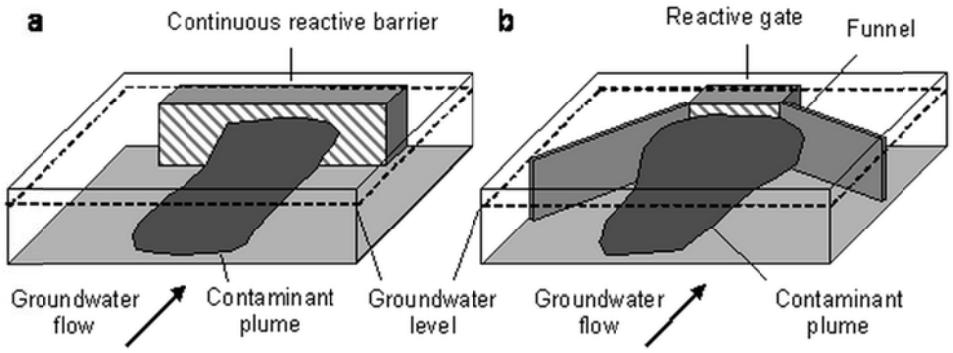


Figure 2.13 PRB configurations: (a) continuous reactive barrier (CRB) and (b) funnel-and-gate (F&G) GW is groundwater (Kaksonen, 2000)

## 2.4 Selection of reactive medium

Selection of correct material is the first important step involved in PRB design as it determines its reactivity, contaminant removal capacity and most significantly, longevity. According to Gavaskar et al. (1998), the reactive material should be fully characterised to confirm:

- adequate reactivity to reduce contaminants;
- maintain the reactivity and ability to run over long periods of time;
- low cost and readily available
- to make sure the reactions taking place between contaminants and reactive material in stable and environmentally friendly forms;
- do not generate adverse chemical reactions and do not serve as a source of contaminants (different or same contaminants);
- minimise precipitation, to allow continued flow of water with time; and
- comprise of the correct particle size for the anticipated porosity.

## 2.5 Types of reactive material used for acidic water remediation

The reactive material should be capable of remediating the groundwater in a timely manner and without clogging or weakening, as stated in Section 2.4. Therefore, the reactive materials are chosen such that they react with the contaminants to convert them to harmless products by the time they pass out the other side of the PRB. Some of the most common reactive materials used to treat acidic groundwater worldwide are organic carbon-rich materials, ZVI and acid neutralising materials. Their characterisation, application in PRBs and long-term performance are described below.

***Organic Carbon-rich Materials***

Acidic groundwater generated from acid mine drainage (AMD) enriched with $SO_4^{2-}$ and heavy metals have being treated with microbial-based PRBs consisting of organic carbons such as wood chips, municipal compost and paper mill pulp (Benner et al., 1999b, Benner et al., 2000). These organic carbons can reduce the $SO_4^{2-}$ and extensively precipitate the metal sulfides (Blowes et al., 2003, Waybrant et al., 1998). The SRB oxidise organic carbon by using $SO_4^{2-}$ and generate $H_2S$. This would result in increasing the alkalinity and pH. Dissolved $H_2S$ has the ability to combine with metal cations to form metal sulfide precipitates, which are stable below the water table inside the PRB (Waybrant et al., 1998). However, it is a drawback as the extensive precipitation in addition to the growth of bacteria can armour the reactive surface of organic carbon-rich materials.

***Zero-valent Iron (ZVI)***

About three-quarters of all full-scale PRBs used worldwide for acidic groundwater remediation use ZVI as the reactive media (Blowes et al., 2000). It has the capacity to remove a range of contaminants such as inorganic contaminants like radionuclides, nickel (Ni), chromium (Cr), arsenic (As), uranium (U), $SO_4^{2-}$ and $NO_3^{2-}$ and chlorinated organic solvents (Gillham and O'Hannesin, 1994, Regmi at al., 2011a, Blowes et al., 2000, Blowes et al., 1997). Jenk et al. (2003) examined the use of ZVI to remediate mine waste containing high concentrations of acid, $SO_4^{2-}$, Fe and Al. ZVI was mixed with chips and lignitic coal and the whole mixture was capable of neutralising acid and removing contaminants in the mine water. As groundwater flows through the PRB, DO and water rust the ZVI, elevating the groundwater pH and precipitating the secondary minerals from the dissolved Fe from

the influent. However, ZVI PRBs too have limitation as same as in organic carbon-rich material by both the corrosion of the reactive material as well as by mineral precipitation hence reducing the anticipated porosity of the PRB (Phillips et al., 2000, Liang et al., 2003, Li and Benson, 2005).

***Acid neutralisation materials***

Due to the disadvantage of extensive precipitation caused by using organic rich material and ZVI, the need for alternative reactive materials to treat acidic groundwater arose. Blowes et al. (1997) reported that mine waste had a self-neutralisation capacity because the amount of carbonate minerals present in mine waste exceeds that of the sulfide minerals. The most significant pH buffering minerals in the mine waste were carbonate minerals; calcite ($CaCO_3$), dolomite ($CaMg(CO_3)_2$) and ankerite ($Ca(Fe,Mg,Mn)(CO_3)_2$) (Jurjovec et al., 2002). The small amount of Ca-bearing minerals present in the soil about 3.1% by weight, could suggestively increase the groundwater pH to near-neutral pH of 6 (Figure 2.14). The effluent pH was controlled by dissolution-precipitation of carbonate, Al and Fe hydroxides and aluminosilicates present in the soil as shown by long plateaus at ~pH 6.0, 4.0 and 1.5, respectively (Figure 2.14).

The research carried out by Jurjovec et al. (2002) supported the application of acid neutralisation materials in PRBs. Following this, different types of acid neutralising materials such as Bauxsol$^{TM}$, lime have been examined, in laboratory scale, for the treatment of acidic groundwater. Lime is not ideal as it is slightly soluble in water and when in contact with acidic groundwater it can be leached out from a PRB. However, hydrated lime ($Ca(OH)_2$), can be a better alternative for this purpose

(McElnea and Ahern, 2002). Bauxsol$^{TM}$ is a by-product from the Bayer process. It contains caustic red mud residues formed during alumina production (Lin et al., 2002, McConchie et al., 2002a). It consists of minerals such as gibbsite ($Al(OH)_3$), hematite ($Fe_2O_3$), boehmite (γ-AlO(OH)), quartz ($SiO_2$), sodalite ($Na_4AI_3Si_3O_{12}Cl$) and cancrinite ($Na_6Ca_2[(CO_3)_2|Al_6Si_6O_{24}]\cdot 2H_2O$), and a little of calcite ($CaCO_3$), aragonite ($CaCO_3$), brucite ($Mg(OH_2)$), gypsum ($CaSO_4\cdot 2H_2O$), diaspore (α-AlO(OH)), ferrihydrite ($(Fe^{3+})_2O_3\bullet 0.5H_2O$), hydrocalumite ($Ca_2Al(OH)_7.3H_2O$), hydrotalcite ($Mg_6Al_2CO_3(OH)_{16}\cdot 4(H_2O)$), portlandite ($Ca(OH)_2$), ilmenite ($FeTiO_3$), lepidocrocite (γ-FeO(OH)) and p-alumohydrocalcite ($CaAl_2(CO_3)2(OH)_4\bullet 3H_2O$) (McConchie et al., 2002a). PRBs containing Bauxsol$^{TM}$ can operate under oxic or anoxic conditions. Most importantly, neither gypsum precipitation nor armouring reduces the performance of the Bauxsol$^{TM}$ PRB. Bauxsol$^{TM}$ also increases the nutrient retention capacity of soil (McConchie et al., 2002b).

Limestone has been used as a suitable reactive material for remediating acidic groundwater in limestone ponds, constructed wetlands, successive alkalinity producing systems (SAPS), open limestone channels (OLC) and oxic limestone drains (OLD). The acidity in groundwater is reduced, by using limestone as an ameliorant, therefore turbulence or mechanical aeration is required to degas carbon dioxide ($CO_2$) from the water (Pearson and McDonnell, 1975a, Webb and Sasowsky, 1994). Pearson and McDonnell (1975b) reported that armouring in an OLD hinder the remediation process. However, when significant concentrations of Fe and Al metals exist in groundwater, the reactivity of the limestone will be severely exhausted.

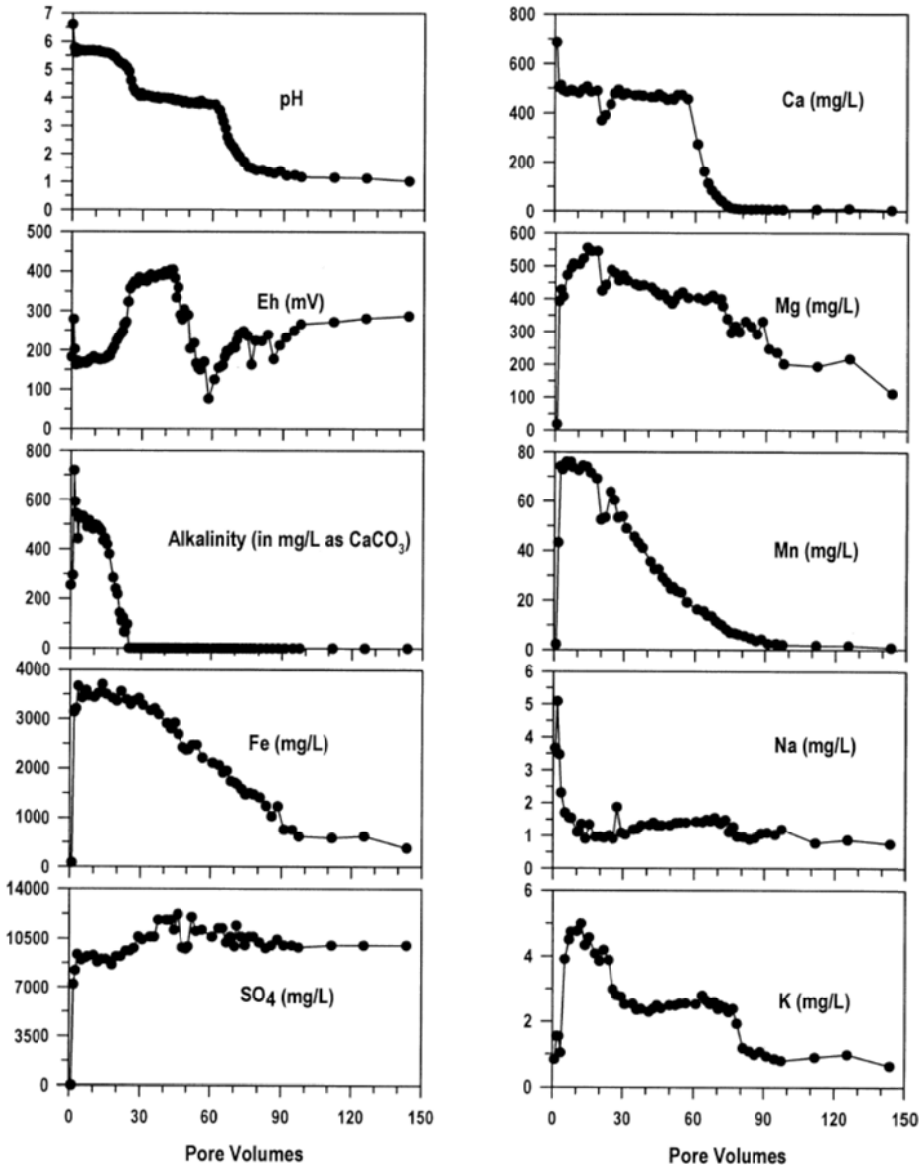


Figure 2.14 Self neutralisation behaviour of soil in acid mine tailing (Jurjovec et al., 2002)

Laboratory column tests are commonly carried out with wide range of alkaline reactive material to determine the potential reactive materials' effectiveness while continuous flow of contaminated groundwater is simulated, prior to the installation of a PRB (Gillham and O'Hannesin, 1994, Mackenzie et al., 1999, Park et al., 2002, Waybrant et al., 2002, Kamolpornwijit et al., 2003, Amos et al., 2004, Logan et al., 2005, Indraratna et al., 2010, Regmi et al., 2011b). Amos and Younger (2003) conducted batch tests for four alkaline reactive mixtures consisting of limestone

chips, cattle slurry, compost, and pea gravel for a possible PRB to treat AMD run-off. The mixtures consisted of different percentages of each material: (i) 50% limestone chips, 25% cattle slurry screenings, 25% compost; (ii) 50% pea gravel, 25% slurry screenings, 25% compost; (iii) 75% limestone chips, 12.5% slurry screenings, 12.5% compost; and (iv) 50% limestone chips, 50% compost. Komnitsas et al. (2004) examined the possibility of a limestone and red mud mixed PRB to remove heavy metals from AMD by precipitation and adsorption using column tests. The main remediation mechanism was the precipitation of contaminants such as Mn, Zn, Fe, Al, Cu, Co, $SO_4^{2-}$ and Ni as hydroxides and also through sorption of Cd. High contaminant concentration may create adverse effects within the reactive media by accelerated reductions in reactivity and longevity of a PRB due to fast consumption of alkalinity, decrease in the reactive surface area due to armouring effect by secondary mineral precipitation, and the desorption of heavy metals.

A number of recycled material from chemical and metallurgical processes have been explored for the suitability of PRBs in order to remediate acidic groundwater via precipitation, degradation or immobilisation of contaminants (Amos and Younger, 2003, Golab et al., 2006, Regmi et al., 2011b). The reason for using recycled material as the reactive media is that the cost of an in-situ PRB system is quite high when pure reactive materials are used. Therefore it is important to find out a cost effective reactive medium in the selection process (Gavaskar, 1999). Recycled concrete, zeolitic breccia, air-cooled blast-furnace slag (ACBFS) and red mud, with a suitable grain size, can be used for the removal of metals and the successive neutralisation of acidic groundwater (Komnitsas et al., 2004, Golab et al., 2006). The screening

process and selection of cost-effective alkaline materials for this current research is elaborated in Chapter 3.

## 2.6 Long-term performance of PRBs

Most of the previous literature is available for ZVI and SRB PRBs and their long-term performance, as they were extensively used in the early development stage of PRB technology. The performance of PRBs is decreasing basically due to the armouring effect from secondary mineral precipitation (Indraratna et al., 2012, Regmi et al., 2009a, Li and Benson, 2005, Wilkin et al., 2003). Armouring is defined as the strong adhesion and complete pacification of the reactive surface by encrustation (coating by the secondary minerals). Armouring will result in decreasing the rate and extent of dissolution of reactive material and capability to remove contaminants (Hedin and Watzlaf, 1994, Cravotta and Watzlaf, 2002). Depending on the groundwater chemistry and composition of the reactive materials inside the barrier, different types of surface coatings have been observed (Puls et al., 1999b, Puls et al., 1999a). Therefore, the methods to quantitatively analyse the secondary minerals and modelling techniques vary accordingly.

Clogging of the porous media can be divided into three main categories; physical clogging by soil particles (Reddi and Bonala, 1997, Indraratna and Vafai, 1997, Reddi et al., 2000), chemical clogging by the accumulation of precipitated compounds (Li and Benson, 2005, Pathirage et al., 2012, Regmi et al., 2011b) and by biological clogging from the growth of bacteria within pores (Rowe, 2005, Fleming and Rowe, 2004, VanGulck and Rowe, 2004). Any of this clogging would result in accumulation in the pore spaces and a decrease in porosity and hydraulic

conductivity. Such a decrease in porosity and hydraulic conductivity inside a PRB reduces flow through the barrier, which has a consequence in changing the flow paths, residence time and probably bypassing the barrier (Mackenzie et al., 1999, Phillips et al., 2000, Roh et al., 2000, Wilkin et al., 2003, Li et al., 2006). Therefore, clogging inside a PRB can decrease the lifetime of a PRB before the reactivity of the material diminishes (Gavaskar, 1999). The following literature shows various studies carried out for performance monitoring and longevity predictions.

***ZVI PRB, Y-12 plant site, Oak Ridge, USA***

Phillips et al. (2000) carried out a comprehensive mineralogical analysis of cores (Figures 2.15 and 2.16) from a field-scale ZVI PRB to study the armouring and clogging effect by secondary minerals precipitation after 15 months following the installation. The intention of this PRB was to remove U from contaminated groundwater at the Y-12 plant site, Oak Ridge, USA. It was reported that corrosion of ZVI and the consequent precipitation of secondary minerals (Figure 2.15) might lead to strong cementation, affecting its long-term performance. This led to a decrease in porosity and permeability of the reactive material. Furthermore, the precipitation of secondary minerals would decrease the reactivity due to surface coating which shortens the longevity of the PRB to less than a decade.

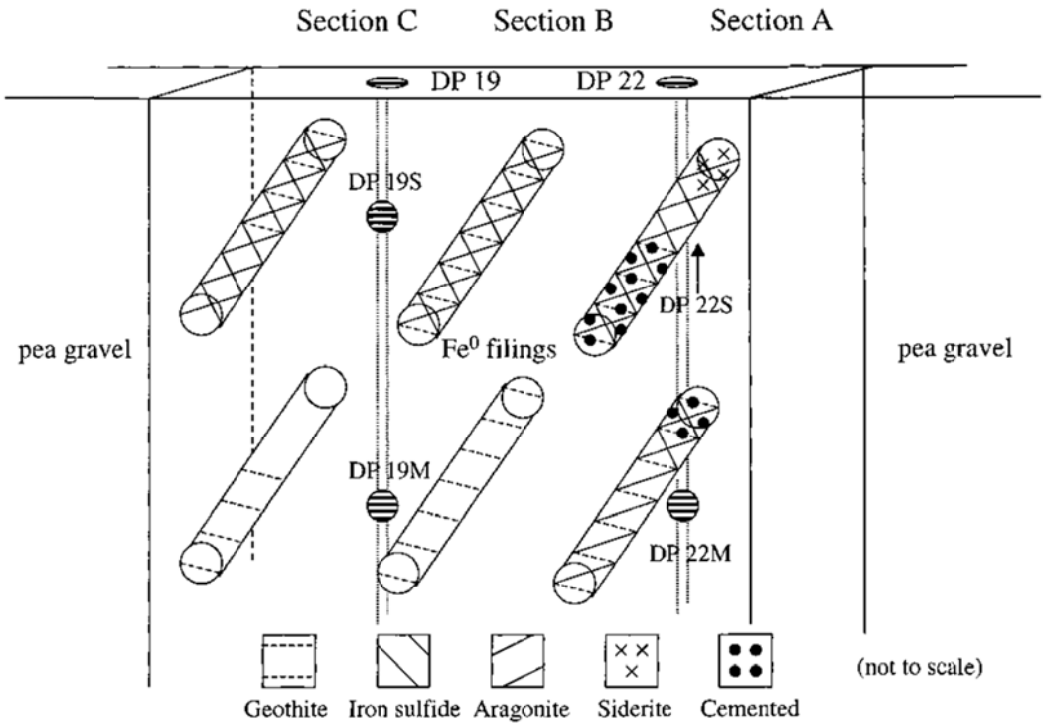


Figure 2.15 The distribution of minerals of the cores from the ZVI portion of the barrier. Note: Akaganeite, which is not shown in the diagram, was present throughout all the cores collected from the PRB (Phillips et al., 2000)

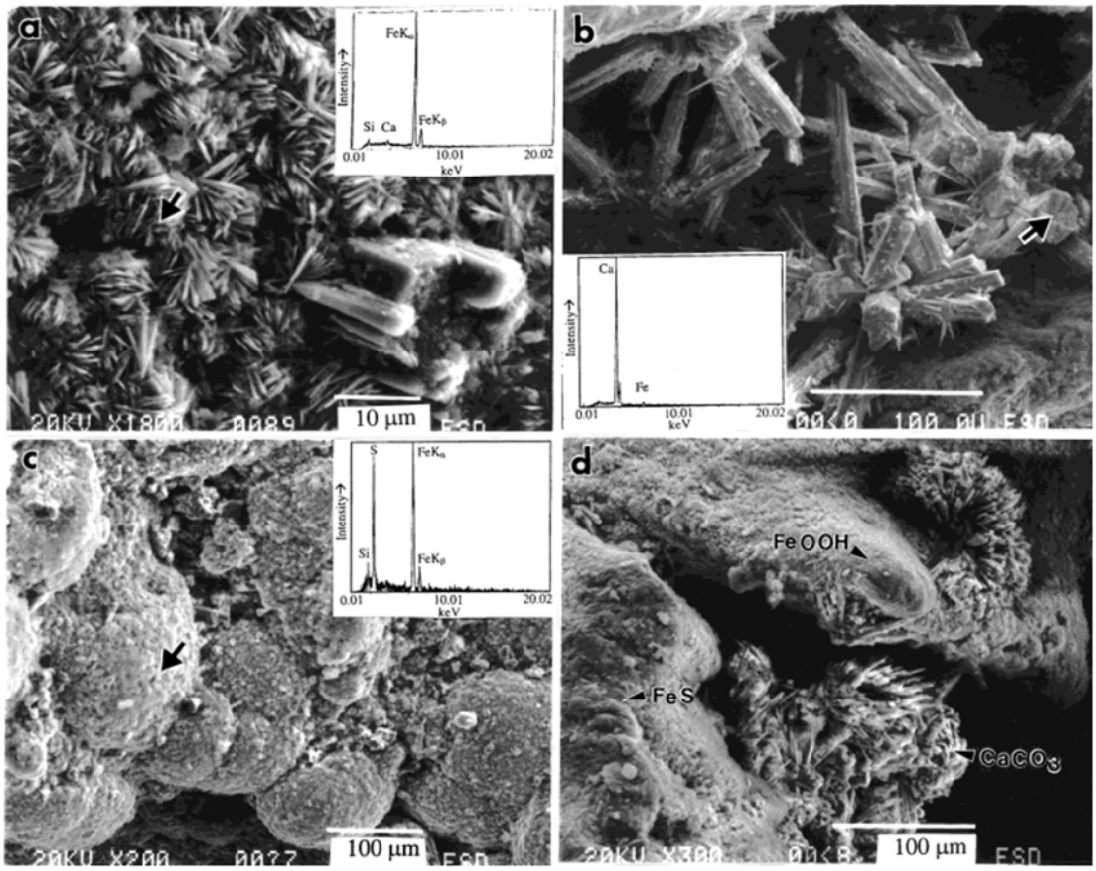


Figure 2.16 SEM-EDX results on the surfaces of ZVI in the barrier: (a) hexagonal shaped crystals of goethite (*â*-FeOOH) around an aragonite crystal (lower right corner), (b) aragonite (CaCO3) crystals (c) amorphous FeS, and (d) precipitates of aragonite, amorphous FeS and FeOOH on the surfaces of an ZVI filing from the shallow down-gradient of the soil and barrier (Phillips et al., 2000)

***ZVI PRBs, Elizabeth City, North California and Denver Federal Centre, Colorado***

Two ZVI PRBs used for the removal of Cr and chlorinated solvents were installed at Elizabeth City, North California and Denver Federal Centre, Colorado. In both these PRBs mineral precipitation was detected after four years of installation (Puls et al., 1999a, Puls et al., 1999b, Furukawa et al., 2002). The PRB at Elizabeth City was a continuous wall barrier and the PRB at Denver Federal Centre was a funnel-and-gate configuration. Puls et al. (2000) reported that the corrosion layer was highest within the first 50 mm and decreased considerably within 200 mm from the up-gradient

aquifer/Fe interface. XRD data from Furukawa et al. (2002) listed all the possible secondary minerals precipitated in the Elizabeth City PRB. The Elizabeth City fine-grained fraction show all the major peaks for magnetite, mackinawite and carbonate green rust as well as three major peaks for calcite, aragonite, siderite, goethite and lepidocrocite (Figure 2.17).

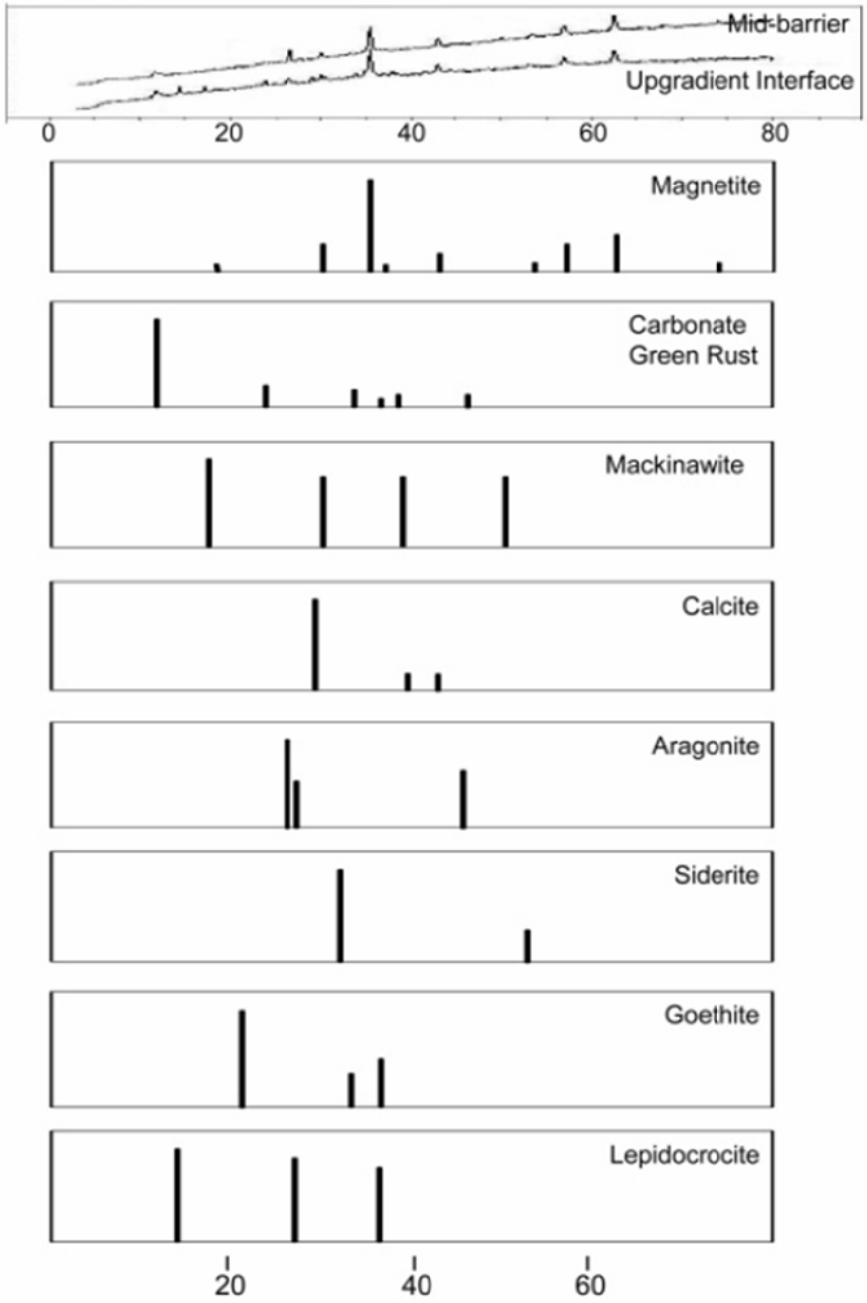


Figure 2.17 XRD results of Elizabeth City samples from near the up-gradient boundary and mid-barrier (Furukawa et al., 2002)

After four years of operation, Wilkin et al. (2003) calculated the rate of inorganic carbon and sulfur accumulation as 0.09 and 0.02 kg/$m^2$/yr, respectively, at Elizabeth City PRB; and 2.16 and 0.80 kg/$m^2$/yr, respectively, at the Denver Federal Centre PRB. The maximum porosity reductions due to secondary mineral precipitation and microbial activity were 0.032 and 0.062 at Elizabeth City and Denver Federal Centre, respectively. USEPA (2004) report mentions the maximum and minimum porosity reductions were 5.9% in the first 25 mm of the ZVI material and 0.1% in 80 mm from the up-gradient interface. This is a small decrease in porosity; therefore it would not have any adverse effect from clogging the pore spaces of the reactive material. Although, there might be a negative affect for the long-term reactivity of ZVI particles by decreasing the reaction kinetics due to the biofilm coverage and surface coating (armouring) by mineral precipitation (Wilkin et al., 2003).

***ZVI and sand PRB, Canadian Force Base, Ontario***

A PRB composed of 22% granular ZVI and 78% sand was installed in 1991, for treating chlorinated organic compounds at the Canadian Force Base, Ontario. These have been running over 5 years, and were the longest available documented PRB performance at the time. The results showed this PRB could remove about 90% of chlorinated organic compounds through reductive dechlorination (O'Hannesin and Gillham, 1998). Moreover, O'Hannesin and Gillham (1998) reported that there was little evidence of precipitation and cementation of $CaCO_3$, hence proving negligible armouring/clogging within the barrier.

***ZVI PRB, New York***

A pilot-scale ZVI PRB was installed at a formal industrial facility in New York to remove volatile organic compounds (VOC). According to Vogan et al. (1999) the performance of the PRB for two year operational period was satisfactory. The porosity was decreased from ~0.5 to 0.45 (10% loss). From this, 6% was due to carbonate precipitation observed towards the up-gradient interface. Nevertheless, the performance of the PRB was not affected since microbial populations did not increase in the ZVI zone compared to the aquifer and the minerals formed in the ZVI zone.

***ZVI PRB, Monticello, Utah, USA***

Morrison (2003) installed a full-scale PRB in Monticello, Utah, USA for the treatment of contaminated groundwater containing 295 mg/L Ca, 1180 mg/L $SO_4^{2-}$, 118 mg/L $NO_3^{2-}$, 173 mg/L chlorite and 430 mg/L alkalinity, and observed 8.8 tonnes of $CaCO_3$ and 24 kg of U- and V-bearing minerals precipitate. Figure 2.18 shows the distribution of solid-phase U and V concentrations. These large amounts of precipitates decreased the porosity of the PRB by 9.3% in the up-gradient gravel/ZVI zone and 3.2% within the ZVI zone 2.7 years after PRB installation.

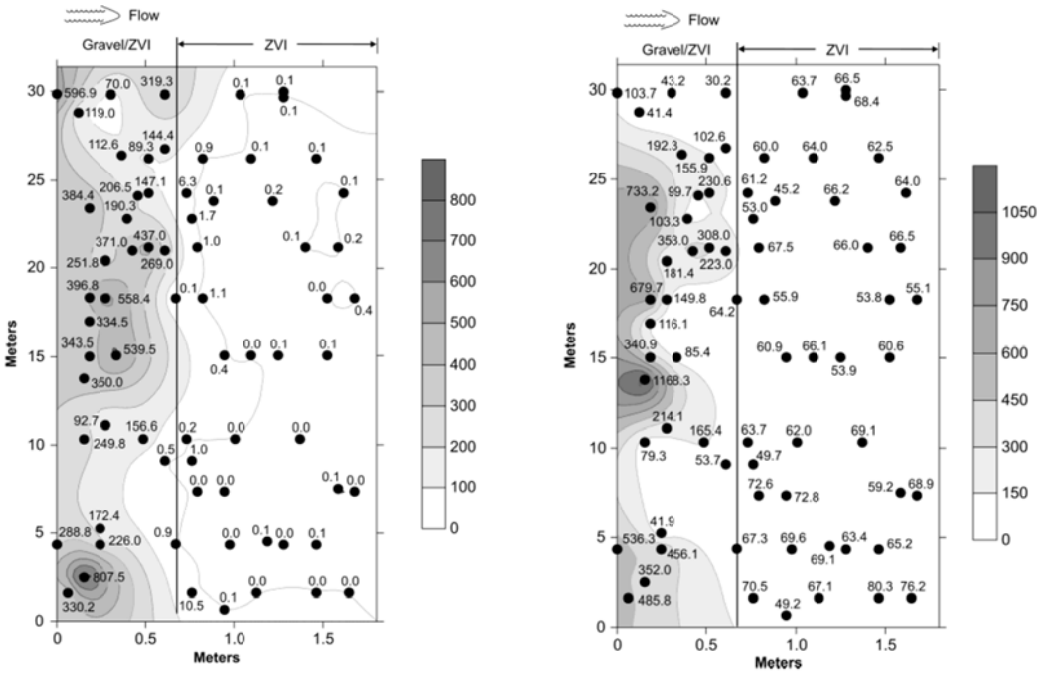


Figure 2.18 Contour maps of means of solid-phase (a) U concentrations (b) V concentrations in samples from four random depths (mg/kg) (Morrison, 2003)

***Mixed-media PRB, British Columbia, Canada***

Ludwig et al. (2002) installed a PRB composed of 15% leaf compost, 84% pea gravel and 1% limestone by volume to treat a site contaminated by heavy metals in British Columbia, Canada. The leaf compost was used as laboratory column experiments proved that it is a fine substrate for SRB. The use of pea gravel was to achieve a minimum desired hydraulic conductivity of $10^{-3}$ m/s to guarantee favoured flow through the barrier. After two months of operation there was hardly any change in the hydraulic conductivity within the barrier (0.0018 m/s). Furthermore, there was no any indication of change in hydraulic conductivity after 9 and 21 months. This pointed out that there were no significant precipitation reactions of secondary minerals taking place in the barrier which could have reduced the hydraulic conductivity.

The majority of literature is mainly on ZVI and SRB PRBs, while research has only just begun on other alkaline reactive materials such as Ca-bearing minerals. Therefore, very small amount of literature is present on the long-term performance of PRBs utilising Ca-bearing minerals (limestone) for the remediation of acidic groundwater. Desmier et al. (2002) and Indraratna et al. (2012) reported that armouring is a problem in PRBs if limestone or recycled concrete are used to remediate acidic groundwater, respectively. Limestone or recycled concrete PRBs become less effective when the reactive surface is armoured by Fe and Al precipitates, which can lead to clogging and failure in the future (Regmi et al., 2009a, Regmi et al., 2011b).

Although field PRBs have shown good performance in remediating contaminated groundwater, there are some concerns and drawbacks of this remediating strategy (Vidic, 2001). The main reason is the lack of information on reaction kinetics and geochemistry, insufficient information on the economic viability of PRBs (Birke et al., 2003) and inability to verify hydraulic performance (Vidic, 2001). Some laboratory and field investigations show that mineral fouling can be favourable in PRBs in terms of better flow and/or blockage of flow (Sarr, 2001, Kamolpornwijit et al., 2004, Kamolpornwijit et al., 2003). However, many researchers reported that the rate of porosity reduction depends on groundwater chemistry and flow rates (Blowes et al., 2000, Phillips et al., 2000). Therefore, a detailed and comprehensive assessment of mineral fouling in PRBs using field data and laboratory experiments is important with special reference to site-specific geochemical and hydro-geological conditions (Phillips et al., 2000), aquifer heterogeneity (Li et al., 2006), and the reactive times of mineral precipitation/dissolution (Vikesland et al., 2003).

In view of the above, it is impractical to carry out field work for performance monitoring of a PRB to find out when the reactivity or the treatment capacity will diminish. Therefore, it is difficult to make any precise conclusions on the longevity of PRB. As a solution for this, numerical modelling has come in to play, which can couple the geochemistry with groundwater flow. Previous researchers (Mayer et al., 2001, Yabusaki, 2001, Li and Benson, 2005, Li et al., 2006, Liang et al., 2003) have used various numerical modelling codes and software to capture the chemical reactions inside PRB including mineral dissolution and precipitation and the effect of mineral precipitation on hydraulic properties of PRBs. A detailed literature review on numerical modelling applications for the long term performance monitoring in PRBs is described in the following section.

## 2.7 Numerical modelling of PRBs

Contaminant transport models contain the governing equations together with the boundary and initial conditions. Once a model has been formed and the proper parameters have been finalised, a solution to the governing equations has to be found with accordance to the suitable boundary and initial conditions. There are mainly five categories of models used to get a solution to the governing equations; analytic, boundary element, finite layer, finite element and finite difference techniques (Rowe et al., 2004).

The finite layer techniques can be applicable when the properties of the system can be idealised as horizontally layered as well as the soil properties stay at the same horizontal location within the layer. The governing equations can be simplified by using a Laplace and/or Fourier transform (the latter is applicable only for 2D or 3D

problems). The transformed equations can then be solved. The difference between the solutions from finite layer technique and analytic approach is that in the finite layer technique, the solution is found numerically rather than analytically. This allows to examine more complicated and accurate situations such as when dealing with larger domains and a lot of unknown parameters. The advection-dispersion equation is usually solved by the boundary element technique. Its main benefit over finite layer technique is its ability to model more complicated geometries. Boundary element approach has not been widely used for contaminant migration studies to date (Rowe et al., 2004).

On the other hand, extensive research has been carried out using the finite difference and finite element methods for the analysis of contaminant migration through soils. These numerical methods are useful for;

i. to define the velocity field by calculating the steady state flow pattern within the hydro-geological system;
ii. to solve the advection dispersion equation (using velocities determined from (i)) by calculating the rate of contaminant migration (Rowe et al., 2004).

The steady state modelling techniques are well established and many commercial software packages are available. The finite element technique is so powerful that it has the capability to model problems with complicated geometries, complex flow patterns, non-linearity and heterogeneity. There are plenty of literatures dealing with different algorithms, which can be used to solve the advection dispersion equation. Some of them are discussed in Section 2.8.

The transportation of reactive contaminants through any reactive material comprises a high complexity, as they are mutual and concurrent. The physical transportation, chemical reactions and the mutual interaction of chemical species can be hard to predict (Mayer, 1999). Contaminant transport modelling within the last three decades mainly focus on developing equilibrium models for assessing geochemistry of reactions (Parkhurst et al., 1980, Ball and Nordstrom, 1991, Wolery et al., 1990, Allison et al., 1991). Geochemical equilibrium reactions include hydrolysis, ion exchange and sorption, complexation, redox and dissolution-precipitation reactions. Some of the geochemical equilibrium models frequently found in literature are MINTEQA2 (Allison et al., 1991), PHREEQE (Parkhurst et al., 1980), PHREEQC V1.6-2 (Parkhurst and Appelo, 1999) and EQ 3/6 (Wolery et al., 1990). Liang et al. (2003) and Wilkin et al. (2003) mentioned that the equilibrium models are less useful for predicting the quantitative accumulation of minerals with respect to space and time but are helpful to understand the qualitative approximation of minerals likely to form within the PRB.

In order to get a better idea about the fate and transport of contaminants, these equilibrium models have also been coupled with advective-dispersive transport models. Multi-component reactive transport models are very versatile compared to equilibrium models as they can be applied to partially saturated and fully saturated porous material. Different types of kinetic relationships have been developed according to the contamination, such as kinetically-controlled reactions (Sverdrup and Warfvinge, 1988), Monod kinetics (Borden and Bedient, 1986, Borden et al., 1986) and the development of reactive networks (Hunter et al., 1998). Coupled hydro-geochemical models are extremely useful for PRB studies to understand the

groundwater quality and mineralogical composition of different systems and trial run the conceptual models (Mayer et al., 2001, Li and Benson, 2005). In contrast to equilibrium models, kinetic reactive models describe the rate at which the geochemical reactions occur and produce the concentrations of dissolved/precipitated ions as a function of time.

## 2.8 Case studies carried out using numerical modelling

Mayer (1999) developed a three dimensional reactive transport code: MIN3P for simulating flow and multi-component reactive transport incorporating a kinetic geochemical algorithm. MIN3P has the ability to solve the governing equation for Darcy-type fluid flow in a variably saturated porous medium. Neuman (1973) and Huyakorn et al. (1984) defined the governing equation for variably saturated flow (Eqn. (2.11)). They adopted some assumptions as the fluid is incompressible, there is no hysteresis and/or a passive air phase and came up with Eqn. (2.11) to calculate the hydraulic head:

$$S_a\, S_s \frac{\partial h}{\partial t} + \emptyset \frac{\partial S_a}{\partial t} - \nabla.\,[k_{ra}\mathbf{K}\,\nabla h] - Q_a = 0 \qquad (2.10)$$

where, $S_a$ is the volumetric water saturation of the aqueous phase ($m^3/m^3$); $S_s$ is the specific storage coefficient (1/m); $h$ is the hydraulic head (m); $t$ is time (s); $\emptyset$ is the porosity of the media ($m^3/m^3$); $k_{ra}$ is the relative permeability of the porous medium with respect to the water phase (dimensionless); $\mathbf{K}$ ($\rho_a g\mathbf{k}/\mu_a$) is the saturated hydraulic conductivity tensor (m/s), $\rho_a$ is the aqueous phase density ($kg/m^3$), g is the gravitational acceleration, ($m/s^2$), $\mu_a$ is the aqueous phase viscosity and k is the intrinsic permeability tensor ($m^2$); and $Q_a$ is a source–sink term (1/s).

The reactive transport equation for advective–dispersive transport is written in global implicit form in MIN3P as (Lichtner, 1996, Mayer and MacQuarrie, 2010, Mayer et al., 2002):

$$\frac{\partial}{\partial t}\left[S_a \emptyset . T_j^a\right] + \frac{\partial T_j^s}{\partial t} + \nabla . \left[q_a T_j^a\right] - \nabla . \left[S_a \emptyset D_a \nabla T_j^a\right] - Q_j^{ext} - Q_j^{int} = 0, j = 1, N_c \quad (2.11)$$

where, $T_j^a$ (kg/m$^3$ $H_2O$) is the total water phase concentration of component $j$; $T_j^s$ is the total adsorbed component concentration, $q_a$ is the Darcy fluid flux (m/s); $D_a$ is the dispersion tensor for the water phase components (including both hydrodynamic dispersion and diffusion); $Q_j^{ext}$ and $Q_j^{int}$ represent external and internal source–sinks, respectively, and $N_c$ defines the number of components.

Mayer et al. (2001) used MIN3P to simulate the flow and mineral precipitation in the ZVI PRB at the US Coast Guard Support Center, Elizabeth City, North Carolina. This PRB was used for treating contaminated groundwater enriched with hexavalent Cr (Cr(VI)) and trichloroethylene. Mayer et al. (2001) carried out simulations for the degradation of chlorinated solvents, transformation of Cr(VI), reduction of DO, $NO_3^-$ and $SO_4^{2-}$ in groundwater. Moreover, he carried out simulations for Fe corrosion by contaminated groundwater, precipitation of secondary minerals, microbial mediated $SO_4^{2-}$ reduction, and hydrogen gas evolution within the PRB. The results showed altogether, twenty-five constituents and seventy-nine reactions possibly occurring and eight possible secondary minerals assumed to form in the ZVI PRB ($CaCO_3$, $CaMg(CO_3)_2$, $MnCO_3$, $FeCO_3$, $Fe(OH)_3$, FeS (am), $Fe(OH)_2$ (am) and $Mn(OH)_2$ (am)). Transition state theory (Eqn. 2.12)) was used to model secondary mineral formation in treatment zone and surface area reduction method to model the depletion of the ZVI reactive material (Eqn. 2.13)).

$$r = -k_{eff}\left(1 - \frac{IAP}{K_{eq}}\right) \tag{2.12}$$

$$S_{Fe^0} = S^0_{Fe^0}\left(\frac{\varphi_{Fe^0}}{\varphi^0_{Fe^0}}\right)^{2/3} \tag{2.13}$$

where, $r$ is the reaction rate ($molm^{-3}_{bulk}s^{-1}$), $k_{eff}$ is the effective rate coefficient ($molm^{-3}_{bulk}s^{-1}$), IAP = ion activity product (depends on the reaction), $K_{eq}$ is the solubility constant (depends on the reaction), $S_{Fe^0}$ is the current reactive surface area of zero-valent iron ($m^2$), $S^0_{Fe^0}$ is the initial reactive surface area of zero-valent iron ($m^2$), $\varphi_{Fe^0}$ is the current volume fraction of zero-valent iron and $\varphi^0_{Fe^0}$ is the initial volume fraction of zero-valent iron.

The simulated results indicated that porosity reduction was high at the entrance of the PRB, which decreased towards the down-gradient zone. The predicted results showed average porosity near the entrance of the PRB was decreased by 28% from 0.50 to 0.36 over 20 years of operation (Figure 2.19).

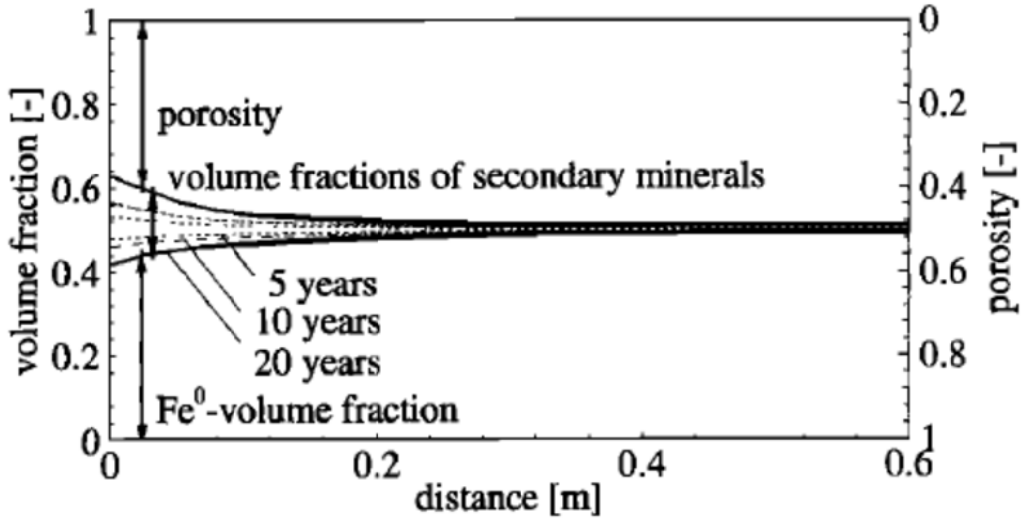


Figure 2.19 Porosity change associated with Fe corrosion and secondary mineral formation (Mayer et al., 2001)

MIN3P has been extensively used for numerous applications including AMD generation and attenuation (Bain et al., 2001, Brookfield et al., 2006), biodegradation of organics (Watson et al., 2003), AMD remediation using PRBs (Mayer et al., 2006), and the evaluation of redox stability in deep crystalline rock formations considered for deep geologic repositories for nuclear waste (Spiessl et al., 2008).

Li et al. (2005) carried out a comprehensive numerical model that could capture the reaction kinetics inside the PRB and most importantly the influence of mineral fouling on the long-term performance of two PRBs using ZVI. MODFLOW (McDonald and Harbaugh., 1988) and the reactive transport model RT3D (Clement, 1997) were used to predict the performance of PRBs at Moffett Federal Airfield and the US Coast Guard Support Centre. They developed a geochemical algorithm coupling all the redox and mineral precipitation-dissolution reactions occurring in the ZVI PRBs with the groundwater flow model (Li, 2004). Moreover, an assessment of

mineral fouling and its effect on the longevity, due to the change in porosity and hydraulic conductivity were predicted by the model.

Li et al. (2005) stated that both average and maximum porosity reductions in the PRB was observed at the entrance face about 0.1 m in to the barrier, and then decreased and remained constant for about 0.8 m from the entrance for different simulation periods of 10, 30, and 50 years. Those results are shown in Figure 2.20. It can be seen that both the average and maximum porosity reductions increased with time, reaching a maximum porosity reduction in 50 years. It is obvious that they could observe from the simulations that the maximum porosity reductions were at the entrance zone of the PRB. That was probably due to the impact of flow heterogeneity on the rate of mineral precipitation.

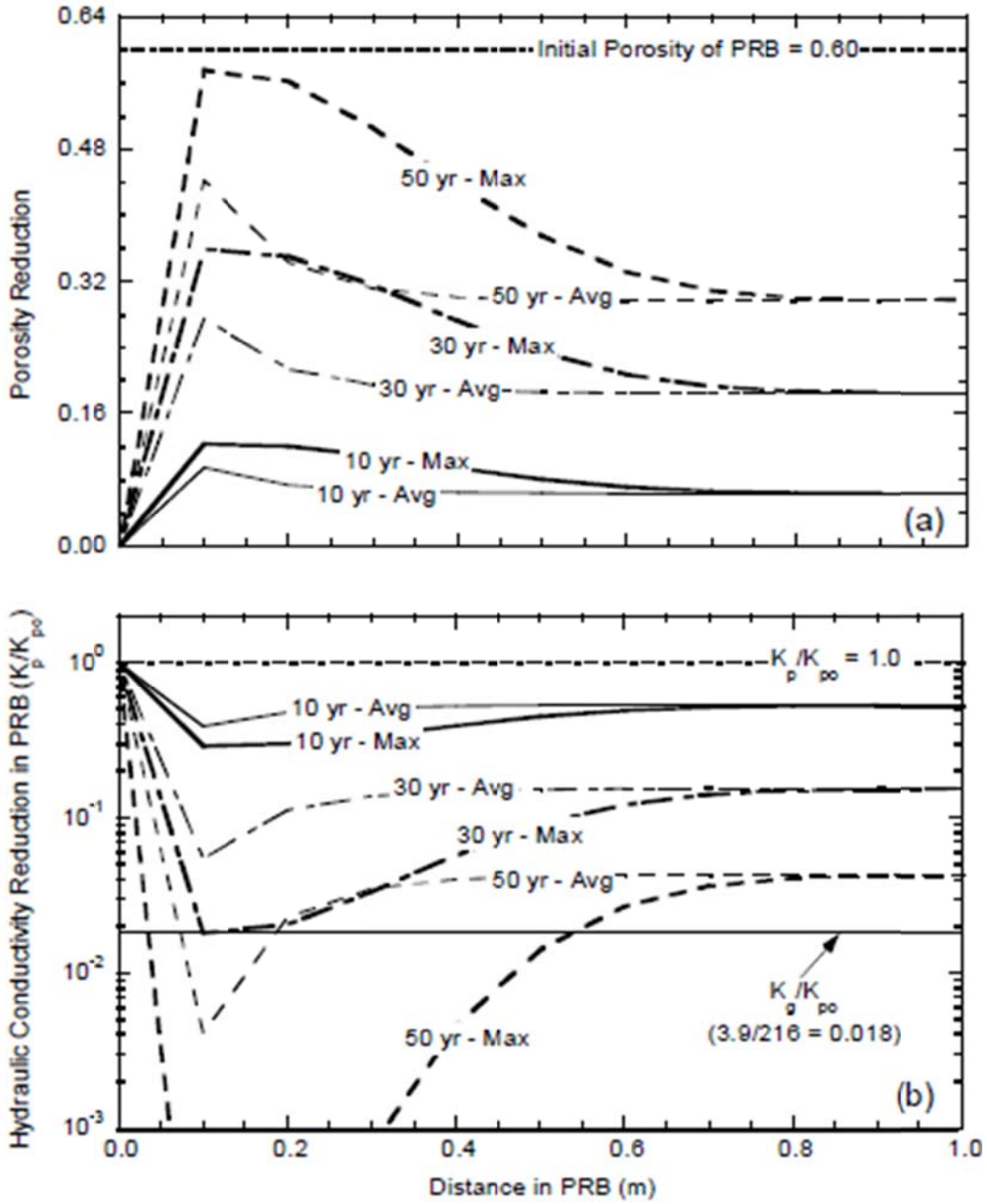


Figure 2.20 Change in (a) porosity and (b) hydraulic conductivity as a function of distance from the entrance face of the PRB for different time intervals (10, 30, and 50 years) (Li and Benson, 2005)

From the results obtained for first 10 year period, decrease in hydraulic conductivity was not much, probably because of the negligible clogging effect during this period. Noteworthy reductions in both porosity and hydraulic conductivity were observed for the simulations carried out for 50 year of operation as a result of predicted complete

blockage of pore spaces of the PRB (Figure 2.20). According to Li (2004), these porosity changes depend on the flow rate and concentration of the influent groundwater. When the influent groundwater flow is high, the reductions in porosity and hydraulic conductivity would be faster because of the increase in contaminants passing through the barrier. As a result of that reactions take place more and precipitate secondary minerals out of solution, which would accumulate on the pore spaces and armour the reactive surface. Figure 2.21 shows the results obtained for different velocities and associated porosity reductions (Li and Benson, 2005).

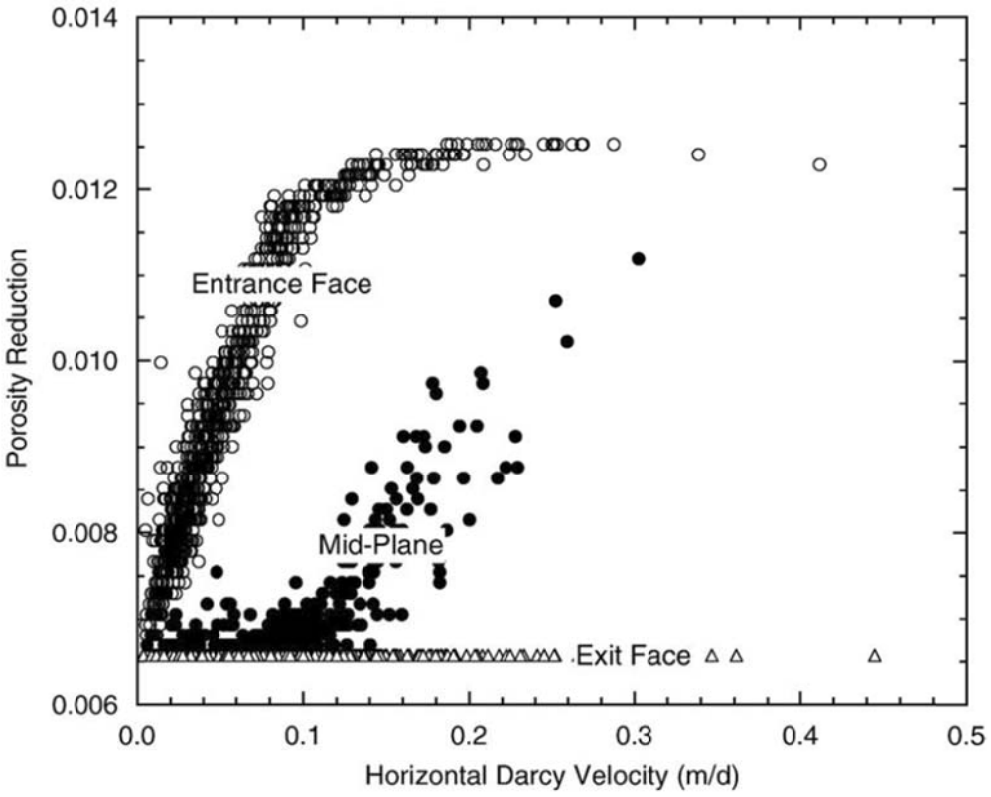


Figure 2.21 Porosity reduction at entrance face, mid-plane and exit face after 1 year of operation as a function of Darcy velocity (Li et al. (2006))

OS3D (three-dimensional reactive transport code) is another multi component transport model developed by Steefel and Yabusaki (1996) which can couple kinetic geochemical algorithms with flow through saturated porous media. This code was used to predict the mineral precipitation and associated porosity reductions in a pilot-scale ZVI PRB at Moffett Federal Airfield, CA, USA. The results obtained from the model and the field data for the concentration profiles for TCE, DCE, pH, alkalinity, total Mg, total $SO_4^{2-}$, and $NO_3^{2-}$ were in good agreement (Figure 2.22). According to Yabusaki (2001), porosity changes were predicted to reduce by 0.030 and 0.014 annually towards the entrance and middle zones of the PRB respectively.

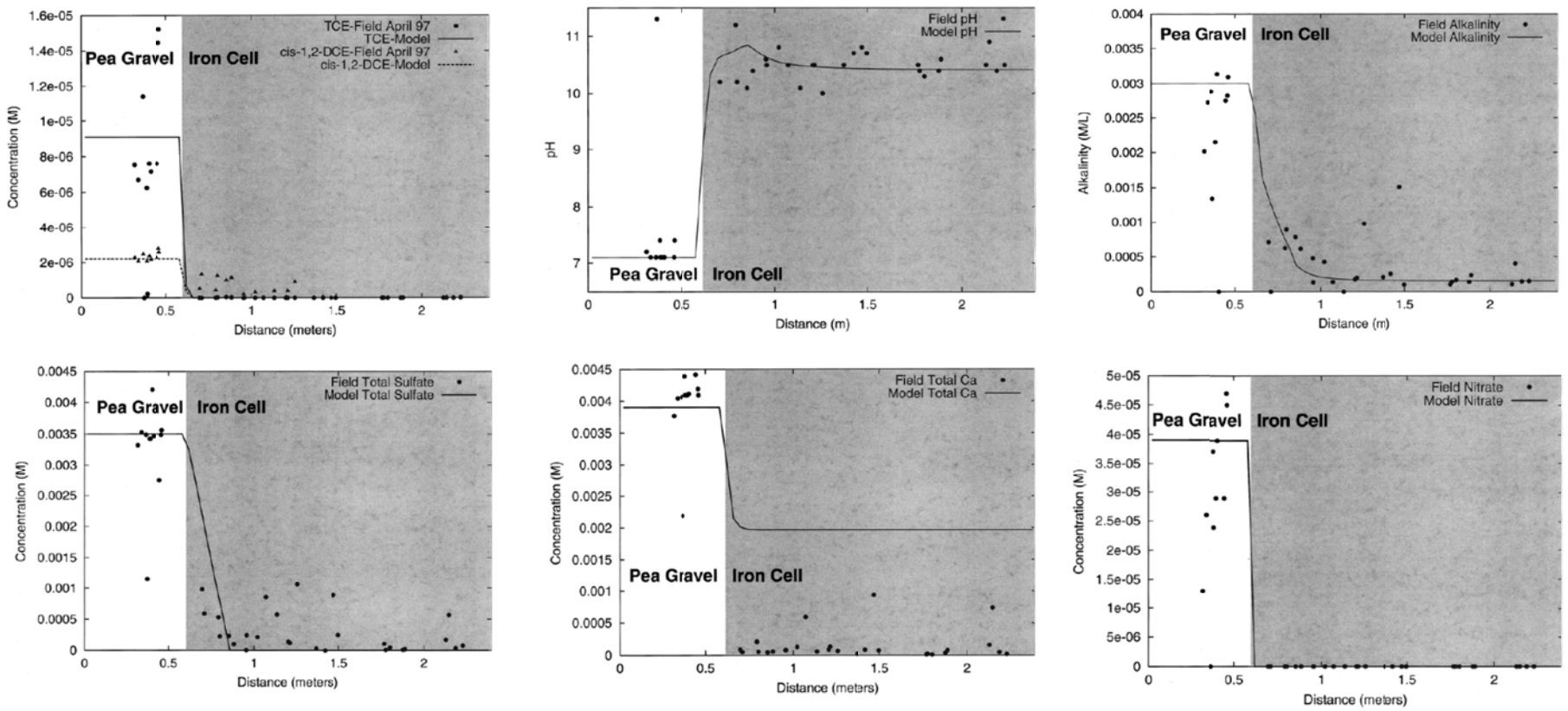


Figure 2.22 Model predicted and field observed results after 1 year of operation in the PRB located at Moffett Federal Airfield, CA, USA (Yabusaki, 2001)

## 2.9 Summary

The acidic groundwater resulting from pyrite oxidation in ASS is a major environmental and socio-economic problem in coastal Australia. Previous research demonstrated that groundwater manipulation using engineering solutions such as weirs and modified two-way floodgates in creeks and flood mitigation drains was not effective in low-lying floodplains due to the risk of flooding and the occurrence of pyrite oxidation even under submerged conditions.

PRBs have been widely used worldwide for the remediation of contaminants such as AMD, chlorinated organic compounds, chromate, heavy metals and radionuclides. However, their application for ASS problems has been very rare to date, except for one trial OLD reported by Waite et al. (2002), which failed in a short period probably due to rapid armouring and clogging by secondary mineral precipitation.

The performance of different types of reactive material used for remediating contaminated groundwater highlighting laboratory and field monitoring data was briefly illustrated in this chapter. The risk of armouring and clogging hindered the performance of reactive materials in many literatures. Moreover, a critical overview of the performance of PRBs and the numerical approaches used to clarify their long-term performance is analysed. The results of the numerical models predicted that the porosity reductions were a maximum at the entrance phase of the PRB due to secondary mineral precipitation.

# Chapter 3 Laboratory column experiments

## 3.1 Introduction

This chapter examines the potential of recycled concrete aggregates to remediate acidic groundwater through detailed laboratory column experiments. Stepwise acid neutralisation behaviour is observed, which is attributed to (a) bicarbonate buffering zone, (b) re-dissolution of Al minerals and (c) re-dissolution of Fe minerals as similar to that reported by Regmi et al. (2011a). The reason to carry out column experiments apart from the results provided by Regmi et al. (2011a) was to determine the mineral precipitation/dissolution behaviour along the column. The results obtained in this study are used to validate the developed model in Chapter 6. The efficiency of acid neutralisation behaviour is hindered by chemical armouring and clogging due to secondary mineral precipitation and accumulation on void spaces. This is evident from the calculated porosity from the volumes of precipitated secondary minerals and calculated hydraulic conductivity reduction from the pressure transducers throughout the column length.

## 3.2 Potential Reactive Material

Apart from cost-effectiveness, the reactive material should be entirely characterised before implementing so that they maintain their reactivity over a long period of time, do not cause any adverse chemical reactions with the constituents of the contaminated plume, and have low cost (Gavaskar et al., 1998). Many alkaline materials can be used to remediate the acidity in groundwater as described in Chapter 2. As the main contaminants in groundwater associated with ASS are acidity, soluble

$Al^{3+}$ and total Fe, the reactive material should be able to increase the pH to a level that causes Al and Fe to precipitate out of solution.

Previous UOW researcher, Golab et al. (2006) tested a total of 25 different possible alkaline materials in a series of batch tests followed by short-term column tests (Golab et al., 2009a, Golab and Indraratna, 2009) using the acidic groundwater collected from the same study site. The materials used by Golab et al. (2009b) were basically waste materials, including fresh and recycled concrete, oyster shells, calcite-bearing zeolitic breccias, ACBFS, lime and fly-ash, with some pure materials such as limestone and lime. Recycled concrete was collected from a demolished construction site.

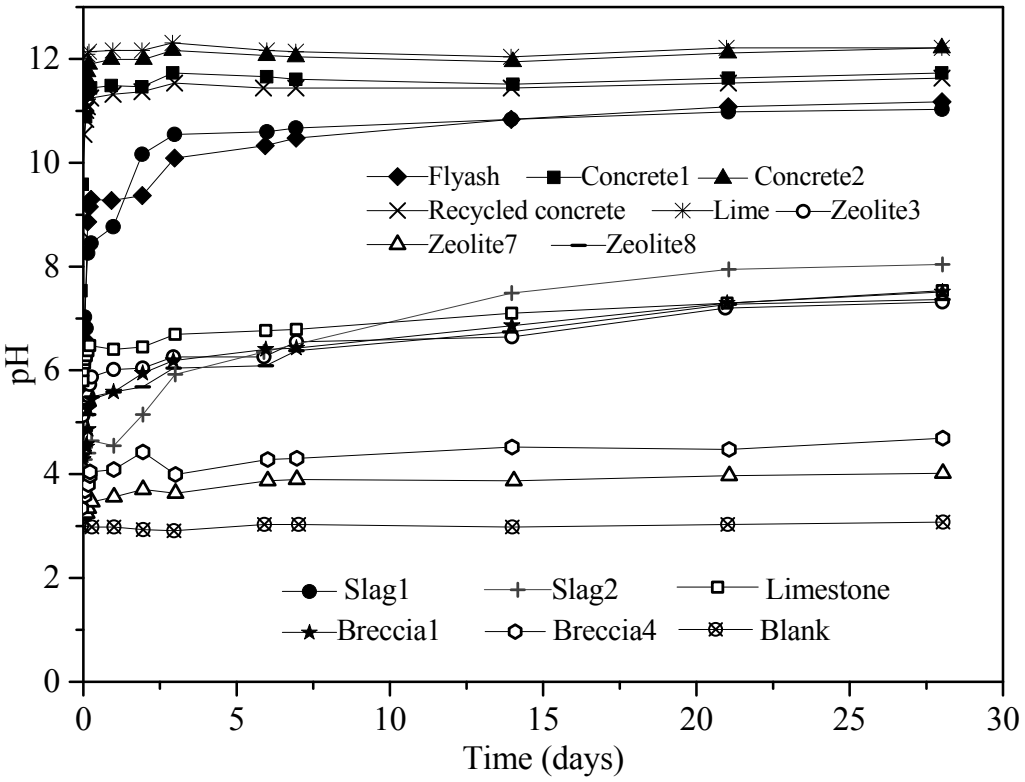


Figure 3.1 pH vs. time for the selected reactive materials (Adapted from Golab et al., 2006)

The results of these batch tests are shown in Figure 3.1. All the above mentioned reactive materials achieved a better pH (a pH above the acidic groundwater) due to the Ca-bearing alkaline material present within them such as $Ca(OH)_2$ and $CaCO_3$ (Golab et al., 2006). The fresh concretes (concrete 1 and concrete 2), recycled concrete, lime and ACBFS, all achieved a consistent pH with the dissolution of portlandite/lime (pH 11 to 12) in the batch tests. The limestone and zeolitic breccia achieved a consistent pH with the dissolution of calcite (~ pH 7.4). Lime and fly ash were considered unsuitable for different reasons including excessively small grain size. ACBFS had insufficient ANC and breccia gave insufficient removal of Al and Fe (Golab et al., 2006). The results of the batch tests showed that recycled concrete performed well by neutralising large volumes of acidity and removing Al and Fe from solution without leaching harmful ions into the groundwater (Golab et al., 2006, Golab et al., 2009a).

In this research, the recycled concrete aggregates used in the laboratory column experiments were collected from a refuse depot, after the demolition of old concrete elements from road expansion works in rural NSW. They were from the same batch of concrete used in the pilot-scale PRB installed in ASS terrain, Nowra. Large pieces of the recycled concrete were crushed to smaller particle sizes to suit the column. Accurate identification of the composition of hydration products in the concrete was complicated due to the physical, chemical and mechanical changes in solidified cementitious systems. Additionally, accurate quantification of the minerals was a challenge due to the heterogeneity of the concrete particles. Regmi et al. (2009b) carried out chemical analysis to determine the elementary composition of recycled concrete by inductively coupled plasma–mass spectrometry (ICP-MS) with 1:1 nitric

acid/hydrochloric acid ($HNO_3$/HCl) digestion following APHA 3120. The recycled concrete contained a negligible amount of heavy metals compared to the major cations (Table 3.1).

Quantitative X-ray diffraction (QXRD) analysis carried out by Regmi et al. (2011a) lists the chemical composition of the major cations present in the recycled concrete as shown in Figure 3.2. The large amount of extractable Ca (58%) and Ca-bearing minerals (anorthite, calcite and feldspars) indicate that recycled concrete can generate significant amounts of alkalinity to neutralise the acidic water.

Table 3.1 Elemental analysis of major elements in recycled concrete by ICP-MS (Regmi et al., 2009b)

| Metals | (mg/kg) | Metals | (mg/kg) |
|---|---|---|---|
| Calcium (Ca) | 63,935 | Copper (Cu) | 85 |
| Iron (Fe) | 23,909 | Vanadium (V) | 75 |
| Aluminium (Al) | 10,984 | Nickel (Ni) | 70 |
| Magnesium (Mg) | 5,872 | Zinc (Zn) | 64 |
| Silica (Si) - acid soluble | 3,416 | Barium (Ba) | 49 |
| Phosphorus (P) | 993 | Chromium (Cr) | 31 |
| Manganese (Mn) | 877 | Lead (Pb) | 9 |
| Potassium (K) | 770 | Cobalt (Co) | 9 |
| Sodium (Na) | 413 | Mercury (Hg) | < 0.01 |

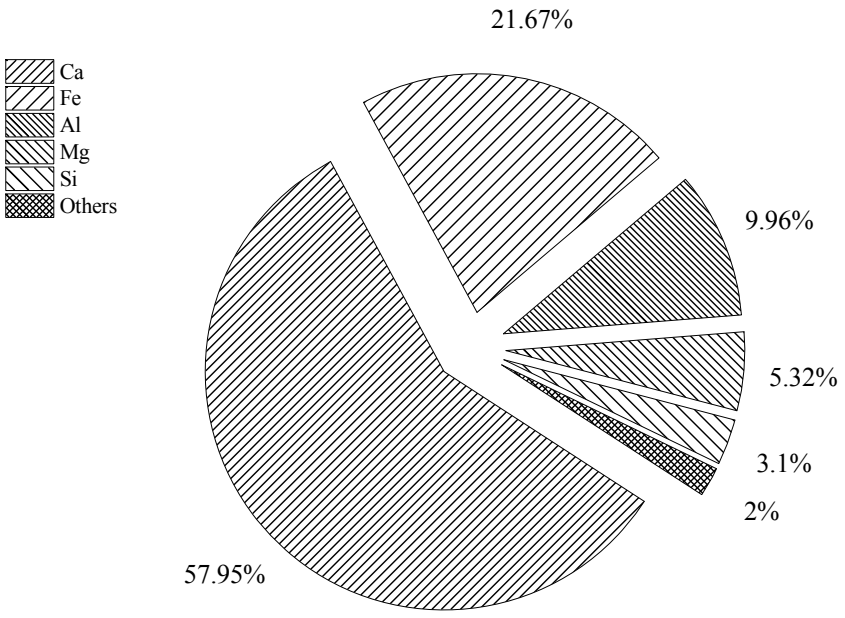


Figure 3.2 Elemental composition of the recycled concrete used in the column experiments (Regmi et al., 2011a)

### 3.3 Laboratory experimental set up

The input solution for the column was a synthetic acidic water (Table 3.2) prepared as to be comparable to the average groundwater from ASS terrain in southeast NSW, Australia as presented by Indraratna et al. (2014) and Pathirage et al. (2012). Previous investigators (Regmi et al., 2011b, Jurjovec et al., 2002, Komnitsas et al., 2004, Waybrant et al., 2002) have also used synthetic water in laboratory experiments to understand the geochemistry behind the remediation of contaminated groundwater as it provides consistent influent characteristics throughout the experimental period.

Table 3.2 Water Chemistry of the influent solution prepared for column experiment simulating the water chemistry of the acidic groundwater in ASS terrain presented in Indraratna et al. (2014) and Pathirage et al. (2012).

| Parameter | Values |
|---|---|
| pH | 2.67 |
| ORP [a] (mV) | 610 |
| Acidity [b] (mmol eq/L) | 6.45 |
| $Na^+$ (mg/L) | 504.2 |
| $K^+$ (mg/L) | 50.1 |
| $Ca^{2+}$ (mg/L) | 152.2 |
| $Mg^{2+}$ (mg/L) | 118.0 |
| $Al^{3+}$ (mg/L) | 54.0 |
| $Fe^{3+}$ (mg/L) | 49 |
| $Cl^-$ (mg/L) | 849.0 |
| $SO_4^{2-}$ (mg/L) | 1450.0 |

Note: [a] ORP – Oxygen Reduction Potential, [b] Acidity was measured equivalent with respect to $CaCO_3$.

Laboratory column experiments were carried out under constant flow condition. A flow rate of 1.2 mL/min was applied using a Masterflex peristaltic pump (Figure 3.3). Two simultaneous column experiments were run as suggested by Johnson et al. (2005). One column was for sampling and the other one to take pressure readings along the column length at every 100 mm interval. The purpose of running two simultaneous columns instead of one column was to eliminate the impact of sampling activities on the pressure in the column (Johnson et al., 2005). It was important to not disturb the pressure of the column, because pressure readings collected by pressure transducers were used to calculate the hydraulic conductivity along the column. The inlet and outlet column pressures at the onset were measured, which were almost the same. The input and environmental conditions were

maintained the same for both columns, so the pressure readings calculated at each port was assumed similar to the respective sampling port at the same height in the other column. The experiments were conducted in transparent acrylic columns (Figure 3.3; Internal diameter × Length = 50 mm × 650 mm). The columns had 100 mm of silica sand at the bottom followed by 500 mm of crushed recycled concrete, and topped with another 50 mm of silica sand. Pure silica sand (chemically inert) placed at the top and bottom of the columns provided effective filtration for the simulated groundwater. The influent and effluent ports were separated from the silica sand using a geotextile separator to prevent physical clogging by sand. The water flow was directed from bottom to top to maintain saturated conditions. The physical parameters of the packing materials and flow rate used in these columns are shown in Table 3.3. The porosity was determined by dividing the total void volume by the volume of the column while the total void volume was determined by weighing the column dry and fully saturated.

Table 3.3 Physical parameters of the column experiments.

| Physical parameters | SC | PTC |
|---|---|---|
| Porosity (%) | 69 | 69 |
| Mass of concrete (g) | 1415 | 1413 |
| Bulk density ($g/cm^3$) | 1.22 | 1.22 |
| Flow rate (mL/min) | 1.2 | 1.2 |
| ANC (g/Kg) | 146 | 146 |

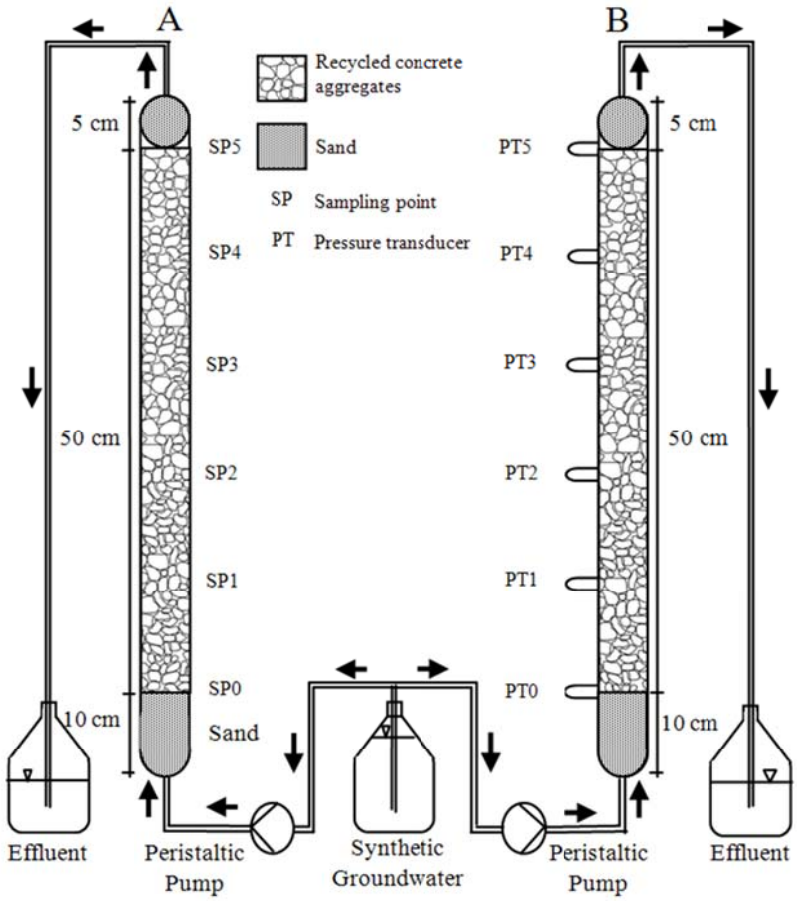


Figure 3.3 Schematic diagram of the laboratory column experiments: A is the sampling column and B is the pressure measuring column

The packed columns were flushed with 4 to 5 pore volumes (PV, defined here as the void volume of the column) of deionised water before commencing the experiments. All column experiments were conducted at room temperature, which varied from 14.9 to 24°C as the experiments were carried out during the winter and spring seasons. The pH, temperature, EC and ORP were measured immediately after the samples were collected, after which they were filtered through 0.45 μm cellulose acetate filter paper. Both acidified and non-acidified samples were collected and stored in a refrigerator at 4°C prior to analysis.

Major cations ($Na^+$, $K^+$, $Ca^{2+}$, $Mg^{2+}$, total Fe, and $Al^{3+}$) in the samples were determined using inductively coupled plasma optical emission spectroscopy (ICP-OES) and atomic absorbance spectroscopy (AAS). Anions ($SO_4^{2-}$ and $Cl^-$) were measured using ion chromatography (IC). All chemical analyses (acidity, alkalinity, major cations, major anions and other trace metals) were performed following standard methods for the examination of water and wastewater (APHA, 1998).


Figure 3.4: Photo of the laboratory column experiments using constant flow method (Left: Sampling column, Right: Pressure transducer column).

## 3.4 Results and Discussion

### 3.4.1 Acid neutralisation behaviour

A step-wise decrease in pH profile was observed in the sampling column (SC) and pressure transducer column (PTC) as the number of PVs passed through the column increased (Figure 3.5). The pH of the effluent collected at the beginning of the experiment for the SC and PTC was high (pH 9.69 and 9.14, respectively). From here onwards the change in pH will be discussed for the results obtained with respect to the SC as both SC and PTC have a similar pH profile. The reaction between the acidic water and the concrete that caused leaching of the Ca also reduced the pH of the effluent from pH 9.7 initially to 8 within 15 PVs (Figure 3.5), after which there was a slow decrease (pH dropped from 7.9 at 25 PV to 7.5 at 125 PV), a faster drop from pH 7.5 at 125PV to about 6.8 at about 185 PV, a rapid drop from pH 6.8 at 185 PV to 4 at about 215 PV, and then another period with a slower rate of decrease from pH 4 at 215 PV to 3.1 to about 295 PV at test termination. According to Indraratna et al. (2010), the initial drop in pH (after 15 PVs was passed through the column) was assumed to be due to the depletion of carbonate alkalinity. However, after reaching a pH value of 6.8 (after 190 PVs), it subsequently diminishes to 4 (Figure 3.5). This is probably due to the $OH^-$ being in equilibrium during the depletion of carbonate minerals (Indraratna et al., 2010). Overall, the three different pH plateaus in Figure 3.5 can be attributed to three distinct pH-buffering reactions as similar to seen in Regmi et al. (2011a):

(1) dissolution of carbonate/bicarbonate alkalinity from the concrete at near-neutral pH,

(2) re-dissolution of Al hydroxide minerals at pH ~4.5, and

(3) re-dissolution of ferric oxyhydroxide minerals at pH < 3.7.

***Bicarbonate Buffering***

Among the above mentioned three buffering reactions, carbonate/bicarbonate buffering was the most significant for remediating acidic groundwater by maintaining an almost neutral pH and complete removal of $Al^{3+}$ and total Fe from the influent solution. The effluent collected after flushing the recycled concrete column with deionised water had a high pH (~9.7) due to the dissolution of a minor amount of portlandite, which when reacted with acid maintained alkaline pH (pH above 8). This initial condition lasted for 20 PVs corresponding to an ORP of 200 mV, which indicates weak oxidising conditions inside the column (Figures 3.5 and 3.7). As shown in Eqns. (3.1) and (3.2), hydroxyl and carbonate alkalinity are released by the dissolution of portlandite and through carbonation, respectively.

$$Ca(OH)_2 + 2H^+ \rightarrow Ca^{2+} + 2H_2O \quad (3.1)$$

$$Ca(OH)_2 + CO_2 \rightarrow CaCO_3 + H_2O \quad (3.2)$$

The total alkalinity released was not strong enough to buffer the pH for a long period. This is evident from the rapidly decreasing pH at around 25 PVs Figure 3.5. Therefore, the buffering effect from Eqns. (3.1) and (3.2) are not significant enough for acid neutralisation. Moreover, total alkalinity decreased due to calcite precipitation during this buffering period (Figure 3.8). Subsequently, the effluent pH remained near-neutral (pH ~6.7-7.9) until ~180 PVs (Figure 3.8) due to the dissolution of calcium aluminate hydrated compounds (C-A-H) with continuous contact of acid with the reactive media (Eqn. (3.3)).

$$CaAl_2SiO_8 + 8H^+ \rightarrow Ca^{2+} + 2Al^{3+} + 2H_4SiO_4 \quad (3.3)$$

After about 25 PVs bicarbonate alkalinity is generated according to Eqns. (3.4)-(3.5) resulting in an increase in alkalinity in the column.

$$CaCO_3 + 2H^+ \Leftrightarrow Ca^{2+} + H_2CO_3 \quad (3.4)$$

$$CO_2 + H_2O \Leftrightarrow H_2CO_3 \quad (3.5)$$

Figure 3.8 shows the alkalinity generation by the dissolution of Ca-bearing minerals from recycled concrete according to Eqns. (3.1)-(3.5). Al et al. (2000) observed that armouring of reactive carbonate mineral grains by the accumulation of secondary mineral precipitates during acid neutralisation diminished the rate of primary mineral dissolution. In the same manner, in this column experiment the pH decreased slowly when the mineral precipitates gradually coated the surface of the recycled concrete at the first plateau reaching a pH of 6.7 at 180 PVs. The pH then dropped immediately reaching the next plateau (pH 4.5-4.0) after the complete depletion of bicarbonate alkalinity at 190 PVs.

The experimental values of pH at sampling points along the SC are shown in Figure 3.6. In the SC, the rapid drop in effluent pH to 6.5 or below is attained within 25 PVs (Figure 3.6), which is fast due to the rapid neutralisation of acidity and the exhaustion of the reactive material at the entrance of the column. In contrast in SP1, 2, 3, 4 and 5, excessive sampling of the column was avoided in order to ensure minimum disturbance to the flow. That is probably the reason why a rapid drop was not observed for the pH values inside the column (Figure 3.6).

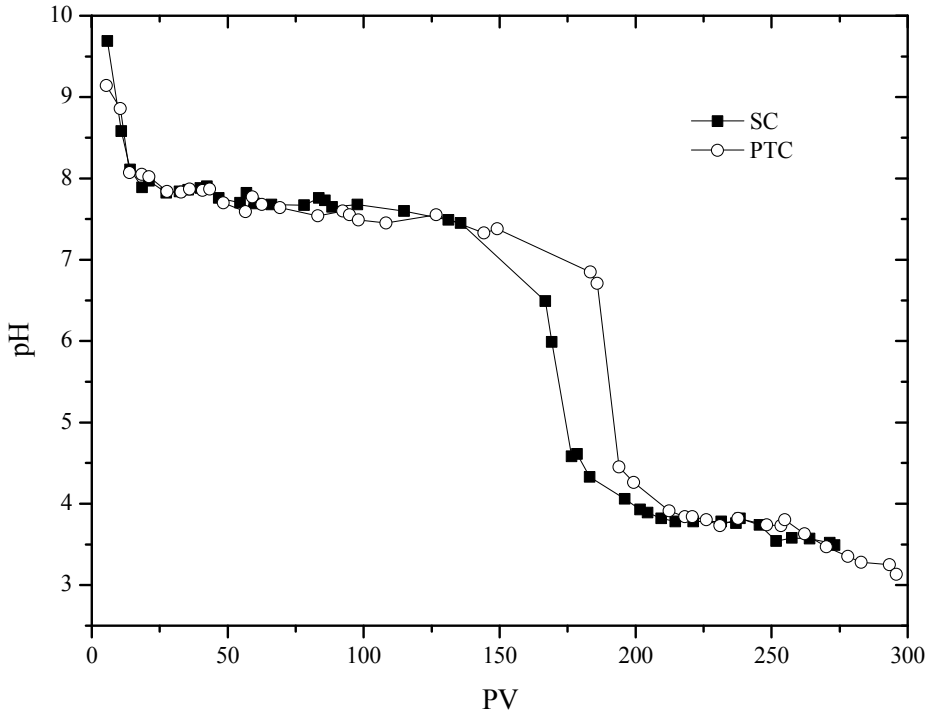


Figure 3.5 Effluent pH of the sampling column (SC) and pressure transducer column (PTC)

As shown in Figure 3.6, the pH at different sampling ports decreased rapidly in the lower parts of the column, corresponding to a sharp increase in ORP (Figure 3.7) due to a fast depletion of alkalinity at the advancing acid front. As a result of the decrease in pH (Figure 3.6) and increase in ORP (Figure 3.7), the depletion of both alkalinity (Figure 3.8) and Ca released from the system was slower in the top part of the column relative to the bottom part of the column.

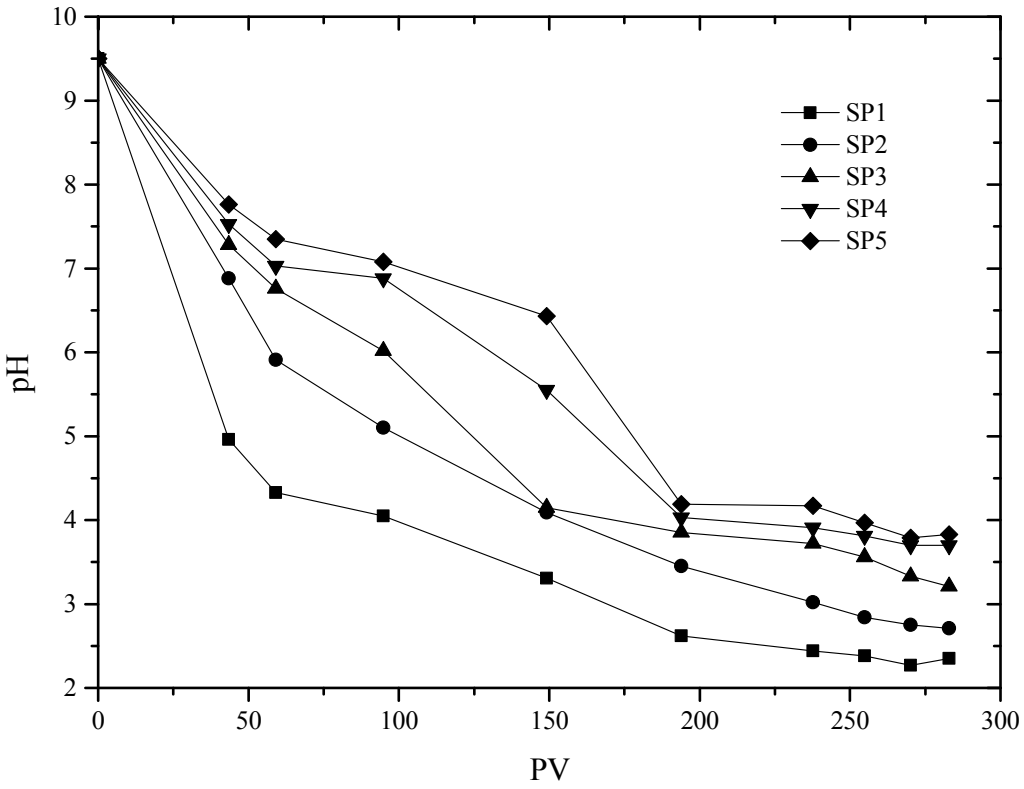


Figure 3.6 pH at sampling points along the column

The increase in pH due to acid neutralisation reactions can lead to a prominent decline in the concentration of dissolved metals, mainly $Al^{3+}$ and total Fe ($Fe^{2+}$ and $Fe^{3+}$) due to precipitation. However, the observed concentrations of $K^+$, $Mg^{2+}$, $Na^+$, $Cl^-$ and $SO_4^{2-}$ at the sampling points were comparatively constant throughout the entire experiment (Figure 3.9), which indicates that they were unaffected and were not influenced by the neutralisation reactions. In the same manner, Watzlaf et al. (2000) also reported that in 10 different anoxic limestone drains (ALDs), $SO_4^{2-}$ levels were unaffected by the ALDs.

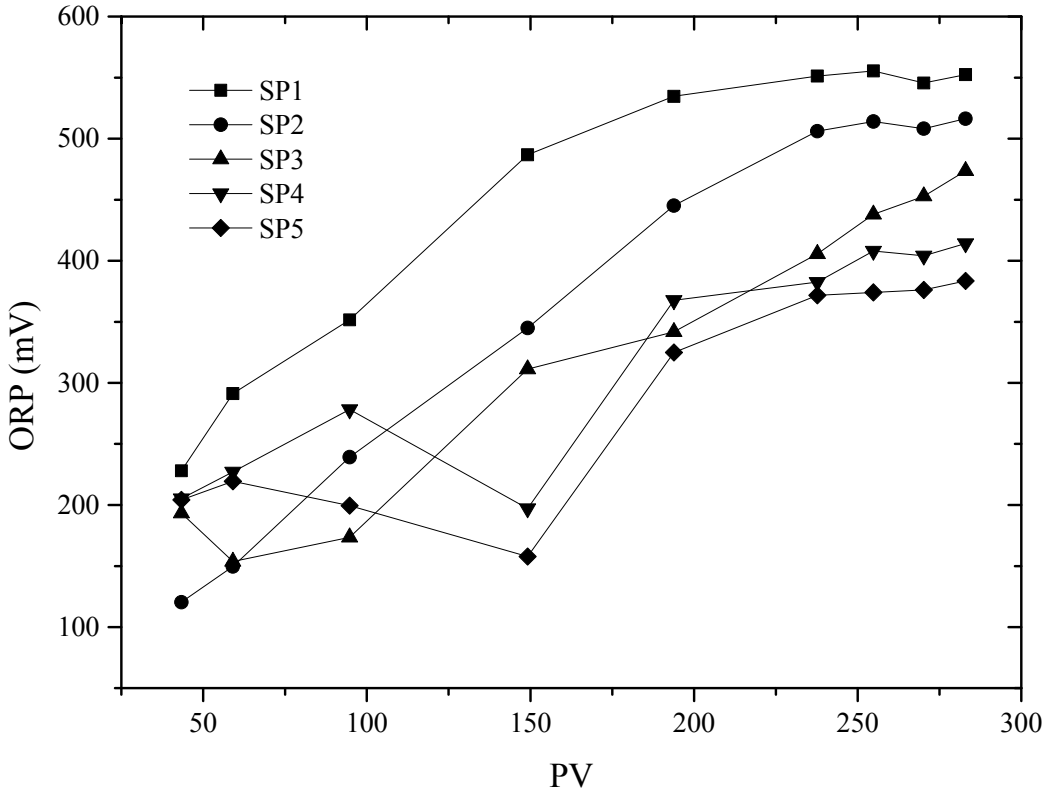


Figure 3.7 ORP at sampling points along the column

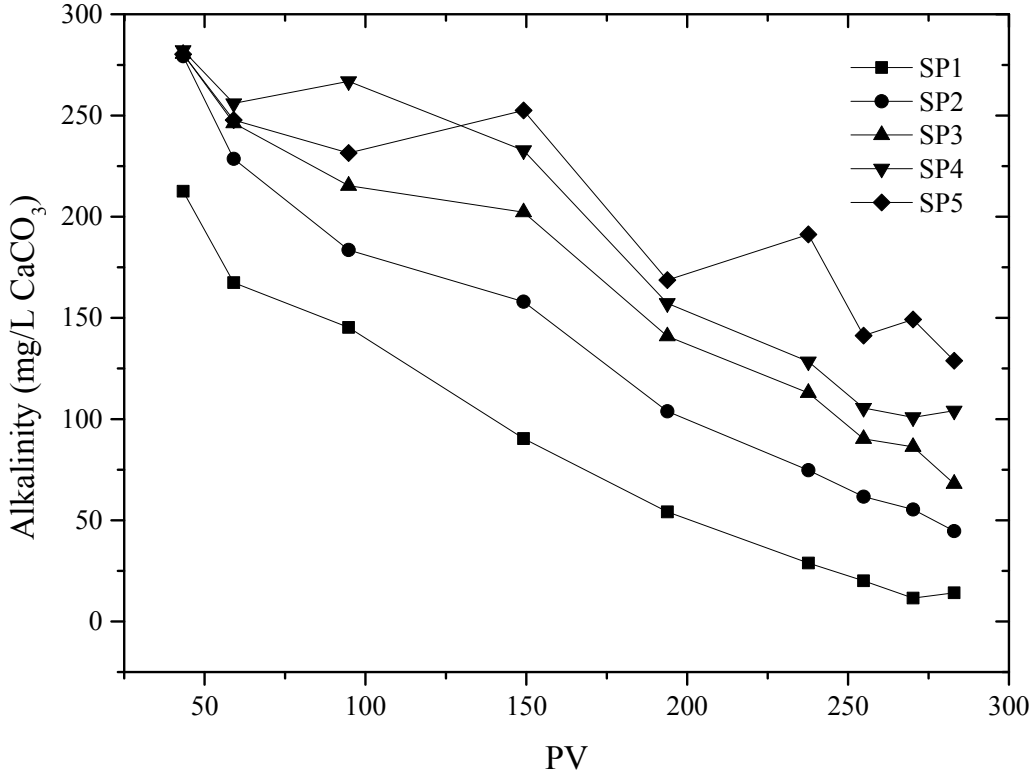


Figure 3.8 Alkalinity at sampling points along the column

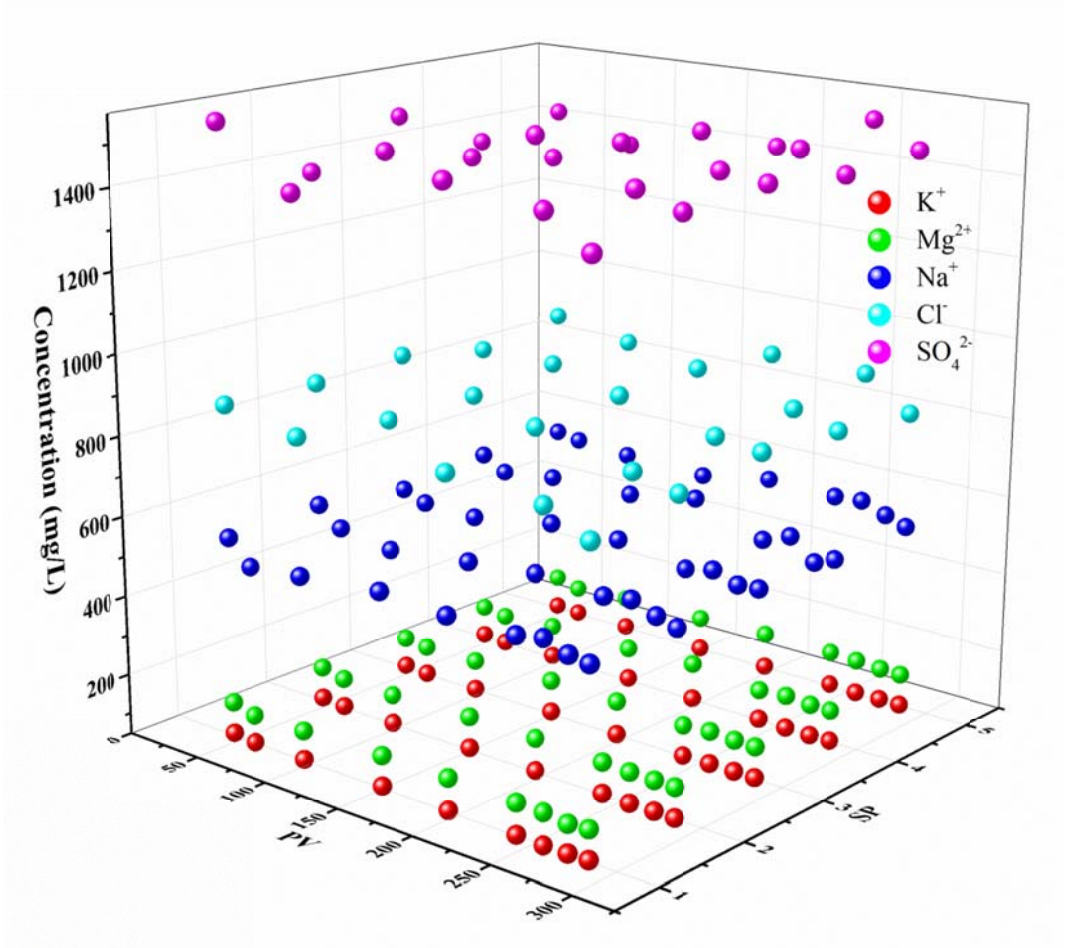


Figure 3.9 Concentration of other ions at different sampling points along the column

***Aluminium oxy/hydroxide buffering***

The Al oxy/hydroxide buffer zone is considered to occur after the rapid drop in pH between 190 and 250 PVs when the effluent pH stabilised at ~4.5-3.7 (Figure 3.5). This plateau was possibly due to the equilibrium reached by the re-dissolution of Al precipitates similar to that reported by Blowes et al. (2003) and Jurjovec et al. (2002) for AMD. Moreover, this interpretation is evident by the sharp increase in $Al^{3+}$ concentration in the effluent at 190 PVs (Figure 3.10).

***Ferric oxy/hydroxide buffering***

After the exhaustion of Al oxy/hydroxide buffering, the next pH plateau was observed at around 270 PVs where the pH dropped to 3.5. This plateau was identified as the Ferric oxy/hydroxide buffering zone, which reached a pH of 3.1 at 295 PVs (Figure 3.5). After that the column experiments were terminated as the effluent pH almost reached the acidic influent pH. This interpretation is also supported by the increase in the total Fe concentration after reaching the third pH plateau at 265 PVs (Figure 3.10).

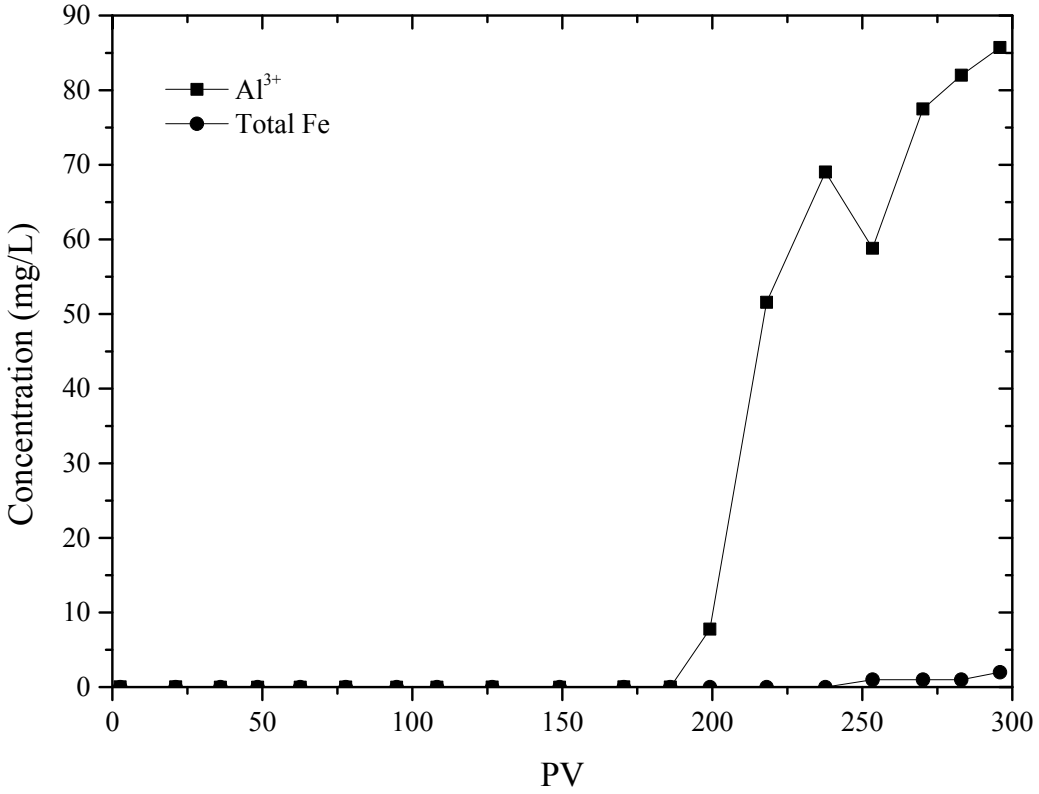


Figure 3.10 Effluent concentrations of $Al^{3+}$ and total Fe

3.4.2 Al and Fe precipitation

Two of the most important attributes in the bicarbonate buffering zone are the almost complete removal of $Al^{3+}$ (> 99%) (Figure 3.11) and total Fe (Figure 3.12). This indicated that the $Al^{3+}$ and total Fe precipitated out of solution. In the early stages of

the experiment, most of the Al in the synthetic groundwater precipitated shortly after entering the column and was no longer in the pore water (Figure 3.11).

$Al^{3+}$ tends to precipitate when the pH is above 4.5. $Al^{3+}$ was observed in the effluent water for the first time when the pH of the effluent dropped to 4, after which the concentration of $Al^{3+}$ continued to increase (Figure 3.11) because of its high solubility at pH<4. Correspondingly, Fe also precipitated when the pH exceeded 3.5. Until 205 PV, the effluent pH did not drop below pH 3.5; accordingly, the Fe content of the effluent (<1 mg/L) was negligible throughout the duration of the column test (Figure 3.12).

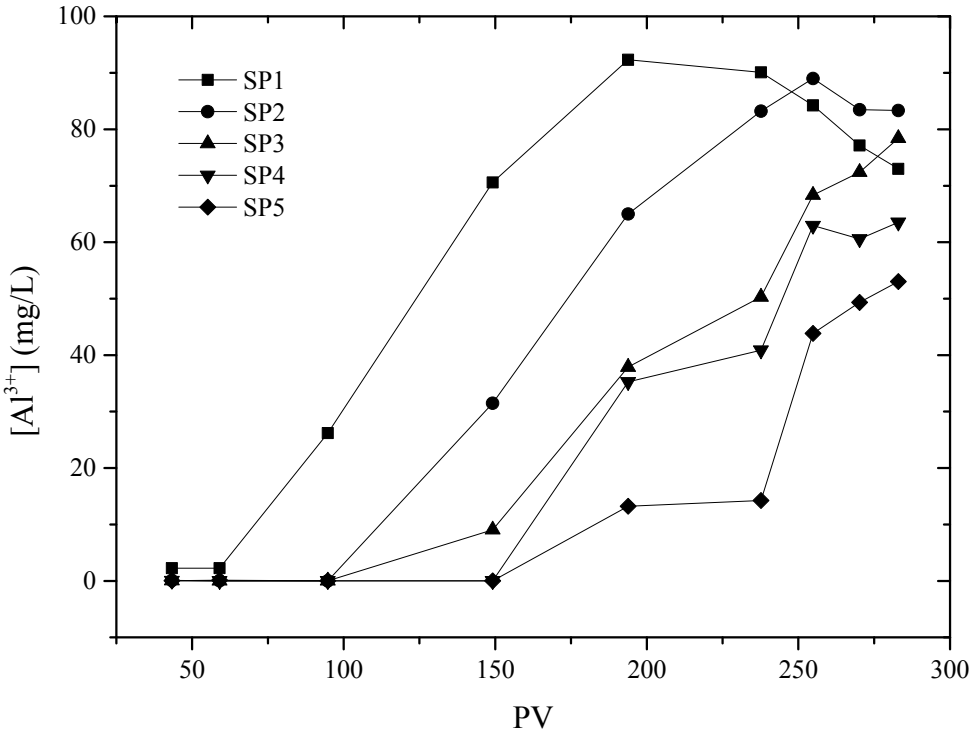


Figure 3.11 $Al^{3+}$ concentration at the sampling points along the column

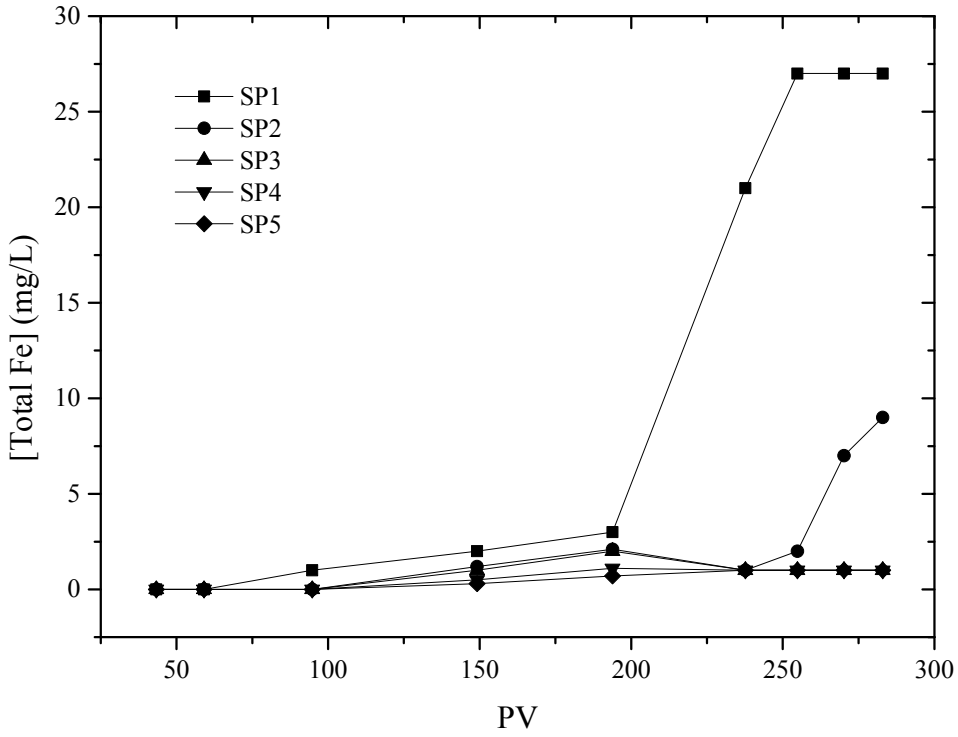


Figure 3.12 Total Fe ($Fe^{2+}$ and $Fe^{3+}$) concentration at the sampling points along the column

In order to study the mineral precipitation out of solution, especially taking $Al^{3+}$ and Total Fe ($Fe^{2+}$ and $Fe^{3+}$) into account, saturation indices (SI) were calculated using PHREEQC software. The calculated SIs of minerals at all the sampling points is illustrated in the geochemical algorithm development section in Chapter 5. These results demonstrate that the effluent was saturated with respect to Al minerals (gibbsite, boehmite and diaspore) and Fe minerals (hematite, maghemite, goethite, lepidocrocite, ferrihydrite) in the first pH plateau, where almost neutral pH was observed (Figure 3.5). Likewise, previous studies of field installations of PRBs and column tests also report precipitates of ferrous/ferric (oxy/hydroxide) oxides and Al hydroxides (Mackenzie et al., 1999, Puls et al., 1999a, Vogan et al., 1999, Phillips et al., 2000, Roh et al., 2000, Golab et al., 2009b).

Furthermore, in this study, the precipitation was evidenced by the hydraulic conductivity reductions calculated using the pressure transducer data (from PTC) at the corresponding sampling points. The hydraulic conductivity reductions were a maximum near where the water entered the column (Zone 1) and decreased with distance along the column (i.e. clogging in Zone 1 > Zone2 > Zone 3 etc.) (Figure 3.13). The precipitation of secondary minerals significantly decreases the efficiency of the reactive material due to the armouring effect (armouring is the coating of reactive surfaces of recycled concrete by precipitating minerals) (Indraratna et al., 2014).

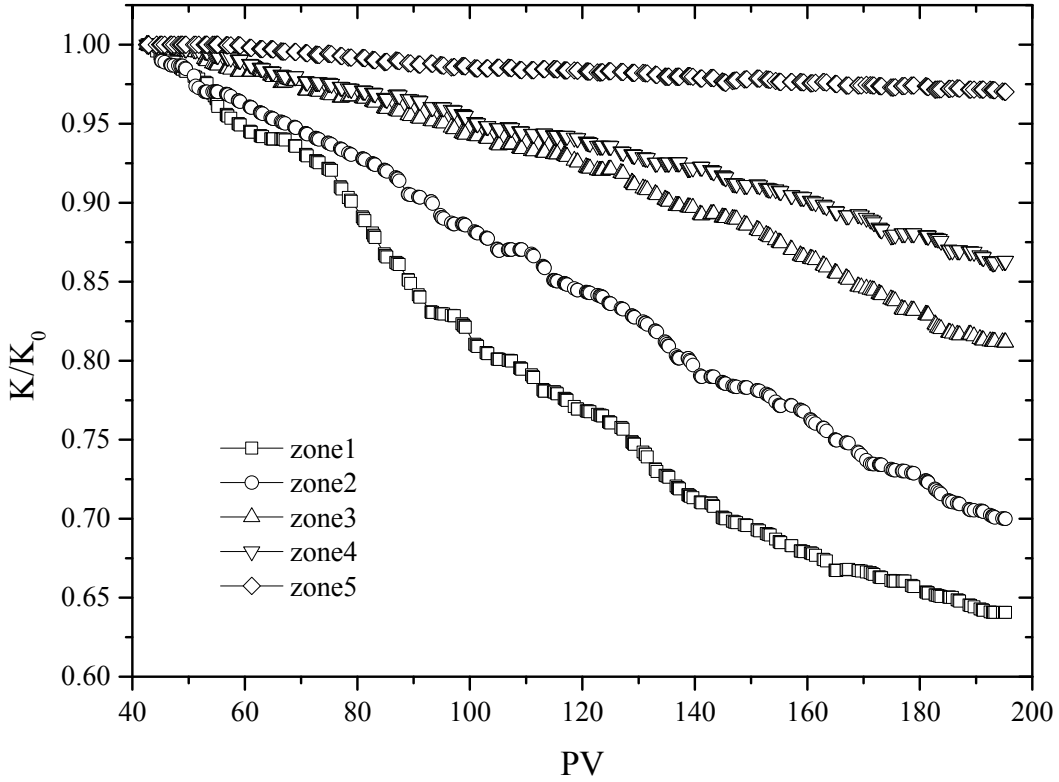


Figure 3.13 Hydraulic conductivity values in Zone (1): SP0-SP1, Zone (2): SP1-SP2, Zone (3): SP2-SP3, Zone (4): SP3-SP4, Zone (5): SP4-SP5

Direct measurement of porosity using the porosity meter (Trani and Indraratna, 2010) did not provide reliable readings due to the internal disturbance of the specimen surrounding the probe tip. In order to get a basic idea of changes in

porosity within the column due to the precipitation of Al- and Fe-bearing minerals, the method adopted by Banasiak et al. (2014) was used. First, the influent and effluent concentration of Al and total Fe throughout the column experiment was plotted. As a constant influent concentration was employed, the volume of $Al^{3+}$ and total Fe retained within the column was obtained through subtraction of the integrated data of the influent curve (computed using OriginPro 9) from the integrated data of the effluent curve. This was then multiplied by the pore volume of the column (0.8035 L) to give the volume of $Al^{3+}$ and total Fe precipitated. Using the molar volume of the predominant Al- and Fe-bearing precipitates formed within the column (gibbsite $Al(OH)_3$ 31.97 $cm^3$/mole; goethite FeOOH 20.33 $cm^3$/mole), the volume occupied by each mineral ($V_P$) was calculated. $V_T$ is the total volume of the column. The porosity within the column ($n_t$) at different PVs with the change of precipitated minerals with time was calculated using Eqn. (3.6):

$$n_t = n_0 - \left( \frac{V_P}{V_T} \right) \tag{3.6}$$

It is evident from Figure 3.14, that at SP1, 2 and 3 the porosity reductions were taking place due to Al and Fe mineral precipitation. When Al oxy/hydroxide buffering started at 190 PVs the change in porosity started to increase further proving the re-dissolution of Al minerals in this zone. Furthermore, the reduction in porosity at SP2 and 3 slowed down after 250 PVs due to the re-dissolution of Fe minerals. Once the ANC was exhausted at the entrance and middle zones (SP1, 2 and 3), the neutralisation process started to take place at the exit zone of the column (SP4 and 5). As a result, a rapid decrease in porosity was observed at SP4 and 5 after 200 PVs till the end of the experiment.

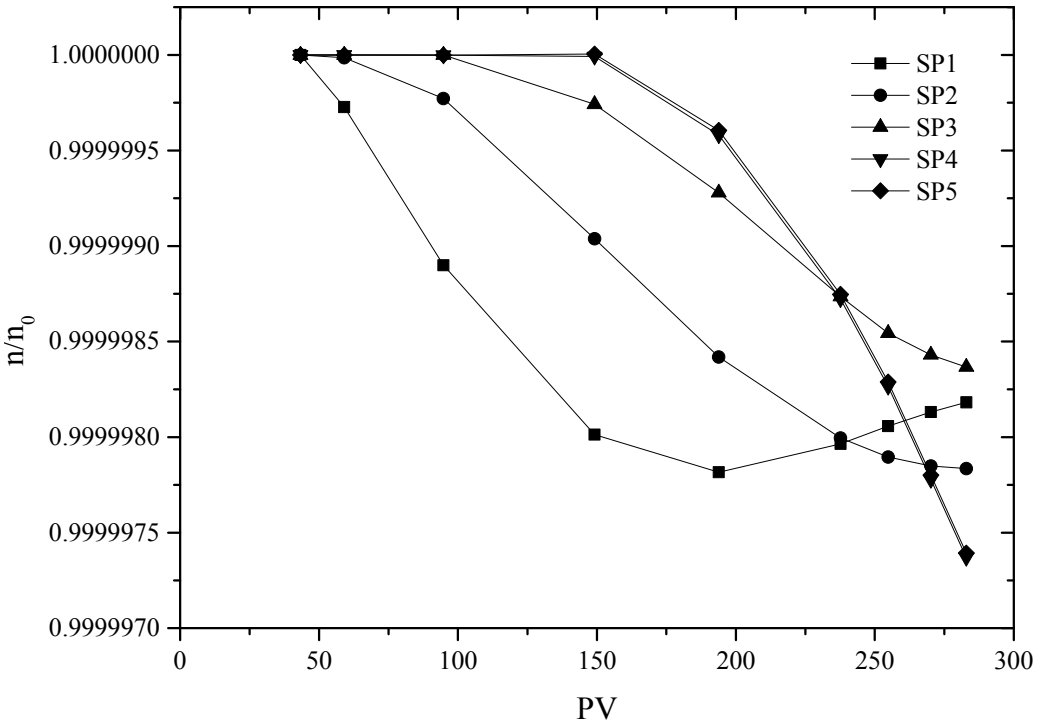


Figure 3.14 Normalised porosity (manually calculated) within the column

The efficiency of recycled concrete would already have decreased to some extent by the exhaustion of the alkalinity of the materials. The theoretical ANC of the recycled concrete in the columns was 146 g/Kg. ANC of the recycled concrete was analysed following the Acid Sulfate Soil Laboratory Method Guidelines 2004 (Ahern et al., 2004). The actual ANC was measured as the number of PVs of acidic water treated before the pH fell below the near-neutral value, and the theoretical ANC was the total PVs of the acid that the material should treat without armouring. Likewise, the column (PTC) treated 185 PVs (Figure 3.5). However, the theoretical ANC of the concrete until the complete depletion of alkalinity without armouring was 400 PVs. Therefore, the loss in ANC of the reactive material by armouring was considerable (>50% in all cases) compared to the loss of ANC efficiency by exhaustion of alkalinity. This situation arises because of the reduction in dissolved ions in the solution available to precipitate as the water moves through the column. The pores in

the column were large enough that complete occlusion of the pores did not occur due to secondary mineral precipitation and hence the flow could be maintained (with an increase in pressure) throughout the experiment (Indraratna et al., 2014). Although accelerated field conditions were provided in the column experiment, the clogging amount was not significant to totally clog the porous media. This provides stable information that the longevity of the field PRB would not significantly be hindered due to clogging. A similar trend in hydraulic properties was observed by Li et al. (2005) for the pilot-scale PRB (containing granular Fe) conducted at Moffett Federal Airfield and U.S. Coast Guard Support Centre.

## 3.5 Summary

This chapter described the laboratory column experiments carried out to confirm the suitability of the reactive material for remediating the acidic leachate full with high concentrations of metal ions such as Al and Fe. Two laboratory column tests were conducted with synthetic groundwater to evaluate the acid neutralisation behaviour and assess the capacity of recycled concrete for treating acidic water under accelerated flow conditions. The results confirmed that the treatment mechanism is mainly controlled by the release of carbonate/bicarbonate alkalinity into the system and the precipitation of Al and Fe in forms of oxide, oxy-hydroxide and hydroxide minerals. The results established that recycled concrete could effectively treat acidic groundwater from ASS terrain, resulting in near-neutral effluent pH over a long period with complete removal of $Al^{3+}$ and total Fe.

The accumulation of secondary minerals on the reactive surface of recycled concrete and in the void spaces decreased the reactivity of the reactive medium. Chemical armouring decreased the ANC of the recycled concrete more than 50% compared to

its theoretical ANC. Furthermore, high concentrations of $Al^{3+}$ and total Fe caused a rapid decrease in ANC efficiency due to neutralisation. As a result of that hydraulic conductivity reduction was evident from the pressure transducer data. The hydraulic conductivity reductions were a maximum near where the water entered the column (Zone 1) and decreased with distance along the column (i.e. clogging in Zone 1 > Zone2 > Zone 3 etc.)

# Chapter 4 Permeable Reactive Barrier

## 4.1 Introduction

This chapter outlines the information pertaining to the study site information of the pilot-scale PRB installed in the Shoalhaven Floodplain, about 100 km south of Sydney, Australia. This PRB was installed in a shallow aquifer containing acidic water from ASS affected agricultural farmland, near Bomaderry, in October 2006. Moreover, this chapter provides detailed information of the monitoring network used to analyse performance of the PRB and a brief outlook for the chemical properties of the soil and groundwater parameters at the field site. Finally, this chapter examines the performance of the PRB by comparing water quality data up-gradient, inside and down-gradient of the PRB over a 6.5 year monitoring period. pH, ORP, concentration of major anions and cations of groundwater at the study site are the main parameters discussed.

## 4.2 Study site

The study site is situated in the Lower Shoalhaven Floodplain, near Bomaderry (34°49'S, 150°39'E), south-eastern NSW, Australia (Figure 4.1). The PRB is installed in farming land (1000 ha) on Manildra Group's Environmental Farm. The study site is adjacent to a flood mitigation drain that flows into Broughton Creek, a left bank tributary of the Shoalhaven River. A DEM of the catchment (Figure 4.1) shows that the topography of the study site is very low-lying (prone to flood in heavy rainfall events) with an elevation ranging from 0 to 1.25 m AHD (Australia height datum).

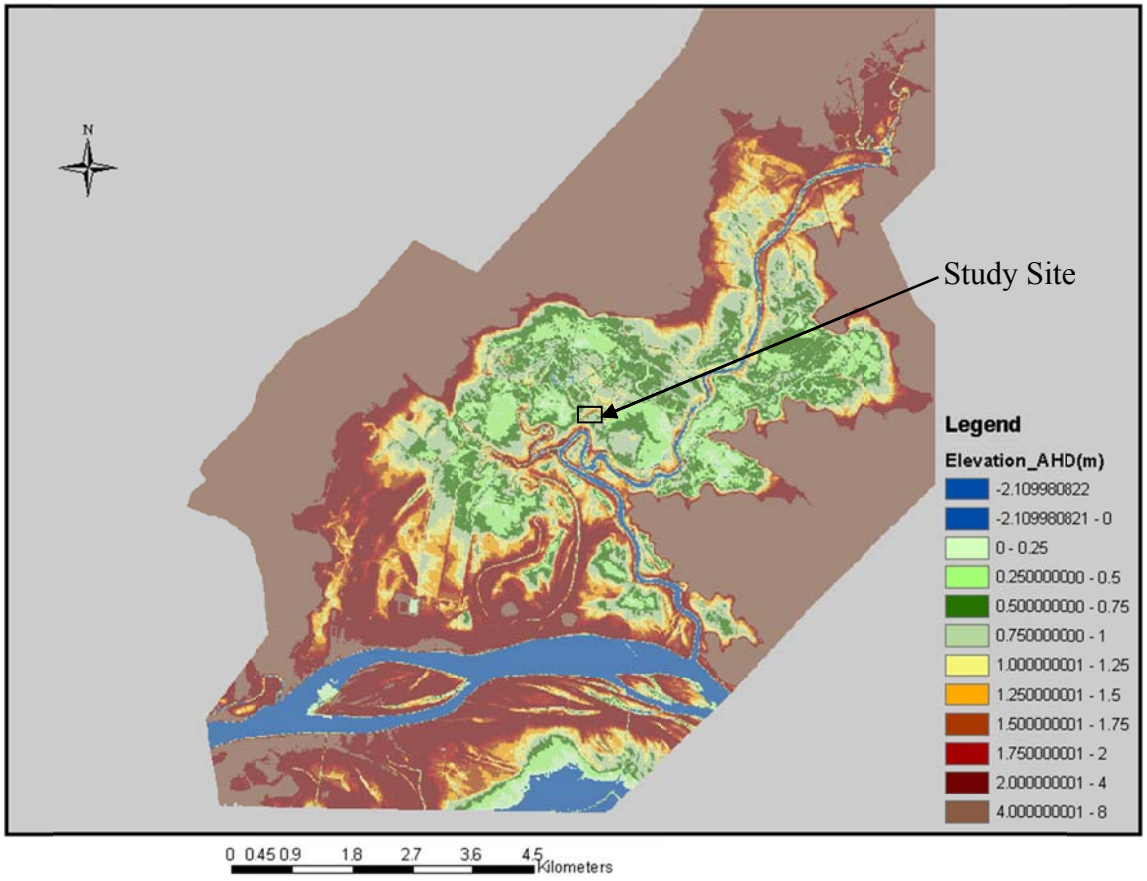


Figure 4.1 DEM of the Broughton Creek catchment

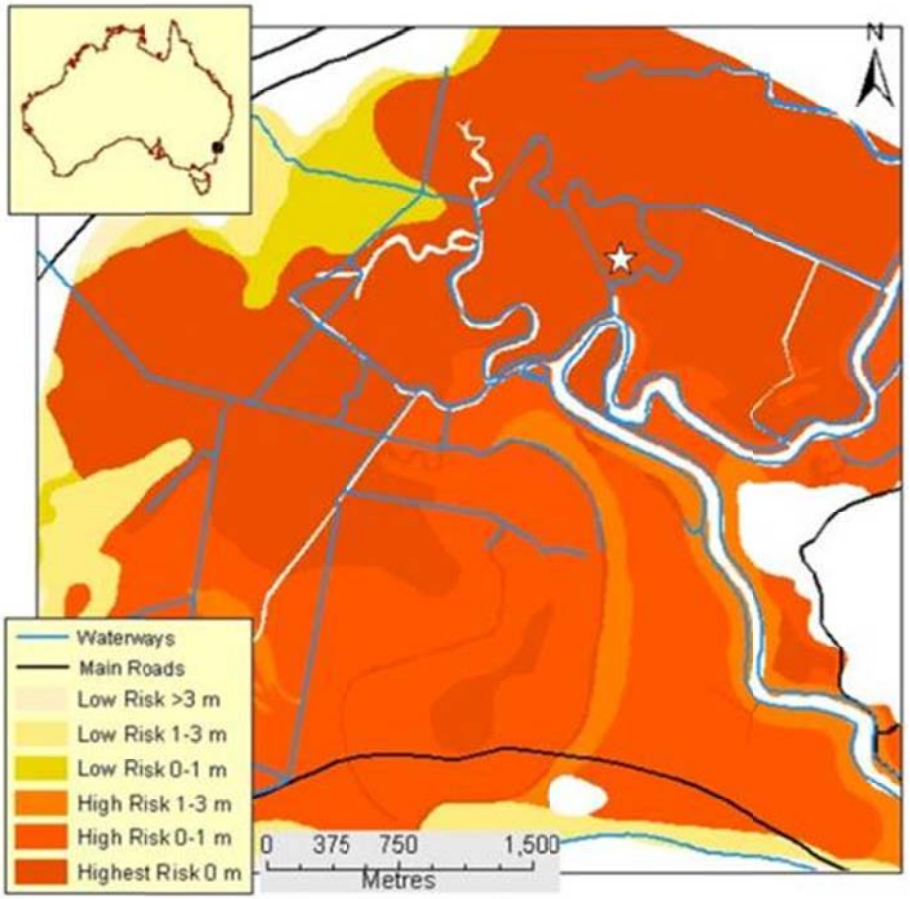


Figure 4.2 Location of the study site, as indicated by star, showing ASS high risk areas (Indraratna et al., 2010)

The distribution and location of ASS in the Broughton Creek catchment with different level of risks susceptible to acidification are shown in Figure 4.2. Both the DEM and ASS risk map of the Broughton Creek catchment (Figures 4.1 and 4.2, respectively) show that the surface topography of the study site is typical of ASS sites found in low-lying landscapes throughout NSW.

A detailed site characterisation was carried out for over a year prior to installing the PRB to understand the site specific parameters, which include monitoring of variations in the phreatic surface and chemical composition of the groundwater, analysis of soil hydraulic conductivity, porosity and grain size, and the geophysical techniques to estimate the hydraulic conductivity of the area (Indraratna et al., 2010).

The PRB site has the following properties (Golab and Indraratna, 2009, Indraratna et al., 2010):

1) The groundwater is acidic with high Al (≤ 60 mg/L) and Total Fe (≤ 300 mg/L) concentrations;
2) A drain is in close proximity for the treated groundwater to flow into;
3) The site is low-lying (0-1 m AHD) and, therefore, not suitable for weirs or two-way floodgates because of the elevated risk of flooding;
4) Easily accessibility, thus allowing monitoring during both wet and dry periods; and
5) No man-made structures present at the site; therefore, providing easy access for excavators and other heavy equipment to be brought to the site.

In early October 2006, a pilot-scale PRB (17.7 m long, 1.2 m wide and 3 m deep) was installed by cut and fill method, parallel and 15 m from the flood mitigation drain to intersect the zone of maximum groundwater flow. The PRB was designed to maximise the groundwater residence time within the barrier and to minimise bypassing of the barrier. The excavation and backfilling techniques were used based on careful geotechnical testing and calculations to ensure that the trench did not collapse during the installation process. A geotextile fabric was stretched over the trench and was backfilled with the crushed recycled concrete ($d_{50}$ = 40 mm) (Figure 4.3). This geotextile fabric was used to protect the reactive media (i.e. recycled concrete) from physical clogging by soil and other fine particles entering the barrier. Figure 4.4 shows current appearance of the study site with monitoring wells and data loggers installed in the PRB.

Figure 4.3 Installation of PRB at the study site


Figure 4.4 (A) and (B) Pilot-scale PRB and monitoring network at study site

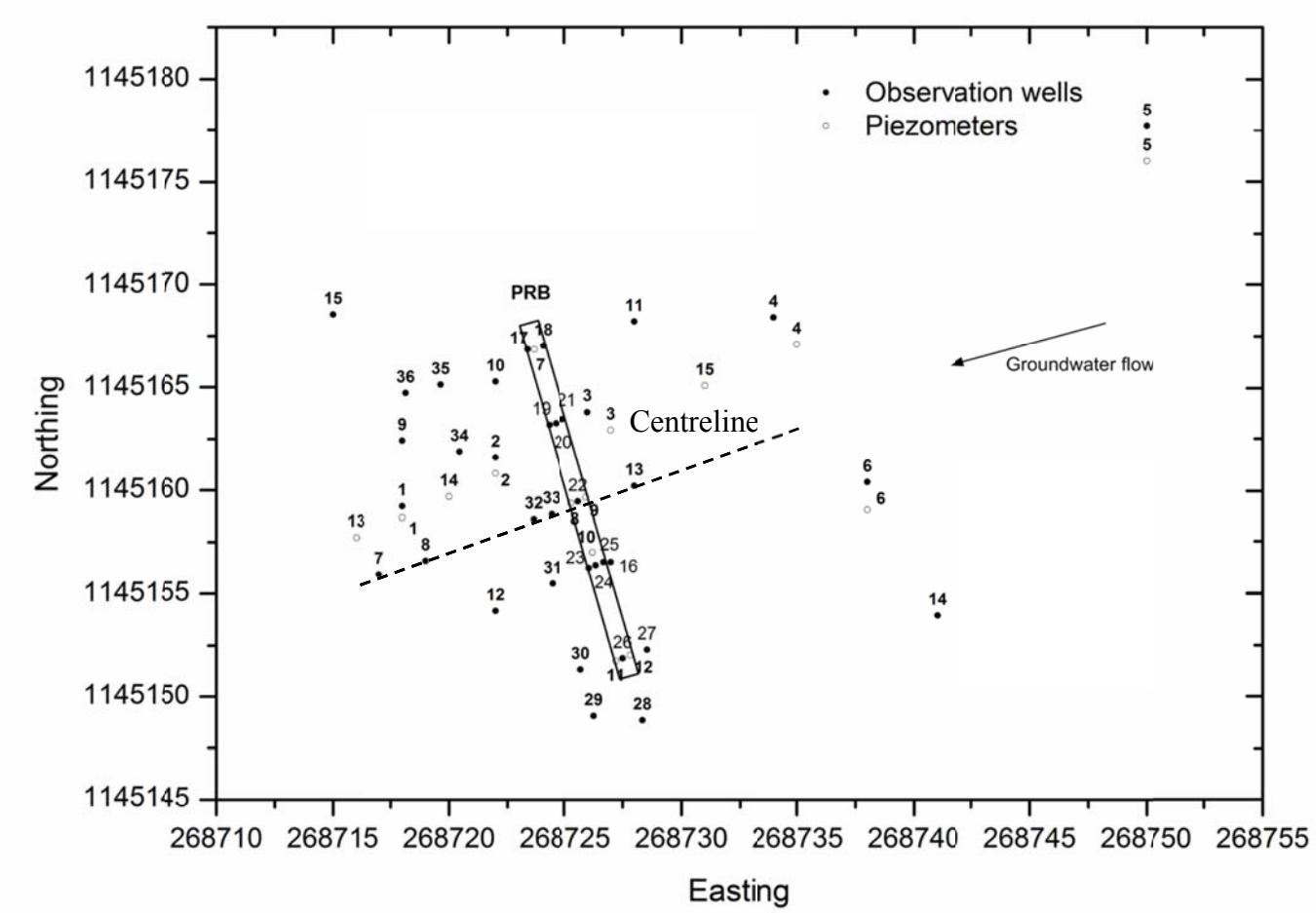


Figure 4.5 Layout of PRB and monitoring network at the study site

Observation wells and data loggers were installed to obtain the water quality parameters in a timely manner to monitor the performance of the PRB. In total, 10 observation wells (50 mm in diameter), two wells for data loggers (100 mm in diameter) and six piezometers were initially installed inside the PRB along five transects roughly parallel to the groundwater flow, as shown in Figure 4.5. Two multi-parameter automated data loggers were mounted to the data logger wells so that the tip of each data logger was around 300 mm from the well base, to ensure that the data logger probes are submersed in groundwater, even in extreme drought conditions. Each data logger was calibrated and set to record pH, DO, water pressure and temperature every hour. In addition, 20 more observation wells (2 m deep, 50 mm external diameter) were installed up and down-gradient of the PRB. Overall, a total of 36 observation wells and 15 piezometers were installed inside, up-gradient and down-gradient of the PRB to monitor phreatic surface variations, hydraulic gradients, permeability and groundwater chemistry (Figure 4.4).

## 4.3 Properties of soil at the study site

Soil samples were collected at two bore holes to characterise the vertical distribution of soil at the study site. A wide range of soil chemical properties can be used to describe pyritic soils, such as, total actual acidity (TAA) and reduced organic sulfur content. A Drillmite petrol fuelled hydraulic powered auger was used to excavate the boreholes. The auger was fitted with a 63 mm cutting head that had a 300 mm length hollow section for soil retrieval. Measurement marks were made along the auger shaft to make excavation depth more easily identifiable during the drilling process. Two boreholes were sampled and soil was extracted at 500 mm intervals starting 0.5 m below the ground level. The first bore, was located up-gradient of the PRB and

samples were taken to 2 m depth below ground level. The second borehole was down-gradient of the PRB and samples were extracted to 2.5 m below the ground level.

***Total Actual Acidity (TAA)***

The TAA is the amount of acidity stored in the soil. This does not include un-oxidised pyrite or any potential acid sources. Analysis was conducted by Southern Cross University Environmental Analysis Laboratory for net acidity in mole $H^+$/ tonne. This Net acidity value is derived from Eqn. (4.1) showing that the key elements are TAA and reduced inorganic sulfur or potential sulfidic acidity. As the values for retained acidity and acid neutralising factor are zero they have no significance.

$$NA = TAA + PSA + RA - ANC/FF \quad (4.1)$$

where, NA is the net acidity, PSA is the potential sulfidic acidity, RA is the retained acidity and ANC/FF is the acid neutralising factor with an FF of 1.5, all in moles $H^+$/tonne.

As can be seen in Figure 4.6 there is a significant change in acidity below a depth of 1.5 m in both the up-gradient and down-gradient samples. The soils below this depth have a relatively lower TAA. This indicated the transition of AASS into PASS. The higher TAA values at 1.5 m demonstrate the generation of acid from past pyrite oxidation. Under acidic conditions, the hydrolysis of ferrous sulfate ions (Fanning, 1993), and the dissolution of Fe oxyhydroxide mottles and/or jarosite, can generate acid in or above the AASS layer and add to the TAA concentration according to Eqns. (4.2)-(4.4).

$$FeSO_4 + \tfrac{1}{2} H_2SO_4 + \tfrac{1}{4} O_2 \rightarrow \tfrac{1}{2} Fe_2(SO_4)_3 + \tfrac{1}{2} H_2O \quad (4.2)$$

$$FeSO_4 + \tfrac{1}{4} O_2 + \tfrac{5}{2} H_2O \rightarrow Fe(OH)_3 + H_2SO_4 \quad (4.3)$$

$$KFe_3(SO_4)_2(OH)_6 + 3H_2O \rightarrow 3Fe(OH)_3 + SO_4^{2-} + K^+ + 3H^+ \quad (4.4)$$

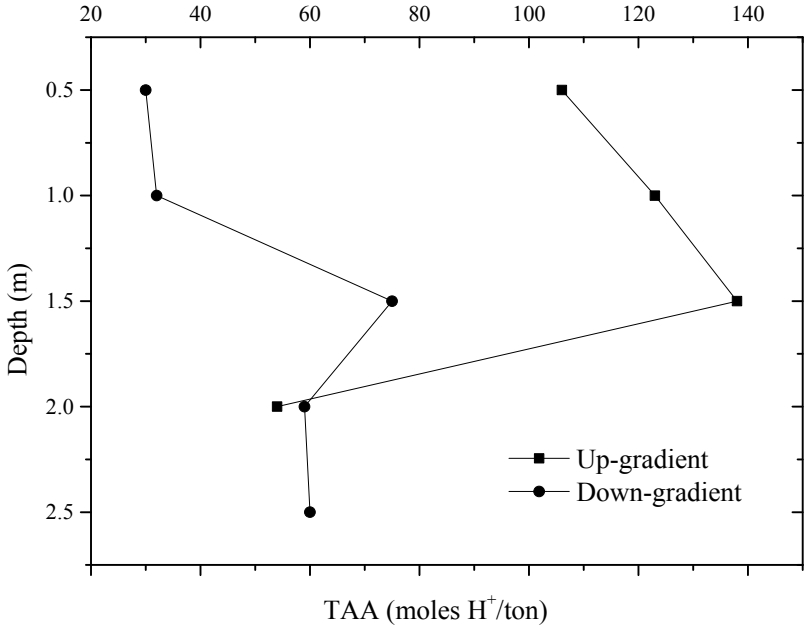


Figure 4.6 Titratable actual acidity at different depths in the up-gradient and down-gradient of PRB

As can be seen in Figure 4.7 (A) at 0.6 m below the soil surface, evidence of ASS oxidation can be observed by the presence of yellow jarosite mottles. Jarosite is a by-product of the pyrite oxidation process. This formation is dependent on the pH being less than 4. The resulting jarosite further hydrolyses the soil producing more acidity.


Figure 4.7 (A) and (B): Excavated pits showing the different layer with iron oxide mottling in the study site ((B) photo courtesy of A. Golab)

Soil stratigraphy at the study site can be described based on the visual information from an excavated pit (Figure 4.7 (B)). In general, Holocene estuarine deposits overlie undisturbed Pleistocene clays, but within the Holocene sediments, an AASS soil layer commonly overlies a PASS layer. Above the estuarine clays, alluvial deposits, formed within the past 4000 years (Umitsu et al., 2001), range in thickness depending on their geomorphic location (i.e. levee banks, levee toe or back swamp). In the Shoalhaven Floodplain, the layer of loamy alluvium overlying the AASS layer increases in thickness moving from the backswamp (0.5 m) to the levee toe (0.75 m) (Blunden, 2000). The soil layers at the study site can be generally divided into four (Figure 4.7 (B)): (i) topsoil enriched with organic soil and peat loam; (ii) AASS layer with Fe oxy/hydroxide mottles and/or jarosite; (iii) transition layer which includes seasonally oxidized sulfidic minerals; and (iv) PASS layer. Orange Fe oxy/hydroxide mottles and rusty yellowish mottles of jarosite are commonly found in the AASS layer. The elevation of this pyritic layer gradually increases towards the back swamps in the Shoalhaven Floodplain (Blunden, 2000, Glamore, 2003).

***Reduced Inorganic Sulfur Content***

Reduced inorganic sulfur (Stratful et al., 2001) is present in the form of pyrite for this particular site. Although the pyrite is not yet oxidised, should oxidisation occur then sulfur becomes soluble producing further acidity which mobilises heavy metals. In contrast to TAA, reduced inorganic sulfur content measures the potential for further acid generation under oxidising conditions. Therefore, reduced inorganic sulfur content is used to identify ASS and to estimate the amount of acid that could be formed by complete oxidation of the soil (Blunden and Naylor, 1995). As per the guidelines provided by Ahern et al. (2004), the classification of potential acid sulfate

material for fine grain soils is $S_{CR} \geq 0.1\%$ or 62 mole $H^+$/tonne. From the graph in Figure 4.8, it can be seen that there is a significant change in reduced inorganic sulfur from 1.5 m depth. The values are over 0.1% indicating that un-oxidised pyrite is present at this depth. There is significant variation in values between the up-gradient and down-gradient sample. This graphical representation can be compared to that of the TAA results. As would be expected, typically where TAA is high, reduced inorganic sulfur is low and similar can be said for the reverse. Comparison of TAA and $S_{CR}$ shows the extensive storage of potential acidity throughout the PASS layer at this study site.

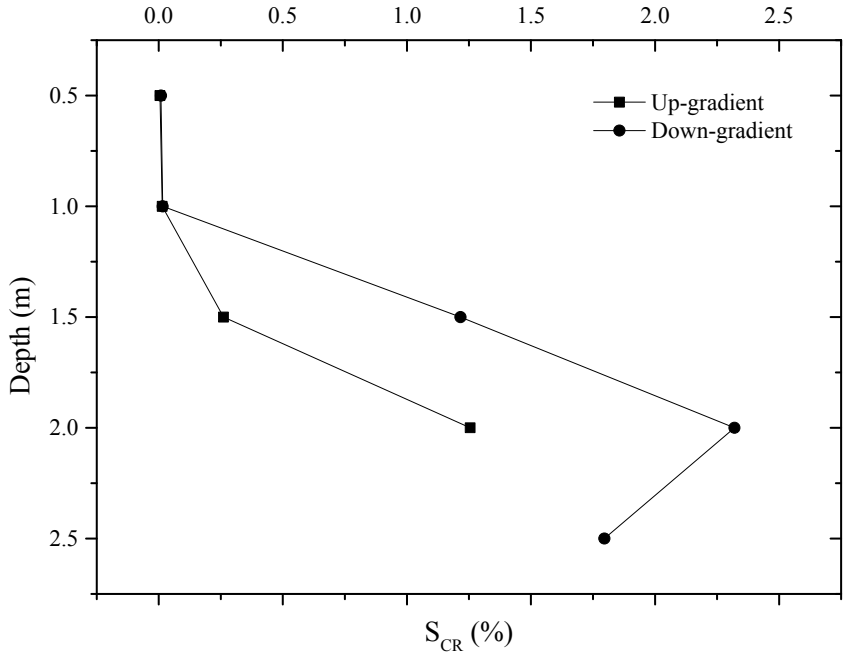


Figure 4.8 Inorganic reduced sulfur ($S_{CR}$, %) at different depths in the up-gradient and down-gradient of PRB

## 4.4 Performance monitoring in the PRB

The performance of the pilot-scale PRB is demonstrated by the spatial and temporal distribution of water quality parameters such as groundwater pH and different ion concentrations after installation of the PRB. Groundwater quality parameters up-

gradient, inside and down-gradient of the PRB were compared. Groundwater samples were collected monthly from the observation wells in acid washed polyethylene plastic bottles and analysed for basic cations ($Ca^{2+}$, $Mg^{2+}$, $Na^{+}$, $K^{+}$), acidic cations ($Al^{3+}$ and total Fe), anions ($Cl^{-}$ and $SO_4^{2-}$), acidity and alkalinity. Ca and Al were analysed using ICP-MS and Fe was analysed using AAS. All chemical analyses were performed following the standard method for water and wastewater (APHA, 1998). Results from column experiments confirmed that $Ca^{2+}$, $Al^{3+}$ and total Fe were the elements of primary importance in the acid neutralisation procedure taking between the recycled concrete and the acidic groundwater. Therefore, these three ions were monthly measured in the field samples. The remaining ions had no significant change, therefore, they were measured quarterly each year (Figures 4.15 (B, C and D) and 4.16.

### 4.4.1 Acid neutralisation

After installation of the PRB on 20$^{th}$ October 2006, the groundwater pH inside the PRB increased slowly from 7.0 to 10.2 (Figure 4.9 (A)). In the same manner, a high pH value of 9.7 was observed at the start of the column experiments (Figure 3.5). The significant increase of pH in the PRB at the early stage was because at the start the recycled concrete in PRB was not fully saturated. Therefore, the PRB monitoring period was considered unstable until the concrete was fully saturated by heavy rainfall in March 2007 (Figure 4.9 (B)). Since then, the groundwater inside the PRB has consistently been alkaline to neutral ranging from pH 10.2 to 7.2 till now. This illustrates the success of the pilot-scale PRB in neutralising the acidic groundwater. Due to variability in groundwater flow patterns soon after the installation of PRB, pH down-gradient of the PRB did not increase immediately. However, after reaching

steady-state flow in February 2007, the average pH down-gradient of the PRB started to increase and reached ~6.2. The lower pH in the down-gradient compared with that inside the PRB is due to: (i) dilution of the effluent from the PRB and (ii) occasional mixing of acid generated in the soil because the PRB cannot control acid generation in the soil by pyrite oxidation. In addition, low pH at some observation wells down-gradient during some dry periods (e.g. November 2006 and 2008) is possibly due to the flushing of large amounts of acidity stored within the soil by small rainfall events.

The groundwater pH along the centreline shows significant improvement in groundwater inside and down-gradient of the PRB (Figure 4.10). This clearly illustrates the potential of the recycled concrete's alkalinity generation to improve the down-gradient water quality. The groundwater pH in the observation wells varied greatly from 4.2 to 7.5 which are 4-12 m away from PRB (Figure 4.10). This is lower than the pH inside the PRB, but certainly higher than the acidic pH up-gradient of the PRB.

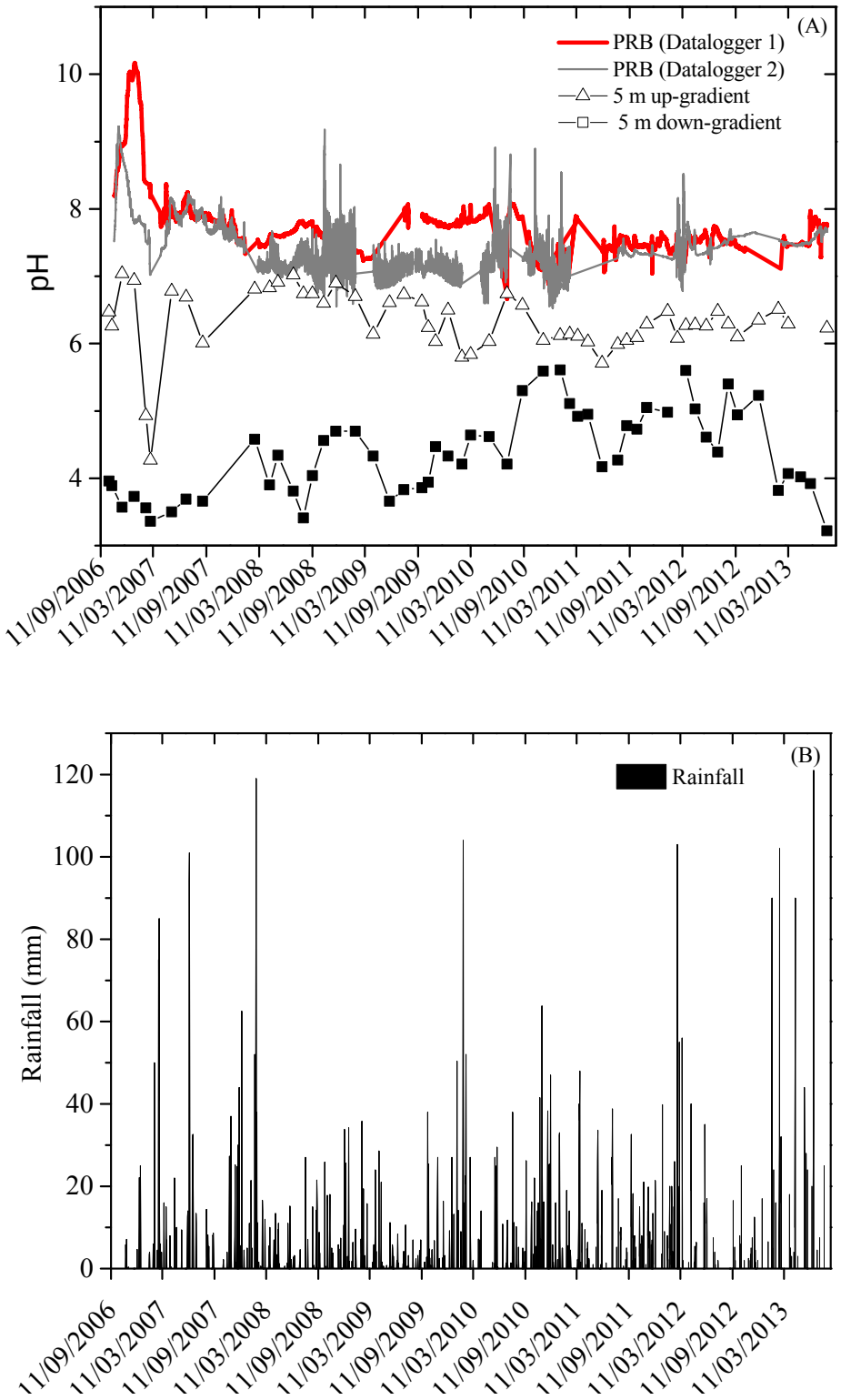


Figure 4.9 (A) Average groundwater pH up-gradient (from 8 observation wells), inside (from 10 observation wells and 2 data loggers) and down-gradient (from 12 observation wells) of the PRB (B) Rain fall
(updated after Regmi (2012))

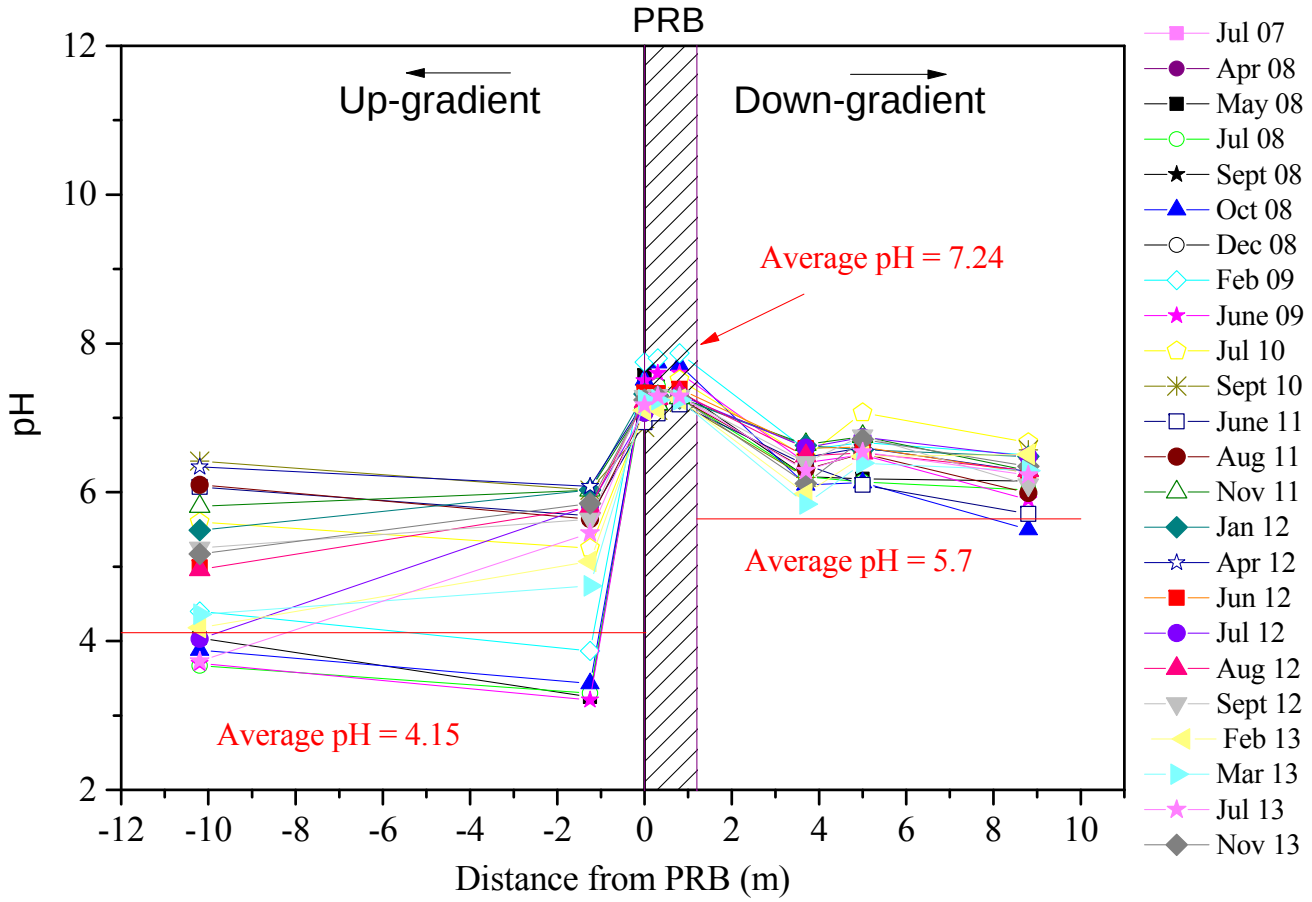


Figure 4.10: Groundwater pH along the centreline of the PRB at different time intervals (updated after Regmi (2012))

Figure 4.11 shows pH values of all the observation wells up-gradient of the PRB. All of them have very acidic pH below 4 from 2006 to 2013 indicating the widespread nature of acidic conditions at the study site.

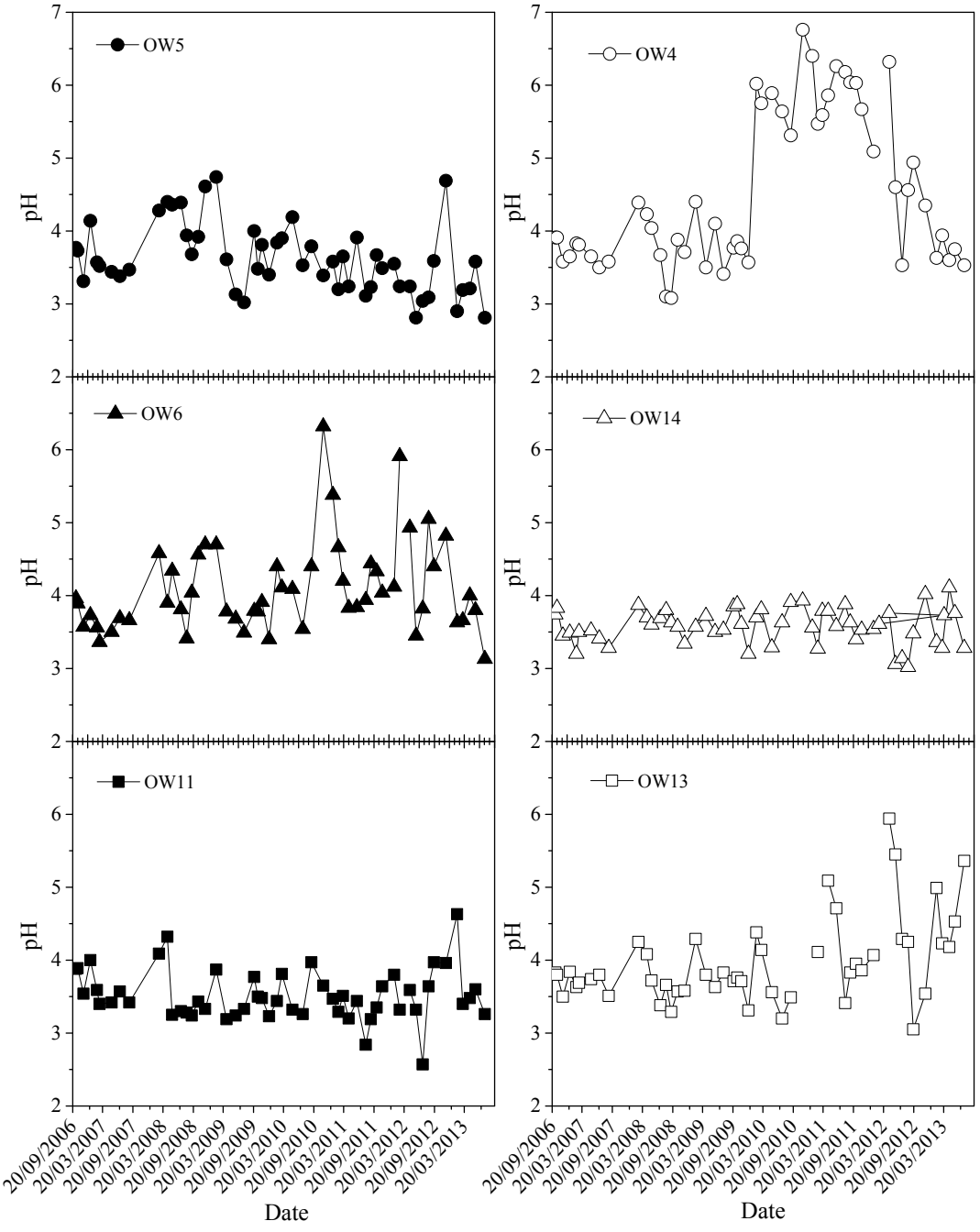


Figure 4.11: Groundwater pH up-gradient of the PRB (OW-Observation Well) (updated after Regmi (2012))

The ORP in groundwater up-gradient of the PRB varies from 20 mV to 470 mV (Figure 4.12) indicating strong oxidising conditions. In ASS, high ORP measurements indicate the potential for pyrite oxidation. The variation in ORP depends on the diffusion of atmospheric oxygen into the soil matrix and is controlled by the groundwater elevation.

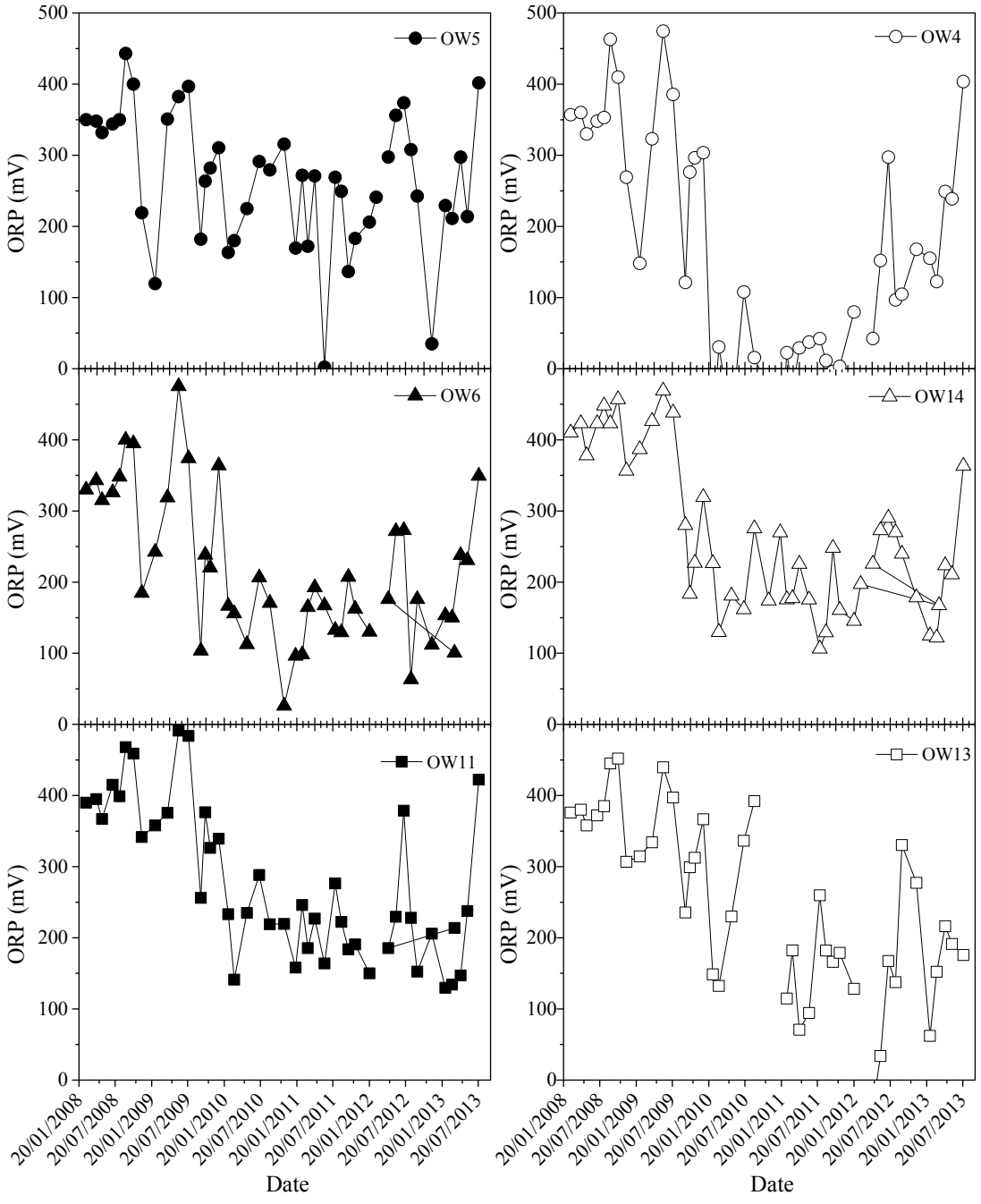


Figure 4.12 Groundwater ORP up-gradient of the PRB (updated after Regmi (2012))

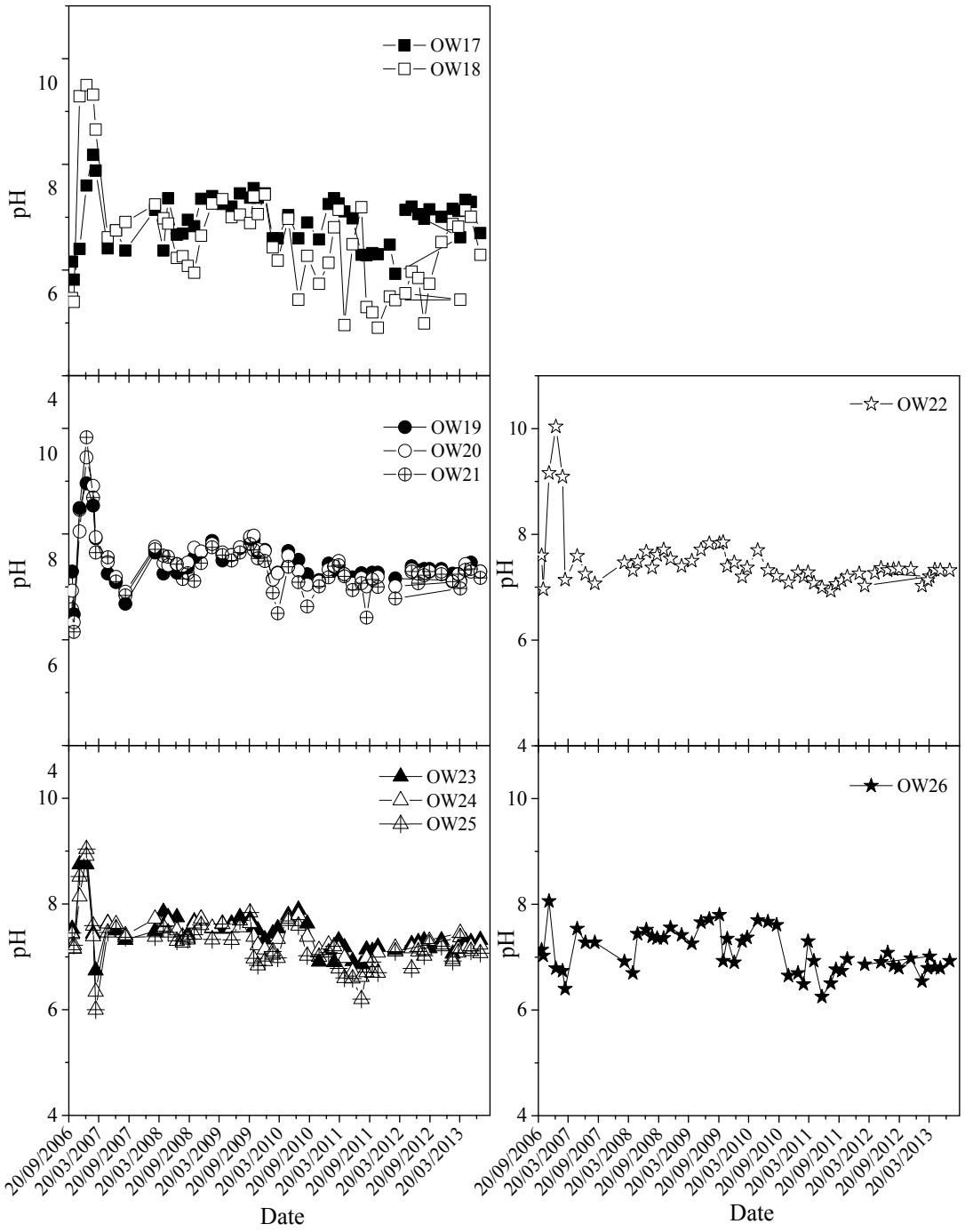


Figure 4.13 Groundwater pH inside the PRB (Entrance zone: OW18, OW21, OW25; Middle zone: OW20, OW22, OW24, OW26; Exit zone: OW17, OW19, OW23) (updated after Regmi (2012))

The pH values in all the observation wells inside the PRB are neutral from the day it was installed and to date (Figure 4.13). This pH plateau observed inside the PRB is consistent with the first pH plateau observed in the column experiments caused by

the buffering by Ca-bearing minerals (i.e. anorthite, feldspars and calcite). These field conditions of 6.5 years further emphasize that recycled concrete is a promising and cost-effective alkaline material for the long-term remediation of acidic groundwater. However, the pH of some of the observation wells inside the PRB has been decreasing slowly at the entrance zone (i.e. OW18 and OW25, Figure 4.13). This might be due to exhaustion of the alkalinity generating minerals within the recycled concrete at the first point of contact with the acidic groundwater as well as assumed armouring of the reactive surface of the concrete by precipitates.

### 4.4.2 Removal of $Al^{3+}$ and total Fe ($Fe^{2+}$ and $Fe^{3+}$) from groundwater

High concentrations of Al and Fe were observed up-gradient of PRB ranging from 1.5-60 mg/L and 2-290 mg/L, respectively (Figure 4.14). The results obtained during the 6.5 years monitoring period in the PRB showed that most of the $Al^{3+}$ and Fe contained in the groundwater precipitated rapidly when Ca-bearing alkaline minerals from the recycled concrete started to dissolve and thereby increased the groundwater pH. A rapid decrease in $Al^{3+}$ and Total Fe can be seen inside the PRB and most importantly has been consistently less than 2 and 0.5 mg/L, respectively (Figure 4.14).

The concentrations of Al and Fe in the down-gradient increased with distance away from the PRB. This is probably due to the active and ongoing oxidation of pyrite in the soil, generating fresh acid, and the release of these metals from the clay minerals in the soil. During rainfall events, the treated groundwater from the PRB would mix with the in-situ acidic groundwater, thus causing an increase in Al and Fe concentration and decrease in pH. Furthermore, there is a chance that some untreated

groundwater from above, below and to the side of the PRB flows towards the down-gradient monitoring area. Although, the concentrations down-gradient were higher than those inside the PRB, they were still lower than those up-gradient of the PRB.

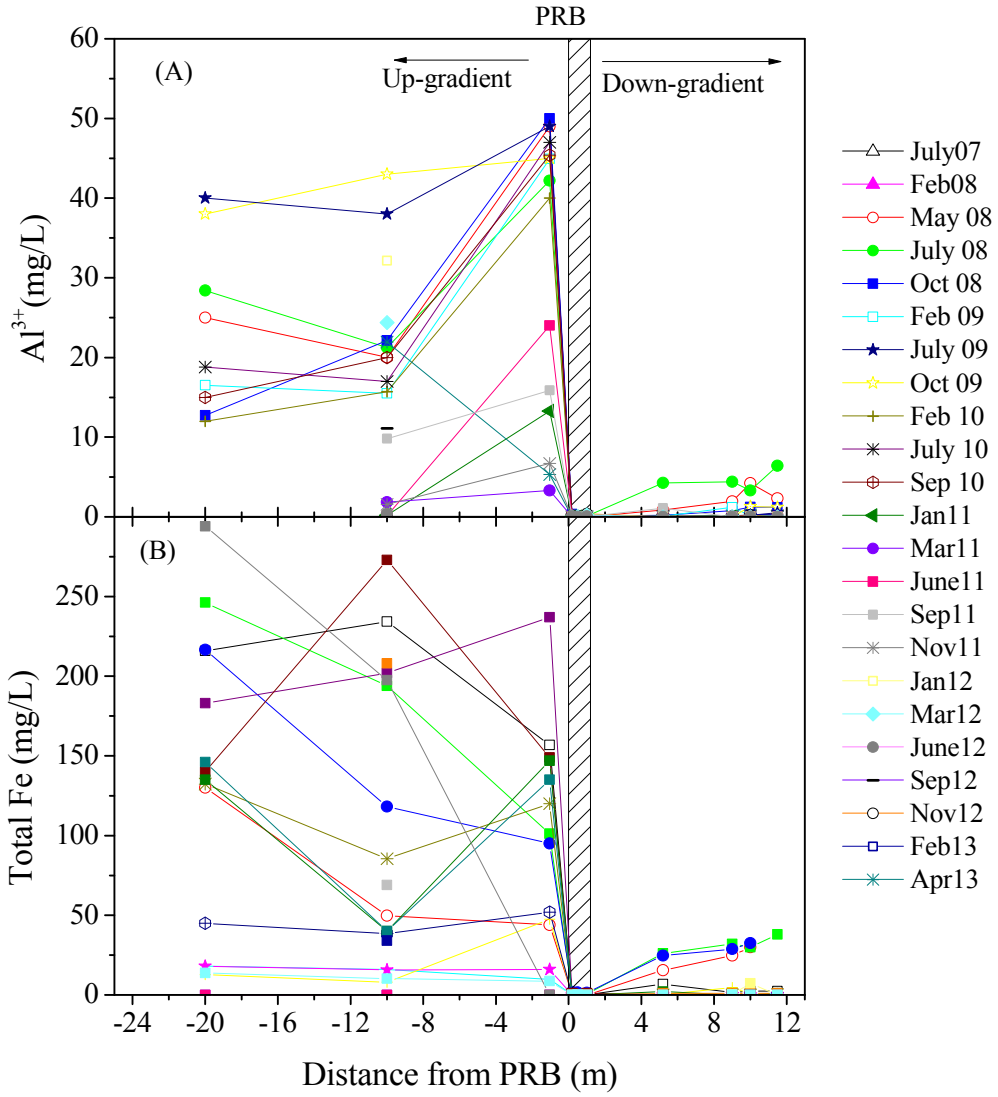


Figure 4.14 (a) $Al^{3+}$ and (b) Total Fe concentrations in groundwater along the centreline of PRB from July 2007 to April 2013 (updated after Regmi (2012))

Although the PRB cannot prevent further pyrite oxidation in the soil, the treated groundwater leaving the PRB can significantly improve the down-gradient water quality. These results indicate the outstanding removal efficiency (~95%) of the recycled concrete for both $Al^{3+}$ and total Fe.

### 4.4.3 Other ions in groundwater chemistry

Except for $Ca^{2+}$, there is no apparent change in $Na^{+}$, $K^{+}$, $Mg^{2+}$, $Cl^{-}$ and $SO_4^{2-}$ concentrations in the groundwater up-gradient and within the PRB as plotted in Figures 4.15 and 4.16. This confirms that these ions are not influenced by the neutralisation reactions occurring within the PRB. The inert nature of these ions is discussed in Chapter 5, where the geochemical algorithm is developed considering the most significant chemical reactions.

$Ca^{2+}$ was continuously released from the recycled concrete inside the PRB throughout the monitoring period. The dissolution of Ca-bearing minerals such as anorthite and calcite present in the recycled concrete has the potential to generate large amounts of carbonate/bicarbonate alkalinity to bring the pore water to near-neutral pH. Chapter 5 elaborates all the associated chemical reactions in this carbonate/bicarbonate alkalinity buffering process.

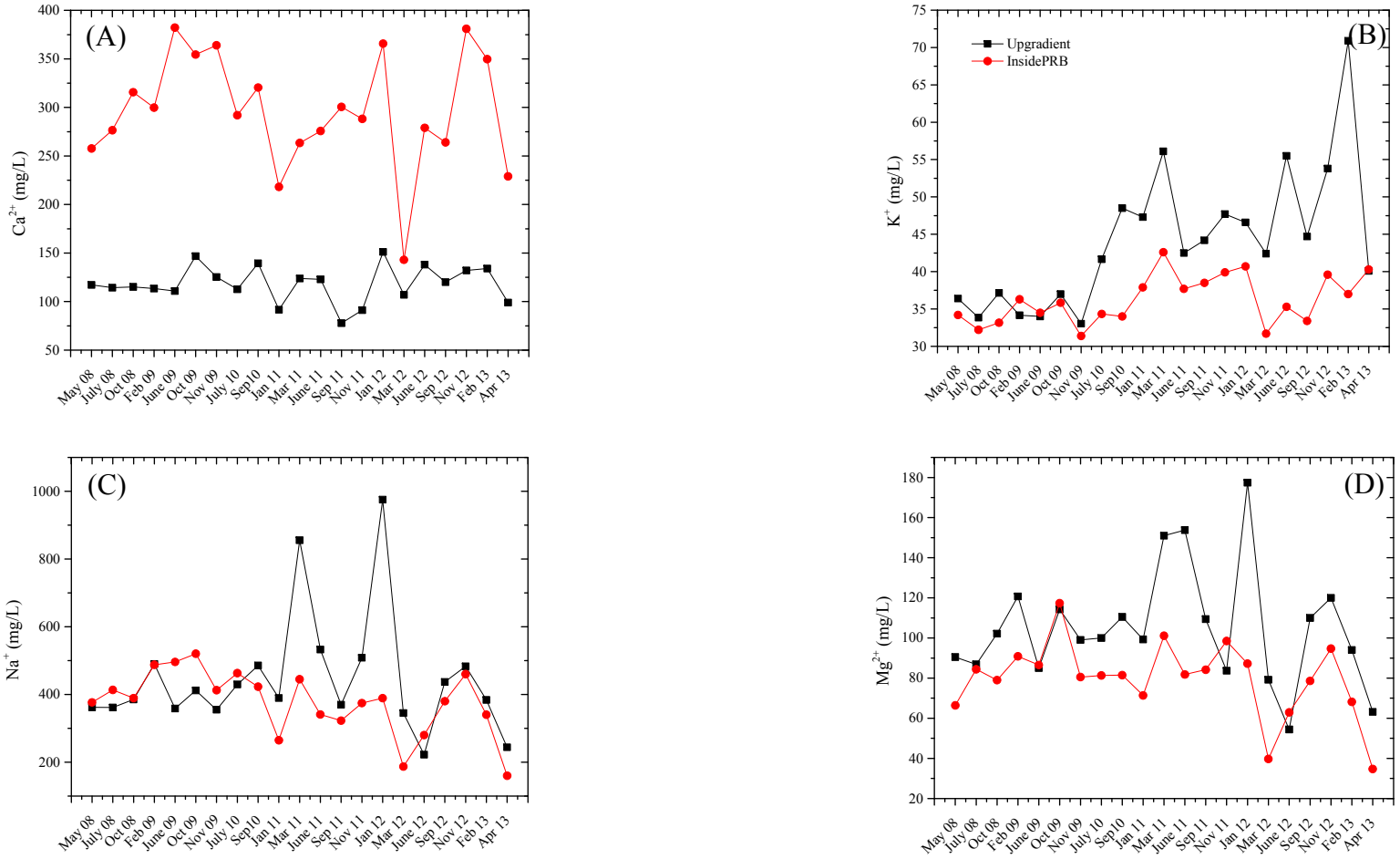


Figure 4.15 Concentration of cations: (A) $Ca^{2+}$, (B) $K^{+}$, (C) $Na^{+}$ and (D) $Mg^{2+}$ in the groundwater inside and up-gradient of the PRB (updated after Regmi (2012))

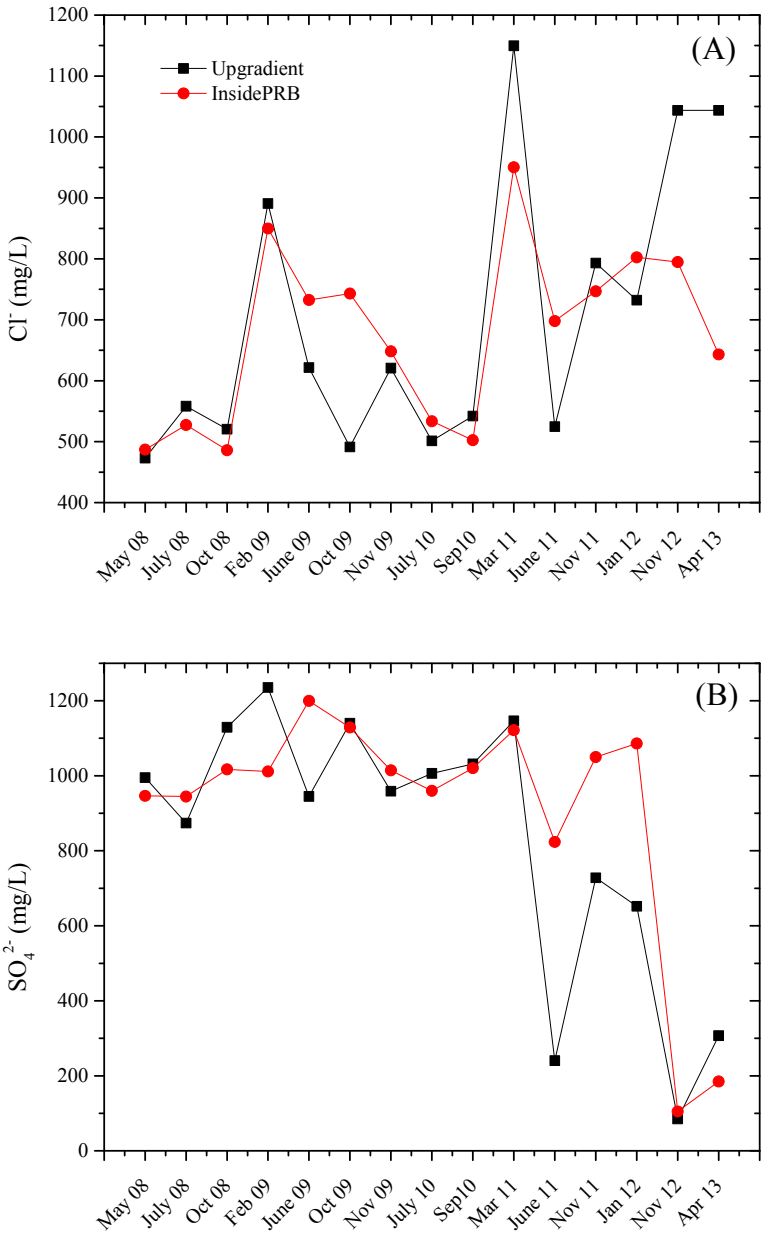


Figure 4.16 Concentration of anions: (A) $Cl^-$ and (B) $SO_4^{2-}$ in the groundwater inside and up-gradient of the PRB (updated after Regmi (2012))

All the above data presents the performance of PRB over 6.5 years since the time it was installed. The neutral to alkaline pH and ~95% removals of $Al^{3+}$ and total Fe from groundwater inside the PRB (Figure 4.13 and 4.14) shows its ability to remediate the acidic groundwater in ASS terrain. Concrete samples were removed from the PRB near OW26 (i.e. 40 cm from PRB entrance) 6.5 years after the PRB

was installed in order to study chemical armouring. These concrete samples had a negligible amount of precipitates coating the surface. The mineralogical analysis of these specimens is discussed later in Chapter 6.

## 4.5 Summary

This chapter described the outcomes of the first pilot-scale PRB using recycled concrete as the reactive media for the in-situ remediation of acidic groundwater in ASS terrain. Monitoring data showed that the recycled concrete could effectively sustain a near-neutral pH removing the main heavy metals, Al and Fe from groundwater over the 6.5 year monitoring period following installation of the PRB. However, it managed to improve the groundwater chemistry for some extent only in the down-gradient of the PRB due to on-going pyrite oxidation.

Overall, the PRB has shown satisfactory performance over a 6.5 year time period, although a slight decrease in the pH and removal efficiencies (~95%) of Al and Fe towards the entrance zone of the PRB was observed. This was because that, some chemical armouring on the surface of the reactive media has occurred and affected the reactivity of the recycled concrete in that zone. Continuous precipitation within the PRB would decrease the surface area of the reactive material available for neutralising acidity over time, thereby, decreasing the longevity of the PRB. Hence, armouring is most likely the limiting factor on the performance of the PRB similar to that explained earlier in Chapter 3 through the results of column tests.

In addition, the application of larger size concrete particles decreased the threat of clogging by the accumulation of precipitates in the pore spaces even under high

influent concentrations of $Al^{3+}$ and total Fe. The recycled concrete is a suitable material because of its ability to effectively neutralise acidity and remove $Al^{3+}$ and total Fe in conjunction with chemical armouring, in PRBs for the treatment of acidic water in ASS terrain.

# Chapter 5 Development of the Geochemical Algorithm

## 5.1 Introduction

This chapter presents the development of the geochemical algorithm. This is the first step involved in modelling the groundwater flow and contaminant transport through PRB in ASS terrain. Chapter 3 described the acid neutralisation behaviour and metal removal capacity of the recycled concrete. This chapter will focus on the chemical reactions involved in the acid neutralisation and metal removal, and most importantly how they could be captured in the geochemical model.

## 5.2 Bicarbonate buffering

Regmi et al. (2009a) and (2011b) proposed three buffering reactions attributed to three distinct pH plateaus:

1. dissolution of carbonate/bicarbonate alkalinity from the concrete at near-neutral pH,
2. re-dissolution of Al hydroxide minerals at pH ~4.5, and
3. re-dissolution of ferric oxyhydroxides minerals at pH < 3.7.

Among these three buffering reactions, carbonate/bicarbonate buffering was the most significant and vital in terms of remediating acidic groundwater by maintaining an almost neutral pH and complete removal of $Al^{3+}$ and total Fe from the influent solution. The cementitious minerals responsible for alkalinity generation in the concrete are portlandite ($Ca(OH)_2$) and C-A-H (Regmi et al., 2011b). Additionally, some $CaCO_3$ may have already formed in the recycled concrete aggregate due to the

carbonation of these minerals present in hydrated cementitious materials (Tam et al., 2005). Dissolution of the Ca-bearing minerals from the concrete, as shown in Eqns. (5.1)-(5.5), released Ca and increased the alkalinity with a potential to maintain the effluent pH near-neutral.

$$Ca(OH)_2 + 2H^+ \rightarrow Ca^{2+} + 2H_2O \quad (5.1)$$

$$Ca(OH)_2 + CO_2(aq) \rightarrow CaCO_3 + H_2O \quad (5.2)$$

$$CaAl_2Si_2O_8 + 8H^+ \rightarrow Ca^{2+} + 2Al^{3+} + 2H_4SiO_4 \quad (5.3)$$

$$CaCO_3 + 2H^+ \Leftrightarrow Ca^{2+} + H_2CO_3 \quad (5.4)$$

$$CO_2(aq) + H_2O \Leftrightarrow H_2CO_3 \quad (5.5)$$

## 5.3 Precipitation of Al- and Fe-bearing minerals

The near-neutral pH maintained by carbonate/bicarbonate buffering favoured the precipitation of Al and Fe as oxides, oxyhydroxides and hydroxides as shown in the following chemical reactions in Eqns. (5.6)-(5.12) (Regmi et al., 2009a).

$$Fe^{3+} + 3H_2O \rightarrow Fe(OH)_{3(S)} + 3H^+_{aq} \quad (5.6)$$

$$Fe^{3+} + 2H_2O \rightarrow Fe(OOH) + 3H^+_{aq} \quad (5.7)$$

$$2Fe^{3+} + 3H_2O \rightarrow Fe_2O_3 + 6H^+_{aq} \quad (5.8)$$

$$Al^{3+} + 3H_2O \rightarrow Al(OH)_{3(S)} + 3H^+_{(aq)} \quad (5.9)$$

$$Fe^{2+} + 2(OH)^- \leftrightarrow Fe(OH)_{2(S)} \quad (5.10)$$

$$Fe^{2+} + CO_3^{2-} \leftrightarrow FeCO_{3(S)} \quad (5.11)$$

$$Ca^{2+} + CO_3^{2-} \leftrightarrow CaCO_{3(S)} \quad (5.12)$$

## 5.4 Geochemical Algorithm

A systematic geochemical algorithm was developed using the Transition State Theory (TST) used by Jeen et al. (2012), Li and Benson (2005), Mayer et al. (2006), Regmi et al. (2011a) and Yabasuki (2001). This is the first time, a geochemical algorithm has been developed for treating acidic groundwater using a recycled concrete filled PRB. There are twelve primary mineral dissolution-precipitation reactions as shown in Regmi et al. (2009b).

The Transition State Theory (TST) (Eyring, 1935) is used to model a hypothetical transition state which exists between reactants and products during a chemical reaction. The species formed during this hypothetical transition state is called the activated complex, which is used to explain how chemical reactions take place (Petrucci et al., 2006a). Transition state theory can be classified under three main headings: (1) thermo-dynamic treatment, (2) kinetic-theory treatment, and (3) statistical-mechanical treatment. The theory suggests that as reactant molecules approach each other (closely), they are momentarily in a less stable state than either the reactants or the products. The example below shows the transition stage clearly.

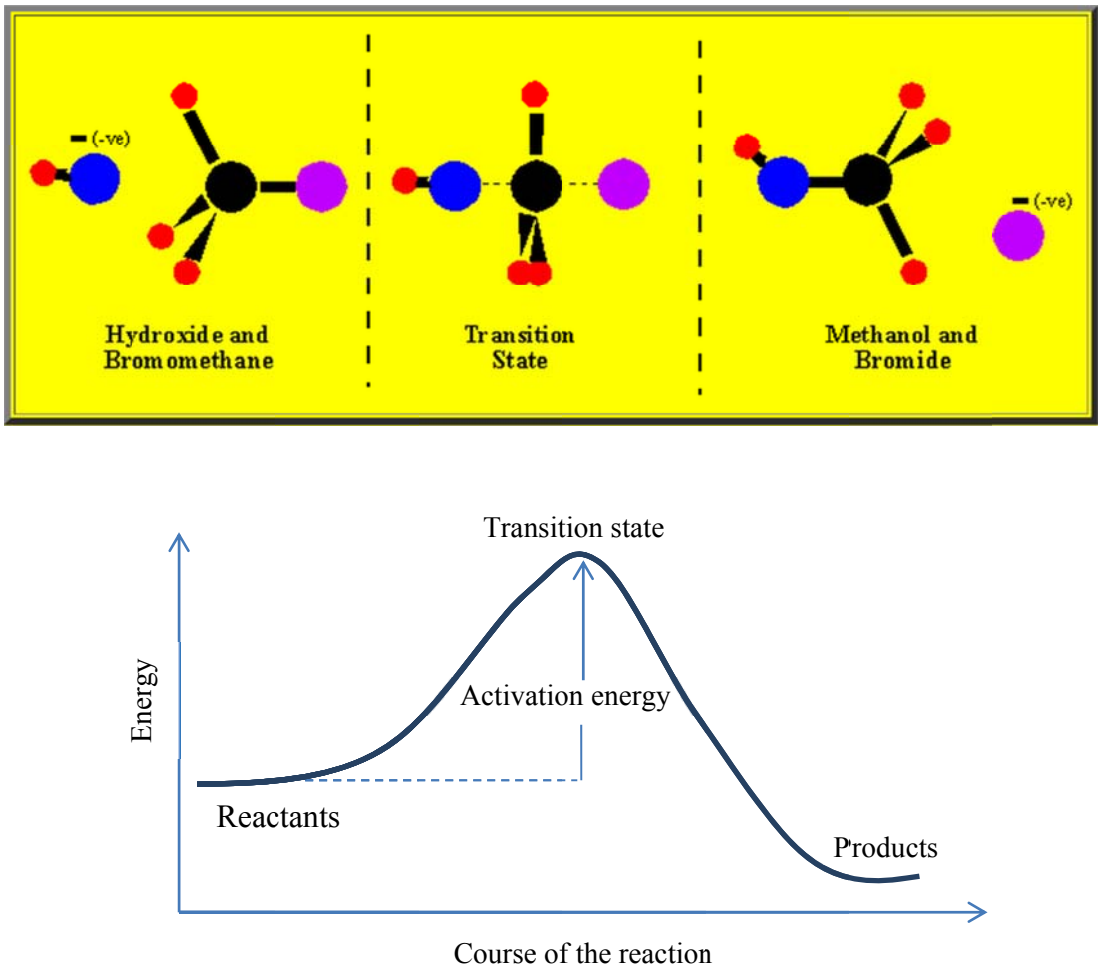


Figure 5.1 Hypothetical schematic of the transition state

The above theory suggests that there are three major factors that determine whether a reaction will occur or not:

1. The concentration of the activated complex (the species of the transition state)
2. The rate at which the activated complex breaks apart, and
3. The way in which the activated complex breaks apart: i.e., whether it breaks apart to reform the reactants or whether it breaks apart to form a new complex (products).

TST has been widely used because if it relatively ease the application in comparison to other treatments of rates. Most importantly, TST approach gives a better understating of how even very complicated reactions take place, in which other complex reaction models require much more labour and time (Laidler and King, 1983).

To confirm the adoption of these twelve reaction equations in the geochemical algorithm, inverse geochemical modelling has been carried out by Regmi et al. (2009a) because the speciation calculation through equilibrium modelling could not predict the minerals that were deposited by chemical reactions. This inverse modelling considered all the possible mineral phases obtained in the speciation calculation of the water sample up-gradient and inside the PRB. The phase mole transfer in inverse geochemical modelling (Table 4.1) for different minerals which confirms the precipitation of Fe and Al in different forms of hydroxides and oxyhydroxides and carbonates. This verifies the possible reactions described in Eqns. (5.6)-(5.12) (Regmi et al., 2009a).

Table 4.1 Phase Mole Transfer of minerals from inverse geochemical modelling (+ sign: Dissolution, – sign: Precipitation) (Regmi et al., 2009a)

| Minerals | Chemical Formula | Phase mole transfer | |
|---|---|---|---|
| | | minimum | Maximum |
| $Al(OH)_3$ | $Al(OH)_3$ | $-7.51\times 10^{-4}$ | $-4.57\times10^{-4}$ |
| Alunite | $KAl_3(SO_4)_2(OH)_6$ | $-2.73\times10^{-4}$ | $-1.27\times10^{-4}$ |
| Anhydrite | $CaSO_4$ | $-1.04\times10^{1}$ | $-6.58\times10^{0}$ |
| Aragonite | $CaCO_3$ | $-1.54\times10^{1}$ | $+8.55\times10^{-3}$ |
| Calcite | $CaCO_3$ | $-1.54\times10^{1}$ | $+8.55\times10^{-3}$ |
| Dolomite | $CaMg(CO_3)_2$ | $-9.5\times10^{-4}$ | $-9.47\times10^{-3}$ |
| $Fe(OH)_3$ | $Fe(OH)_3$ | $-3.47\times10^{-3}$ | $-2.89\times10^{-7}$ |
| Gibbsite | $Al(OH)_3$ | $-6.23\times10^{-4}$ | $-1.10\times10^{-4}$ |
| Goethite | FeOOH | $-3.47\times10^{-3}$ | $-2.89\times10^{-7}$ |
| Gypsum | $CaSO_4{:}2H_2O$ | $+6.58\times10^{0}$ | $+1.04\times10^{1}$ |
| Halite | NaCl | $+3.89\times10^{-3}$ | $+5.57\times10^{-3}$ |
| Hematite | $Fe_2O_3$ | $-1.74\times10^{-3}$ | $-1.45\times10^{-7}$ |
| Siderite | $FeCO_3$ | $-3.37\times10^{-3}$ | $-7.64\times10^{-4}$ |

The user-defined geochemical algorithm employs many of the principles and approaches in Li (2004), Mayer et al. (2001) and Yabusaki (2001). The geochemical reactions included in the model are from Eqns. (5.1)-(5.12). All these geochemical reactions are assumed to take place in the column or in the PRB in parallel and are solved simultaneously. The concentration of each species is calculated for each cell in the domain during each time step. The kinetics of mineral precipitation was assumed to follow transition state theory (Lichtner, 1996, Hunter et al., 1998, Steefel and Lasaga, 1994, Mayer et al., 2001, Yabusaki, 2001, Li et al., 2006). The reaction rate is expressed as:

$$r = -k_{eff}\left(1 - \frac{IAP}{K_{eq}}\right) \tag{5.13}$$

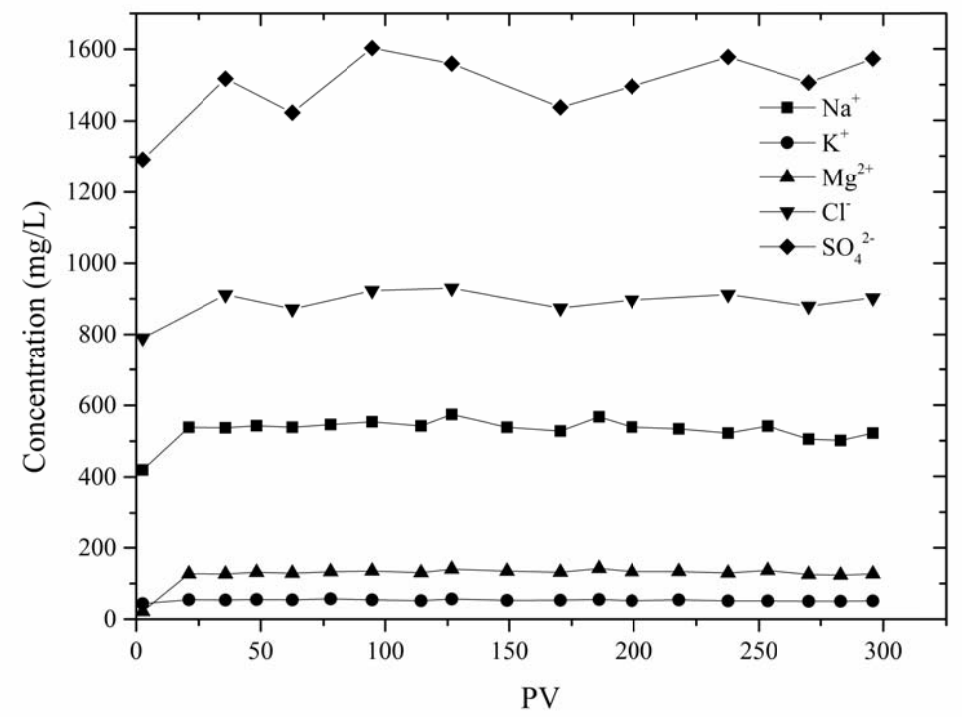


Figure 5.2 Concentration of other ions in the effluent as a function of pore volume (Indraratna et al., 2014)

where, $r$ is the rate of mineral precipitation ($r > 0$) or dissolution ($r < 0$), $k_{eff}$ is an effective rate coefficient, $IAP$ is the ion activity product, and $K_{eq}$ is the solubility constant for the reaction. The overall reaction rates for each aqueous and solid species are shown in the following algorithm:

$$\frac{d[m_{Ca(OH)_2}]}{dt} = \frac{1}{2}\frac{d[H^+]}{dt} = -\frac{d[Ca^{2+}]}{dt} = r_{1[Ca^{2+}]} = k_{[Ca^{2+}]}\left[\frac{a_{Ca^{2+}}a_{OH^-}^2}{K_{eq,Ca^{2+},OH^-}} - 1\right]$$

$$\frac{d[m_{CaAl_2Si_2O_8}]}{dt} = \frac{1}{8}\frac{d[H^+]}{dt} = -\frac{d[Ca^{2+}]}{dt} = -\frac{1}{2}\frac{d[Al^{3+}]}{dt} = r_{[Ca^{2+}Al^{3+}]} = k_{[Ca^{2+}Al^{3+}]}\left[\frac{a_{Ca^{2+}}a_{Al^{3+}}^2}{K_{eq,Ca^{2+}Al^{3+}}} - 1\right]$$

$$\frac{d[m_{CaCO_3}]}{dt} = \frac{1}{2}\frac{d[H^+]}{dt} = -\frac{d[Ca^{2+}]}{dt} = -\frac{d[H_2CO_3]}{dt} = r_{2[Ca^{2+}]} = k_{[Ca^{2+}]}\left[\frac{a_{Ca^{2+}}a_{CO_3^{2-}}}{K_{eq,Ca^{2+},CO_3^{2-}}} - 1\right]$$

$$\frac{d[Fe^{3+}]}{dt} = -\frac{d[m_{Fe(OH)_3}]}{dt} = -\frac{1}{3}\frac{d[H^+]}{dt} = r_{1[Fe^{3+}]} = k_{[Fe^{3+}]}\left[\frac{a_{Fe^{3+}}a_{OH^-}^3}{K_{eq,Fe^{3+},OH^-}} - 1\right]$$

$$\frac{d[Fe^{3+}]}{dt} = -\frac{d[m_{Fe(OOH)}]}{dt} = -\frac{1}{3}\frac{d[H^+]}{dt} = r_{2[Fe^{3+}]} = k_{[Fe^{3+}]}\left[\frac{a_{Fe^{3+}}a_{OOH^{3-}}}{K_{eq,Fe^{3+},OOH^{3-}}} - 1\right]$$

$$\frac{1}{2}\frac{d[Fe^{3+}]}{dt} = -\frac{d[m_{Fe_2O_3}]}{dt} = -\frac{1}{6}\frac{d[H^+]}{dt} = r_{3[Fe^{3+}]} = k_{[Fe^{3+}]}\left[\frac{a_{Fe^{3+}}^2a_{O^{2-}}^3}{K_{eq,Fe^{3+},O^{2-}}} - 1\right]$$

$$\frac{d[Al^{3+}]}{dt} = -\frac{d[m_{Al(OH)_3}]}{dt} = -\frac{1}{3}\frac{d[H^+]}{dt} = r_{[Al^{3+}]} = k_{[Al^{3+}]}\left[\frac{a_{Al^{3+}}a_{OH^-}^3}{K_{eq,Al^{3+},OH^-}} - 1\right]$$

$$\frac{d[Fe^{2+}]}{dt} = \frac{1}{2}\frac{d[OH^-]}{dt} = -\frac{d[m_{Fe(OH)_2}]}{dt} = r_{1[Fe^{2+}]} = k_{[Fe^{2+}]}\left[\frac{a_{Fe^{2+}}a_{OH^-}^2}{K_{eq,Fe^{2+},OH^-}} - 1\right]$$

$$\frac{d[Fe^{2+}]}{dt} = \frac{d[CO_3^{2-}]}{dt} = -\frac{d[m_{FeCO_3}]}{dt} = r_{2[Fe^{2+}]} = k_{[Fe^{2+}]}\left[\frac{a_{Fe^{2+}}a_{CO_3^{2-}}}{K_{eq,Fe^{2+},CO_3^{2-}}} - 1\right]$$

$$\frac{d[Ca^{2+}]}{dt} = \frac{d[CO_3^{2-}]}{dt} = -\frac{d[m_{CaCO_3}]}{dt} = r_{4[Ca^{2+}]} = k_{[Ca^{2+}]}\left[\frac{a_{Ca^{2+}} a_{CO_3^{2-}}}{K_{eq,Ca^{2+},CO_3^{2-}}} - 1\right]$$

The overall reactive kinetics for each species in the algorithm is listed as:

$$\frac{d[Ca^{2+}]}{dt} = -r_{1[Ca^{2+}]} - r_{[Ca^{2+}Al^{3+}]} - r_{2[Ca^{2+}]} + r_{4[Ca^{2+}]}$$

$$\frac{d[Fe^{3+}]}{dt} = r_{1[Fe^{3+}]} + r_{2[Fe^{3+}]} + 2r_{3[Fe^{3+}]}$$

$$\frac{d[Fe^{2+}]}{dt} = r_{1[Fe^{2+}]} + r_{2[Fe^{2+}]}$$

$$\frac{d[Al^{3+}]}{dt} = r_{[Al^{3+}]} - 2r_{[Ca^{2+}Al^{3+}]}$$

$$\frac{d[H^{+}]}{dt} = 2r_{1[Ca^{2+}]} + 8r_{[Ca^{2+}Al^{3+}]} + 2r_{2[Ca^{2+}]} - 3r_{1[Fe^{3+}]} - 3r_{2[Fe^{3+}]} - 6r_{3[Fe^{3+}]} - 3r_{[Al^{3+}]}$$

$$\frac{d[HCO_3^{-}]}{dt} = -r_{2[Ca^{2+}]} + r_{2[Fe^{2+}]} + r_{4[Ca^{2+}]}$$

All the $m_i$ values are considered for a volume of $10^{-3}$ $m^3$, which is equivalent to 1 L ($i$ = all the solid phase minerals) (Indraratna et al., 2014).

### 5.5 Saturation index (SI)

Li (2005) used the extended Debye-Huckle equation for the activity correction and data provided in Krauskopf et al. (1995) for the solubility constants. In this study, saturation indices (SI), which can be calculated from PHREEQC software, were used to get the value for $IAP/K_{eq}$ as given in Eqn. 5.14 (Regmi et al., 2011b, Walter et al., 1994a).

$$SI = \log(IAP) - \log(K_{eq}) \quad (5.14)$$

SIs for minerals dissolving ($SI$<0) and precipitating ($SI$>0) were calculated from PHREEQC software based on the concentration of $Na^+$, $K^+$, $Ca^{2+}$, $Mg^{2+}$, $Al^{3+}$, $Fe^{3+}$, $Cl^-$ and $SO_4^{2-}$in the influent water along with alkalinity, pH and temperature. The mineral reactions and geochemical algorithm are given in Sections 5.3 and 5.4, respectively. The effective rate coefficient ($k_{eff}$) was assumed to be time invariant and spatially homogeneous throughout the simulation (Li and Benson, 2005).

Figures 5.3-5.9 show the saturation indices of Ca, Al and Fe minerals for the column experiments. PHREEQC was run for five different zones as the model output was expected to give effluent concentrations at five different heights along the column. At Zone 1, influent concentrations were the synthetic water prepared at the laboratory. For Zone 2, the effluent water concentrations coming out of Zone 1 from the model output was used as influent concentrations. Likewise for Zone 3, model output from Zone 2, for Zone 4: model output from Zone 3 and for Zone 5: model outputs from Zone 4 were used as the input concentrations. The results obtained for SIs show a promising trend of precipitating and dissolving minerals.

The SIs of Ca-bearing minerals (Figure 5.3 A) in the recycled concrete are negative, implying that they dissolve at that stage (Zone 1) of the experiment. These dissolved Ca-bearing minerals provide the alkalinity to remediate the acidity and precipitate out the Al and Fe as their oxyhydroxides and/or hydroxides. Positive SI values shown in Figure 5.3 B and C indicate the precipitation of these minerals. This model was run from 40 PV, and that is why the Al minerals still show negative SI values,

suggesting re-dissolution of some Al minerals that precipitated during the early phase of the experiment from the bottom of the column. This supposition was supported by rapid depletion of pH and alkalinity the bottom of the column at all sampling points (Chapter 3 Figures 3.6 and 3.8, respectively).

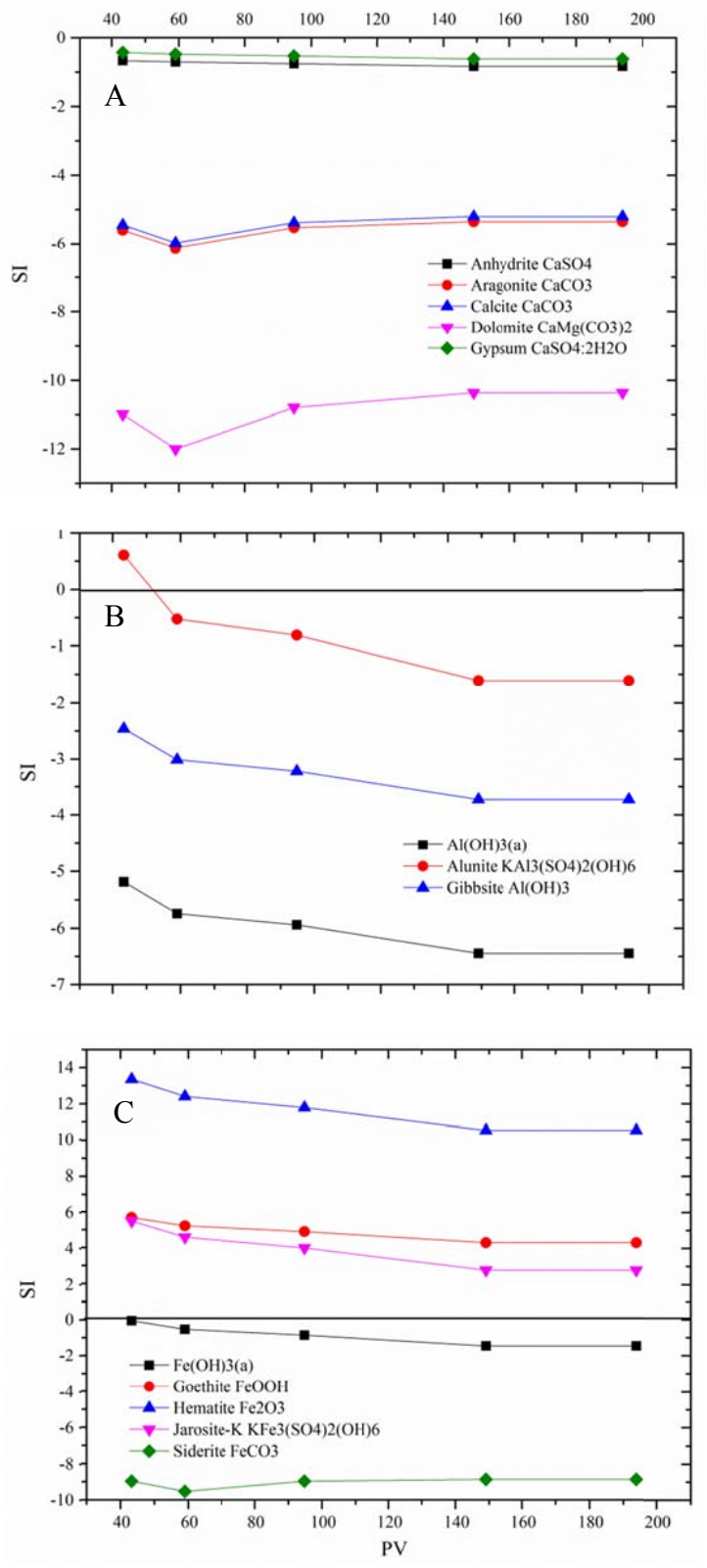


Figure 5.3 SI of different (A) calcium, (B) aluminium and (C) iron minerals calculated using PHREEQC with respect to the PV of synthetic groundwater passed through Zone 1 during the column experiment

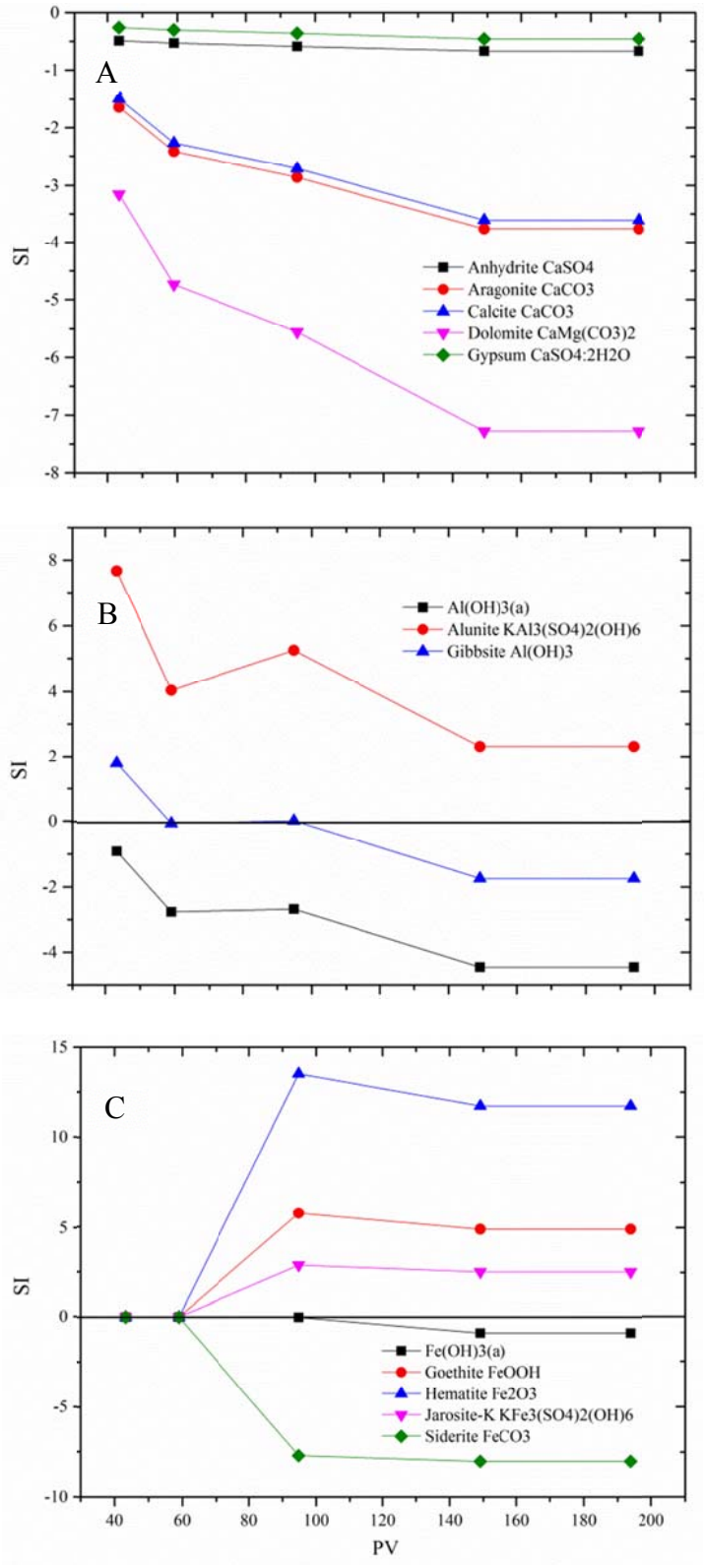


Figure 5.4 SI of different (A) calcium, (B) aluminium and (C) iron minerals calculated using PHREEQC with respect to the PV of synthetic groundwater passed through Zone 2 during the column experiment

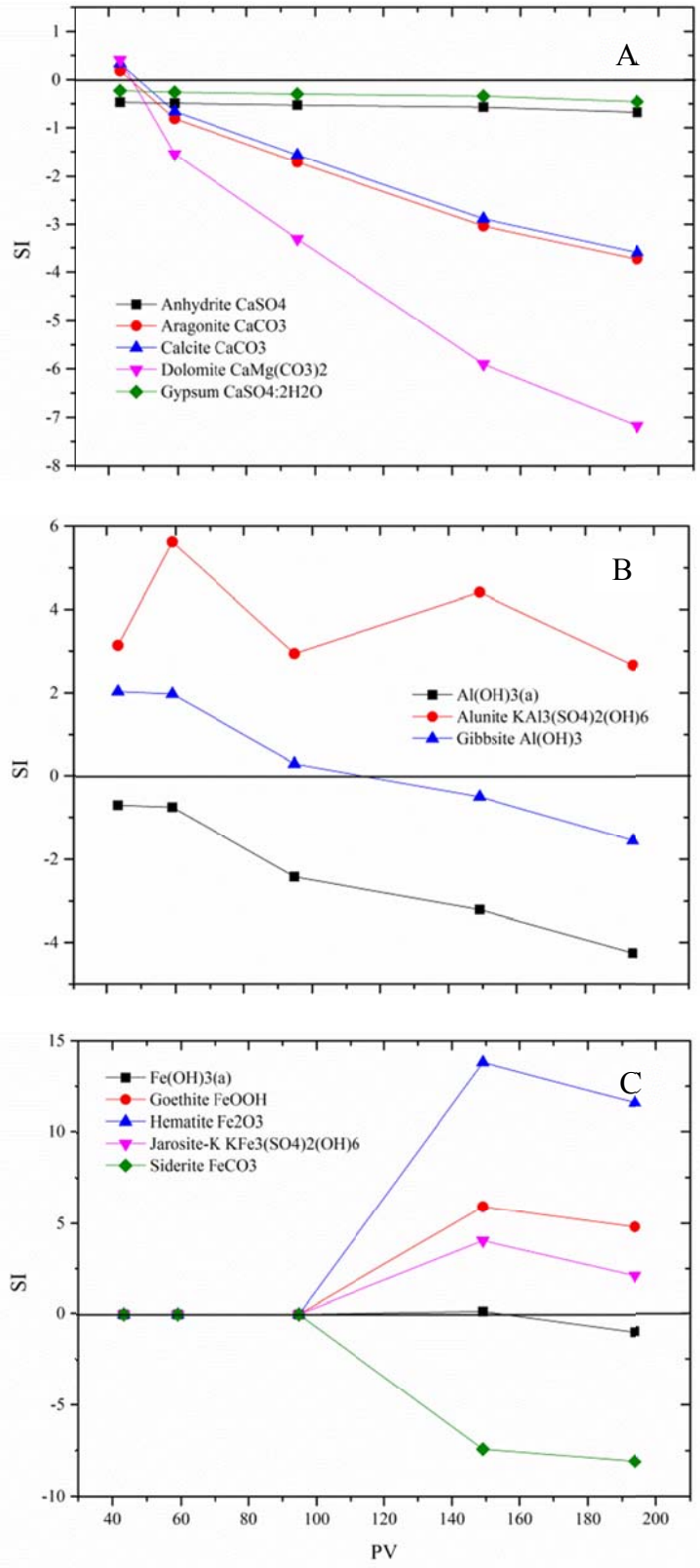


Figure 5.5 SI of different (A) calcium, (B) aluminium and (C) iron minerals calculated using PHREEQC with respect to the PV of synthetic groundwater passed through Zone 3 during the column experiment

Figure 5.4 A, clearly indicates the dissolution of Ca bearing minerals in Zone 2 and the associated precipitation of Al and Fe oxyhydroxides/hydroxides. Compared to the precipitation of Al and Fe oxyhydroxides/hydroxides in Zone 1 (Figure 5.3), Zone 2 and 3 had more Al and Fe oxyhydroxides/hydroxides precipitating (Figure 5.4 B, C and Figure 5.5 B and C).

Moreover, with the saturation indices being positive, there is evidence of Ca bearing minerals getting precipitated out of solution as calcite ($CaCO_3$), dolomite ($CaMg(CO_3)_2$) and gypsum ($CaSO_4.2H_2O$) in Zone 3 (Figure 5.5 A). Almost similar behaviour can be seen at the exit face (Zone 4 and 5) of the column as shown in Figures 5.6 and 5.7, respectively. The saturation indices of Al and Fe are also higher than that of seen in the entrance and middle zones of the column (Figure 5.6 B, C and Figure 5.7 B, C). This implies that the favourable condition of neutral pH is available at the exit zones throughout the experiment until the termination of the experiment.

The laboratory column experiments were terminated soon after the effluent concentration dropped to around pH 3.5, because as a whole, the reactive material in the column gets exhausted. The reactivity or the alkalinity produced by the recycled concrete was not enough to cope up with the influent acidity. If the column experiment was run for some more time, the reactivity of the recycled material present at Zones 3, 4 and 5 would also be exhausted totally and the precipitated Al and Fe oxyhydroxides/hydroxides would start to re-dissolute as seen in Zone 1 (Figure 5.3).

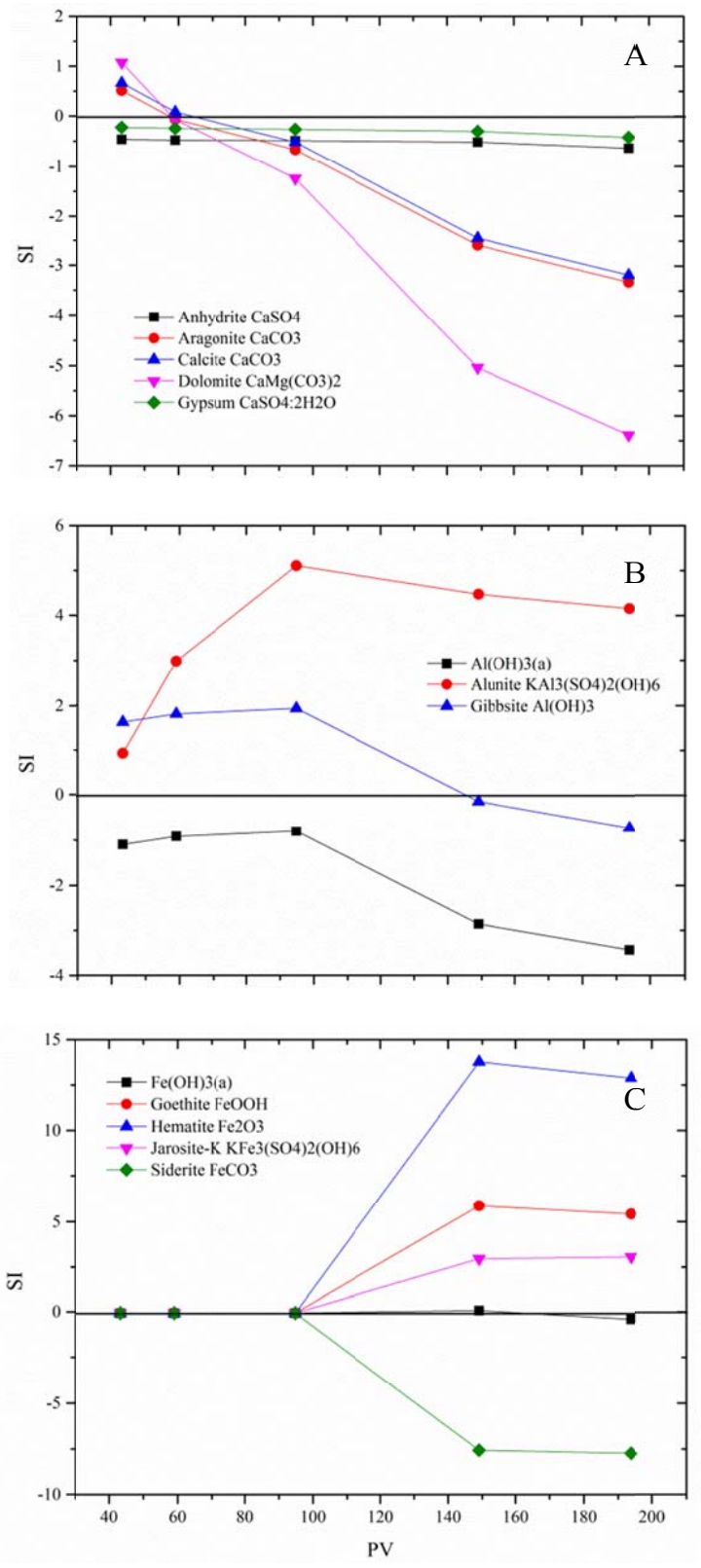


Figure 5.6 SI of different (A) calcium, (B) aluminium and (C) iron minerals calculated using PHREEQC with respect to the PV of synthetic groundwater passed through Zone 4 during the column experiment

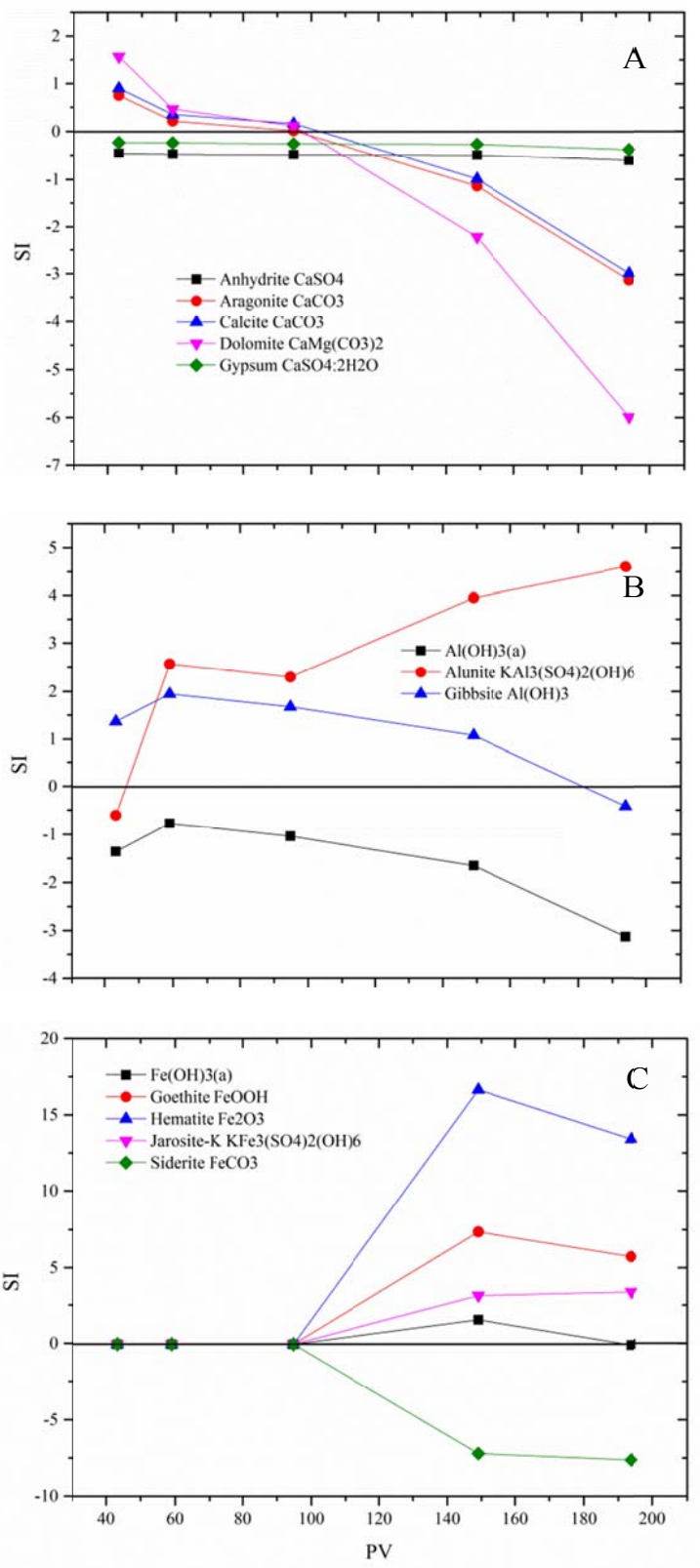


Figure 5.7 SI of different (A) calcium, (B) aluminium and (C) iron minerals calculated using PHREEQC with respect to the PV of synthetic groundwater passed through Zone 5 during the column experiment

## 5.6 Summary

Development of the geochemical algorithm was the first step involved in modelling the groundwater flow and contaminant transport through PRB in ASS terrain. Twelve primary chemical reactions involved in the acid neutralisation and metal removal were captured in the geochemical model. These reactions are responsible for the most important phase of the acid neutralisation: bicarbonate buffering zone, for the ability to remediate acidic groundwater by maintaining an almost neutral pH and complete removal of $Al^{3+}$ and total Fe from the influent solution. The kinetics of mineral precipitation/dissolution was assumed to follow transition state theory. SIs for minerals dissolving ($SI<0$) and precipitating ($SI>0$) were calculated from PHREEQC software based on the concentration of $Na^{+}$, $K^{+}$, $Ca^{2+}$, $Mg^{2+}$, $Al^{3+}$, $Fe^{3+}$, $Cl^{-}$ and $SO_4^{2-}$in the influent water along with alkalinity, pH and temperature for all 5 zones in the column.

# Chapter 6 Model application to column experiment and field PRB

## 6.1 Introduction

This chapter elaborates the multi-component reactive transport model developed for acidic groundwater remediation with the use of recycled concrete. It shows how the geochemical algorithm developed (in Chapter 5) for the reactions taking place between recycled concrete and acidic groundwater will be used to model the fate and transport of contaminants. Commercially available numerical codes, MODFLOW and RT3D were used for this purpose. Formulation of these finite difference codes is introduced and the mathematical model to calculate the head of groundwater flow has been developed and illustrated. One-dimensional reactive transport modelling was conducted based on data from laboratory column experiments to describe the geochemical evolution of groundwater along a flow path in the column experiment. Moreover, the model was applied to the field PRB, along a transect passing through the centreline of the PRB. Changes in the geochemical composition of the contaminated groundwater within the PRB after treatment with recycled concrete are also addressed. The processes potentially affecting the long-term performance of the PRB were investigated. The optimum width for another possible PRB is calculated considering the reaction kinetics and residence times.

## 6.2 MODFLOW and RT3D

The software codes MODFLOW and RT3D were used to simulate the transport and fate of contaminants in the PRB. In MODFLOW, groundwater flow is simulated

using a block-centred finite-difference approach (Harbaugh, 2005). The three-dimensional movement of groundwater of constant density through porous material is described by the following partial differential Eqn. (6.1):

$$\frac{\partial}{\partial x}\left(K_{xx}\frac{\partial h}{\partial x}\right)+\frac{\partial}{\partial y}\left(K_{yy}\frac{\partial h}{\partial y}\right)+\frac{\partial}{\partial z}\left(K_{zz}\frac{\partial h}{\partial z}\right)+W=S_s\frac{\partial h}{\partial t} \tag{6.1}$$

where, $K_{xx}$, $K_{yy}$, and $K_{zz}$ are values of hydraulic conductivity along the $x$, $y$, and $z$ coordinate axes, which are assumed to be parallel to the major axes of hydraulic conductivity (L/T), $h$ is the potentiometric head (L), $W$ is volumetric flux per unit volume representing sources and/or sinks of water, with $W<0.0$ for flow out of the groundwater system, and $W>0.0$ for flow into the system ($T^{-1}$), $S_S$ is the specific storage of the porous material (the volume of water that can be injected per unit volume of aquifer material per unit change in head) ($L^{-1}$), and $t$ is time (T).

Eqn. (6.1) describes groundwater flow under non-equilibrium conditions in a heterogeneous and anisotropic medium, provided that the principal axes of hydraulic conductivity are aligned with the coordinate directions *x, y* and *z*. Eqn. (6.1), implies that the flow and/or head conditions at the boundaries of an aquifer and specification of initial head conditions constitutes a mathematical representation of a groundwater flow system. An analytical solution of Eqn. (6.1) is the algebraic expression giving *h(x,y,z,t)* when the derivatives of *h* with respect to space and time are substituted into Eqn. (6.1), provided that the equation and its initial and boundary conditions are satisfied. A time varying head distribution of this nature characterises the flow system. It measures both the energy of flow and the volume of water in storage, and can be used to calculate directions and rates of movement. Except for very simple systems, analytical solutions of Eqn. (6.1) are rarely possible, so various numerical

methods must be employed to obtain approximate solutions (Harbaugh, 2005, Rowe et al., 2004).

One such approach is the finite difference method, wherein the continuous system described by Eqn. (6.1) is replaced by a finite set of discrete points in space and time. The partial derivatives are replaced by terms calculated from the differences in head values at these points. The process leads to systems of simultaneous linear algebraic difference equations. Their solution yields values of head at specific points and times. These values represent an approximation to the time varying head distribution that would be given by an analytical solution of the partial differential equation of flow. In Eqn. (6.1), head ($h$) is a function of time as well as space. Therefore, in the finite difference formulation, discretisation of the continuous time domain is also required. Time is broken into time steps, and the head is calculated at each time step.

Development of the groundwater flow equation in finite difference form pursues from the application of the continuity equation. In the continuity equation, the sum of all flows in and out of the cell must be equal to the rate of change in storage within the cell. Assuming that the density of groundwater is constant, the continuity equation expressing the balance of flow for a cell is:

$$\sum Q_i = SS \frac{\Delta h}{\Delta t} \Delta V \tag{6.2}$$

where, $Q_i$ is the flow rate into the cell ($L^3T^{-1}$), $\Delta V$ is the volume of the cell ($L^3$), and $\Delta h$ is the change in head over a time interval of $\Delta t$.

The right side of the continuity equation is equivalent to the volume of water taken into storage over a time interval of $\Delta t$ given a change in head of $\Delta h$. Eqn. (6.2) is stated in terms of inflow and storage gain. Outflow and loss are represented by defining outflow as negative inflow and loss as negative gain, respectively (Harbaugh, 2005).

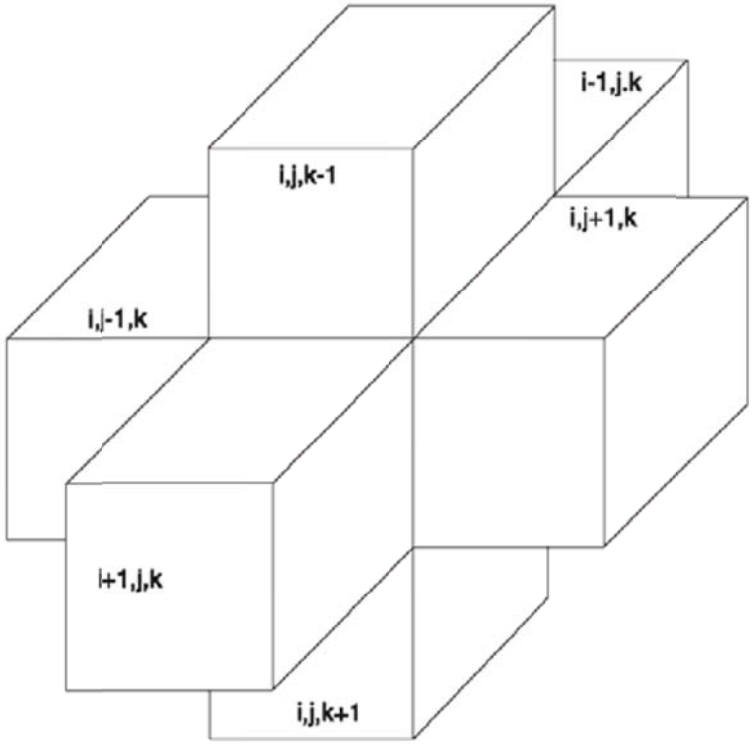


Figure 6.1 Indices for the six adjacent cells surrounding cell *i,j,k* (hidden) (Harbaugh, 2005)

Figure 6.1 shows six aquifer cells adjacent to cell *i,j,k* (hidden) — *i-1,j,k; i+1,j,k; i,j-1,k; i,j+1,k; i,j,k-1;* and *i,j,k+1*. The flows are considered positive if they are entering cell *i,j,k* (the negative sign usually incorporated in Darcy's law has been dropped from all terms). Following these conventions, flow into cell *i,j,k* in the row direction from cell *i,j-1,k* (Figure 6.2), is given by Darcy's law as:

$$q_{i,j-1/2,k} = KR_{i,j-1/2,k}\Delta c\Delta v_k \frac{\left(h_{i.j-1,k} - h_{i,j,k}\right)}{\Delta r_{j-1/2}} \tag{6.3}$$

where, $h_{i,j,k}$ is the head at node *i,j,k*, and $h_{i,j-1,k}$ is the head at node *i,j-1,k*, $q_{i,j-1/2,k}$ is the volumetric flow rate through the face between cells *i,j,k* and *i,j-1,k* ($L^3T^{-1}$), $KR_{i,j-1/2,k}$ is the hydraulic conductivity along the row between nodes *i,j,k* and *i,j-1,k* ($LT^{-1}$), $\Delta c_i \Delta v_k$ is the area of the cell faces normal to the row direction; and $\Delta r_{j-1/2}$ is the distance between nodes *i,j,k* and *i,j-1,k* (L).

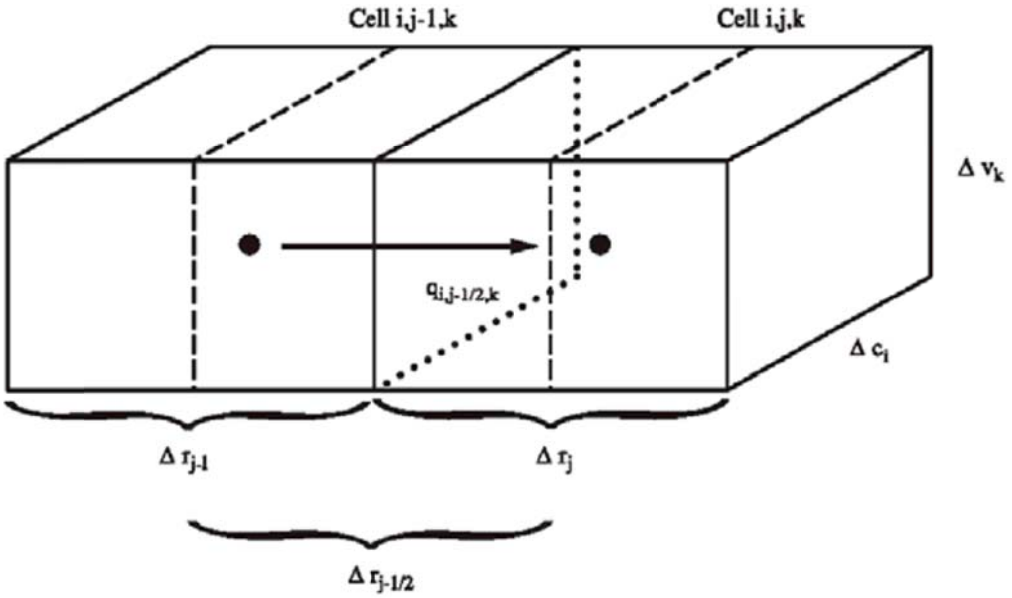


Figure 6.2 Flow into cell i,j,k from cell i, j-1,k (Harbaugh, 2005)

MODFLOW (a modular three dimensional finite difference groundwater flow model) employs iterative methods to obtain the solution to the finite difference equations for each time step. In the example given in Figure 6.3, a total of *n* iterations are required to achieve closure for the heads at the end of time step *m*. Therefore, the array of final head values for the time step is designated $h^{m,n}$. Figure 6.3 also shows that the array of final head values for the end of the earlier time step is

$h^{m-1,n}$. Again it is assumed that $n$ iterations were required for convergence. Because they represent heads for the preceding time step, for which computations have already been completed, they appear as predetermined constants in the equation for time step $m$; thus they retain the same value in each iteration of the time step. Similarly, the final values of head for time step $m$ are used as constants in the storage term during calculations for time step $m+1$.

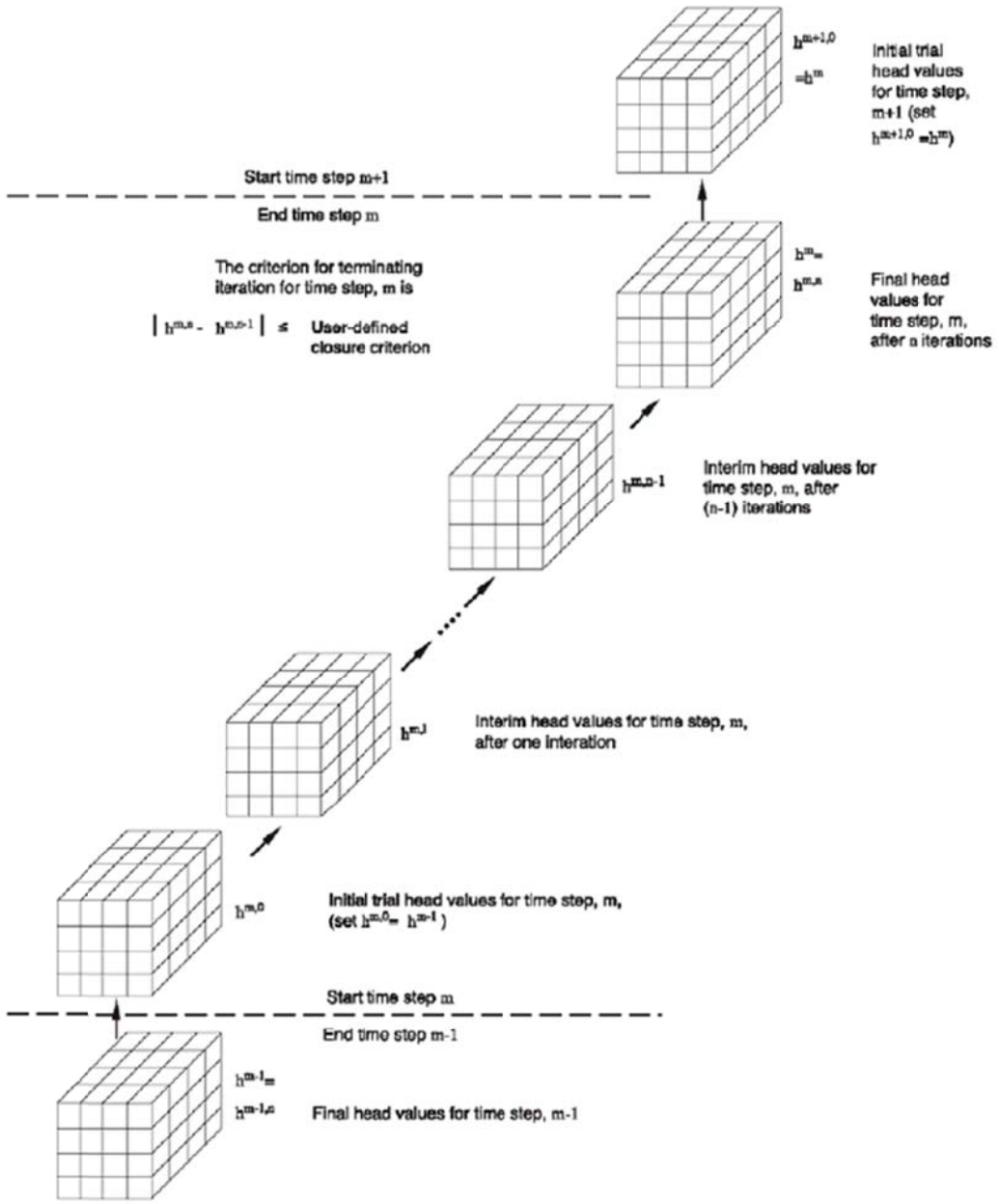


Figure 6.3 Iterative calculation of head distribution (McDonald and Harbaugh., 1988)

RT3D is a computer code which solves the coupled partial differential equations that describe reactive flow and transport of multiple mobile and/or immobile species in three dimensional saturated groundwater systems. The RT3D code includes an implicit reaction solver. It makes the code sufficiently flexible for simulating various types of chemical and microbial reaction kinetics. RT3D supports seven pre-programmed reaction modules that can be used to simulate different types of reactive contaminants. They are benzene-toluene-xylene mixtures (BTEX) of instantaneous aerobic degradation, kinetic limited degradation, rate limited sorption reactions, double monod model, sequential decay reactions, and chlorinated solvents such as tetrachloroethene (PCE) and TCE. In addition, RT3D has a user-defined reaction option that can be used to simulate any other type of user specified reactive transport systems. In this study, a user-defined reaction module was used with the geochemical algorithm explained in Chapter 5.

The general macroscopic equations describing the fate and transport of aqueous (Eqn. (6.4)) and solid phase species (Eqn. (6.5)), in multi-dimensional saturated porous media are written as:

$$\frac{\partial C_k}{\partial t} = \frac{\partial}{\partial x_i}\left( D_{ij} \frac{\partial C_k}{\partial x_j} \right) - \frac{\partial}{\partial x_i}\left(v_i C_k\right) + \frac{q_s}{\phi} C_{s_k} + r_c \text{, where } k = 1, 2,...,m \tag{6.4}$$

$$\frac{d\widetilde{C}_{im}}{dt} = \widetilde{r}_c \text{, where, } im = 1, 2,... \tag{6.5}$$

where, $k$ is the total number of species, $m$ is the total number of aqueous-phase (mobile) species (thus, $k$ minus $m$ is the total number of solid phase or immobile species), $C_k$ is the aqueous phase concentration of the $k^{th}$ species [$ML^{-3}$], $C_{im}$ is the

solid phase concentration of the $im^{th}$ species [either $MM^{-1}$ (contaminant mass per unit mass of porous media) or $ML^{-3}$ (contaminant mass per unit aqueous phase volume) unit basis can be used], $D_{ij}$ is the hydrodynamic dispersion coefficient [$L^2T^{-1}$], $v$ is the pore velocity [$LT^{-1}$], $\phi$ is the soil porosity, $q_s$ is the volumetric flux of water per unit volume of aquifer representing sources and sinks [$T^{-1}$], $C_s$ is the concentration of source/sink [$ML^{-3}$], $r_c$ represents the rate of all reactions that occur in the aqueous phase [$ML^3T^{-1}$], and $\widetilde{r}_c$ represents the rate of all reactions that occur in the soil phase (either $MM^{-1}T^{-1}$ or $ML^3T^{-1}$ can be used).

RT3D code was developed to solve the multi-species reactive transport, Eqns. (6.4) and (6.5). The code employs a reaction operator-split (OS) numerical strategy to solve the coupled transport equations (of the form Eqn. (6.4) and Eqn. (6.5)). Walter et al. (1994b) have successfully used a similar OS approach to solve multi-component transport with geochemical reactions. Moreover, Clement et al. (1996) used the OS strategy to solve a biologically reactive flow problem in a radial system. Valocchi et al. (1992) and Kaluarachchi et al. (1995) brought attention to the fact that the splitting the reaction terms using the standard OS strategy may have numerical limitations. They recommended an improved alternative OS strategy that may give more accurate numerical results. Nevertheless, Barry et al. (1995) states that the improvement provided by the alternative OS may not be applicable for multi-component nonlinear problems. In addition, they demonstrated the efficiency of the standard OS approach, by solving a two-species reactive transport problem. In this work, we used the standard OS strategy, to develop a general numerical solution scheme for solving the coupled partial/ordinary differential Eqns. (6.4) and (6.5).

Utilising the OS strategy, the mobile species transport equation (Eqn. (6.4)) is first divided into four distinct equations: the advection equation:

$$\frac{\partial C}{\partial t} = -\frac{\partial (v_i C)}{\partial x_i} \tag{6.6}$$

the dispersion equation:

$$\frac{\partial C}{\partial t} = -\frac{\partial}{\partial x_i}\left( D_{ij} \frac{\partial C}{\partial x_j} \right) \tag{6.7}$$

the source/sink mixing equation:

$$\frac{\partial C}{\partial t} = \frac{q_s}{\phi} C_s \tag{6.8}$$

and, the reaction equation:

$$\frac{\partial C}{\partial t} = r \tag{6.9}$$

where, the term $r$ represents all possible reaction terms that appear in a typical mobile species transport equation. Note that in Eqn. (6.9), which is for a typical immobile species, the advection, dispersion, and source-sink mixing terms are zero and only the reaction term exists. The advection equation can be solved by the method of characteristics, a modified method of characteristics, a hybrid method of characteristics, or by the upstream finite difference solution scheme (Zheng and Wang, 1999). The dispersion and source-sink mixing packages use explicit finite difference approximations.

The reaction Eqn. (6.9) can be adjusted according to the study and the reactions taking place. This is the most versatile option available in RT3D. Using this option, one can describe and solve any type of kinetic-limited reactive transport problem.

The reaction information is input through a Fortran 90 subroutine, which should be compiled as a dynamic link library (DLL) using either the Microsoft Fortran Power station 4.0 or the Digital DVF Fortran compiler (Clement, 1997).

## 6.3 Change of mineral quantity over time

The intent of this study was to develop a model to understand mineral fouling in PRBs in ASS terrain, incorporating a calibrated flow and a reactive transport model to simulate mineral deposition and its effects on hydraulic parameters. It has been found that the key factors reducing PRB longevity and efficiency are geochemical factors such as armouring and/or clogging. Chemical armouring is the strong adhesion and entire pacification of the reactive surface by encrustation leading to a decrease in the rate and extent of reactive material dissolution and alkalinity production of the reactive material (Cravotta and Trahan, 1999, Indraratna et al., 2014). Clogging is the accumulation of precipitates in the void spaces between the reactive materials (Gavaskar, 1999). Both these phenomena directly affect the change of porosity and, hence, decrease in hydraulic conductivity. Moreover, this will result in reducing flow through the barrier, therefore changing the flow paths, residence time and finally bypassing the PRB altogether (Johnson et al., 2005, Mackenzie et al., 1999, Wilkin et al., 2002). Therefore, it is of utmost importance to study the armouring and clogging behaviour in order to monitor the efficiency and longevity of PRB.

Secondary minerals precipitated in the recycled concrete media were assumed to be immobile. The pore space occupied by each mineral was calculated from the respective molar volume. The volume prediction at a given location due to secondary

mineral precipitation was computed as the total volume occupied by the mineral precipitates minus the volume achieved by the dissolution of Ca-bearing minerals in recycled concrete. The associated porosity reductions (Eqn. (6.11)) were calculated using Eqn. (6.10) as suggested by Steefel and Lasaga (1994), thus:

$$\frac{\partial \Phi_k}{\partial t} = M_k R_k \tag{6.10}$$

Hence, the change in porosity with time can be obtained from:

$$n_t = n_0 - \sum_{k=1}^{N_m} M_k R_k t \tag{6.11}$$

where, $\Phi_k$ is the volume fraction of mineral, $M_k$ is the mineral molar volume ($m^3mol^{-1}$), $R_k$ is the overall reaction rate for the mineral ($molm^{-3}{}_{bulk}s^{-1}$), $N_m$ is the number of minerals, $t$ is the time $n_o$ and $n_t$ are the porosities at the start and at time $t$, respectively.

The product of $M_kR_k$ is constant for a given time step. In the next time step, the new value of $R_k$ is introduced to the equation based on the results obtained from Eqns. 5.14 and 5.15 (in Chapter 5) for respective time steps. The Kozeny Carmen equation can be used to estimate the hydraulic conductivity at different PVs with the change of dissolved/precipitated minerals with time:

$$K = \frac{1}{5M^2}\left(\frac{\rho_w g}{\mu}\right)\frac{n^3}{(1-n)^2} \tag{6.12}$$

where, $n$ is the porosity of the reactive medium, $M$ is the specific surface of the recycled concrete particles (ratio of surface area and bulk volume), $\rho_w$ is the density of water, $g$ is the gravitational constant, and $\mu$ is the absolute viscosity of water. Mineral precipitation and dissolution may change the value of $M$. However, the

relationship is a complex function of the geometry of the recycled concrete particles, the shape of the minerals being precipitated, and the location of the mineral precipitates. Therefore, *M* was assumed constant, which is a conservative approach (Li et al. 2005).

The normalised Kozeny Carmen equation (Eqn. (6.13)) was used to estimate the hydraulic conductivity at different pore volumes (PV) with the change of dissolved/precipitated minerals with time (Li et al., 2006, Pathirage et al., 2012, Indraratna et al., 2014).

$$K = K_0 \left[ \frac{n_0 - \Delta n_t}{n_0} \right]^3 / \left[ \frac{1 - n_0 + \Delta n_t}{1 - n_0} \right]^2 \tag{6.13}$$

where, $\Delta n_t$ is the reduction in porosity at time *t*.

It is important to capture this change of porosity and hydraulic conductivity in the groundwater flow model. The head solution for transient groundwater flow in one dimension is given by Eqn. (6.16), which was used to calculate the starting head for MODFLOW at every time step. The reason to adopt this approach was because MODFLOW does not have a way of automatically changing the porosity or hydraulic conductivity unless they are manually entered. It was important to update these values at every time step due to the changes in volume fractions of primary and secondary minerals. For instance, when the model is run for the 1$^{st}$ time step, the corresponding values of porosity and hydraulic conductivity are updated for the 2$^{nd}$ time step, and Eqn. (6.16) is now required to determine the resulting head as that is an essential input for MODFLOW to continue the analysis for subsequent time steps (Indraratna et al., 2014). MODFLOW was used to couple the chemical reaction

component developed in RT3D with advection, diffusion and dispersion (Eqn. (6.4)) using finite difference method. Once the starting head was calculated by the analytical model, the results were put into MODFLOW. Then MODFLOW and RT3D were run in tandem to get the concentrations of reactants at every time step.

Transient groundwater flow in one dimension is governed by:

$$\frac{\partial^2 h}{\partial x^2} = \frac{S}{T}\left(\frac{\partial h}{\partial t}\right) \tag{6.14}$$

$$T = Kb \tag{6.15}$$

The variation in hydraulic conductivity due to dissolution/precipitation of minerals can be calculated from Eqn. (6.13). The solution for Eqn. (6.14) considering the changes in hydraulic conductivity (Eqn. (6.13)) can be written as:

$$h = \left( \exp\left[ -\frac{\mu^2 b K_0}{S\sum_{k=1}^{N_m} M_k R_k} \frac{(1-n_0)^2}{n_0^3} \left\{ \alpha^2 \left( 1.5 + {}^{1}\!/\!_{\beta} \right) - 3(\alpha + \ln\beta) \right\} \right] \right) \cdot \tag{6.16a}$$

$$\left(C \sin \mu x + D \cos \mu x\right)$$

where,

$$\alpha = n_0 + \sum_{k=1}^{N_m} M_k R_k t \tag{(6.16b)}$$

$$\beta = 1 - n_0 - \sum_{k=1}^{N_m} M_k R_k t \tag{(6.16c)}$$

The step by step procedure for obtaining Eqn. (6.16) is illustrated in Appendix I.

The following initial conditions can be used to calculate the values for $\mu$, $C$ and $D$.

$h = h_1$ at $x=0$ and $t=0$, (6.17)

$h = h_2$ at $x=l$ and $t=0$, (6.18)

$$\frac{\partial h}{\partial t} = 0 \text{ at } x=0 \text{ and } t=0 \tag{6.19}$$

## 6.4 Step by step involved in the model development

1. Groundwater flow through porous media is modelled by the 1D formulation of Eqn. (6.1) in MODFLOW.

$$\frac{\partial}{\partial x}\left(K_{xx}\frac{\partial h}{\partial x}\right)+\frac{\partial}{\partial y}\left(K_{yy}\frac{\partial h}{\partial y}\right)+\frac{\partial}{\partial z}\left(K_{zz}\frac{\partial h}{\partial z}\right)+W=S_s\frac{\partial h}{\partial t} \tag{6.20}$$

2. Change of mineral quantity over time is calculated by the reaction kinetics and molar volume of each mineral using Eqn. (6.10).

$$\frac{\partial \Phi_k}{\partial t} = M_k R_k \tag{6.21}$$

3. Change in porosity due to change in mineral fractions are captured by Eqn. (6.11).

$$n_t = n_0 - \sum_{k=1}^{N_m} M_k R_k t \tag{6.22}$$

4. The normalised Kozeny Carmen equation (Eqn. 6.13) is used to calculate the associated change in hydraulic conductivity.

$$K = K_0\left[\frac{n_0-\Delta n_t}{n_0}\right]^3 / \left[\frac{1-n_0+\Delta n_t}{1-n_0}\right]^2 \tag{6.23}$$

5. MODFLOW does not have a way of automatically changing the porosity or hydraulic conductivity unless they are manually entered. It is important to

capture this change of porosity and hydraulic conductivity in the groundwater flow model. Thus Eqn. (6.1) is solved to capture the change in head with respect to change in hydraulic conductivity from mineral dissolution and precipitation. The solution is given by Eqn. (6.16).

$$h = \left( \exp\left[ -\frac{\mu^2 b K_0}{S\sum_{k=1}^{N_m} M_k R_k} \frac{(1-n_0)^2}{n_0^3} \left\{ \alpha^2 \left( 1.5 + {}^{1}\!/\!_{\beta} \right) - 3(\alpha + \ln\beta) \right\} \right] \right) \cdot \tag{6.24a}$$

$$\left(C \sin \mu x + D \cos \mu x\right)$$

where,

$$\alpha = n_0 + \sum_{k=1}^{N_m} M_k R_k t \tag{6.16b}$$

$$\beta = 1 - n_0 - \sum_{k=1}^{N_m} M_k R_k t \tag{6.16c}$$

For instance, when the model is run for the 1st time step, the corresponding values of porosity and hydraulic conductivity are updated for the 2nd time step, and Eqn. (6.16) is now required to determine the resulting head as that is an essential input for MODFLOW to continue the analysis for subsequent time steps.

6. The advection, diffusion and dispersion equation (Eqn. (6.4)) is used for the contaminant transport. This equation is available in RT3D.

$$\frac{\partial C_k}{\partial t} = \frac{\partial}{\partial x_i}\left( D_{ij} \frac{\partial C_k}{\partial x_j} \right) - \frac{\partial}{\partial x_i}\left( v_i C_k \right) + \frac{q_s}{\phi} C_{s_k} + r_c \tag{6.25}$$

For the dissolution/precipitation reactions taking place between acidic groundwater and recycled concrete, the kinetic reaction expression ($r$) in Eqn. 5.14 multiplied by $M$ (molar volume of the mineral) can be replaced by $r_c$ in Eqn. 6.4.

7. Then MODFLOW and RT3D were run in tandem to get the concentrations of reactants at every time step.

8. Although, a 2D grid is used to show the discretisation of finite different domain, 1D transport is considered in the mathematical model development and model application to both column experiment and field PRB.

## 6.5 Model application to column experiment

Firstly, multi-component reactive transport simulations were undertaken for quantitative simulation of the remediation process for more controlled conditions in the laboratory column experiments. The focus was to develop a simple conceptual model using reactive transport modelling, based on the detailed data obtained from the column influent and effluent chemistry. Therefore, to investigate how the mineralogical assembly within the recycled concrete affects the change in pH and long-term metal removal capability of the reactive mixture. Secondly, the model was applied for performance monitoring in the field PRB under varying field conditions.

The column experiment was considered to be a confined aquifer with transient flow conditions. The crushed concrete in the column was assumed to be homogeneous and isotropic. A relatively uniform particle gradation was selected for the column test and also it was assumed that the particle angularity is generally similar (as it was impossible to find all rounded particles of broken concrete aggregates). Therefore, for simplicity the assumption of a continuum with homogeneity and isotropy is made along the column length. Since, the flow is only vertical (one dimensional) in the column, the negative implications of this assumptions are expected to be minimal.

Indraratna et al. (1993) indicated that for granular media, the width or diameter of the test chamber to maximum particle size ratio > 8 would make boundary effects generally insignificant. The same concepts have been applied for filtration testing of rail ballast and other rockfill for dams (Indraratna et al., 1998). In this study, given the diameter of the column as 50 mm, and the maximum particle size approximately 4-5 mm, the corresponding ratio is above 10, hence, boundary effects can be considered to be insignificant.

In the 1D column domain, 50 cm of recycled concrete was divided into five zones, where the bottom most one is Zone 1 and the topmost one is Zone 5. This whole domain was discretised uniformly into 50 × 5 sections, where 1 unit is 100 mm. A schematic diagram of the boundary conditions is shown in Figure 6.4. The sides of the column are no flow boundaries.

Table 6.1 summarises the experimental parameters and model inputs. Mineral dissolution-precipitation reactions were modelled as kinetically-controlled reactions. Because of their potential variability of in-situ rate coefficients (Li et al., 2006), the kinetic reaction rate coefficient ($k_{eff}$) was obtained for $Ca^{2+}$, $Al^{3+}$ and total Fe ($Fe^{2+}$ and $Fe^{3+}$) (Table 6.2) by calibrating the model against the laboratory column data provided by (Regmi et al., 2011b) and using the molar weights of $Ca^{2+}$, $Al^{3+}$, $Fe^{2+}$ and $Fe^{3+}$. The total Fe was calculated by adding the $Fe^{2+}$ and $Fe^{3+}$ according to their stoichiometric relationships as illustrated in the geochemical algorithm in Chapter 5.

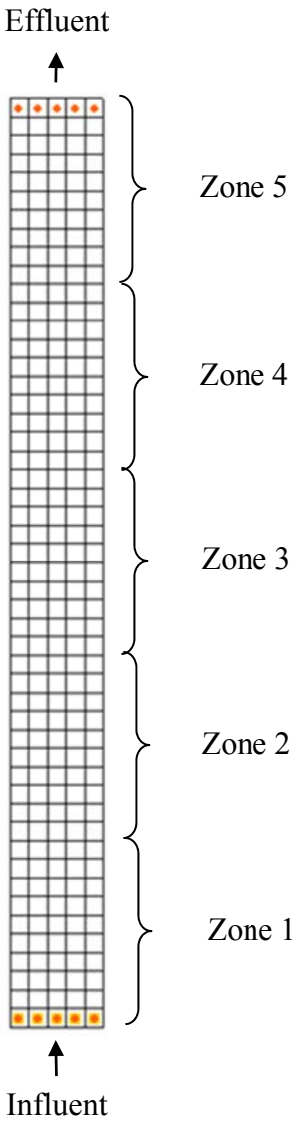


Figure 6.4 Boundary conditions in 1D discretised solution domain of the column

Table 6.1 Experimental and model parameters

| Property | Experiment | Model (Lab) | Model (Field) |
|---|---|---|---|
| Flow | 1.2 mL/min | 1.2 mL/min | 1.1 x $10^6$ L/year |
| Initial porosity ($n_0$) | 0.69 | 0.69 | 0.5 |
| Initial hydraulic conductivity ($K_0$) | 0.9565 m/d | 0.9565 m/d | 0.1 m/s |
| pH of influent | 2.8 | 2.8 | 3.6 |

The calibrated rate coefficients were obtained by manual trial and error as undertaken by Li et al. (2006). The corresponding reaction kinetics (listed in Table

6.2) were then used to validate the current model using the column experiment data in this study. The calibration was done for the 40-190 PV range using data from Regmi et al. (2011b) and the current model was validated for the same PV range. This is an important experimental phase for maintaining neutral pH and for 100% removal of Al and Fe ions. Model parameters used for calibration and validation process are listed in Table 6.3.

Table 6.2 Kinetic reaction rate coefficients ($k_{eff}$) for the mineral dissolution/precipitation which are calibrated values from the data provided by (Regmi et al., 2011b).

| Mineral phase | Kinetic reaction rate coefficient ($k_{eff}$) (mol/L.s) | Kinetic reaction rate coefficient ($k_{eff}$) (mol/L.s) in literature[e] |
|---|---|---|
| $Ca^{2+}$ | $2.27 \times 10^{-7}$ | $(1 \times 10^{-6})$ |
| $Al^{3+}$ | $6.86 \times 10^{-8}$ | $(9.0 \times 10^{-7} – 1.0 \times 10^{-8})$ |
| Total Fe ($Fe^{2+}$ and $Fe^{3+}$) | $5.87 \times 10^{-8}$ | $(1.0 \times 10^{-7} – 1.2 \times 10^{-8})$ |

Note: [e] Source: (Ouangrawa et al., 2009) and (Jurjovec et al., 2004)

Table 6.3 Calibration and validation parameters used in the model application for range 40-190 PV.

| | Calibration | Validation |
|---|---|---|
| Data set | | |
| $k_{eff}$ for $Ca^{2+}$, $Al^{3+}$ and Total Fe ($Fe^{2+}$ and $Fe^{3+}$) | Data from Regmi et al. (2011a) | Current data |
| State variables | | |
| $[Ca^{2+}]$, $[Al^{3+}]$, $[Fe^{2+}]$ and $[Fe^{3+}]$ | Effluent concentrations (after Regmi et al. (2011a)) | Current data on effluent concentration |

The reaction between the acidic water and the concrete that caused leaching of the Ca also reduced the pH of the effluent from pH 9.6 initially to 8 within 15 PVs

(Figure 6.5), after which there was a slow decrease (pH dropping from 7.9 at 25 PV to 7.5 at 125 PV), a faster drop from pH 7.5 at 125 PV to about 6.8 at about 185 PV, a rapid drop from pH 6.8 at 185 PV to 4 at about 215 PV, and then another period with a slower rate of increase from pH 4 at 215 PV to 3.1 to about 295 PV at test termination. According to Indraratna et al. (2010), the initial drop in pH (after 15 PVs passed through the column) was assumed to be due to the depletion of carbonate alkalinity. The model predicted values for the first pH plateau is shown in Figure 6.5. In this model prediction, $OH^-$ in the aqueous phase was assumed to be in equilibrium.

However, after reaching a pH value of 6.8 (after 190 PVs), the pH subsequently diminishes to 4 (Figure 6.5). This is probably due to the $OH^-$ ion in equilibrium state during the depletion of carbonate minerals (Indraratna et al., 2010). The experimental and predicted values of pH along the column are shown in Figure 6.6. In SP1, the rapid jump occurred at pH 6.5, (Figure 6.5) which took place within 25 PVs, which is fast due to the rapid neutralisation of acidity and the exhaustion of the reactive material at the entrance of the column. In contrast in SP1, 2, 3 and 4, excessive sampling of the column was avoided in order to ensure minimum disturbance to the flow. That is probably the reason why a rapid jump was not visible in the pH values inside the column. In the early stages of the experiment, most of the Al in the synthetic groundwater precipitated shortly after entering the column and was no longer in the pore water (Figure 6.8 and Figure 6.11). Al precipitates when the pH is above 4.5. Al was observed in the effluent water for the first time when the pH of the effluent dropped to 4, after which the concentration of Al continued to increase (Figure 6.8) because of its high solubility at pH<4. Similarly, Fe also precipitated when the pH exceeded 3.5. Until 255 PV, the effluent pH did not drop below pH 3.5;

accordingly, the Fe content of the effluent (<1 mg/L) was negligible throughout the duration of the column test (Figure 6.9 and Figure 6.12).

The predicted and measured concentration profiles of $Ca^{2+}$, $Al^{3+}$ and total Fe (Figures 6.7-6.9) are in very good agreement. Figures 6.10-6.12 show the model outputs for $Ca^{2+}$, $Al^{3+}$ and total Fe. In the model, $Fe^{2+}$ and $Fe^{3+}$ are considered separately and later combined to compare with the experiment values (Indraratna et al., 2014). The precipitation of secondary minerals (i.e. $Fe(OH)_3$, $Fe(OOH)$, $Fe_2O_3$, $Fe(OH)_2$, $FeCO_3$, $Al(OH)_3$) significantly decreases the efficiency of the reactive material due to the armouring effect.

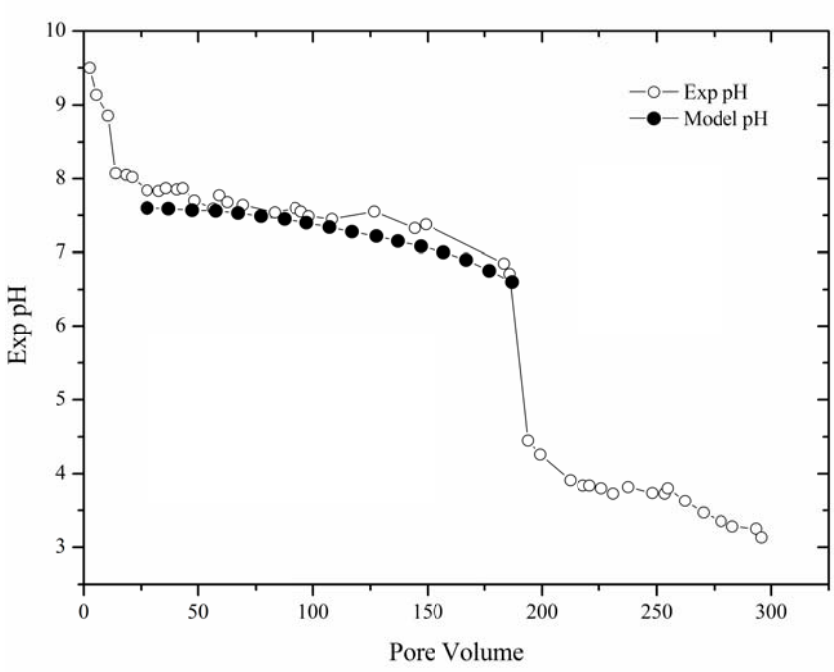


Figure 6.5 Predicted and experimental results of pH at the effluent (Indraratna et al., 2014)

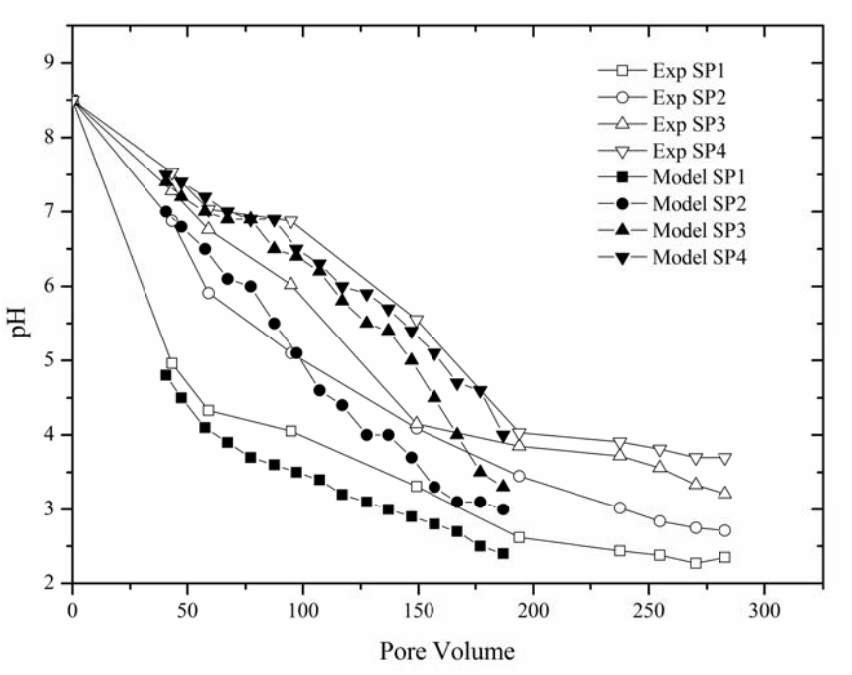


Figure 6.6 Predicted and experimental results of pH at the sampling points along the column (Indraratna et al., 2014)

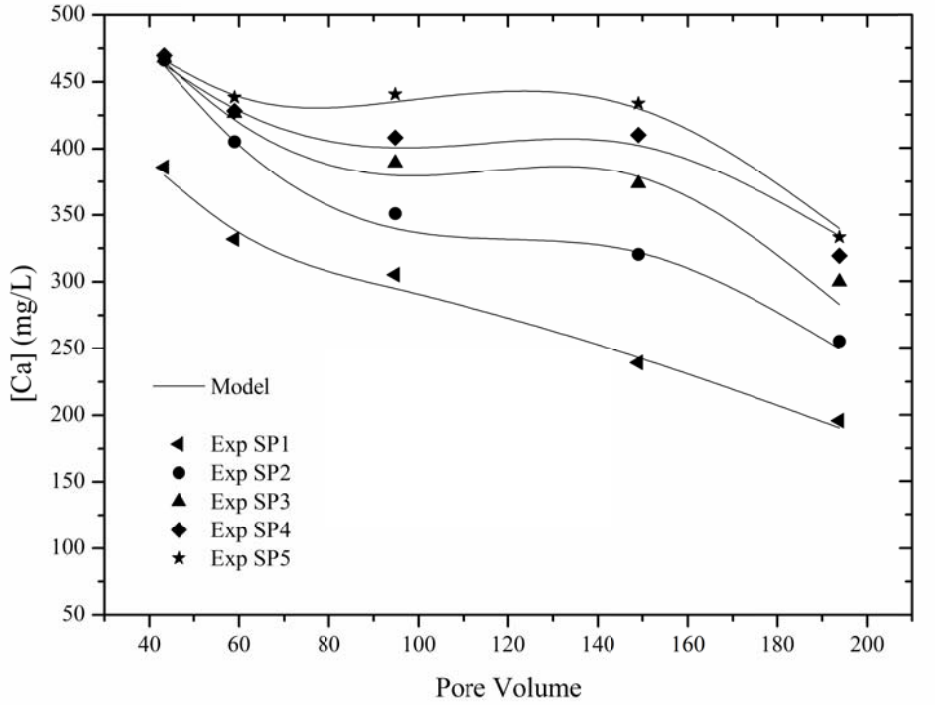


Figure 6.7 $Ca^{2+}$ concentrations of model predicted values vs. experimental values at sampling points along the column (Indraratna et al., 2014)

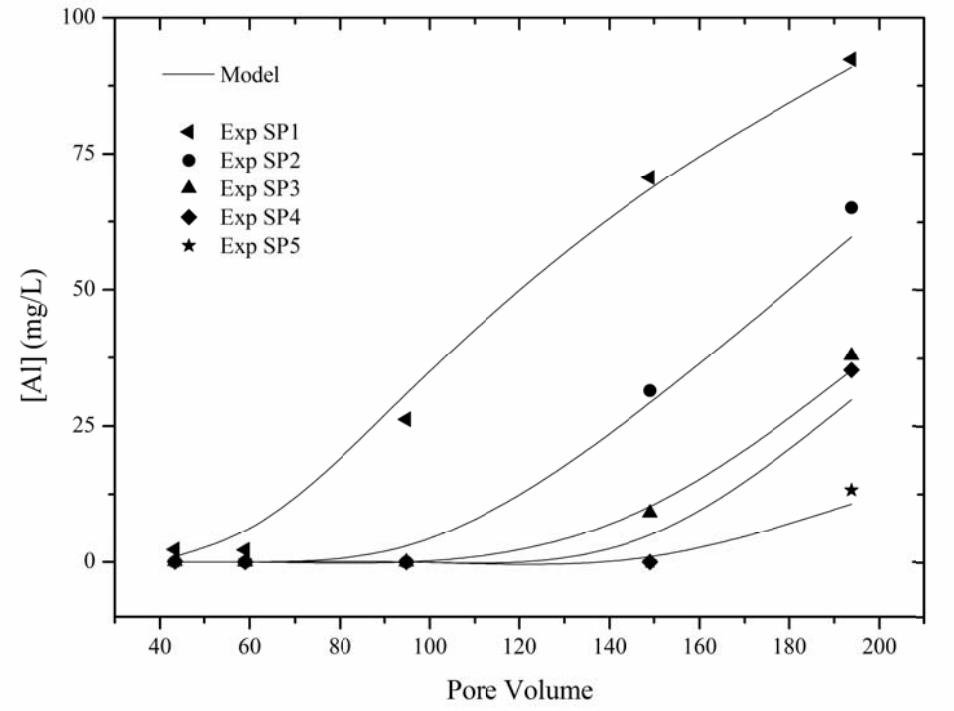


Figure 6.8 Calculated and measured $Al^{3+}$ concentrations at sampling points along the column (Indraratna et al., 2014)

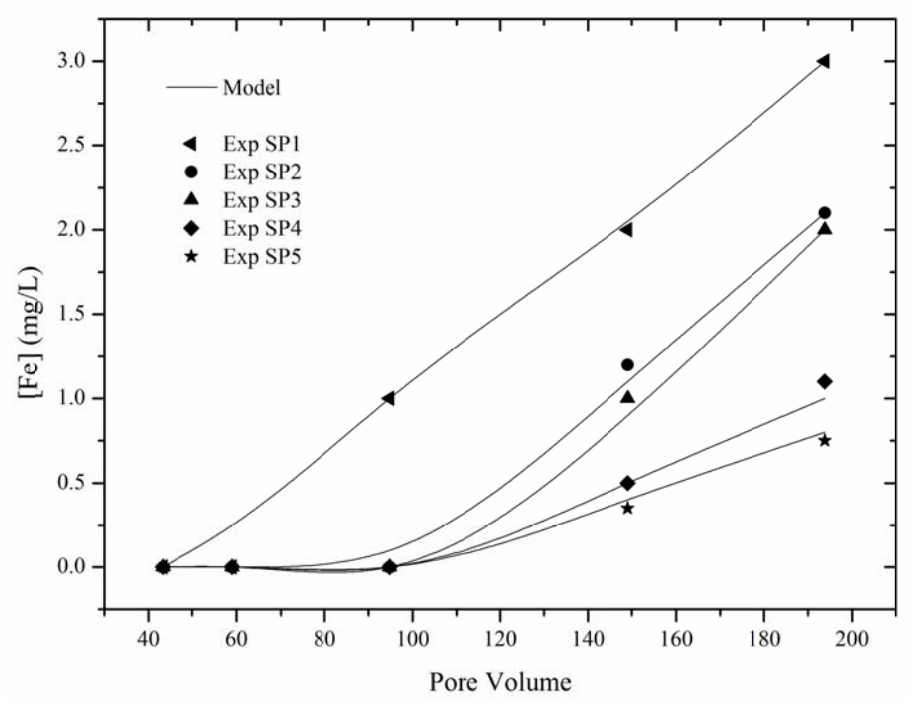


Figure 6.9 Calculated and measured total Fe ($Fe^{2+}$ and $Fe^{3+}$) concentrations at sampling points along the column (Indraratna et al., 2014)

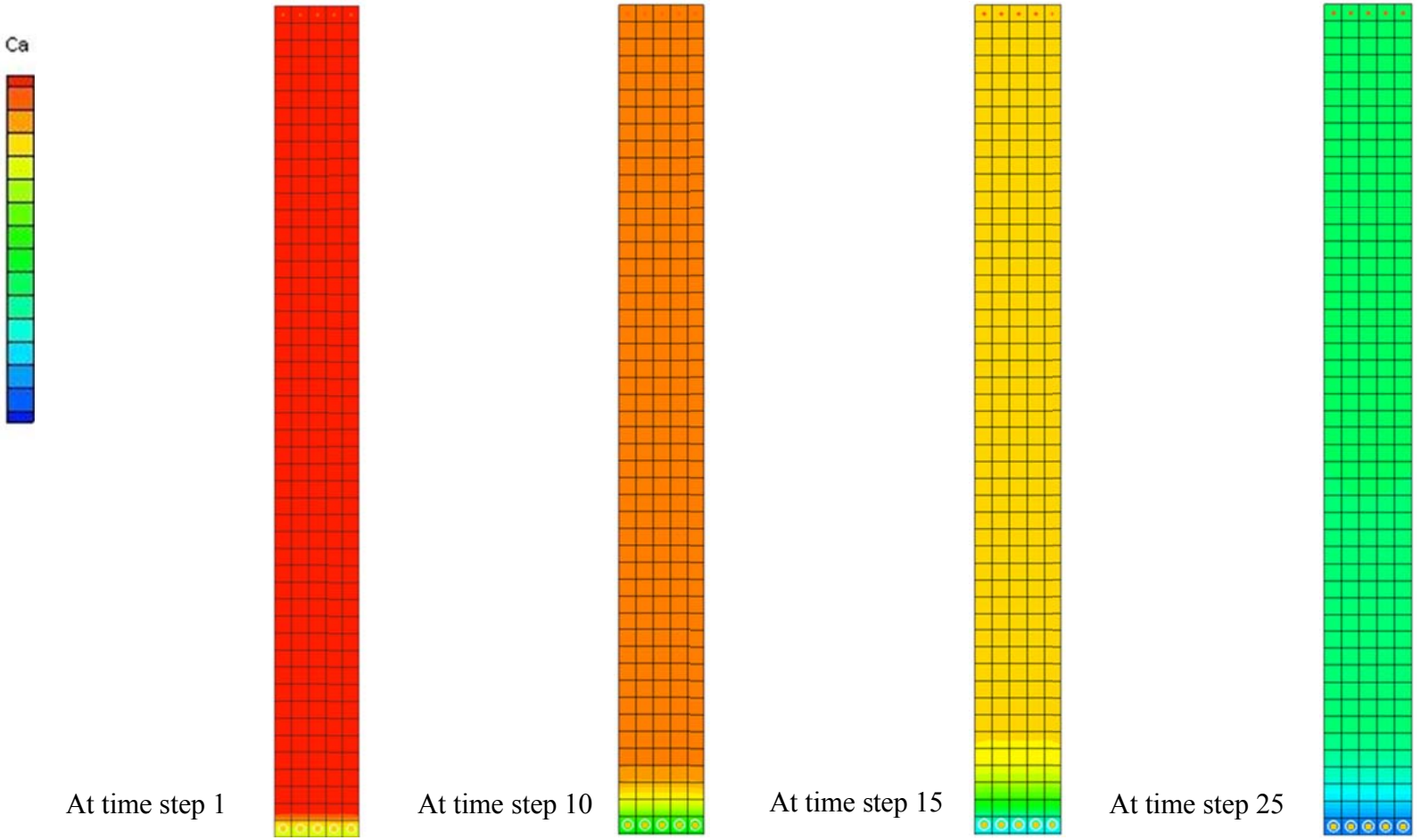


Figure 6.10 Model outputs for the $Ca^{2+}$ concentrations along the column

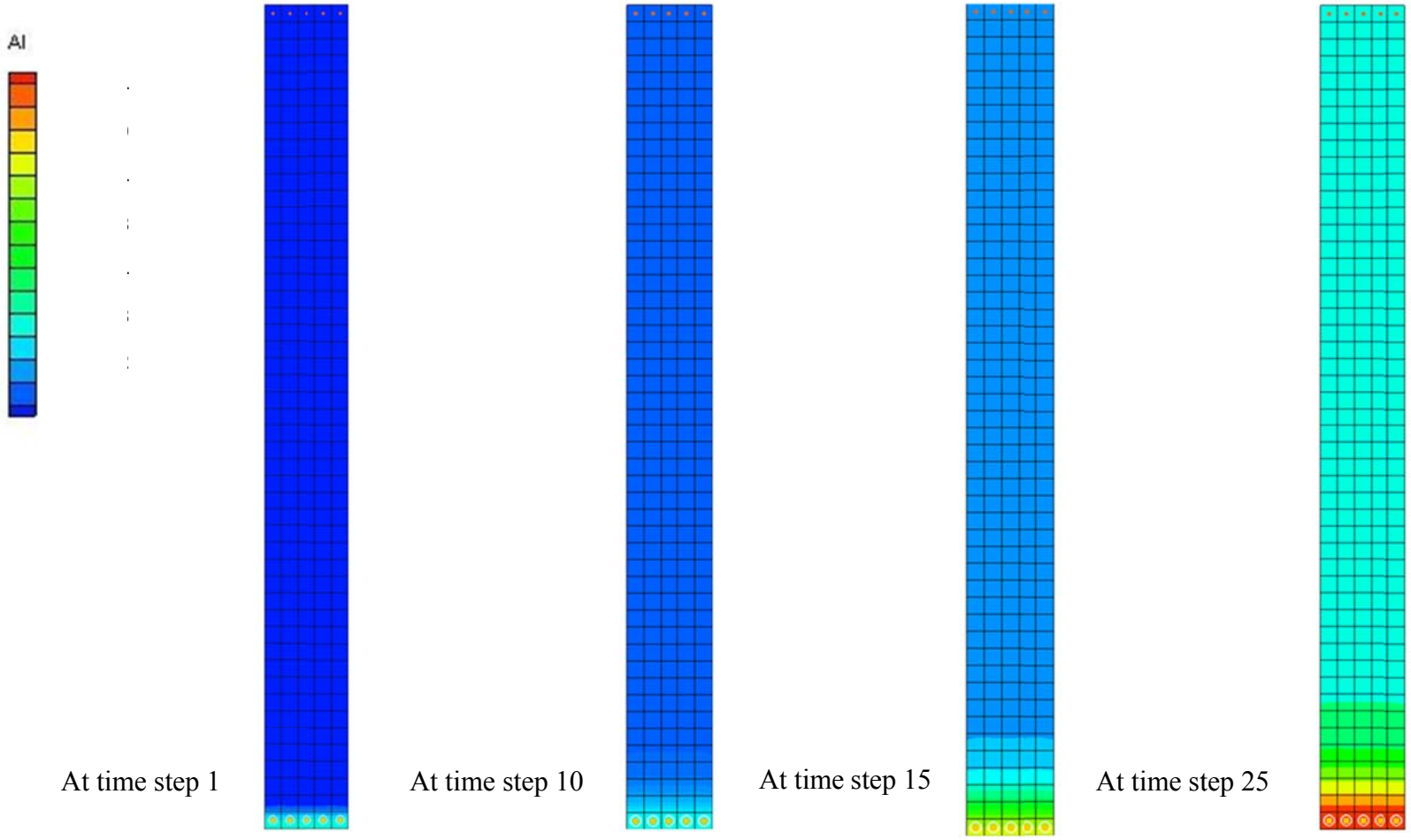


Figure 6.11 Model outputs for the $Al^{3+}$ concentrations along the column

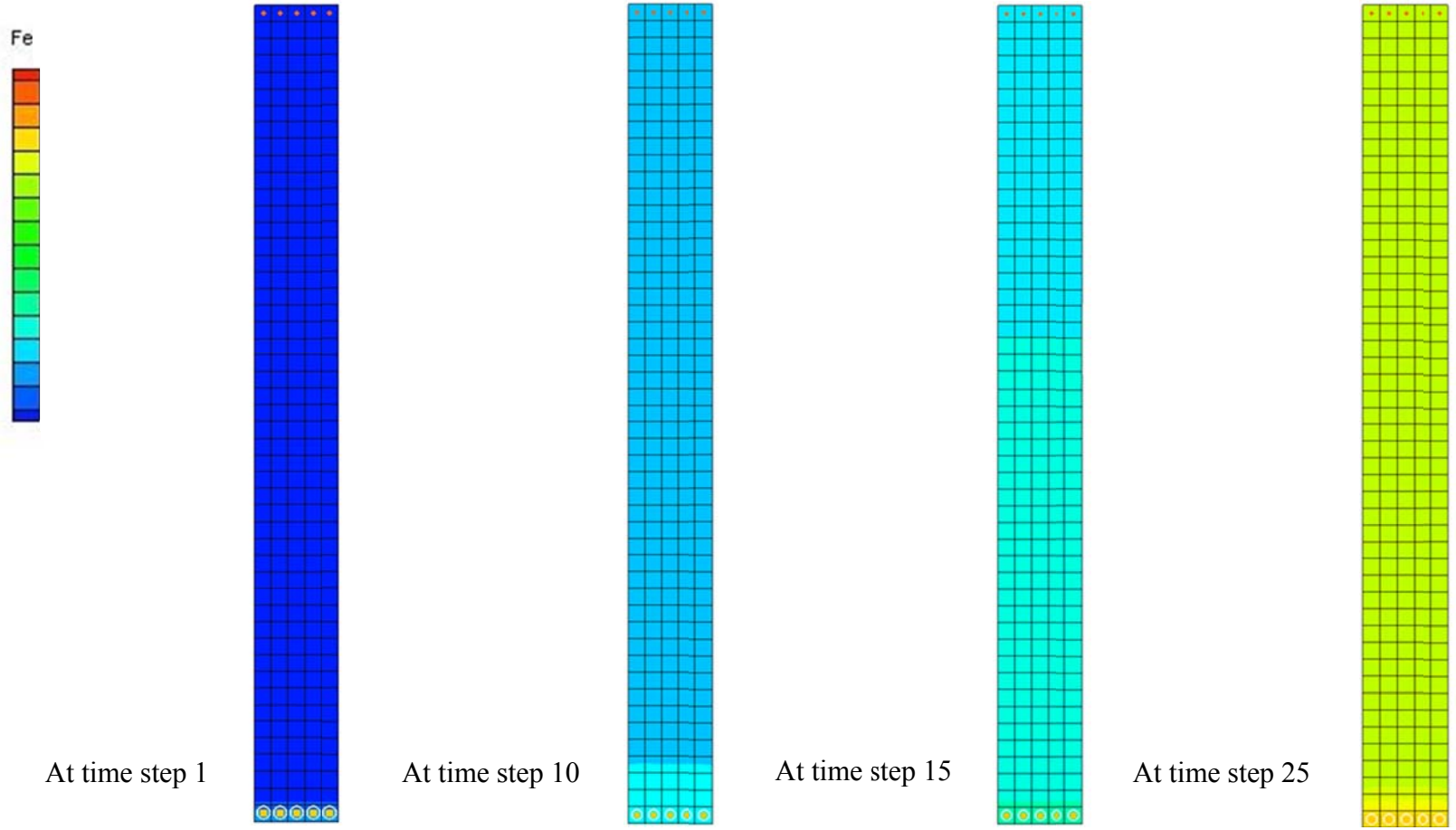


Figure 6.12 Model outputs for the total Fe concentrations along the column

The efficiency of recycled concrete would already have decreased to some extent by the exhaustion of the alkalinity of the materials. The model results obtained for porosity show that the precipitated secondary minerals subsequently reduce the porosity and hydraulic conductivity. Direct measurement of porosity using the porosity meter (Trani and Indraratna, 2010) did not provide reliable readings due to the internal disturbance of the specimen surrounding the probe tip. Therefore, some porosity values were back calculated from the Kozeny Carmen equation (Eqn. (6.13)) using the hydraulic conductivity data from experiment at different PVs (Table 6.4). The results are very similar to the predicted porosity values from Eqn. (6.11), further confirming the accuracy of the developed model.

Table 6.4: Comparison of porosities based on Kozeny Carmen relationship with the model predictions (Eqn. (6.11)).

| PV | Experimental $k$ (m/d) based on Darcy's Law | $n$ back-calculated from Kozeny-Carmen equation (Eqn. (6.13) | $n$ predicted from geochemical model (Eqn. (6.11) |
|---|---|---|---|
| 43 | 0.957 | 0.690 | 0.690 |
| 59 | 0.919 | 0.685 | 0.687 |
| 95 | 0.808 | 0.673 | 0.679 |
| 149 | 0.682 | 0.656 | 0.668 |
| 194 | 0.628 | 0.648 | 0.663 |

Several studies carried out for zero-valent Fe columns (Li and Benson, 2005, Kamolpornwijit et al., 2004), organic sediment columns (Bilek, 2006), glass bead columns (Rowe et al., 2000) and recycled concrete columns (Regmi et al., 2011b) have reported that excessive clogging is greatest near the inlet to the column (reactive materials) and is not uniform throughout the column. For the current case, the porosity and hydraulic conductivity reductions due to mineral precipitation and

dissolution were calculated from Eqns. (6.11) and (6.13) for each 100 mm interval along the column (Figures 6.13 and 6.14). The porosity and hydraulic conductivity reductions were maximum near the column inlet (Zone 1) and decreased with distance along the column (i.e. clogging in Zone 1 > Zone 2 > Zone 3 etc.). This situation arises because of the reduction in dissolved ions in the influent available to precipitate as the water moves through the column. The pores in the column were large enough that complete occlusion of the pores did not occur and, hence, the flow could be maintained (with an increase in pressure) throughout the experiment. A similar trend in hydraulic properties was observed by Li et al. (2006) for the pilot-scale PRB (containing granular Fe) conducted at Moffett Federal Airfield and U.S. Coast Guard Support Centre.

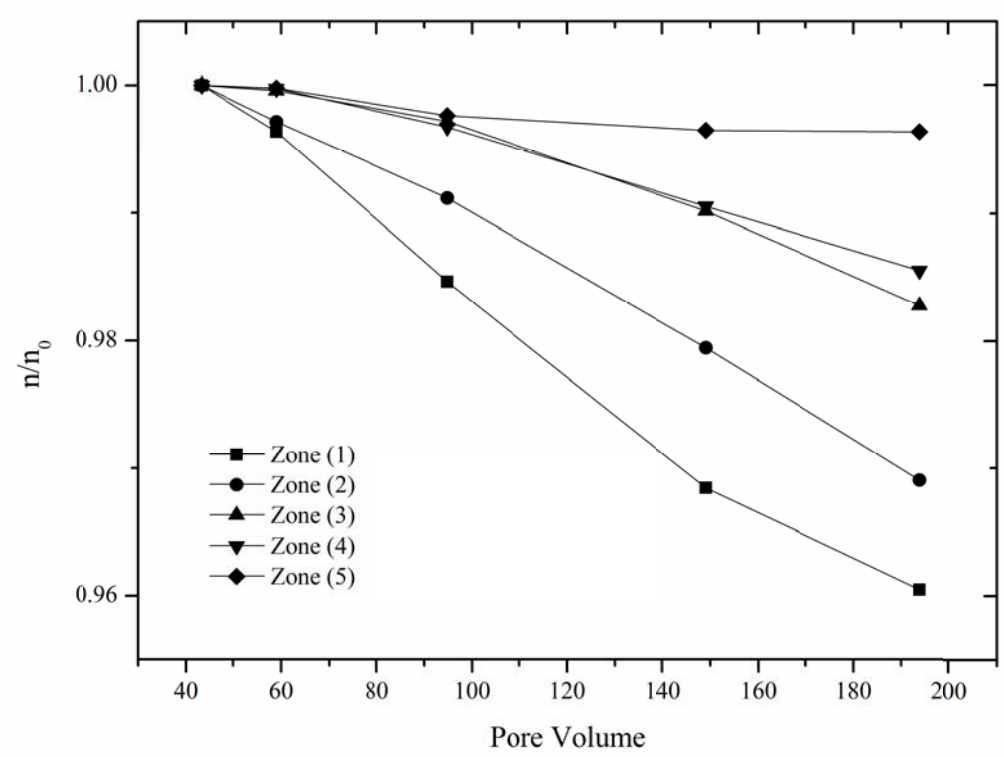


Figure 6.13 Normalised porosity values in Zone (1): SP0-SP1, Zone (2): SP1-SP2, Zone (3): SP2-SP3, Zone (4): SP3-SP4, Zone (5): SP4-SP5 (Indraratna et al., 2014)

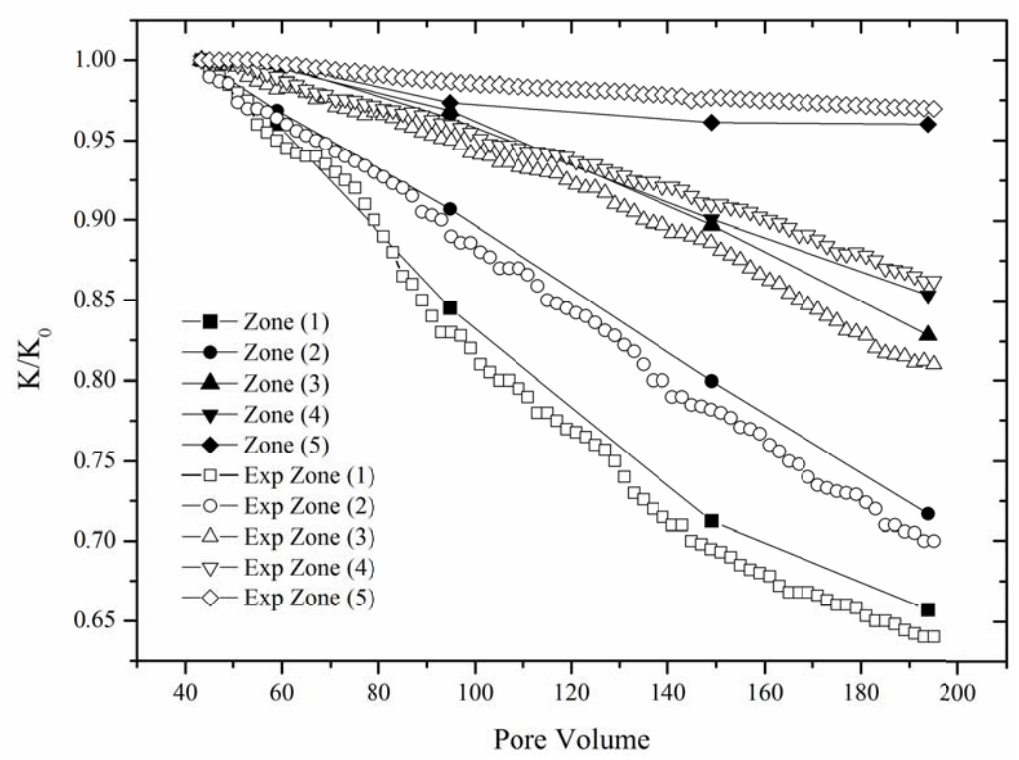


Figure 6.14 Experimental and predicted (normalised) hydraulic conductivity values in Zone (1): SP0-SP1, Zone (2): SP1-SP2, Zone (3): SP2-SP3, Zone (4): SP3-SP4, Zone (5): SP4-SP5 (Indraratna et al., 2014)

The largest porosity reduction during the experiment was most significant (4%) near the influent end of the column and this reduced to 3% midway along the column and 0.5% near the end of the column. The porosity reduction arose from the precipitation of secondary minerals (i.e. $Fe(OH)_3$, $Fe(OOH)$, $Fe_2O_3$, $Fe(OH)_2$, $FeCO_3$, $Al(OH)_3$). The largest hydraulic conductivity reduction was 34% near the inlet to the column, with a 27% reduction mid-way along the column and 4% near the end of the column.

## 6.6 Model application to field PRB

PRB performance modelling using numerical solutions and field data is not simple or straightforward because of several factors that govern the field conditions from being constant and unique for a specific site. Some of them are site-specific geochemical and hydro-geological conditions (Phillips et al., 2000), aquifer heterogeneity (Warner and Sorel, 2002, Li et al., 2006) and the relatively long period over which mineral deposition occurs inside the PRB (Vikesland et al., 2003). Analysing the field data with a calibrated flow and reactive transport model that simulates mineral precipitation and the impact on hydraulic behaviour of PRBs (Liang et al., 2000, Mayer et al., 2001, Yabusaki, 2001) can be an alternative approach. One-dimensional numerical simulation would be helpful in order to capture the full range of reactive processes and the complex geochemical reactions occurring inside the PRB (Bain et al., 2001).

The conceptual model for this purpose was a continuous trench PRB, containing recycled concrete aggregates, that was placed in a homogeneous shallow aquifer. The conceptual model of the field PRB was divided into three zones: Zone 1 (entrance), Zone 2 (middle) and Zone 3 (exit). One-dimensional reactive transport analysis was conducted considering a section passing through the centreline of the PRB. The discretised solution domain is shown in Figure 6.15. In this zone, contaminants are transformed by reduction reactions and immobilised by subsequent precipitation. A number of secondary reactions occur simultaneously in this zone. The alkaline pH promotes the precipitation of a number of secondary minerals throughout the treatment zone. These reactions consume alkalinity and act to buffer further increasing the groundwater pH. The groundwater leaving this treatment zone is

characterised by low concentrations of dissolved total Fe and $Al^{3+}$ and exhibits near-neutral pH (7.9-7.3 pH).

Reactive contaminant transport analysis was conducted along the centreline of the PRB. A discretisation interval of 0.1 m in the horizontal direction was adopted for a total width of 1.2 m (Figure 6.15). All the equations used in the model application to the column experiment which was a vertical flow, was assumed equivalent to the horizontal flow along the centreline of the field PRB. The geochemical algorithm is independent of the effect of gravity. On the basis of field data observed during the period from October 2006 to January 2012, the flow domain was simulated as a fully saturated system with specified head boundaries and a mean hydraulic gradient of 0.006 to represent realistic field conditions. Table 6.5 lists all the input parameters of the groundwater chemistry.

Table 6.5: Initial conditions (concentrations) of the model

| Parameter | Initial conditions |
|---|---|
| pH | 3.6 |
| $Na^+$ (mg/L) | 435 |
| $K^+$ (mg/L) | 48 |
| $Ca^{2+}$ (mg/L) | 115 |
| $Mg^{2+}$ (mg/L) | 90 |
| $Al^{3+}$ (mg/L) | 27 |
| Total Fe (mg/L) | 80 |
| $Cl^-$ (mg/L) | 825 |
| $SO_4^{2-}$ (mg/L) | 1135 |

The reaction rates for simulating the PRB conditions were the same as those corresponding to laboratory column experiments albeit different boundary

conditions. In addition, the primary and secondary mineral components considered in the field were the same as those in the column experiments.

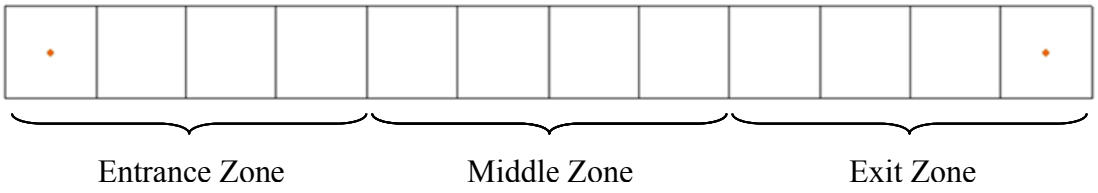


Figure 6.15 Discretisation of the field PRB

In the application of the model to the field PRB, favourable comparisons were obtained between the predictions and field measurements for pH, Al and total Fe concentrations. Figures 6.16-6.18 show the model predictions and field results for pH, Al and total Fe concentrations respectively for 2012, after 6 years of operation. The pH of groundwater up-gradient of the PRB varied between 3.2 and 4.1 with an average of 3.6, whereas inside the PRB, the pH was higher and varied from 6.7 to 7.4 with an average of 7. Table 6.6 summarises the model inputs and averaged values of field data and model outputs. The predicted pH values are in agreement with the sharp increase in pH observed at the near-neutral plateau inside the PRB.

Table 6.6: Model predicted and measured pH, Al and total Fe concentrations in the field PRB

| | Input values | Averaged measured values | Averaged model predicted values |
|---|---|---|---|
| pH | 3.6 | 7 | 7.3 |
| [Al] (mg/L) | 27 | 1 | 0.5 |
| [Total Fe] (mg/L) | 80 | 1 | 0 |

Field monitoring and column experiments indicate that the concentrations of $Al^{3+}$ and total Fe reduce rapidly within the PRB to very low levels, in accordance with the model output. The rapid decrease in these cations indicates that secondary minerals precipitate inside the PRB resulting in a decrease in porosity and hydraulic conductivity. However, the computed decrease in hydraulic conductivity from October 2006 to October 2012 is only 3% at the entrance zone, which is not surprising given the larger sized recycled concrete aggregates ($d_{50}$=40 mm) used in the PRB that prolong total clogging within relatively large pores of a coarse aggregate assembly. Several researchers have reported that chemical precipitation and clogging may occur excessively near the inlet of the reactive materials and not homogeneously distributed throughout the barrier (Li et al., 2005; Bilek, 2006).

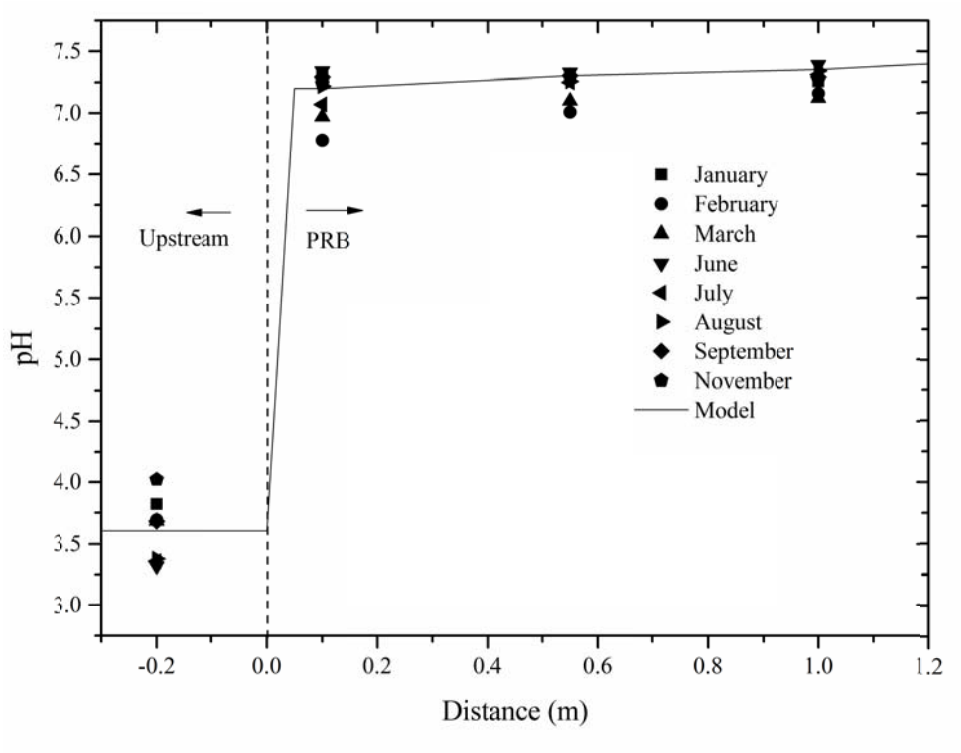


Figure 6.16 Measured and predicted pH values for field PRB for 2012 (Indraratna et al., 2014)

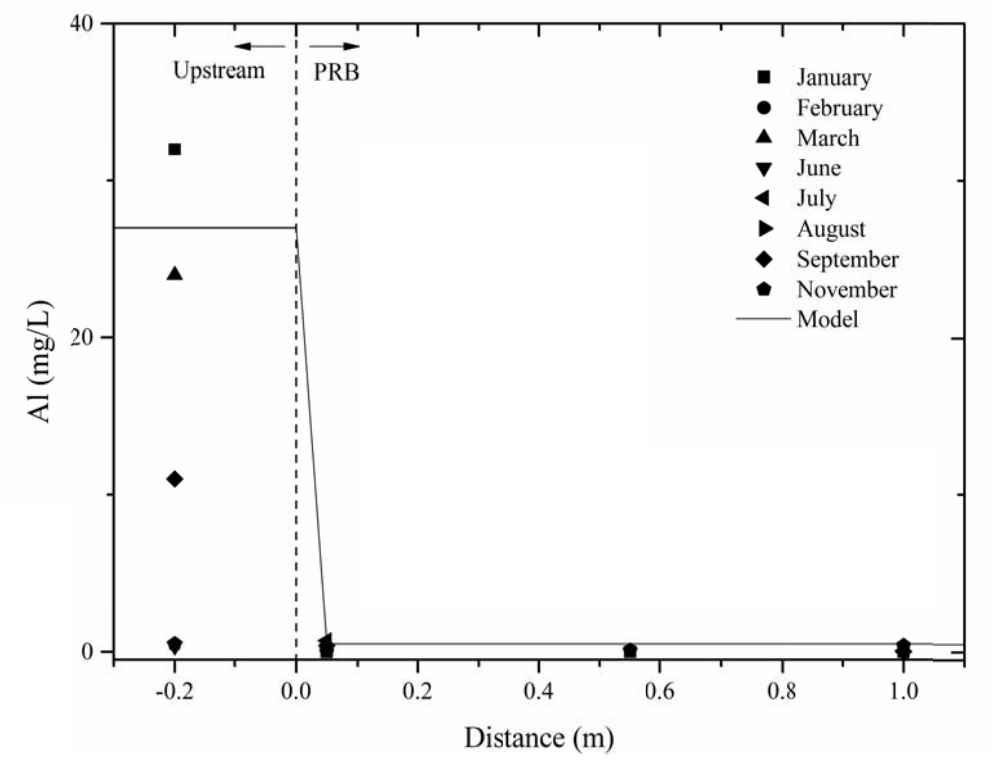


Figure 6.17 Measured and predicted Al concentrations for field PRB for 2012 (Indraratna et al., 2014)

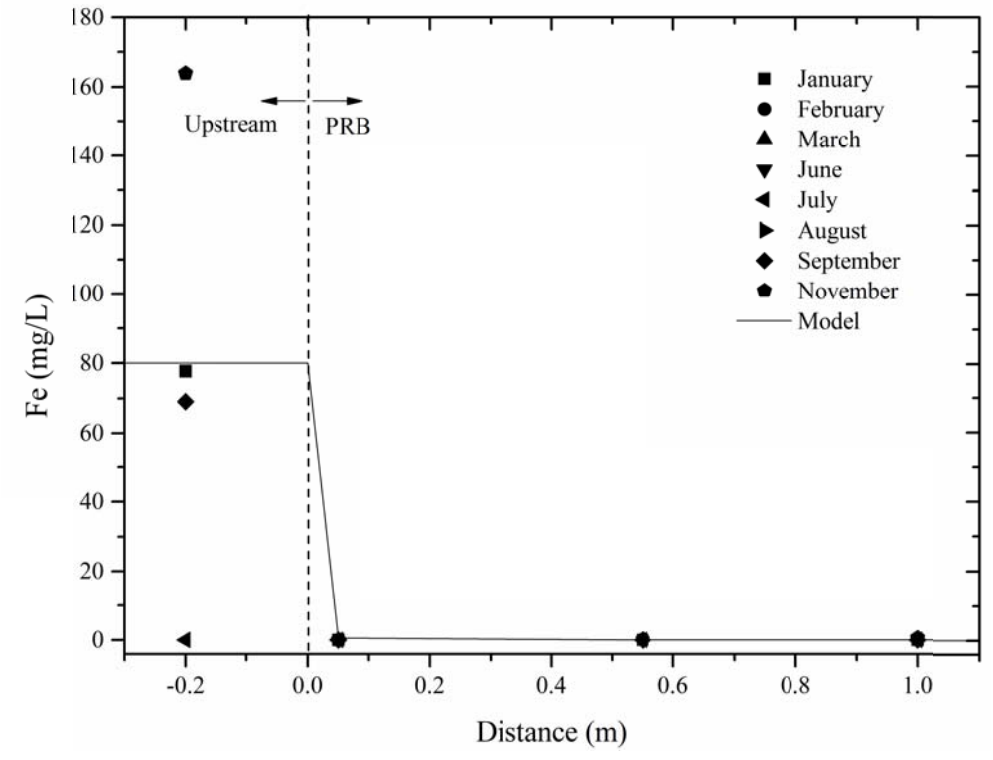


Figure 6.18 Measured and predicted Fe concentrations for field PRB for 2012 (Indraratna et al., 2014)

## 6.7 Mineralogical analysis

The PRB was excavated in selected locations to obtain the recycled concrete specimens of the barrier in October 2013. One sample was collected at the entrance zone of the PRB near observation well 22 (Figure 4.5 in Chapter 4). The purpose was to compare them with the virgin recycled concrete samples in terms of mineralogy. XRF, XRD and SEM/EDS analyse were undertaken to determine precipitation of the secondary minerals. These analyses gave quantitative and qualitative measures of the precipitates.

Due to the maintenance of neutral pH inside the PRB, Al and Fe precipitated out of solution (e.g. low concentrations inside the PRB shown in (Figures 6.17 and 6.18) as hydroxides or oxyhydroxides (Indraratna et al., 2014, Regmi et al., 2009a). Orange and white precipitates on these specimens indicated that some chemical armouring of the surface of the reactive media had occurred, which affected the reactivity of the recycled concrete at the entrance of PRB. However, these concrete samples had a negligible amount of precipitates coating the reactive surface (Figure 6.19). This is probably due to a slow distribution of the precipitation as the groundwater velocity within the site is very small (<10 cm/day). Furthermore, the porosity of the PRB is high due to large sized recycled concrete and precipitates might have collected in the voids towards the entrance of the PRB over time, which will take longer to fill due to the slow groundwater flow rate. While chemical armouring was not significant at the entrance of the PRB, it was evident that the precipitates would not be high towards the middle of the PRB and at the exit face of the PRB. The precipitates were probably causing armouring on the surface of the reactive materials towards the

entrance of the PRB where the acidic groundwater enriched with Fe and Al directly is exposed to the recycled concrete.

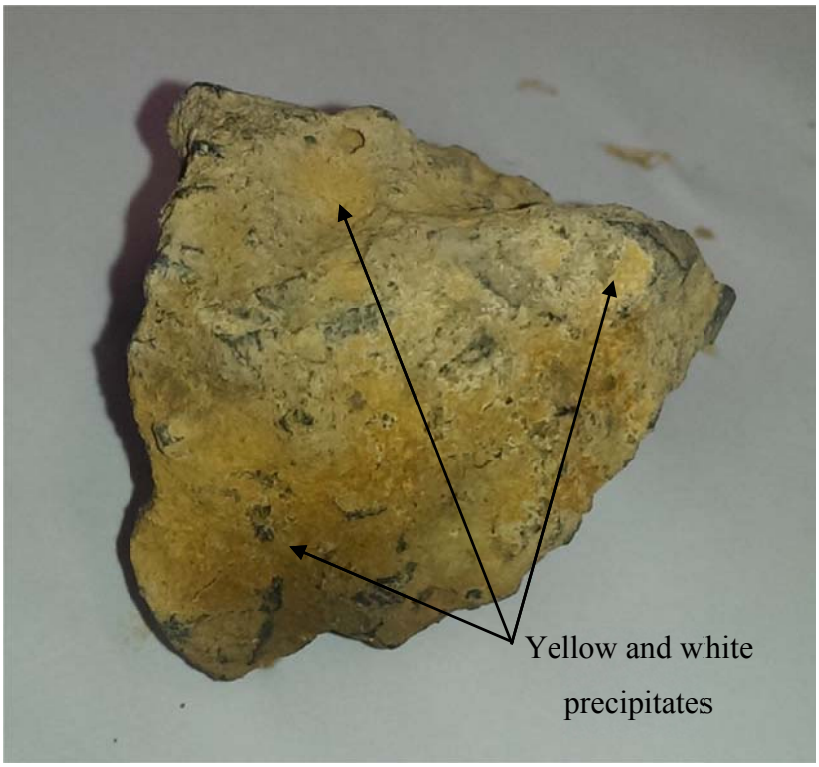


Figure 6.19 Precipitates coating the surface area of a recycled concrete sample collected at the entrance zone of the PRB

Identification of the minerals in the precipitates was an important task for the study of the acid neutralisation behaviour and chemical armouring of the recycled concrete aggregates. Mineralogical characterisation of the recycled concrete and the precipitates by XRD and XRF confirmed that Ca-bearing minerals were the primary source of alkalinity, whereas Al and Fe minerals were the main precipitates formed during the acid neutralisation process (Table 6.7).

The recycled concrete aggregates used in the PRB are based on OPC (Ordinary Portland Cement) of grades M25 and M30 with water to cement ratio of 0.4:0.43 (Indraratna et al., 2010) and from an ungraded mixture of concrete waste material. The high amount of $SiO_2$ present in the recycled concrete was chemically inert in the acid neutralisation processes. The presence of CaO supported the role of the dissolution of C-A-H compounds (e.g. anorthite ($CaAl_2SiO_8$)], portlandite ($Ca(OH)_2$) and calcite ($CaCO_3$)), from the recycled concrete in generating alkalinity and buffering the acidic influent in the PRB. Armouring on the surface of the recycled concrete could result in a decrease in the rate of mineral dissolution, finally decreasing the ANC of the reactive material.

SEM-EDS analysis was also carried out on a cut section of the armoured concrete to compare the SEM image and EDS results of the armoured surface with the unarmoured recycled concrete (Figure 6.20). Further EDS analysis showed the large peaks of Si, moderate peaks for Ca and Al, and the small peaks for K, Fe and other elements support the XRD and XRF results for the recycled concrete. Conversely, higher peaks were obtained for Al and Fe in the armoured concrete, confirming the precipitates were primarily Al and Fe-bearing precipitates in the form of hydroxide and oxyhydroxides. Mineralogical analysis of the recycled concrete confirms the presence of a significant amount of Ca-bearing minerals in the virgin concrete minerals. Solidly cloudy images of the precipitates observed in SEM analysis with high amounts of Al and Fe also confirmed that the precipitates were primarily Al and Fe-bearing precipitates in the form of hydroxide and oxyhydroxides. Al- and Fe-bearing minerals within the precipitates were in the ratio of 41:59 (by mass). These results gave a clear idea about the dominant precipitating minerals but these values

could not conclude the quantitative presence of minerals exactly, as the SEM-EDS equipment in UOW was not calibrated for semi-quantitative compositional analysis. In order to get a more precise analysis in terms of quantitative presence of minerals, more sophisticated equipment is required.

Table 6.7: Comparison of metal oxide composition of the virgin concrete and precipitates analysed by quantitative SEM-EDS

| Element | Mass (%) | |
|---|---|---|
| | Virgin recycled concrete | Armoured concrete from field PRB |
| C | 17.46 | 14.91 |
| O | 44.57 | 57.5 |
| Na | 0.5 | - |
| Mg | 0.76 | - |
| Al | 3.21 | 4.61 |
| Si | 19.8 | 12.25 |
| S | 0.15 | - |
| K | 1.08 | - |
| Ca | 8.87 | 4.17 |
| Fe | 3.6 | 6.55 |

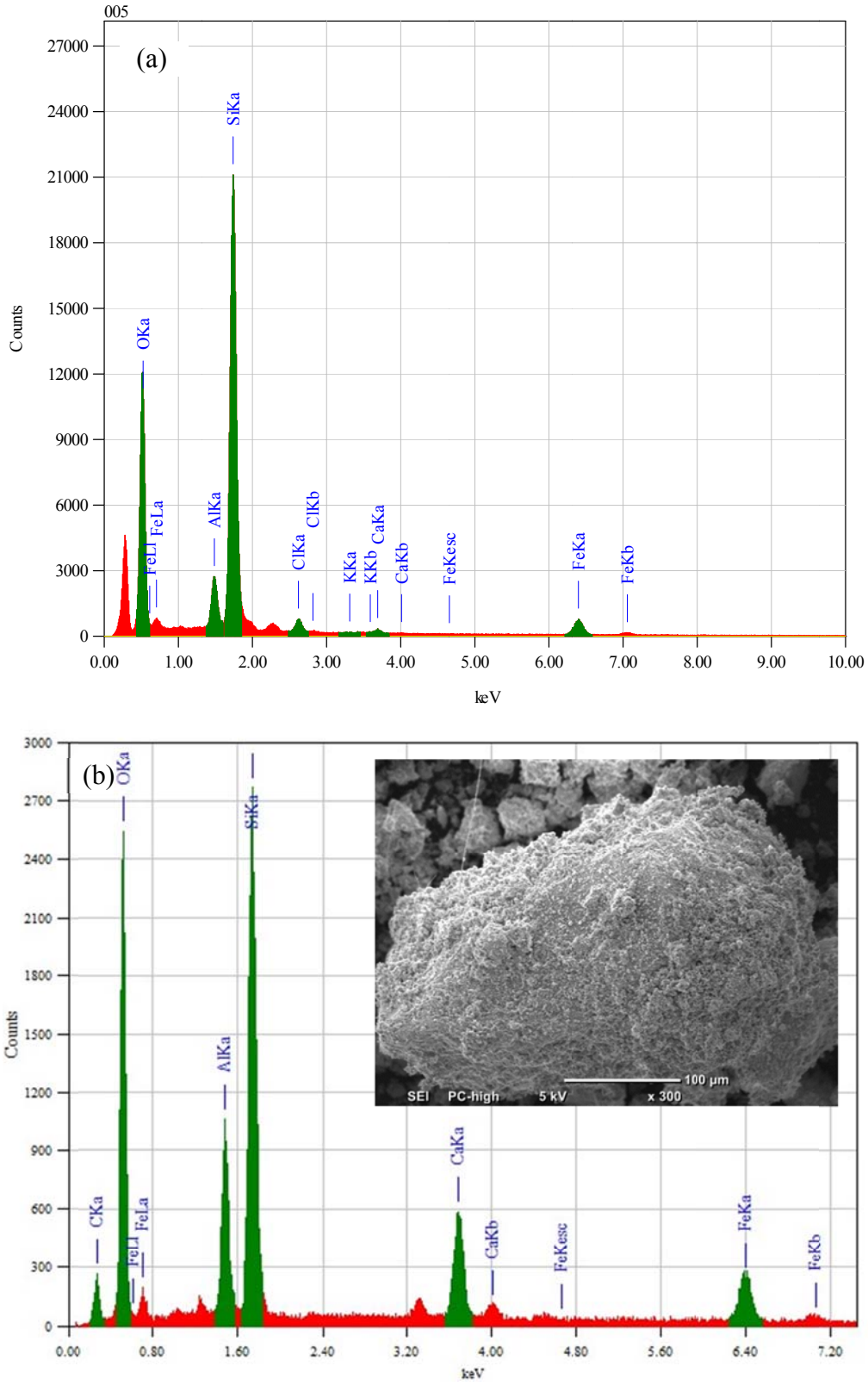


Figure 6.20: EDS analysis of (a) recycled concrete (Regmi et al., 2011a) (b) armoured concrete from PRB. Corresponding SEM image (inset) shows area analysed.

## 6.8 Optimum width of PRB

A PRB is commonly built with a reactive material having a higher hydraulic conductivity than the surrounding soils. As a result, the contaminated groundwater is forced to pass through the barrier itself, moving under its natural hydraulic gradient. The mechanism of the remediation process of a PRB depends on the reactive material chosen to build the barrier.

Before designing a barrier it is necessary to properly characterise the site, to assess the contaminant properties, distribution and tracking; to describe the groundwater flow within the aquifer; to determine the chemical-physical phenomena involved in the reaction process and to meaningfully represent the results. The site characterisation of this particular site is described in Chapter 4. The most important thing when designing a PRB is that the residence time of the contaminated flow travelling through the barrier should be long enough for the reaction processes to take place. Therefore, the barrier width ($W$) must satisfy the following inequality:

$$\frac{W}{v_b} > -\frac{\ln\left(C_e / C_{in}\right)}{k} \tag{6.26}$$

where, $v_b$ represents groundwater flow velocity through the barrier, $k$ is the overall reaction rate and $C_e$ and $C_{in}$ represents the external effluent and influent concentrations, respectively. It must be considered that influent concentrations may vary due to the seasonal changes. Therefore, the barrier must be designed both to retain intense concentration peaks and to guarantee long term performances.

PRB sizing is obtained iteratively, as reported schematically in the flow chart in Figure 6.21. Specifically, after defining boundary conditions and all input data such

as $K$ (hydraulic conductivity), $n$ (porosity), $h$ (initial hydraulic head from Eqn.), $C_0$ (initial pollutant concentrations), $k$ (overall reaction kinetics), MODFLOW simulation was carried out, choosing $W$ (PRB width), in order to calculate $h(x,t)$ and $u(x,t)$. Next step is RT3D simulation to compute pollutant concentration $C_e(x,t)$. When $C_e$ is lower than an acceptable limit value ($C_{lim}$), PRB width is correct, otherwise it must be increased until $C_e < C_{lim}$. The $C_{lim}$ values were taken from Australian water guidelines (Sundaram et al., 2009) where the $C_{lim}$ for both Al and Fe were 0.2 mg/L.

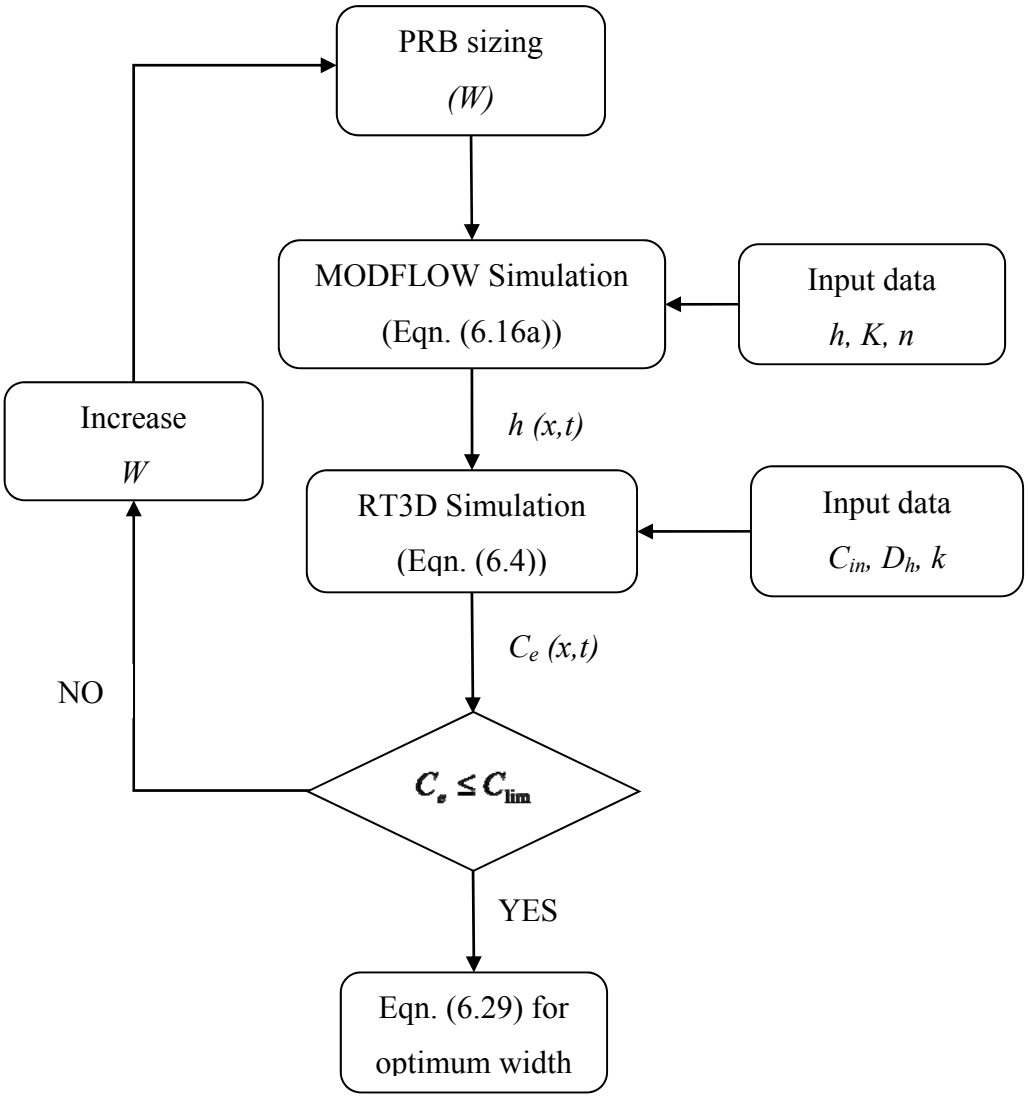


Figure 6.21 Flow chart of the optimum PRB width determination process

Moreover, it is important to consider the different influent concentrations and check whether the optimum width of the barrier can provide a reasonable residence time especially in high concentrations. In order to accommodate the above, iterations were carried out for several influent concentrations and then the optimum width was finalised. Results shown in Figure 6.22 conclude the optimum width to be 0.45 m for a range of influent concentrations from 50 to 250 mg/L. By applying a safety factor (Eqn. (6.29)) of two, as suggested by Gavaskar (1998) and Nardo et al. (2010), the width of the PRB would be 0.9 m. The pilot-scale PRB installed at Nowra has a width of 1.2 m, which is allowable for the remediation of acidic groundwater with the use of recycled concrete aggregates.

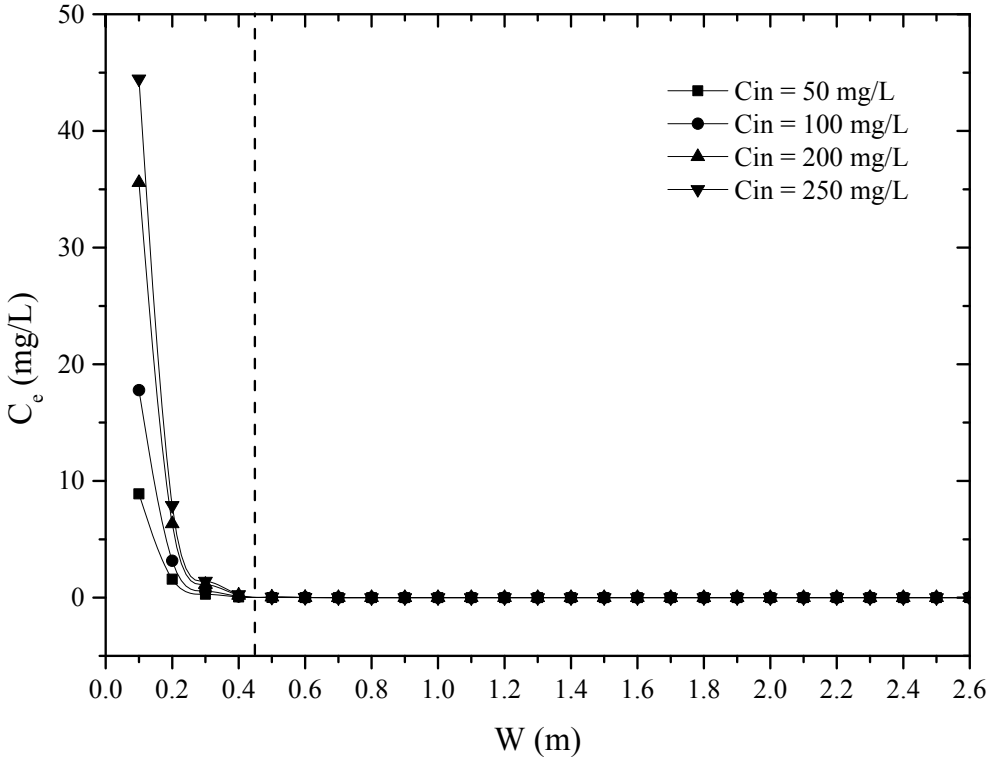


Figure 6.22 Effluent concentrations vs. PRB width for different influent concentrations

$$C_e = C_{in} \exp\left(\frac{-kW}{v_b}\right) \tag{6.27}$$

$$k = -\frac{\ln\left(C_e / C_{in}\right)}{t} \tag{6.28}$$

$$\text{Optimum W} = \text{W} \times \text{SF} \tag{6.29}$$

## 6.9 Longevity prediction

The ultimate success of the PRB will be determined by the longevity over which Ca-bearing mineral dissolution and metal oxy/hydroxide precipitation is maintained. Due to maintenance of neutral to alkaline pH inside the PRB, Al and Fe precipitated out of solution (e.g. low concentrations inside the PRB shown in Figures 6.17 and 6.18) as hydroxides or oxyhydroxides as indicated by the XRD, XRF and SEM results. Observed steady piezometric head within the PRB over the 6 year monitoring period after attaining steady state conditions in February 2007 (Figure 6.23) indicates no threat of failure of the PRB from clogging. The continuous mineral precipitation inside the PRB over time indicates that the effectiveness of the PRB may decrease rapidly in the future due to the decreased surface area of the concrete by armouring effect, further decreasing the longevity of the PRB as demonstrated by column experiments.

PRB longevity can be estimated by comparing the column experiment results discussed in Chapter 3 with respect to the PRB dimensions and groundwater velocity. The synthetic water used in column experiment (~pH 2.67 and acidity 645 mg/L $CaCO_3$) was slightly more acidic than the groundwater in the field (average pH ~3.7 and average acidity ~550 mg/L eq. as $CaCO_3$) (Indraratna et al., 2010).

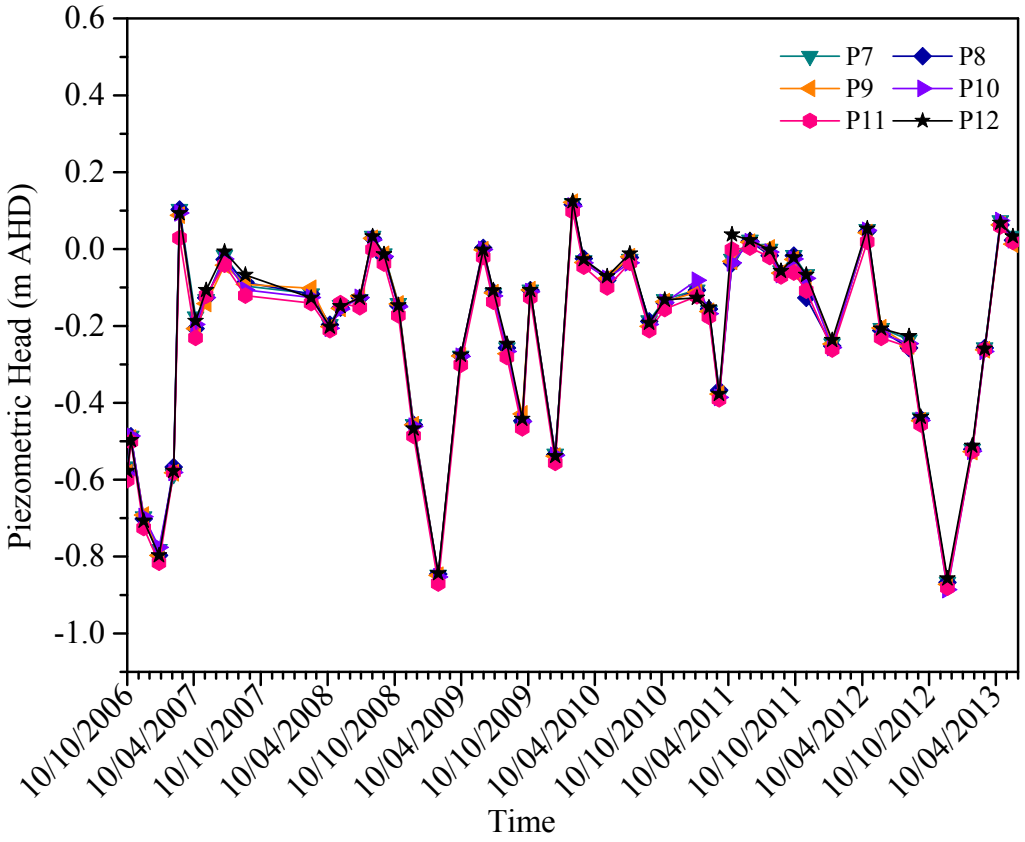


Figure 6.23: Groundwater elevation inside the PRB with respect to time. (P7-P12 are the six piezometers inside the PRB) (updated after Regmi (2012))

In the column experiment, 49 mg/L Fe and 54 mg/L Al, and 645 mg/L $CaCO_3$ equivalent acidity were removed with a residence time of 11.8 hr for a travel path length of 0.5 m. Assuming a groundwater velocity in the aquifer of 10 cm/day (based on the piezometric head and hydraulic conductivity), estimated residence time through the PRB is 12 days for a PRB thickness of 1.2 m. Therefore, the corresponding PRB residence time is around 24 times higher than the residence time in column experiment run with medium flow rate of 1.2 mL/min.

Moreover, the longevity of the PRB depends on the amount of concrete used and the seasonal changes in groundwater qualities in the field. The mass of the concrete used inside the PRB was 80 tonnes, and the ANC of the recycled concrete is 146 g/kg,

corresponding to which a theoretical total neutralisation capacity of the concrete used inside the PRB is 11.6 tonnes (Indraratna et al., 2010). Considering a maximum groundwater velocity of 0.1 m/day, the amount of acid passed through the PRB per year is estimated to be ~1100 × $10^3$ L and the consumption of the reactive material is predicted to be ~0.70 tonnes per year. This indicates that the material will be exhausted after 17 years, if there is no chemical armouring of the reactive media by Al and Fe precipitates. However, it was observed from the column experiments carried out by Regmi et al. (2011b) and Pathirage et al. (2012) that the recycled concretes ANC could be reduced by ~50% due to armouring. Considering this, the longevity of the PRB considering armouring and based on the acid flux passed through the PRB per year would be 8.5 years for a groundwater velocity of 0.1 m/day (Figure 6.24). However, the groundwater velocity at the PRB site is usually less than 0.1 m/day, which implies that the longevity of the barrier would be more than 8.5 years.

The estimated longevity from the pH profile and the current performance of the PRB indicates that recycled concrete in the field will treat the acidic water for a longer period, fulfilling the expectations of the local government for improving water quality to protect the aquatic environments of nearby surface water sources.

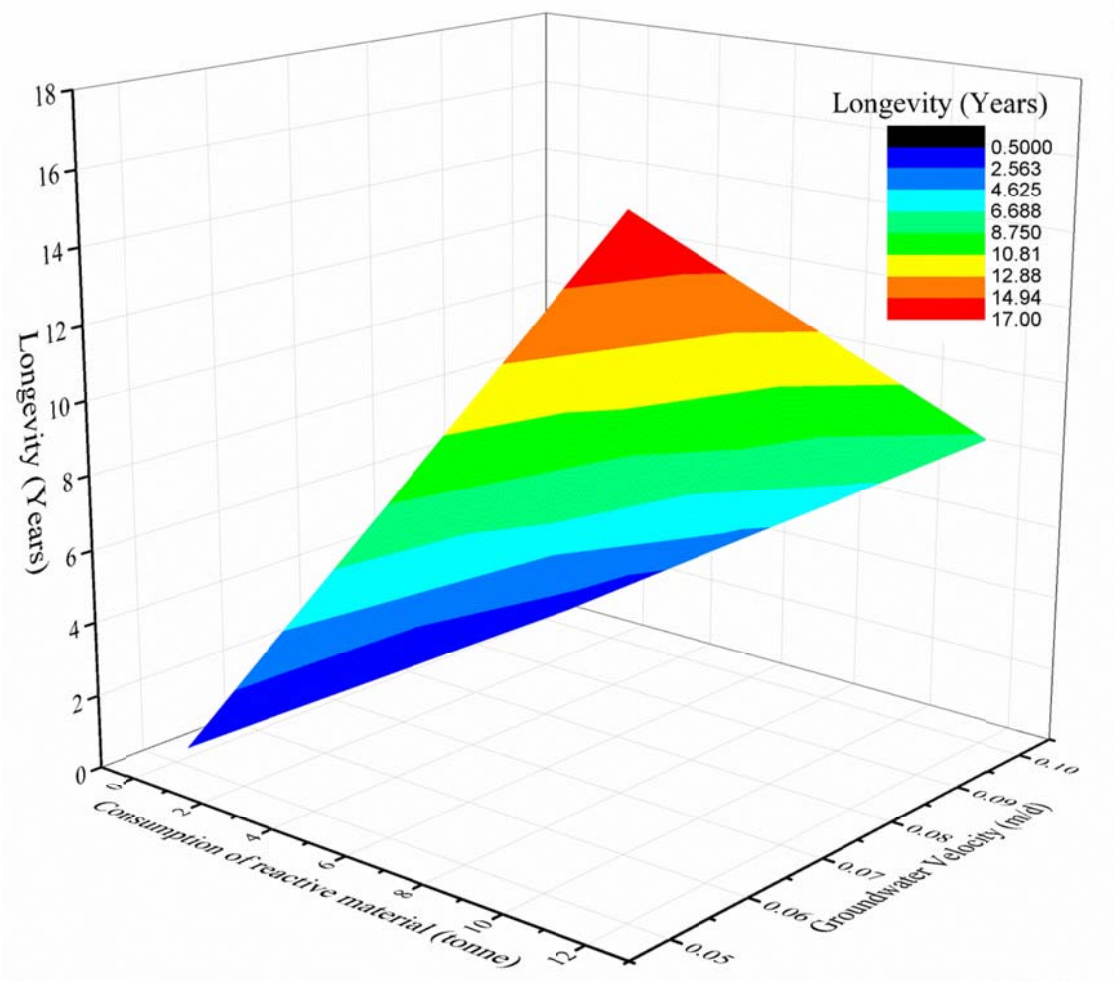


Figure 6.24 Longevity of the PRB

## 6.10 Summary

The software codes MODFLOW and RT3D were used to simulate the transport and fate of the major cations ($Ca^{2+}$, $Al^{3+}$ and total Fe) in the column experiment. Eqn. (6.16) was used to calculate the starting head for MODFLOW at every time step. Eqn. (6.16) captured the change in head due to hydraulic conductivity reduction by secondary mineral precipitation. The reason to adopt this approach was because MODFLOW did not have a way of automatically changing the porosity or the hydraulic conductivity unless they were manually entered. Once the starting head was calculated by the analytical model, the results were put into MODFLOW. Then

MODFLOW and RT3D were run in tandem to get the concentrations of reactants at every time step.

The predicted and measured concentration profiles of $Ca^{2+}$, $Al^{3+}$, and total Fe were found to be in very good agreement and hence confirming the feasibility of the coupled hydro-geochemical model developed in this study. The precipitation of secondary minerals (i.e. $Fe(OH)_3$, $Fe(OOH)$, $Fe_2O_3$, $Fe(OH)_2$, $FeCO_3$, $Al(OH)_3$) significantly decreased the efficiency of the reactive material due to armouring and clogging in the column experiments. The model results obtained for porosity showed that the precipitated secondary minerals subsequently reduced the porosity and hydraulic conductivity. The largest porosity reduction during the experiment was most significant (4%) near the influent end of the column and this reduced to 3% midway along the column and 0.5% near the end of the column. The largest hydraulic conductivity reduction of 34% was found to be near the inlet to the column, with a 27% reduction mid-way along the column and 4% near the end of the column.

In the application of the model to field PRB, favourable comparisons were obtained between the predictions and field measurements for pH, $Al^{3+}$ and total Fe concentrations. Field monitoring and column experiments indicated that the concentrations of $Al^{3+}$ and total Fe reduced rapidly within the PRB to very low levels, in accordance with the model output. The rapid decrease in these cations indicated that secondary minerals precipitate inside the PRB resulting in a decrease of porosity and hydraulic conductivity. However, the computed decrease in hydraulic conductivity from October 2006 to October 2012 was noticed to be only 3%, which

was not surprising given the larger sized recycled concrete aggregates ($d_{50}$=40 mm) used in the PRB that prolong total clogging within relatively large pores of a coarse aggregate assembly.

MODFLOW and RT3D simulations were carried out to find the optimum width of PRB. The model was run for different influent contaminant concentrations and till the inequality, $C_e < C_{lim}$ satisfied (when the effluent concentration ($C_e$) is lower than an acceptable limit value ($C_{lim}$). The optimum width of the PRB was 0.9 m from these iterative simulations. The pilot-scale PRB installed at Nowra consisted of a width of 1.2 m, which was allowable for the remediation of acidic groundwater with the use of recycled concrete aggregates. The longevity prediction of the PRB considering armouring and based on the acid flux passed through the PRB per year was 8.5 years for a maximum groundwater velocity of 10 cm/day. However, the groundwater velocity at the PRB site is usually less than 10 cm/day, which implies that the longevity of the barrier would be more than 8.5 years.

# Chapter 7 Conclusions and Recommendations

## 7.1 Introduction

This chapter is a synopsis of all the major findings of the research and its practical implications, followed by recommendations for future research. This study monitors the performance of a novel PRB for the remediation of contaminated groundwater from ASS terrain. The application of recycled concrete as the reactive material was thoroughly studied through laboratory column experiments and validated with a groundwater flow model coupled with contaminant transport and geochemistry. Commercially available numerical codes, MODFLOW and RT3D were used for this purpose. Moreover, the model was applied to the field PRB, along a transect passing through the centreline of the PRB. Changes in the geochemical composition of the contaminated groundwater within the PRB after treatment with recycled concrete are also addressed.

## 7.2 Conclusions

Laboratory column experiments carried out using synthetic groundwater confirm the suitability of the reactive material in decontaminating acidic leachate consisting of high concentrations of dissolved acidic cations $Al^{3+}$ and total Fe ($Fe^{2+}$ and $Fe^{3+}$). The results of the column experiments proposed conceptual acid neutralisation reactions, i.e. the pH of the effluent groundwater is controlled by a series of dissolution-precipitation reactions, namely Ca-bearing minerals (portlandite, anorthite, and calcite) and Al and Fe oxy/hydroxides. Three distinct pH plateaus observed during the column experiments can be attributed to three different pH-buffering reactions:

1. dissolution of carbonate/bicarbonate alkalinity from the concrete at near-neutral pH (bicarbonate buffering zone),
2. re-dissolution of Al hydroxide minerals at pH ~4.5, and
3. re-dissolution of ferric oxy/hydroxide minerals at pH < 3.7.

The results confirmed that recycled concrete is an effective and promising reactive medium, especially considering the long-term treatment of acidic groundwater from ASS terrain.

The dissolution potential of Ca-bearing minerals in recycled concrete and precipitation potential of secondary minerals out of acidic groundwater has been examined with particular attention to their impact on the hydraulic properties of crushed recycled concrete in a test column and a pilot-scale PRB. MODFLOW and RT3D were used to simulate flow and the reactive transport of mineral components. A geochemical algorithm was developed for the input in RT3D specifically for simulating the geochemical reaction that occur in PRBs composed of recycled concrete for the treatment of acidic groundwater. The calculated concentrations of $Ca^{2+}$, $Al^{3+}$ and total Fe were found to be in good agreement with the observed experimental and field values. Based on the results reported herein, the following conclusions can be derived:

- The dissolved $Al^{3+}$ and total Fe were precipitated out of solution as their oxy/hydroxides (i.e. $Fe(OH)_3$, $Fe(OOH)$, $Fe_2O_3$, $Fe(OH)_2$, $FeCO_3$, $Al(OH)_3$);
- Chemical armouring/clogging of the reactive material due to the secondary mineral precipitation, decreased the ANC of the recycled concrete by up to 50% compared to its theoretical ANC;

- Clogging, and hence the reduction in porosity and hydraulic conductivity, was most significant where the groundwater entered the column and decreased with distance along the column. The largest porosity reduction during the experiment was most significant (4%) near the influent end of the column and this reduced to 3% midway along the column and 0.5% near the end of the column;
- The largest hydraulic conductivity reduction was 34% near the inlet of the column, with a 27% reduction mid-way along the column and 4% near the end of the column;

Field monitoring data over 6.5 years is reported in this thesis. They indicate that the recycled concrete has effectively maintained near-neutral pH and removed $Al^{3+}$ and total Fe in a manner similar to the column experiments. These findings further confirm that the groundwater chemistry inside the PRB is primarily controlled by the alkalinity generated by the dissolution of Ca-bearing minerals in the concrete and the precipitation of insoluble Al- and Fe-hydroxides and oxy-hydroxides. The competence of the PRB to remove $Al^{3+}$ and total Fe depends on the variation of the acidity of the groundwater due to pyrite oxidation, the long-term generation of alkalinity by the minerals present in the recycled concrete and the reduction of the reactive surface area by chemical armouring/clogging due to the precipitated minerals. Despite the excellent performance of the recycled concrete inside the PRB, groundwater chemistry down-gradient of the PRB could be improved to some extent only, due to the dilution of the effluent from the PRB and the occasional mixing of acid generated in the soil by pyrite oxidation.

Overall, the PRB has performed well so far but a slight decrease in the pH and Fe and Al removal efficiencies towards the entrance of the PRB was observed due to the chemical armouring of the surface of the reactive media which affected the reactivity of the recycled concrete in that zone.

Model results were validated using the data from the pilot-scale PRB along the centreline of the PRB. The predicted values from MODFLOW and RT3D simulations for pH, concentrations of $Al^{3+}$ and total Fe are found to be in good agreement with the observed field values throughout 2012. The average pH was around 7 within the PRB. The pH of the PRB has been decreasing slowly, attributed to exhaustion of the alkalinity generating materials as well as fouling by precipitates over the surface of the reactive materials.

Mineralogical analysis of the recycled concrete confirms the presence of a significant amount of Ca-bearing minerals in the virgin concrete minerals. Solidly cloudy images of the precipitates observed in SEM analysis with high amounts of Al and Fe also confirmed that the precipitates were primarily Al and Fe-bearing precipitates in the form of hydroxide and oxyhydroxides. Al- and Fe-bearing minerals within the precipitates were in the ratio of 41:59 (by mass).

Clogging, and hence the reduction in porosity and hydraulic conductivity, was most significant where the groundwater entered the PRB. However, the computed decrease in hydraulic conductivity at the entrance zone from October 2006 to October 2013 was only 3%, which is not surprising given the larger sized recycled

concrete aggregates ($d_{50}$=40 mm) used in the PRB that delays total clogging within relatively large pores of a coarse aggregate assembly.

The optimum PRB sizing is obtained iteratively, defining boundary conditions and input data such as *K* (hydraulic conductivity), *n* (porosity), *h* (initial hydraulic head), $C_0$ (initial pollutant concentrations) and *k* (overall reaction kinetics). MODFLOW and RT3D simulations were carried out till the inequality, $C_e < C_{lim}$ is satisfied (when the effluent concentration ($C_e$) is lower than an acceptable limit value ($C_{lim}$). The model was run for different influent contaminant concentrations and the optimum width of the PRB would be 0.9 m. The pilot-scale PRB installed at Nowra has a width of 1.2 m, thus is acceptable for the remediation of acidic groundwater with the use of recycled concrete aggregates.

The longevity prediction of the PRB considering armouring, and based on the acid flux passing through the PRB per year would be 8.5 years for a maximum groundwater velocity of 100 mm/day. However, the groundwater velocity at the PRB site is usually less than 100 mm/day, which implies that the longevity of the barrier would be more than 8.5 years.

The findings from the pilot-scale PRB confirms that recycled concrete is a suitable environmentally friendly and cost-effective alternative compared to other conventionally utilised techniques (e.g. watertable manipulation, lime neutralisation) for the in-situ treatment of acidic groundwater in ASS terrain. The ability to make comparisons between the geochemically complex transport scenarios coupled with transient groundwater flows within the column experiments and pilot-scale PRB is an

important benefit of this numerical model. Moreover, the models ability to predict the porosity and hydraulic conductivity reductions due to secondary minerals precipitation is of paramount importance to estimate the longevity of the PRB. The developed model can be used as an analysis tool for the performance verification of PRBs in ASS terrain.

## 7.3 Recommendations for Future Research

Field investigations carried out over the 6.5 years monitoring show that although acidic groundwater is neutralised and acidic cations ($Al^{3+}$ and total Fe) were removed significantly by the PRB, acidic conditions still exist with distance down-gradient of the PRB. This is due to the active and ongoing oxidation of pyrite in the soil and generation of acid followed by the liberation of $Al^{3+}$ and total Fe from the clay minerals in the soil, and subsequently mixing with treated groundwater. The amount of mixing of the treated water from the PRB and the acidic water generated at the down-gradient, can be predicted by coupling the PRB effluent from the model predictions with the pyrite oxidation model (Blunden and Indraratna, 2001). This will allow further understanding on the installation distance of a new PRB from the drain or creek to obtain the maximum neutral conditions in groundwater down-gradient of the PRB.

This study revealed that small-sized PRBs would function more effectively for large areas of ASS terrain, if they were constructed in series before discharging the effluent into the surface water. A funnel-and-gate design could be used to decrease the risk of mixing of treated water with untreated groundwater. Hence, the

application of a series of horizontal PRBs or funnel-and-gate PRB can be a potential solution for ASS management that needs to be investigated.

The laboratory column experiments revealed that chemical armouring by the precipitated Al and Fe minerals could decrease the ANC of the recycled concrete by up to 50% compared to its theoretical ANC, which results in decreasing the longevity significantly. The longevity of the PRB and down-gradient water quality could be improved if an alkaline effluent (preferably alkaline waste effluent for cost-effective management) is intermittently injected into the PRB as discussed by Banasiak et al., (2014). Further examination is vital in laboratory scale to quantify the change in porosity and hydraulic conductivity prior to the application of such alkaline effluent as it may shorten the life span of the PRB due to chemical clogging more rapidly.

This study involved the development of a 1D numerical model through the centreline of the PRB, which was useful for evaluating the acid neutralisation behaviour of the recycled concrete and its performance with especial reference to the geochemistry coupled with transient groundwater flows. However, this 1D model cannot capture the lateral groundwater flow and cross flow. The development of a 3D reactive transport model is recommended to quantitatively evaluate changes in flow behaviour due to chemical dissolution/precipitation. This 3D numerical model would be useful to determine the decrease in void space within the PRB per unit volume and analysis of the interconnected effects of acidic flow-induced clogging, PRB effectiveness and longevity.

This study extensively describes and models the chemical clogging phenomena within the reactive medium and acidic groundwater in ASS terrain. However, biological clogging of porous media when exposed to acidic influent has not been investigated or modelled for ASS terrain. The problem of chemical and biological clogging in porous media is of great importance in the fields of geotechnical and geo-environmental engineering and in the application of PRB technology. While bacteria present in soil on the Shoalhaven Floodplain, *A. ferrooxidans*, is acidophilic with optimum growth occurring at a pH < 4, it can survive to a pH as high as 6-7, as currently observed in groundwater within the PRB (Rudens, 2001). Thus, bacterial growth on the recycled concrete within the PRB (as a biofilm) could occur under submerged and anaerobic conditions. The abundance of Fe, as precipitated on the recycled concrete in the PRB, would act as a food source for *A. ferroxidans* and enhance its growth and the subsequent rate of pore space reduction and bioclogging of the PRB with time. Thus, it is of utmost importance to determine the rate of bioclogging and the change in the rate of growth of microorganisms through carefully controlled experiments and the application of mathematic formula, in order to couple the geochemical and biological processes occurring in the PRB. In fact, this will be an area that the writer of this thesis will continue to study in near future.

# References


AHERN, C. R., MCELNEA, A. & SULLIVAN, L. 2004. Acid Sulfate Soils Laboratory Methods Guidelines. Queensland Department of Natural Resources, Mines and Energy, Indooroopilly,Queensland, Australia

AL, T. A., MARTIN, C. J. & BLOWES, D. W. 2000. Carbonate-mineral/water interactions in sulfide-rich mine tailings. *Geochimica et Cosmochimica Acta,* 64**,** 3933-3948.

ALLISON, J. D., BROWN, D. S. & NOVO-GRADAC, K. J. 1991. MINTEQA2/ PRODEFA2, A geochemical assessment model for environmental systems: Version 3.0 User's Manual. Athens, GA, USA: Environmental Research Laboratory, Office of Research and Development, U.S. Environmental Protection Agency.

AMOS, P. W. & YOUNGER, P. L. 2003. Substrate characterisation for a subsurface reactive barrier to treat colliery spoil leachate. *Water Research,* 37**,** 108-120.

AMOS, R. T., MAYER, K. U., BLOWES, D. W. & PTACEK, C. J. 2004. Reactive transport modeling of column experiments for the remediation of acid mine drainage. *Environmental Science and Technology,* 38**,** 3131-3138.

ANZECC & ARMCANZ 2000. *National Water Quality Management Strategy. Australian Guidelines for Water Quality Monitoring and Reporting. Summary (Paper 7a)*, Australia and New Zealand Environment and Conservation Council and Agriculture and Resource Management Council of Australia and New Zealand.

APHA 1998. *Standard Methods for the Examination of Water and Wastewater,* Washington, 20th Edition, American Public Health Association.

AS3798 1996. Australian Standard: Guidelines on earthworks for commercial and residential developments. Sydney: Standards Australia.

BALDWIN, D. 2011. National Guidance for the Management of Acid Sulfate Soils in Inland Aquatic Ecosystems. Canberra, ACT: Environment Protection and Heritage Coincil and Natural Resource Management Ministerial Council.

BAIN, J. G., MAYER, K. U., BLOWES, D. W., FRIND, E. O., MOLSON, J. W. H., KAHNT, R. & JENK, U. 2001. Modelling the closure-related geochemical evolution of groundwater at a former uranium mine. *Journal of Contaminant Hydrology,* 52**,** 109-135.

BALL, J. W. & NORDSTROM, D. K. 1991. User's manual for WATEQ4F, with revised thermodynamic data base and test cases for calculating speciation of major, trace and redox elements in natural waters. U.S. Geological Survey, Open-File Report 91-183.

BANASIAK, L. J. 2004. *The Role of a Subsurface Lime-Fly Ash Barrier in the Mitigation of Acid Sulphate Soils.* Masters, University of Wollongong.

BANASIAK, L. J., INDRARATNA, B., LUGG, G., PATHIRAGE, U., MCINTOSH, G. & RENDELL, N. 2014. Permeable reactive barrier rejuvenation by alkaline wastewater. Available: http://www.icevirtuallibrary.com/content/article/10.1680/envgeo.13.00122.

BENNER, S. G., BLOWES, D. W., GOULD, W. D., HERBERT JR, R. B. & PTACEK, C. J. 1999a. Geochemistry of a permeable reactive barrier for metals and acid mine drainage. *Environ. Sci. Technol.,* 33**,** 2793-2799.

BENNER, S. G., BLOWES, D. W., GOULD, W. D., HERBERTJR, R. B. & PTACEK, C. J. 1999b. Geochemistry of a permeable reactive barrier for metals and acid mine drainage. *Environmental Science & Technology,* 33**,** 2793-2799.

BENNER, S. G., GOULD, W. D. & BLOWES, D. W. 2000. Microbial populations associated with the generation and treatment of acid mine drainage. *Chemical Geology,* 169**,** 435-448.

BERNER, R. A. 1984. Sedimentary pyrite formation: An update. *Geochimica et Cosmochimica Acta,* 48**,** 605-615.

BEST, R. 2005. Browns Oxide Project – Groundwater Assessment, Report B18183/1-G, 1. Coffey Geosciences.

BILEK, F. 2006. Column tests to enhance sulphide precipitation with liquid organic electron donators to remediate AMD-influenced groundwater. *Environmental Geology,* 49**,** 674-683.

BIRKE, V., BURMEIER, H. & ROSENAU, D. 2003. Design, construction, and operation of tailored permeable reactive barriers. *Practice Periodical of Hazardous, Toxic, and Radioactive Waste Management,* 7**,** 264-280.

BLOWES, D. W., PTACEK, C. J., BENNER, S. G., MCRAE, C. W. T., BENNETT, T. A. & PULS, R. W. 2000. Treatment of inorganic contaminants using permeable reactive barriers. *Journal of Contaminant Hydrology,* 45**,** 123-137.

BLOWES, D. W., PTACEK, C. J. & JAMBOR, J. L. 1997. In-situ remediation of Cr(VI)-contaminated groundwater using permeable reactive walls: Laboratory studies. *Environmental Science and Technology,* 31**,** 3348-3357.

BLOWES, D. W., PTACEK, C. J., JAMBOR, J. L. & WEISENER, C. G. 2003. The Geochemistry of Acid Mine Drainage. *In:* TUREKIAN, H. D. H. A. K. K. (ed.) *Treatise on Geochemistry.* Oxford: Elsevier Science Ltd.

BLUNDEN, B. 2000. *Management of Acid Sulfate Soils by Groundwater Manipulation.* PhD, University of Wollongong.

BLUNDEN, B. & INDRARATNA, B. 2001. Pyrite oxidation model for assessing ground-water management strategies in acid sulfate soils. *Journal of Geotechnical and Geoenvironmental Engineering, ASCE,* 127**,** 146-157.

BLUNDEN, B., INDRARATNA, B. & NETHERY, A. 1997. Effect of groundwater table on acid sulphate soil remediation. *In:* BOUAZZA, KODIKARA & PARKER (eds.) *GeoEnvironment 97.* Rotterdam: Balkema.

BLUNDEN, B. & NAYLOR, S. 1995. Assessing and Managing Acid Sulfate Soils. Guidelines for Land Management. Environmental Protection Authority: Chatswood, NSW.

BLUNDEN, B. G. & INDRARATNA, B. 2000. Evaluation of surface and groundwater management strategies for drained sulfidic soil using numerical simulation models. *Australian Journal of Soil Research,* 38**,** 569-590.

BOHN, H. L., FU, Y. & HUANG, C. 1989. Hydrogen Sulfide Sorption by Soils. *Soil Science Society of American Journal,* 53**,** 1914-1917.

BORDEN, R. C. & BEDIENT, P. B. 1986. Transport of dissolved hydrocarbons influenced by oxygen-limited biodegradation: 1. Theoretical development. *Water Resources Research,* 22**,** 1973-1982.

BORDEN, R. C., BEDIENT, P. B., LEE, M. D., WARD, C. H. & WILSON, J. T. 1986. Transport of dissolved hydrocarbons influenced by oxygen-limited biodegradation: 2. Field application. *Water Resources Research,* 22**,** 1983-1990.

BRINKMAN, R. 1982. Directions of further research on acid sulfate soils *In:* DOST & BREEMAN, V., eds. *Proceedings of the Bangkok Symposium on Acid Sulfate Soils*, 1982. ILRI Publication 31, Wageningen, The Netherlands.

BROOKFIELD, A. E., BLOWES, D. W. & MAYER, K. U. 2006. Integration of field measurements and reactive transport modelling to evaluate contaminant transport at a sulfide mine tailings impoundment. *Journal of Contaminant Hydrology,* 88**,** 1-22.

BUSH, R. T. & SULLIVAN, L. A. 1997. Morphology and behaviour of greigite from a Holocene sediment in Eastern Australia. *Australian Journal of Soil Research,* 35**,** 853–861.

CALLINAN, R. B., PACILBARE, J. O., REANTASO, M. B., LUMANLAN-MAYO, S. C., FRASER, G. C. & SAMMUT, J. 1995. EUS outbreaks in estuarine fish in Australia and the Philippines: associations with acid sulphate soils, rainfall, and *Aphanomyces*. *Diseases in Asian Aquaculture II***,** 291-298.

CLEMENT, T. P. 1997. RT3D: A Modeular Computer Code for Simulating Reactive Multi-Species Transport in 3-Dimensional Groundwater Aquifers, PNNL-SA-11720 *In:* LABORATORY, P. N. N. (ed.). Richland, Washington.

CLEMENT, T. P., HOOKER, B. S. & SKEEN, R. S. 1996. Numerical modeling of biologically reactive transport near a nutrient injection well. *ASCE Journal of Environmental Engineering Division,* 122**,** 833-839.

CRAVOTTA, C. A., III & WATZLAF, G. R. 2002. Design and performance of limestone drains to increase pH and remove metals from acidic mine drainage. *In:* NAFTZ, D. L., MORRISON, S. J., FULLER, C. C. & DAVIS, J. A. (eds.) *Handbook of Groundwater Remediation Using Permeable Reactive Barriers: Applications to Radionuclides, Trace Metals, and Nutrients.* San Francisco: Academic Press.

DAVISON, W., LISHMAN, J. P. & HILTON, J. 1985. Formation of pyrite in freshwater sediments: Implications for CS ratios. *Geochimica et Cosmochimica Acta,* 49**,** 1615-1620.

DENT, D. 1986. Acid Sulphate Soils: a baseline for research and development. *In:* IRRI Publication No. 39, Wageningen, the Netherlands.

DENT, D. 1992. Reclamation of acid sulphate soils. *Advances in Soil Science,* 17**,** 79-122.

DENT, D. L. & PONS, L. J. 1995. A world perspective on acid sulphate soils. *Geoderma,* 67**,** 263-276.

DESMIER, R., MACDONALD, B. C. T., MELVILLE, M. D. & WAITE, T. D. 2002. Design, construction and performance of passive and active treatment systems to decrease the acidity export from acid sulfate soils in the Tweed Shire, NSW (Australia). *In:* BUSH, R., ed. *Proc. of the 5th International Acid Sulfate Soils Conference - Sustainable Management of Acid Sulfate Soils*, Tweed Heads, Australia, 71-72.

DICK, T. M. & OSUNKOYA, O. O. 2000. Influence of tidal restriction floodgates on decomposition of mangrove litter. *Aquatic Botany,* 68**,** 273-280.

DOVE, M. C. 2003. *Effects of estuarine acidification on survival and growth of the Sydney rock oyster Saccostrea glomerata.* PhD, University of New South Wales.

DRISCOLL, C. T., BAKER, J. P., BISOGNI, J. J. & SCHOFIELD, C. L. 1980. Effect of aluminium speciation on fish in dilute acidified waters. *Nature,* 284**,** 161-164.

EYRING, H. 1935. The Activated Complex and the Absolute Rate of Chemical Reactions. *Chemical Reviews,* 17**,** 65-77.

FANNING, D. S. 1993. Salinity problems in acid sulfate coastal soils. *In:* LEITH, H. & MASOOM, A. A. (eds.) *Towards the Rational Use of High Salinity Tolerant Plants.* The Netherlands: Kluwer Academic Publishers.

FITZPATRICK, R. W., FRITSCH, E. & SELF, P. G. 1993. Australia's unique saline acid sulphate soils associated with dryland salinity. *In: National Conference of Acid Sulphate Soils*, 24-25 June Coolangatta, Queensland, Australia, 41-56.

FITZPATRICK, R. W., POWELL, B. & MARVANEK, S. 2006. Coastal Acid Sulfate Soils: National Atlas and Future Scenarios. *Coast to Coast 2006: Australia's National Coastal Conference.* Melbourne, Australia.

FLEMING, I. R. & ROWE, R. K. 2004. Laboratory studies of clogging of landfill leachate collection and drainage systems. *Canadian Geotechnical Journal,* 41**,** 134-153.

FREEDMAN, V. L., SARIPALLI, K. P. & MEYER, P. D. 2003. Influence of mineral precipitation and dissolution on hydrologic properties of porous media in static and dynamic systems. *Applied Geochemstry,* 18**,** 589-606.

FURUKAWA, Y., KIM, J.-W., WATKINS, J. & WILKIN, R. T. 2002. Formation of ferrihydrite and associated iron corrosion products in permeable reactive barriers of zero-valent iron. *Environmental Science & Technology,* 36**,** 5469-5475.

GAVASKAR, A. R. 1999. Design and construction techniques for permeable reactive barriers. *Journal of Hazardous Materials,* 68**,** 41-71.

GAVASKAR, A. R., GUPTA, N., SASS, B. M., JANOSY, R. J. & O'SULLIVAN, D. 1998. *Permeable Barriers for Groundwater Remediation: Design, Construction, and Monitoring,* Columbus, Battelle Press.

GILLHAM, R. W. & O'HANNESIN, S. F. 1994. Enhanced degradation of halogenated aliphatics by zero-valent iron. *Ground Water,* 32**,** 958-967.

GLAMORE, W. 2003. *Evaluation and Analysis of Acid Sulphate Soil Impacts via Tidal Restoration.* PhD, University of Wollongong.

GLAMORE, W. & INDRARATNA, B. 2001. The impact of floodgate modifications on water quality in acid sulphate soil terrains. *In:* MCGRATH, B., GOURLAY, M. & NIELSEN, P., eds. 15th Australasian Coastal and Ocean Engineering Conference Proceedings, Gold Coast, Australia. The Institution of Engineers: Sydney, 265-270.

GLAMORE, W. & INDRARATNA, B. 2002. Management of acid sulphate soil drainage via floodgate manipulation. *In:* BUSH, R., ed. *Proceedings of the 5th International Acid Sulfate Soils Conference - Sustainable Management of Acid Sulfate Soils*, Tweed Heads, 75-76.

GLAMORE, W. & INDRARATNA, B. 2004. A two-stage decision support tool for restoring tidal flows to flood mitigation drains affected by acid sulphate soil: case study of Broughton Creek Floodplain, New South Wales, Australia. *Australian Journal of Soil Research,* 42**,** 639-648.

GOLAB, A., PETERSON, M. & INDRARATNA, B. 2009a. Selection of permeable reactive barrier materials for treating acidic groundwater in acid sulphate soil terrains based on laboratory column tests. *Environmental Earth Sciences,* 59**,** 241-254.

GOLAB, A. N. & INDRARATNA, B. 2009. Occurrence and consequences of acid sulphate soils and methods of site remediation. *Geomechanics and Geoengineering: An International Journal,* 4**,** 201 - 208.

GOLAB, A. N., PETERSON, M. A. & INDRARATNA, B. 2006. Selection of potential reactive materials for a permeable reactive barrier for remediating acidic groundwater in acid sulphate soil terrains. *Quarterly Journal of Engineering Geology and Hydrogeology,* 39**,** 209-223.

GOLAB, A. N., PETERSON, M. A. & INDRARATNA, B. 2009b. Selection of permeable reactive barrier materials for treating acidic groundwater in acid sulphate soil terrains based on laboratory column tests. *Environmental Earth Sciences*.

HARBAUGH, A. W. 2005. *MODFLOW-2005,The U.S. Geological Survey modular ground-water model—the Ground-Water Flow Process: U.S. Geological Survey Techniques and Methods 6-A16, variously p*.

HEDIN, R. S. & WATZLAF, G. R. 1994. The effects of anoxic limestone drains on mine water chemistry. Bureau of Mines Special Publication SP 06A.

HUNTER, K. S., WANG, Y. F. & VAN CAPPELLEN, P. 1998. Kinetic modeling of microbially-driven redox chemistry of subsurface environments: coupling transport, microbial metabolism and geochemistry. *Journal of Hydrology,* 209**,** 53-80.

HUYAKORN, P. S., THOMAS, S. D. & THOMPSON, B. M. 1984. Techniques for Making Finite Elements Competitve in Modeling Flow in Variably Saturated Porous Media. *Water Resources Research,* 20**,** 1099-1115.

INDRARATNA, B., BALASUBRAMANIAM, A. S. & KHAN, M. J. 1995a. Effect of fly ash with lime and cement on the behaviour of a soft clay. *Quarterly Journal of Engineering Geology,* 28**,** 131-142.

INDRARATNA, B., GLAMORE, W. C. & TULARAM, G. A. 2002. The effects of tidal buffering on acid sulphate soil environments in coastal areas of New South Wales. *Geotechnical and Geological Engineering,* 20**,** 181-199.

INDRARATNA, B., GOLAB, A., GLAMORE, W. & BLUNDEN, B. 2005. Acid sulphate soil remediation techniques on the Shoalhaven River Floodplain, Australia. *Quarterly Journal of Engineering Geology and Hydrogeology,* 38**,** 129-142.

INDRARATNA, B., GOLAB, A. N. & BANASIAK, L. J. 2006. Installation of a lime injection barrier for the remediation of acid sulphate soil problems. *Quarterly Journal of Engineering Geology and Hydrogeology,* 39**,** 391-401.

INDRARATNA, B., IONESCU, D. & CHRISTIE, H. D. 1998. Shear behaviour of railway ballast on large-scale triaxial tests. *Journal of Geotechnical and Geoenvironmetal Engineering***,** 439-449.

INDRARATNA, B., PATHIRAGE, P. U., BANASIAK, L. J. & NGHIEM, L. D. 2012. Column experiments carried out for the treatment of acidic groundwater in acid sulfate terrain at the Shoalhaven Floodplain, NSW. *In:* CLAY, C., ed. 3rd National Acid Sulfate Soil Conference, 2012 Melbourne. 72-73.

INDRARATNA, B., PATHIRAGE, P. U., KERRY, R. & BANASIAK, L. 2014. Coupled hydro-geochemical modelling of a permeable reactive barrier for treating acidic groundwater. *Computers and Geotechnics,* 55**,** 429-439.

INDRARATNA, B., REGMI, G., NGHIEM, L. & GOLAB, A. 2010. Performance of a permeable reactive barrier (PRB) for the remediation of groundwater in acid

sulphate soil terrain. *Journal of Geotechnical and Geoenvironmental Engineering, ASCE,* 136**,** 897-906.

INDRARATNA, B., SULLIVAN, J. & NETHERY, A. 1995b. Effect of groundwater table on formation of acid sulphate soils. *Minewater and the Environment,* 14**,** 71-84.

INDRARATNA, B. & VAFAI, F. 1997. Analytical model for predicting particle migration within a base soil-filter system. *Journal of Geotechnical and Geoenvironmental Engineering, ASCE,* 123**,** 100-109.

INDRARATNA, B., WIJEWARDANA L.S.S. & BALASUBRAMANIAM, A. S. 1993. Large-scale triaxial testing of greywacke rockfill. *Geotechnique,* 43**,** 37-51.

ITRC 2011. Permeable reactive barrier: Technology update. PRB-5. *In:* INTERSTATE TECHNOLOGY & REGULATORY COUNCIL, P. T. U. T. (ed.). Washington, D.C., US.

JAYNES, D. B., ROGOWSKI, A. S. & PIONKE, H. B. 1984. Acid mine drainage from reclaimed coal strip mines 1. Model description. *Water Resources Research,* 21**,** 233-242.

JEEN, S.-W., AMOS, R. T. & BLOWES, D. W. 2012. Modeling Gas Formation and Mineral Precipitation in a Granular Iron Column. *Environmental Science & Technology,* 46**,** 6742-6749.

JENK, U., SCHREYER, J. & KLINGER, C. 2003. Fe(0)/lignitic coal: an efficient and mechanically stable reactive material for purification of water containing heavy metals, radionuclides, and nitroaromatics. *Environmental Science & Technology,* 37**,** 644-651.

JOHNSON, R. L., TRATNYEK, P. G., MIEHR, R., THOMS, R. B. & BANSTRA, J. Z. 2005. Reduction of Hydraulic Conductivity and Reactivity in Zero-Valent Iron Columns by Oxygen and TNT. *Groundwater Monitoring and Remediation,* 25**,** 129-136.

JOHNSTON, S. G., SLAVICH, P. & HIRST, P. 2002. Floodgate and drainage system management: opportunities and limitations. An acid export perspective. *In:* MACDONALD, B. C. T., KEENE, A. F., CARLIN, G. & SULLIVAN, L. A., eds. *Sustainable Management of Acid Sulfate Soils. Proceedings of Third International Conference on Acid Sulfate Soils*, Tweed Heads, NSW, Australia. Acid Sulfate Soil Working Group, International Union of Soil Sciences, 79-80.

JURJOVEC, J., BLOWES, D. W., PTACEK, C. J. & MAYER, K. U. 2004. Multicomponent reactive transport modeling of acid neutralization reactions in mine tailings. *Water Resources Research,* 40**,** W1120201-W1120217.

JURJOVEC, J., PTACEK, C. J. & BLOWES, D. W. 2002. Acid neutralization mechanisms and metal release in mine tailings: a laboratory column experiment. *Geochimica et Cosmochimica Acta,* 66**,** 1511-1523.

KAKSONEN, A. 2000. *Sulfate-reduction based bioprocesses in mining biotechnology* [Online]. [Accessed].

KALINOVICH, I., RUTTER, A., POLAND, J. S., CAIRNS, G. & ROWE, R. K. 2008. Remediation of PCB contaminated soils in the canadian arctic: Excavation and Surface PRB Technology. *Science of Total Environment,* 407**,** 53-66.

KALINOVICH, I., RUTTER, A., ROWE, R. K. & POLAND, J. S. 2012. Design and application of surface PRBs for PCB remediation in the Canadian Arctic. *Journal of Environmental Management,,* 101**,** 124-133.

KALUARACHCHI, J. & J., M. 1995. Critical assessment of the operator-splitting technique in solving the advection-dispersion-reaction equation: 1. First-order reaction. *Advances in Water Resources,* 18**,** 89-100.

KAMOLPORNWIJIT, W., LIANG, L., MOLINE, G. R., HART, T. & WEST, O. R. 2004. Identification and quantification of mineral precipitation in $Fe^0$ filings from a column study. *Environmental Science & Technology,* 38**,** 5757-5765.

KAMOLPORNWIJIT, W., LIANG, L., WEST, O. R., MOLINE, G. R. & SULLIVAN, A. B. 2003. Preferential flow path development and its influence on long-term PRB performance: column study. *Journal of Contaminant Hydrology,* 66**,** 161-178.

KOMNITSAS, K., BARTZAS, G. & PASPALIARIS, I. 2004. Efficiency of limestone and red mud barriers: laboratory column studies. *Minerals Engineering,* 17**,** 183-194.

KRAUS, M. J. 1998. Development of potential acid sulfate paleosols in Paleocene floodplains, Bighorn Basin, Wyoming, USA. *Palaeogeography, Palaeoclimatology, Palaeoecology,* 144**,** 203-224.

KRAUSKOPF K.B. & D.K., B. 1995. *Introduction to Geochemistry*, McGraw-Hill, New York.

LAIDER, K. J. & KING, M. C. 1983. The development of transition-state theory. *Journal of Physical Chemistry,* 87**,** 2657-2664.

LI, L. 2004. *Fouling and the Long-Term Performance of Permeable Reactive Barriers.* PhD, University of Wisconsin-Madison.

LI, L. & BENSON, C. H. 2005. Impact of fouling on the long-term hydraulic behaviour of permeable reactive barriers. *IAHS-AISH Publication***,** 23-31.

LI, L., BENSON, C. H. & LAWSON, E. M. 2006. Modeling porosity reductions caused by mineraql fouling in continuous-wall permeable reactive barriers. *Journal of Contaminants Hydrology,* 83**,** 89-121.

LIANG, L., KORTE, N., GU, B., PULS, R. & REETER, C. 2000. Geochemical and microbial reactions affecting the long-term performance of in situ 'iron barriers'. *Advances in Environmental Research,* 4**,** 273-286.

LIANG, L., SULLIVAN, A. B., WEST, O. R., MOLINE, G. R. & KAMOLPORNWIJIT, W. 2003. Predicting the precipitation of mineral phases in permeable reactive barriers. *Environmental Engineering Science,* 20**,** 635-653.

LICHTNER, P. C. 1996. Continuum formulation of multicomponent–multiphase reactive transport. *In:* LICHTNER, P. C., STEEFEL, C.I., OELKERS, E.H. (ed.) *Reactive Transport in Porous Media. Reviews in Mineralogy (34).* Washington, D.C.: Mineralogical Society of America.

LIN, C., MADDOCK, G., MCCONCHIE, D., LANCASTER, G. & LIN, J. 2002. The uses of Bauxsol$^{TM}$ for treating sulfidic soils: Laboratory modeling and pot trials. *In:* BUSH, R., ed. *Proceedings of the 5th International Acid Sulfate Soils Conference - Sustainable Management of Acid Sulfate Soils*, Tweed Heads, 157-158.

LIN, C. & MELVILLE, M. D. 1992. Mangrove soil: a potential contamination source to estuarine ecosystems of Australia. *Wetlands,* 11**,** 68-74.

LIN, C., MELVILLE, M. D. & HAFER, S. 1995. Acid sulphate soil-landscape relationships in an undrained, tide-dominated estuarine floodplain, Eastern Australia. *Catena,* 24**,** 177-194.

LIN, C., ROSICKY, M., MCCONCHIE, D., SULLIVAN, L. A. & LANCASTER, G. 2001. Coastal land scalding in NSW, Australia: soil chemical

characteristics and their implications for remediation of the scalded lands. *Land Degradation & Development,* 12**,** 293-303.

LOGAN, M. V., REARDON, K. F., FIGUEROA, L. A., MCLAIN, J. E. T. & AHMANN, D. M. 2005. Microbial community activities during establishment, performance, and decline of bench-scale passive treatment systems for mine drainage. *Water Research,* 39**,** 4537-4551.

LUDWIG, R. D., MCGREGOR, R. G., BLOWES, D. W., BENNER, S. G. & MOUNTJOY, K. 2002. A permeable reactive barrier for treatment of heavy metals. *Ground Water,* 40**,** 59-66.

MACKENZIE, P. D., HORNEY, D. P. & SIVAVEC, T. M. 1999. Mineral precipitation and porosity losses in granular iron columns. *Journal of Hazardous Materials,* 68**,** 1-17.

MAYER, K. & MACQUARRIE, K. 2010. Solution of the MoMaS reactive transport benchmark with MIN3P—model formulation and simulation results. *Computational Geosciences,* 14**,** 405-419.

MAYER, K. U., BENNER, S. G. & BLOWES, D. W. 2006. Process-based reactive transport modeling of a permeable reactive barrier for the treatment of mine drainage. *Journal of Contaminant Hydrology,* 85**,** 195-211.

MAYER, K. U., BLOWES, D. W. & FRIND, E. O. 2001. Reactive transport modeling of an in situ reactive barrier for the treatment of hexavalent chromium and trichloroethylene in groundwater. *Water Resources Research,* 37**,** 3091-3103.

MAYER, K. U., FRIND, E. O. & BLOWES, D. W. 2002. Multicomponent reactive transport modeling in variably saturated porous media using a generalized formulation for kinetically controlled reactions. *Water Resources Research,* 38**,** 1174.

MCCONCHIE, D., CLARK, M., LIN, C., DAVIES-MCCONCHIE, F. & MADDOCKS, G. 2002a. Bauxsol$^{TM}$ - a new treatment for acid sulphate soils and sulphidic mining wastes. *In: Proceedings of the 5th International Acid Sulfate Soils Conference - Sustainable Management of Acid Sulfate Soils*, Tweed Heads, 73-74.

MCCONCHIE, D., CLARK, M., LIN, C., DAVIES-MCCONCHIE, F. & MADDOCKS, G. 2002b. Strategies for the use of Bauxsol$^{TM}$ in the management of acid sulphate soils and sulphidic mining wastes. *In: Proceedings of the 5th International Acid Sulfate Soils Conference - Sustainable Management of Acid Sulfate Soils*, Tweed Heads, 165-166.

MCDONALD, M. G. & HARBAUGH., A. W. 1988. *MODFLOW: A modular three dimensional finite-difference ground-water flow model,* Washington, DC, U.S. Geological Survey Techniques of Water-Resources Investigations, Chapter A1, Book 6, 586 pp.

MCELNEA, A. E. & AHERN, C. R. 2002. Testing the effectiveness of lime and cement kiln dust as acid sulfate soil ameliorants using leaching column experiments. *In:* BUSH, R., ed. *Proceedings of the 5th International Acid Sulfate Soils Conference - Sustainable Management of Acid Sulfate Soils*, Tweed Heads, Australia, 167-168.

MCMAHON, P. B., DENNEHY, K. F. & SANDSTROM, M. W. 1999. Hydraulic and geochemical performance of a permeable reactive barrier containing zero-valent iron, Denver Federal Center. *Ground Water,* 37**,** 396-404.

MORRISON, S. 2003. Performance evaluation of a permeable reactive barrier using reaction products as tracers. *Environmental Science & Technology,* 37**,** 2302-2309.

NAFTZ, D. L., FULLER, C. C., DAVIS, J. A., MORRISON, S. J., FELTCORN, E. M., FREETHEY, G. W., ROWLAND, R. C., WILKOWSKE, C. & PIANA, M. 2002. Field demonstration of three permeable reactive barriers to control uranium contamination in groundwater, Fry Canyon, Utah. *In:* NAFTZ, D. L., MORRISON, S. J., FULLER, C. C. & DAVIS, J. A. (eds.) *Handbook of Groundwater Remediation Using Permeable Reactive Barriers: Applications to Radionuclides, Trace Metals, and Nutrients.* San Francisco: Academic Press.

NEUMAN, S. P. 1973. Saturated-unsaturated seepage by finite elements. *Journal of the Hydraulics Divisions, ASCE,* 99:HY12**,** 2233-2250.

NORDSTROM, D. K. 1982. The effect of sulfate on aluminium concentrations in natural waters: some stability relations in the system $Al_2O_3$-$SO_3$-$H_2O$ at 298 K. *Geochimica et Cosmochimica Acta,* 46**,** 681-692.

O'HANNESIN, S. F. & GILLHAM, R. W. 1998. Long-term performance of an in situ 'iron wall' for remediation of VOCs. *Ground Water,* 36**,** 164-170.

OUANGRAWA, M., MOLSON, J., AUBERTIN, M., BUSSIERE, B. & ZAGURY, G. J. 2009. Reactive transport modelling of mine tailings columns with capillarity-induced high water saturation for preventing sulfide oxidation. *Applied Geochemistry,* 24**,** 1312-1323.

PARK, J.-B., LEE, S.-H., LEE, J.-W. & LEE, C.-Y. 2002. Lab scale experiments for permeable reactive barriers against contaminated groundwater with ammonium and heavy metals using clinoptilolite (01-29B). *Journal of Hazardous Materials,* 95**,** 65-79.

PARKHURST, D. L. & APPELO, C. A. J. 1999. User's Guide to Phreeqc (Version 2) - A Computer Program for Speciation, Batch-Reaction, One-Dimensional Transport, and Inverse Geochemical Calculations. Denver, Colorado: U.S. Geological Survey Water-Resources Investigations Report 99-4259.

PARKHURST, D. L., THORSTENSON, D. C. & PLUMMER, L. N. 1980. PHREEQE - a computer program for geochemical calculations.: US Geological Survey. US Government Printing Office, Washington, DC.

PATHIRAGE, P. U., INDRARATNA, B., NGHIEM, L. D., BANASIAK, L. & REGMI, G. 2012. Armouring by precipitates and the associated reduction in hydraulic conductivity of recycled concrete aggregates used in a novel PRB for the treatment of acidic groundwater. *11th Australia - New Zealand Conference on Geomechanics: Ground Engineering in a Changing World (pp. 828-833). ANZ Geomechanics.* Melbourne, Australia.

PEARSON, F. H. & MCDONNELL, A. J. 1975a. Limestone barriers to neutralize acidic streams. *Journal of the Environmental Engineering Division***,** 425-440.

PEARSON, F. H. & MCDONNELL, A. J. 1975b. Use of crushed limestone to neutralize acid wastes. *Journal of the Environmental Engineering Division***,** 139-158.

PEDERSEN, T. F. 1983. Dissolved heavy metals in a lacustrine mine tailings deposit-Buttle lake, British Columbia. *Marine Pollution Bulletin,* 14**,** 249-254.

PETRUCCI, H. H., HARWOOD, W. S. & MADURA, J. 2006a. *General Chemistry: Principles and Modern Application.*

PETRUCCI, R. H., HARWOOD, W. S., G.E., H. & MADURA, J. 2006b. *General Chemistry: Principles and Modern Application*.

PHILLIPS, D. H., GU, B., WATSON, D. B., ROH, Y., LIANG, L. & LEE, S. Y. 2000. Performance evaluation of a zerovalent iron reactive barrier: Mineralogical characteristics. *Environmental Science & Technology,* 34**,** 4169-4176.

POLLARD, D. A. & HANNAN, J. C. 1994. The ecological effects of structural flood mitigation works on fish habitats and fish communities in the lower Clarence River System of South-Eastern Australia. *Estuaries,* 17**,** 427-461.

PONS, L. J., VAN BREEMEN, N. & DRIESSEN, P. M. 1982. Physiography of Coastal Sediments and Development of Potential Soil Acidity. *In:* KITTRICK, J. A., FANNING, D. S. & HOSSNER, L. R. (eds.) *Acid Sulfate Weathering.* Madison, WI, USA: Soil Science of America.

PORTNOY, J. W. & GIBLIN, A. E. 1997a. Biogeochemical effects of seawater restoration to diked salt marshes. *Ecological Applications,* 7**,** 1054-1063.

PORTNOY, J. W. & GIBLIN, A. E. 1997b. Effects of historic tidal restrictions on salt marsh sediment chemistry. *Biogeochemistry,* 36**,** 275-303.

POWELL, B. & MARTENS, M. 2005. A review of acid sulfate soil impacts, actions and policies that impact on water quality in Great Barrier Reef catchments, including a case study on remediation at East Trinity. *Marine Pollution Bulletin,* 51**,** 149-164.

PULS, R. W., BLOWES, D. W. & GILLHAM, R. W. 1999a. Long-term performance monitoring for a permeable reactive barrier at the U.S. Coast Guard Support Center, Elizabeth City, North Carolina. *Journal of Hazardous Materials,* 68**,** 109-124.

PULS, R. W., KORTE, N., GAVASKAR, A. & REETER, C. 2000. Long-term performance of permeable reactive barriers: an update on a U.S. multi-agency initiative. *In: Proceedings of the 7th International Conference on Contaminated Soil*, 591-594.

PULS, R. W., PAUL, C. J. & POWELL, R. M. 1999b. The application of in situ permeable reactive (zero-valent iron) barrier technology for the remediation of chromate-contaminated groundwater: a field test. *Applied Geochemistry,* 14**,** 989-1000.

REDDI, L. N. & BONALA, M. V. S. 1997. Analytical solution for fine particle accumulation in soil filters. *Journal of Geotechnical and Geoenvironmental Engineering, ASCE,* 123**,** 1143-1152.

REDDI, L. N., XIAO, M., HAJRA, M. G. & LEE, I. M. 2000. Permeability reduction of soil filters due to physical clogging. *Journal of Geotechnical and Geoenvironmental Engineering, ASCE,* 126**,** 236-246.

REGMI, G. 2012. *Performance Validation of a Permeable Reactive Barrier (PRB) for Treating Acidic Groundwater.* Degree of Doctor of Philosophy, University of Wollongong.

REGMI, G., INDRARATNA, B. & NGHIEM, L. 2009a. Long-term Performance of a Permeable Reactive Barrier in Acid Sulphate Soil Terrain. *Water, Air & Soil Pollution: Focus,* 9**,** 409-419.

REGMI, G., INDRARATNA, B. & NGHIEM, L. D. 2009b. Effective remediation of groundwater in acid sulphate soil terrain. *Australian Geomechanics,* 44**,** 33-40.

REGMI, G., INDRARATNA, B., NGHIEM, L. D. & BANASIAK, L. 2011a. Evaluating waste concrete for the treatment of acid sulphate soil groundwater from coastal floodplains. *Desalination and Water Treatment,* 32**,** 126-132.

REGMI, G., INDRARATNA, B., NGHIEM, L. D., GOLAB, A. & GURUPRASAD, B. 2011b. Treatment of Acid Groundwater in Acid Sulphate Soil Terrain Using Recycled Concrete: Column Experiments. *Journal of Environmental Engineering, ASCE,* 137 (6)**,** 433-443.

RITSEMA, C. J., VAN MENSVOORT, M. E. F., DENT, D. L., TAN, Y., VAN DEN BOSCH, H. & VAN WIJK, A. L. M. 2000. Acid Sulfate Soils. *In:* SUMNER, M. E. (ed.) *Handbook of Soil Science.* Boca Raton: CRC Press.

ROH, Y., LEE, S. Y. & ELLESS, M. P. 2000. Characterization of corrosion products in the permeable reactive barriers. *Environmental Geology,* 40**,** 184-194.

RORISON, I. H. 1973. The effect of extreme soil acidity on the nutrient uptake and physiology of plants. *In:* DOST, H., ed. Acid Sulfate Soils: *Proceedings of the International Symposium*, 13-20 August Wageningen, The Netherlands: IRRI, 223-255.

ROWE, R., ARMSTRONG, M. & CULLIMORE, D. 2000. Particle Size and Clogging of Granular Media Permeated with Leachate. *Journal of Geotechnical and Geoenvironmental Engineering,* 126**,** 775-786.

ROWE, R. K. 2005. Long-term performance of contaminant barrier systems. *Geotechnique,* 55**,** 631-678.

ROWE, R. K., QUIGLEY, R. M., BRACHMAN, R. W. I. & BOOKER, J. R. 2004. *Barrier Systems for Waste Disposal,* London, Spon Press.

RUDENS, C. 2001. *The Role of Biotic Oxidation on Acid Production in Potential Acid Sulfate Soils in the Shoalhaven Floodplain.* Honours, University of Wollongong.

RUMER, R. R. & RYAN, M. E. (eds.) 1995. *Barrier Containment Technologies for Environmental Remediation Applications,* New York: John Wiley & Sons.

SAMMUT, J., CALLINAN, R. B. & FRASER, G. C. 1996a. An overview of the ecological impacts of acid sulfate soils in Australia. *In:* SMITH, R. J. & SMITH, H. J., eds. *Proceedings of the 2nd National Conference of Acid Sulfate Soils*, Coffs Harbour: Robert J. Smith and Associates and ASSMAC, 140-145.

SAMMUT, J. & MELVILLE, M. 1994. Impacts of poor water quality on fish. *In:* BRIERLEY, G. J. & NAGEL, F., eds. *Geomorphology and River Health in New South Wales*, Macquarie University, Graduate School of the Environment, Macquarie University, 115-122.

SAMMUT, J., WHITE, I. & MELVILLE, M. D. 1996b. Acidification of an estuarine tributary in eastern Australia due to drainage of acid sulfate soils. *Marine and Freshwater Research,* 47**,** 669-684.

SARR, D. 2001. Zero-valent-iron permeable reactive barriers - How long will they last? *Remediation,* 11**,** 1-18.

SINGER, P. C. & STUMM, W. 1970. Acidic mine drainage: the rate-determining step. *Science***,** 1121.

SPIESSL, S. M., MACQUARRIE, K. T. B. & MAYER, K. U. 2008. Identification of key parameters controlling dissolved oxygen migration and attenuation in fractured crystalline rocks. *Journal of Contaminant Hydrology,* 95**,** 141-153.

STEEFEL, C. I. & LASAGA, A. C. 1994. A coupled model for transport of multiple chemical-species and kinetic precipitation dissolution reactions with

application to reactive flow in single-phase hydrothermal systems. *American Journal of Science,* 294**,** 529-592.

STEEFEL, C. I. & YABUSAKI, S. B. 1996. OS3D/GIMRT – Software for Modeling Multicomponent-Multidimensional Reactive Transport. User Manual & Programmer's Guide. Richland, Washington: Pacific Northwest National Laboratory.

STRATFUL, I., SCRIMSHAW, M. D. & LESTER, J. N. 2001. Conditions influencing the precipitation of magnesium ammonium phosphate. *Water Research,* 35**,** 4191-4199.

STUMM, W. & MORGAN, J. J. 1996. *Aquatic Chemistry,* New York, 3rd Edition, John Wiley and Sons.

SULTAN, M., STURCHIO, N., HASSAN, F. A., HAMDAN, M. A. R., MAHMOOD, A. M., ALFY, Z. E. & STEIN, T. 1997. Precipitation source inferred from stable isotopic composition of Pleistocene groundwater and carbonate deposits in the Western Desert of Egypt. *Quaternary Research,* 48**,** 29-37.

SUNDARAM, B., FEITZ, A. J., DE CARITAT, P., PLAZINSKA, A., BRODIE, R. S., CORAM, J. & RANSLEY, T. 2009. Groundwater Sampling and Analysis - A Field Guild. *In:* AUSTRALIA, G. (ed.).

SVERDRUP, H. & WARFVINGE, P. 1988. Weathering of primary silicate minerals in the natural soil environment in relation to a chemical weathering model. *Water, Air, and Soil Pollution,* 38**,** 387-408.

TAM, V. W. Y., GAO, X. F. & TAM, C. M. 2005. Carbonation around near aggregate regions of old hardened concrete cement paste. *Cement and Concrete Research,* 35**,** 1180-1186.

TRANI, L. D. O. & INDRARATNA, B. 2010. Use of impedance probe for estimation of porosity changes in saturated granular filters under cyclic loading: Calibration and Application. *Journal of Geotechnical and Geo-environemntal Engineers***,** 1469-1474.

UMITSU, M., BUMAN, M., KAWASE, K. & WOODROFFE, C. D. 2001. Holocene palaeoecology and formation of the Shoalhaven River deltaic-estuarine plains, southeast Australia. *The Holocene,* 11**,** 407-418.

USEPA 2002. Field applications of in situ remediation technologies: Permeable reactive barriers. Washington, D.C: Office of Solid Waste and Emergency Response, Technology Office, USEPA/68/W-00/084

USEPA 2004. Evaluation of permeable reactive barrier performance. Washington, D.C: U.S. Environmental Protection Agency, EPA/542/R-04/004.

VALOCCHI, A. J. & MALMSTEAD, M. 1992. Accuracy of operator-splitting for advectiondispersion-reaction problems. *Water Resources Research,* 28**,** 1471-1476.

VAN BREEMAN, N. 1980. Acid sulphate soils. *Land Reclamation and Water Management,* ILRI 27, Wageningen**,** 53-57.

VAN HOLST, A. F. & WESTERVELD, C. J. W. 1973. Corrosion of concrete foundations in potential acid sulphate soils and subsoils in the Netherlands. *In:* DOST, H., ed. Acid Sulfate Soils: *Proceedings of the International Symposium*, 13-20 August Wageningen, The Netherlands: IRRI, 373-382.

VANGULCK, J. F. & ROWE, R. K. 2004. Evolution of clog formation with time in columns permeated with synthetic landfill leachate. *Journal of Contaminant Hydrology,* 75**,** 115-139.

VIDIC, R. D. 2001. Permeable reactive barriers: Case study review. *GWRTAC E-Series Technology Evaluation Rep. TE-01-01.* Pittsburgh: Ground-Water Remediation Technologies Analysis Center.

VIKESLAND, P. J., KLAUSEN, J. R., ZIMMERMANN, H., LYNN ROBERTS, A. & BALL, W. P. 2003. Longevity of granular iron in groundwater treatment processes: changes in solute transport properties over time. *Journal of Contaminant Hydrology,* 64**,** 3-33.

VOGAN, J. L., FOCHT, R. M., CLARK, D. K. & GRAHAM, S. L. 1999. Performance evaluation of a permeable reactive barrier for remediation of dissolved chlorinated solvents in groundwater. *Journal of Hazardous Materials,* 68**,** 97-108.

WAITE, D. T., DESMIER, R., MELVILLE, M., MACDONALD, B. & LAVITT, N. 2002. Preliminary investigation into the suitability of permeable reactive barriers for the treatment of acid sulfate soils discharge. *In:* NAFTZ, D. L., MORRISON, S. J., FULLER, C. C. & DAVIS, J. A. (eds.) *Handbook of Groundwater Remediation Using Permeable Reactive Barriers: Applications to Radionuclides, Trace Metals, and Nutrients.* San Francisco: Academic Press.

WALKER, P. H. 1972. Seasonal and stratigraphic controls in coastal floodplain soils. *Australian Journal of Soil Research,* 10**,** 127-142.

WALTER, A. L., FRIND, E. O., BLOWES, D. W., PTACEK, C. J. & MOLSON, J. W. 1994a. Modeling of multicomponent reactive transport in groundwater, Model development and evaluation. *Water Resour. Res.,* 30**,** 3137-3148.

WALTER, A. L., FRIND, E. O., BLOWES, D. W., PTACEK, C. J. & MOLSON, J. W. 1994b. Modeling of multicomponent reactive transport in groundwater: 1. Model development and evaluation. *Water Resources Research,* 30**,** 3137-3148.

WARNER, S. D. & SOREL, D. 2002. *Ten Years of Permeable Reactive Barriers: Lessons Learned and Future Expectations*, American Chemical Society.

WATSON, I. A., OSWALD, S. E., MAYER, K. U., WU, Y. & BANWART, S. A. 2003. Modeling Kinetic Processes Controlling Hydrogen and Acetate Concentrations in an Aquifer-Derived Microcosm. *Environmental Science & Technology,* 37**,** 3910-3919.

WATZLAF, G. R., SCHROEDER, K. T. & KAIRIES, C. 2000. Long-term performance of anoxic limestone drains for the treatment of mine drainage. *Mine Water and the Environment,* 19**,** 98-110.

WAYBRANT, K. R., BLOWES, D. W. & PTACEK, C. J. 1998. Selection of reactive mixtures for use in permeable reactive walls for treatment of mine drainage. *Environmental Science & Technology,* 32**,** 1972 -1979.

WAYBRANT, K. R., PTACEK, C. J. & BLOWES, D. W. 2002. Treatment of mine drainage using permeable reactive barriers: column experiments. *Environmental Science & Technology,* 36**,** 1349-1356.

WEBB, J. A. & SASOWSKY, I. D. 1994. The interaction of acid mine drainage with a carbonate terrane: evidence from the Obey River, north-central Tennessee. *Journal of Hydrology,* 161**,** 327-346.

WHITE, I., HEATH, L. & MELVILLE, M. 1999. Ecological Impacts of Flood Mitigation and Drainage in Coastal Lowlands. *Australian Journal of Emergency Management***,** 9-15.

WHITE, I., MELVILLE, M. D., WILSON, B. P. & SAMMUT, J. 1997. Reducing acidic discharges from coastal wetlands in eastern Australia. *Wetlands Ecology and Management,* 5**,** 55-72.

WHITE, I., WILSON, B. P., MELVILLE, M. D., SAMMUT, J. & LIN, C. 1996. Hydrology and drainage of acid sulfate soils. *In:* SMITH, R. J. & SMITH, H. J., eds. *Proceedings of the 2nd National Conference of Acid Sulfate Soils*, Coffs Harbour: Robert J. Smith and Associates and ASSMAC, 103-108.

WILKIN, R. T., PULS, R. W. & SEWELL, G. W. 2002. Long-term performance of Permeable Reactive Barriers: An evaluation at two sites. US EPA Environmental Research Brief, EPA/600/S-02/001.

WILKIN, R. T., PULS, R. W. & SEWELL, G. W. 2003. Long-term performance of permeable reactive barriers using zero-valent iron: geochemical and microbiological effects. *Ground Water,* 41**,** 493-503.

WILLIAMS, R. J. & WATFORD, F. A. 1997. Identification of structures restricting tidal flow in New South Wales, Australia. *Wetlands Ecology and Management,* 5**,** 87-97.

WOLERY, T. J., JACKSON, K. J., BOURCIER, W. L., BRUTON, C. J., VIANI, B. E., KNAUSS, K. G. & DELANY, J. M. 1990. Current status of the EQ3/6 software package for geochemical modeling. *Chemical Modeling of Aqueous Systems II.* merican Chemical Society.

YABUSAKI, S. 2001. Multicomponent reactive transport in an in situ zero-valent iron cell. *Environmental Science and Technology,* 35**,** 1493-1503.

ZHENG, C. & WANG, P. P. 1999. MT3DMS: A Modular Three-Dimensional Multispecies Transport Model for Simulation of Advection, Dispersion, and Chemical Reactions of Contaminants in Groundwater Systems; Documentation and User's Guide. US Army Corps of Engineers, Engineer Research and Development Center, Report SERDP-99-1.

# APPENDIX I: Mathematical model derivation

The groundwater flow at transient condition is considered, and the governing equation for one dimension flow is given by;

$$\frac{\partial^2 h}{\partial x^2} = \nabla^2 h = \frac{S}{T}\left(\frac{\partial h}{\partial t}\right) \tag{A.1}$$

$$T = Kb \tag{A.2}$$

The solution for Eq. (A.1) can be written as,

Let b/$S$ =$A$, as $S$ and $b$ are assumed to be constants throughout the simulation, hence,

$$\nabla^2 h = \frac{1}{AK}\left(\frac{\partial h}{\partial t}\right) \tag{A.3}$$

Now, we assume a solution of separating variable type for Eq. (A.1) as follows;

$$h(x,t) = X(x)T(t) \text{ and } K(t_1) = T_1(t_1) \tag{A.4}$$

Substitution of $h$=$X.T$ and $K$=$T_1$ into Eq. (A.3) yields;

$$X''.T = \frac{X}{A}.\frac{T'}{T_1} \tag{A.5}$$

where the prime denotes differentiation with respect to the appropriate variable.

Dividing by X.T, we obtain,

$$\frac{X''}{X} = \frac{1}{A}\cdot\frac{T'}{T}\cdot\frac{1}{T_1} = -\mu^2 \tag{A.6}$$

where μ is an arbitrary constant, thus,

$$\frac{X''}{X} = -\mu^2 \tag{A.7}$$

And

$$\frac{1}{A}\cdot\frac{T'}{T}\cdot\frac{1}{T_1}=-\mu^2 \tag{A.8}$$

$$\frac{T'}{T}=-\mu^2 A T_1 \tag{A.9}$$

$$\int\frac{T'}{T}dt=-\mu^2 A\int T_1 dt \tag{A.10}$$

$$\ln(T)=-\mu^2 A\int\frac{K_0\left(\dfrac{n_0+\sum_{k=1}^{N_m}M_k R_k t}{n_0}\right)^3}{\left(\dfrac{1-\left(n_0+\sum_{k=1}^{N_m}M_k R_k t\right)}{1-n_0}\right)^2}dt \tag{A.11}$$

Let $\alpha=n_0+\sum_{k=1}^{N_m}M_k R_k t$ and $\beta=1-n_0-\sum_{k=1}^{N_m}M_k R_k t$

$$\frac{\partial\alpha}{\partial t}=\sum_{k=1}^{N_m}M_k R_k \tag{A.12}$$

$$\ln(T)=-\frac{\mu^2 A K_0}{\sum_{k=1}^{N_m}M_k R_k}\frac{(1-n_0)^2}{n_0^3}\int\frac{\alpha^3}{(1-\alpha)^2}d\alpha \tag{A.13}$$

$$\ln(T)=-\frac{\mu^2 b K_0}{S\sum_{k=1}^{N_m}M_k R_k}\frac{(1-n_0)^2}{n_0^3}\left[\alpha^2\left(1.5+{}^{1}\!/\!_{\beta}\right)-3(\alpha+\ln\beta)\right] \tag{A.14}$$

$$T=\exp\left[-\frac{\mu^2 b K_0}{S\sum_{k=1}^{N_m}M_k R_k}\frac{(1-n_0)^2}{n_0^3}\left\{\alpha^2\left(1.5+{}^{1}\!/\!_{\beta}\right)-3(\alpha+\ln\beta)\right\}\right] \tag{A.15}$$

From Eq. (B.4);

$$X=C\sin\mu x+D\cos\mu x \tag{A.16}$$

where, $C$ and $D$ are integral constants.

Therefore, the general solution for Eq. (A.3) can be written as,

$$h = \left( \exp\left[ -\frac{\mu^2 b K_0}{S\sum_{k=1}^{N_m} M_k R_k} \frac{(1-n_0)^2}{n_0^3} \left\{ \alpha^2 \left( 1.5 + {}^{1}\!/\!_{\beta} \right) - 3(\alpha + \ln \beta) \right\} \right] \right) \cdot (C \sin \mu x + D \cos \mu x) \tag{A.17}$$

# *APPENDIX II: Field Work*

Yellow mottles of jarosite collected at the field site, Nowra

Collecting undisturbed samples of ASS for permeability test

Surveying the piezometers and monitoring wells to locate them in the map and to determine the water table according to AHD

Collecting the soil and water samples and storing them in an esky till refrigerated

Collecting the bore hole samples using the mechanical auger